

Department of Mechanical and Aerospace Engineering

Hydro-Connected Floating Photovoltaic (FPV) Renewable Energy System with Onshore Wind Potential in Zambia.

Author:

Kumbuso Joshua Nyoni

201984476

Supervisor:

Dr Paul Gerald Tuohy

A Thesis submitted by Kumbuso Joshua Nyoni to the Department of Mechanical and Aerospace Engineering, University of Strathclyde, in part completion of the requirements for the MSc in Sustainable Engineering: Renewable Energy Systems and the Environment.

I, Kumbuso Joshua Nyoni, hereby state that this report is my own work and that all sources used are made explicit in the text.

2020

Copyright Declaration

This thesis is the result of the author's original research. It has been composed by the author and has not been previously submitted for examination which has led to the award of a degree.

The copyright of this thesis belongs to the author under the terms of the United Kingdom Copyright Acts as qualified by University of Strathclyde Regulation 3.50. Due acknowledgement must always be made of the use of any material contained in, or derived from, this thesis.

Signed: **Kumbuso Joshua Nyoni** Date: August 18, 2020

Abstract

An exploitation plan towards a diversification strategy of the energy mix including low water consumptions technologies, such as onshore wind and floating photovoltaics (FPV), will address the consequences of climate change and variability (i.e. extreme weather events like frequent low rainfall periods and droughts) thus improving the resilience of the Zambian hydro-based power system. Moreover, a better water exploitation plan during the year is possible thanks to the time complementarity of wind and solar sources with hydro sources; wind and solar radiation are greater during the dry season and lower during the wet season when more water is available for hydropower.

With this motivation, a site appraisal methodology was developed for the potential of linking existing and future hydro sites with FPV and wind. Thereafter, the methodology was applied to all the 13 existing hydro sites in Zambia of which 3 were filtered off and the remaining 10 ranked according to attribute suitability. A scoping design methodology was then developed and later applied to a case study after stakeholder engagement. The Kafue Gorge Upper case study results revealed that the integration of FPV and onshore wind did not only improve the voltage magnitude profile at nine network buses but also reduced the total network active power loss by 5% as well. The FPV along with onshore wind also added about 341 GWh to the national annual energy generation to meet 3.84 TWh of energy demand, in the presence of 3.2 TWh as well as 286 GWh of hydropower generation and virtual storage respectively. This was achieved at a competitive levelized cost of energy (LCOE) of 4.5 pence/kWh.

Further, it is worth noting that the floating PV is not being presented as a competitor to ground mounted systems, but rather as a complimentary technology in specific applications (i.e. retrofitting on hydro reservoirs). Along with providing such benefits as reduced evaporation and algae growth, FPV systems have lower operating temperatures and potentially reducing the costs of solar energy generation. To put this into perspective, the current study using PVSYST showed that floating photovoltaic has a better energy yield compared to ground mounted system as evidenced by 7.4%, 5.8% and 4.9% increase in energy production for the freestanding, small footprint and large footprint FPV configurations respectively, at a reduced generation cost of 4 pence/kWh. The case study also revealed the hydro reservoir storage potential by throttling down 17 percent of hydrogeneration in the presence of FPV and wind using a customized homerpro and matlab dispatch algorithm.

Therefore, onshore wind and photovoltaic (both land and floating) integration could allow additional technical-economic benefits as a faster commissioning of new capacity with more opportunities for Independent Power Producers (IPPs) investments, new opportunities for the Zambian manufacturing and service sectors, decentralization of the power supply structure thanks to their availability in different regions of the country (i.e. wind and solar sources are more diffused than hydropower which is usually located on large rivers and lakes).

Keywords: Dispatch, Electrical Demand, Energy Mix, Floating Photovoltaics, Grid Integration, Hydro Generation, Levelized Cost of Energy, Onshore Wind, Time Complementarity, Site Appraisal & Ranking.

Acknowledgements

The thesis study outcomes would not have been possible without the positive influence and aid of many people and organizations. Of utmost importance, I would like to express my heartfelt gratitude to the Commonwealth Scholarship Commission for the gesture of the scholarship award and the University of Strathclyde for offering me a place to pursue my master's degree. Many thanks go to Dr Paul Gerald Tuohy for his relentless effort and contributions towards this study. His constructive critiques and guidance throughout this research have made this paper worth contributing to the vibrant conversation about the sustainability of floating photovoltaics and onshore wind in developing countries.

I would like to thank my lovely family for the patience and support rendered during the period of studying for my masters in the United Kingdom. Particularly, I honour and thank my ever loving and outrageously supportive wife Clara M. Nyoni, our lovely daughter Thandeka, my awesome sister Phaidesy and my loving mother Christine, for your sacrifice. Though it was not easy, you were always there for me and only God can reward you.

In addition, I would like to appreciate Mr George Muyunda for the technical support he rendered to me throughout my studies.

Further, I would like to thank the following friends for their constructive philosophical contributions towards this paper: Kelvin Kabwe, Michael Sakala and Katelema Mapoma.

I would like to appreciate the Rural Electrification Authority CEO, Mr. Clement Silavwe and ZESCO management for the support they gave me throughout my study.

Last but not the least, I would like to dedicate this study to my late father, Mr. Joshua Nyoni and the ever faithful and loving Almighty God for the immeasurable contribution in shaping me to be the man I am today.

Table of Contents

Abstract	i
Acknowledgements	iii
List of Figures.....	ix
List of Tables	xiii
List of Symbols, Abbreviations and Acronyms.....	xv
CHAPTER ONE: INTRODUCTION	1
1.1 Background	1
1.2 Problem Statement and Motivation.....	3
1.3 Research Question.....	4
1.4 Aims and Objectives.....	4
1.5 Methodological Approach	5
1.6 Scope Statement	6
1.7 Thesis Structure.....	6
CHAPTER TWO: POWER SECTOR REVIEW & RENEWABLE ENERGY POLICY IN ZAMBIA	8
2.1 Overview.....	8
2.2 Power System Outlook.....	10
2.2.1 Demand and Demand Forecast	10
2.2.2 Power Generation System.....	12
2.2.2.1 Generation Fleet	12
2.2.2.2 Hydropower Generation	13
2.2.2.3 Variable Renewable Energy Sources.....	15
2.2.3 Power Transmission Network.....	16
2.2.3.1 Network Composition.....	17
2.2.3.2 Interconnection with Neighbouring Countries	17
2.3 Renewable Energy Policies (REFiT & GETFiT).....	19
2.4 Summary.....	20
CHAPTER THREE: LITERATURE REVIEW.....	21
3.1 Floating Photovoltaics (FPV) Technology	21
3.1.1 Overview	21
3.1.1.1 Floating PV Typical Components	22
3.1.1.2 Different Floating PV Technologies.....	22

3.1.1.3	Global Market for Floating PV	24
3.1.1.4	Floating PV Pros & Cons.....	25
3.1.2	System Design	27
3.1.2.1	PV Technology.....	27
3.1.3	Analysis of Energy Yield.....	31
3.1.3.1	Insolation and Irradiance on Solar Modules	31
3.1.3.2	Soiling.....	32
3.1.3.3	Shading Losses.....	32
3.1.3.4	Temperature Dependent Losses	32
3.1.3.5	Mismatch, Cabling and Inverter Losses.....	33
3.1.3.6	Water Surface Albedo.....	33
3.1.3.7	Long-Term Degradation Rates.....	34
3.1.3.8	Optimal Tilt Angle	34
3.1.3.9	Cooling Effect	34
3.1.3.10	Performance Ratio.....	35
3.2	Hydro-Connected FPV Potential.....	36
3.3	Onshore Wind Turbine Technology.....	37
3.3.1	Overview	37
3.3.2	Wind Turbine Model Formulation	38
3.3.3	Wind Energy in Zambian Context.....	38
3.4	Selection of Software Analysis Tools	39
3.4.1	Power System Modelling.....	39
3.4.1.1	Comparison of Power System Analysis Tools.....	41
3.4.1.2	Selection Criteria of Power System Tools	44
3.4.2	Renewable Energy Simulation and Optimization Tools.....	44
3.4.2.1	Online Software Tools.....	45
3.4.2.2	Renewable Energy Modelling Tools	45
3.4.2.3	Methodological Approach	47
3.4.2.4	Selection Criteria of Renewable and Optimization Tools.....	51
3.5	Grid Integration of Variable Renewables	54
3.5.1	Overview	54
3.5.2	Impacts on Voltage Magnitude Profile.....	54
3.5.3	Impact on Network Power Losses.....	55
3.5.4	Optimal Power Flow Based Optimization.	55
3.6	Dispatch of Hybrid Energy Systems	56
3.7	The Cost of Variable Renewable Energy	57
3.7.1	Cost Overview	58

3.7.2	The Cost of Floating PV	59
3.7.3	CAPEX of Floating vs Land PV	61
3.7.4	Perceived Costs of VRES in Zambia.....	62
3.7.5	Grid Reinforcement Costs	65
3.8	Literature Review Summary	66
CHAPTER FOUR: SITE ASSESSMENT, SCREENING & RANKING		
METHODOLOGY		67
4.1	Overview.....	67
4.2	Proposed Study Methodology	68
4.3	Criteria Hierarchy Structure.....	69
4.3.1	Optimal FPV Site	69
4.3.2	Optimal Wind Site.....	70
4.4	Site Attribute Suitability Score	71
4.5	Summary.....	72
CHAPTER FIVE: APPLICATION OF SITE ASSESSMENT, SCREENING &		
RANKING METHODOLOGY		74
5.1	Data Collection & Mapping.....	74
5.1.1	Site Identification.....	74
5.1.2	Photovoltaics Parameter QGIS Mapping.....	75
5.1.3	Wind Parameter Mapping.....	77
5.1.4	Google Earth Pro FPV & Wind Site Mapping.....	79
5.1.5	Floating Photovoltaic Output Potential	80
5.1.6	Wind Output Potential.....	82
5.2	Stage 1 Screening.....	84
5.3	Stage 2 Scoring & Ranking.....	86
5.3.1	Hybrid Balanced Ranking.....	87
5.3.2	Floating PV Ranking.....	88
5.3.3	Onshore Wind Ranking	89
5.4	Methodology Application Limitations	90
5.5	Summary.....	90
CHAPTER SIX: SCOPING DESIGN STUDY METHODOLOGY		92
6.1	Design Methodology Formulation	92

6.2	Details of the Hydro-FPV-Wind Daily Dispatch Model	94
6.2.1	VRES Parameter Uncertainty	97
6.2.2	Dispatch Model Objective Function.....	97
6.2.3	Dispatch Model Constraints.....	97
6.2.3.1	Hydro Constraints.....	97
6.2.3.2	Power Balance Constraint.....	98
6.2.3.3	Branch Power flow Constraints.....	98
6.2.3.4	Floating Photovoltaic Power Constraint	98
6.2.3.5	Onshore Wind Power Constraint.....	98
6.3	Methodology Application Flowchart	98
6.4	Summary.....	99
CHAPTER SEVEN: APPLICATION OF SCOPING DESIGN STUDY		
METHODOLOGY.....		
7.1	Grid Assessment for VRES Integration at KGU.....	101
7.1.1	Existing Grid Analysis	102
7.1.1.1	Network Modelling Using Power System Analysis Toolbox (PSAT)	102
7.1.1.2	Simulation Results of Existing Grid.....	103
7.1.2	VRES Integration.....	107
7.1.2.1	VRES Modelling	107
7.1.2.2	Optimal Power Flow Market Model Formulation of National Grid.....	108
7.1.2.3	Optimal Power Flow Model Validation.....	109
7.1.2.4	Simulations Results	111
7.1.3	Results Analysis.....	115
7.2	Assessment of Seasonal Hydro Generation & Grid Demand	116
7.2.1	Kafue Gorge Generation Assessment.....	116
7.2.1.1	Kafue Gorge HVA Table.....	117
7.2.1.2	Kafue Gorge Upper Reservoir Operation Rule Curves	117
7.2.1.3	Hydro Generation Modelling	118
7.2.1.4	Kafue Gorge Generation Scenarios	120
7.2.2	National Electrical Grid Load Assessment.....	122
7.3	Detailed VRES (FPV & Wind) Assessment and Design at KGU	123
7.3.1	KGU Floating Photovoltaics Assessment & Design	123
7.3.1.1	Interrow Spacing of FPV System.....	123
7.3.1.2	System Layout, Design Components & Characteristics	125
7.3.1.3	Yield Comparison Between FPV Configurations and Ground Mounted System	127
7.3.1.4	FPV Shading Scene (large footprint).....	129
7.3.1.5	System Main Results (large footprint).....	130
7.3.1.6	Loss Diagram Assessment (large footprint).....	132

7.3.1.7	Economic Evaluation (large footprint)	133
7.3.1.8	System Optimization (large footprint).....	133
7.3.2	KGU Onshore Wind Assessment and Optimal Placement	135
7.3.2.1	Wind Farm Layout & Capacity Density	135
7.3.2.2	Wind Turbine Characteristics	136
7.3.2.3	Site Wind Variability.....	137
7.3.2.4	Wind Farm Energy Yield Assessment.....	137
7.4	Assessing the Hydro Storage Potential at KGU.....	139
7.5	System Optimization (Maximizing Energy & Reducing Cost)	142
7.5.1	Timeseries Dispatch	142
7.5.2	Cost of VRES (Wind & FPV).....	153
7.5.3	Hybrid System Optimization Using HomerPro Advanced Dispatch.....	154
7.5.3.1	Energy System Model.....	154
7.5.3.2	Homerpro Dispatch Strategy Capabilities.....	158
7.5.3.3	Energy System Optimization	159
7.6	Optimal Dispatch versus Baseline Case	165
7.7	Summary.....	173
CHAPTER EIGHT: DISCUSSION, OUTCOMES, LIMITATIONS, FURTHER WORK & CONCLUSIONS.....		174
8.1	Discussion	174
8.2	Research Outcomes	178
8.3	Project Limitation.....	180
8.4	Further Work.....	180
8.5	Conclusions	181
REFERENCES.....		182
APPENDICES		196
Appendix A – Site Appraisal Data Collection Tables		196
Appendix B – Grid Assessment Models.....		200
Appendix C – Matlab Link Dispatch Code.....		204
A MatlabStartSimulation Function.....		204
B MatlabEndSimulation Function.....		204
C Matlab Dispatch Function		205

List of Figures

Figure 2A: showing the single buyer market model (Source: ERB, 2018; USAID, 2018). -----	9
Figure 2B: National electricity consumption in GWh per economic sector (Source: ERB, 2018) -----	11
Figure 2C: perceived demand by 2030 (Source: USAID, 2018) -----	11
Figure 2D: showing generation expansion plan 2019 – 2030 (Source: CESI, 2020) -----	13
Figure 2E: Installed capacity and expected yearly average generated energy for hydropower plant -----	14
Figure 2F: Average generated power and Capacity Factor for hydropower plant -----	14
Figure 2G: showing the distribution of global horizontal irradiation in Zambia and 6 candidate sites -----	15
Figure 2H: showing mesoscale wind speed at 80m AGL Figure 2I - showing location of installed met masts.	16
Figure 2J: showing Planned and existing transmission system in Zambia. (Source: ZESCO) -----	17
Figure 2K: showing net transfer capacities and interconnections -----	18
Figure 2L - showing planned and existing interconnections within the SAPP system (Source: SAPP, 2017) ----	19
Figure 3A: showing the typical representation of a large floating PV system (Source: SERIS, 2019) -----	22
Figure 3B: showing annual additions and global installed capacity of FPV -----	25
Figure 3C: showing size distribution of FPV as of December 2018 (Source: World Bank, SERIS, 2019) -----	25
Figure 3D: showing equivalent circuit of photovoltaic cell -----	27
Figure 3E: showing IV characteristics of connecting two identical cells -----	30
Figure 3F: showing two identical cells connected in parallel -----	30
Figure 3F: showing FPV capacity potential in GW (top) and electricity generation potential TWh (bottom) ----	36
Figure 3G: showing the power/energy system software selection criteria -----	44
Figure 3H: showing flowchart summarizing the methodology and categorisation -----	49
Figure 3I: showing the renewable energy modelling tool selection criteria -----	53
Figure 3J: showing Global weighted average total installed costs, CFs and LCOE for solar PV -----	58
Figure 3K: Global weighted average total installed costs, CFs and LCOE for onshore wind -----	59
Figure 3L: showing Investment costs of FPV in 2014–2018 (realized and auction results) -----	60
Figure 3M: showing CAPEX of floating vs. land-based (ground-mounted) photovoltaic systems -----	62
Figure 3N: showing comparison between annual LCOE for wind and PV technologies -----	64
Figure 4A: showing typical structure of multicriteria decision method (source: Harper et al., 2017) -----	68
Figure 4B: showing proposed methodology flowchart of study area -----	68
Figure 4C: showing 2 stage hierarchy structure for optimal floating photovoltaics site selection. -----	70
Figure 4D: showing 2 stage hierarchy structure for optimal onshore wind site selection. -----	71
Figure 5A: Direct Normal Irradiation (DNI) in kWh/m ² -----	75
Figure 5B: Diffuse Irradiation (DIF) in kWh/m ² -----	75
Figure 5C: Global Horizontal Irradiation (GHI) in kWh/m ² -----	76
Figure 5D: Global Tilted Irradiation (GTI) in kWh/m ² -----	76
Figure 5E: Temperature Distribution in °C -----	76
Figure 5F: Optimal Tilt Angle (OPTA) in in degrees -----	76

Figure 5G: showing hydro sites & long-term yearly average of potential PV production. ----- 76

Figure 5H: showing average terrain slope distribution in Zambia ----- 77

Figure 5I: showing terrain elevation distribution (source: World Bank & DNV GL 2015) ----- 77

Figure 5J: showing wetlands & important bird areas (source: World Bank & DNV GL 2015) ----- 77

Figure 5K: showing aerodynamic roughness length (source: World Bank & DNV GL 2015) ----- 77

Figure 5L: showing the land tenure distribution (source: World Bank & DNV GL 2015) ----- 77

Figure 5M: showing power generation and transmission (source: World Bank & DNV GL 2015) ----- 77

Figure 5N: showing seasonal distribution of wind at 100m above ground level (AGL) ----- 78

Figure 5O: showing some mapped FPV and wind sites in google earth pro ----- 79

Figure 5P: showing site capacity factors for 2019 weather data from MERRA-2 dataset ----- 80

Figure 5Q: showing site optimal tilt angle based on the updated ESMAP for Zambia ----- 80

Figure 5R: shows the Summation of Monthly Totals of FPV Output (kWh/kWp) & DNI (kWh/m²) ----- 81

Figure 5S: showing the site energy production potential using renewables ninja and GWA. ----- 81

Figure 5T: showing wind potential output for each site ----- 83

Figure 5U: showing FPV stage 1 criteria benchmark ----- 84

Figure 5V: showing the number of FPV sites that passed each defined criterion ----- 85

Figure 5W: showing onshore wind stage 1 criteria benchmark ----- 85

Figure 5X: showing application of the WSM equation under balanced scoring and ranking ----- 87

Figure 5Y: showing application of the WSM equation under FPV scoring & ranking ----- 88

Figure 5Z: showing application of the WSM equation under wind scoring and ranking ----- 89

Figure 6A: showing the schematic for the hydro-FPV-Wind grid tied system ----- 94

Figure 6B: showing systematic flow of decision level to attain optimal hydro-FPV-Wind dispatch ----- 96

Figure 6C - showing methodology application process ----- 99

Figure 7.1A: showing network statistics of main power components ----- 102

Figure 7.1B: showing voltage magnitude profile before addition of compensation equipment. ----- 105

Figure 7.1C: showing voltage magnitude after grid compensation ----- 106

Figure 7.1D: showing the global power summary of the network ----- 106

Figure 7.1E: wind farm modelling with DFIG generator ----- 107

Figure 7.1F: showing the PSAT solar PV generator model ----- 107

Figure 7.1G: showing the PSAT IEEE-06 test system for OPF ----- 109

Figure 7.1H: showing global power summary with VRES integration at constant load ----- 112

Figure 7.1I: showing active generation power before and after VRES integration ----- 113

Figure 7.1J: showing active generation power before and after VRES integration ----- 113

Figure 7.1K: showing transaction level for the different dispatch scenarios ----- 114

Figure 7.1L: showing losses for the different dispatch scenarios ----- 114

Figure 7.1M: showing cost (\$/h) for the different dispatch scenarios ----- 115

Figure 7.2A: showing the upper rule curve for KGU ----- 118

Figure 7.2B: showing the modelled KGU hydrogeneration for one turbine in iHoga software ----- 120

Figure 7.2C: showing current water availability generation first day of each month	121
Figure 7.2D: showing low water availability generation for first day of each month.	121
Figure 7.2E: showing normal water availability generation for first day of each month	122
Figure 7.2F: showing seasonal variation of demand.	122
Figure 7.3A: showing the principle used to calculate interrow spacing	124
Figure 7.3B: showing the solar chart for KGU site	124
Figure 7.3C: showing component layout of photovoltaic system design	126
Figure 7.3D: showing PV module and array characteristics of designed system	127
Figure 7.3E: showing energy production in GWh/year for each system configuration	128
Figure 7.3F: showing performance ratio for each system configuration	128
Figure 7.3G: showing perspective of the PV-field and surrounding shading scene	129
Figure 7.3H: showing the shading loss diagram for the design with pitch 3m	129
Figure 7.3I: showing normalized productions and performance ratio for the large footprint FPV	130
Figure 7.3J: showing array power output for the first day of each month	131
Figure 7.3K: showing the loss diagram of the large footprint FPV at KGU	132
Figure 7.3L: showing the economic evaluation of the large footprint FPV (from PVSYST)	133
Figure 7.3M: showing ground cover ratio optimization of the large footprint FPV	134
Figure 7.3N: showing tilt angle optimization of the large footprint FPV	134
Figure 7.3O: showing pitch optimization of the large footprint FPV	134
Figure 7.3P: showing azimuth angle optimization of the large footprint FPV	134
Figure 7.3Q: showing Kafue Gorge (-15.67064°, 28.32604°) Wind Farm layout for 25 turbines	135
Figure 7.3R: showing turbine power curve	136
Figure 7.3S: showing the turbine losses for the design	136
Figure 7.3T: showing GWA wind variability at Kafue Gorge wind site (-15.67064°, 28.32604°).	137
Figure 7.3U: showing the optimistic daily mean power output and monthly capacity factors	138
Figure 7.3V: showing hourly power output for the first day of each month (from renewables ninja)	138
Figure 7.3W: showing more conservative output simulations in Homerpro	139
Figure 7.4A: showing the customized virtual storage model in homerpro	141
Figure 7.5.1A: showing floating PV and wind dispatch on 1 st January	143
Figure 7.5.1B: showing total generation dispatch on 1 st January	143
Figure 7.5.1C: showing generation dispatch and load on 1 st January	144
Figure 7.5.1D: showing floating PV and wind dispatch on 1 st March	144
Figure 7.5.1E: showing generation dispatch and load on 1 st March	145
Figure 7.5.1F: showing floating PV and wind dispatch on 1 st June	145
Figure 7.5.1G: showing generation dispatch and load on 1 st June	146
Figure 7.5.1H: showing floating PV and wind dispatch on 1 st September	146
Figure 7.5.1I: showing generation dispatch and electrical grid load on 1 st September	147

Figure 7.5.1J: showing floating PV and wind dispatch on 1 st November	147
Figure 7.5.1K: showing generation dispatch and electrical grid load on 1 st November	148
Figure 7.5.1L: showing generation dispatch and electrical grid load on 1 st January	148
Figure 7.5.1M: showing generation dispatch and electrical grid load on 1 st March	149
Figure 7.5.1N: showing generation dispatch and electrical grid load on 1 st June	149
Figure 7.5.1O: showing generation dispatch and electrical grid load on 1 st September	150
Figure 7.5.1P: showing generation dispatch and electrical grid load on 1 st November	150
Figure 7.5.1Q: showing generation dispatch and electrical grid load on 1 st January	151
Figure 7.5.1R: showing generation dispatch and electrical grid load on 1 st March	151
Figure 7.5.1S: showing generation dispatch and electrical grid load on 1 st June	152
Figure 7.5.1T: showing generation dispatch and electrical grid load on 1 st September	152
Figure 7.5.1U: showing generation dispatch and electrical grid load on 1 st November	153
Figure 7.5.2A: showing the LCOE of the large footprint floating PV and Wind at KGU	154
Figure 7.5.3A: showing energy system schematic in Homerpro	155
Figure 7.5.3B: showing sensitivity inputs	155
Figure 7.5.3C: showing sensitivity inputs	155
Figure 7.5.3D: showing national electricity consumption by economic sector	156
Figure 7.5.3E: showing fraction of national load modelled in homerpro	157
Figure 7.5.3F: showing system cost summary of the energy system under HGO strategy	159
Figure 7.5.3G: showing electrical summary of the energy system under HGO strategy.	160
Figure 7.5.3H: showing hydro storage of the energy system under HGO strategy.	160
Figure 7.5.3I: showing system cost summary of the energy system under HP strategy	161
Figure 7.5.3J: showing electrical summary of the energy system under HP strategy	161
Figure 7.5.3K: showing hydro storage of the energy system under HP strategy.	162
Figure 7.5.3L: showing the Matlab link inputs	162
Figure 7.5.3M: showing the process of calculations and function calls between homerpr and matlab	163
Figure 7.6A: showing the generator order dispatch strategy	166
Figure 7.6B: showing the homer predictive dispatch strategy	169
Figure 7.6C: showing timeseries dispatch using Matlab link	171
Figure 7.6D: showing optimal dispatch versus baseline case	172
Figure 7.6E: showing the customized hydro generation with search space of 6 units	172

List of Tables

Table 2A - showing maximum generation fleet for 2019, 2020 and 2030 (Source: CESI, 2020) -----	12
Table 2B: showing the location of selected sites for solar resource (Source: World Bank, 2019)-----	15
Table 2C: showing procurement limits per technology (REFIT, 2016)-----	20
Table 3A: showing description of typical components of FPV system (Oliveira-Pinto, 2020) -----	22
Table 3B: showing the description of commonly applied floating PV technologies in reservoirs -----	23
Table 3C: showing example of supplier for each technology type in table 3B -----	24
Table 3D: shows FPV generation potential in man-made freshwater reservoirs, by continent -----	24
Table 3E: illustrating pros and cons of floating PV technology applications -----	26
Table 3F: describing the three types of photovoltaic modules (ABB Group, 2016) -----	29
Table 3G: showing characterization of floating structures using the heat loss factor (Liu et al., 2018) -----	35
Table 3H: showing estimated power generation and reservoir size to match hydropower capacity -----	37
Table 3I: defines some of the grid and economic analysis features -----	41
Table 3J: shows the comparison of different grid and economic analysis features -----	43
Table 3K: showing a list of modelling tools, developer, availability, relevant software and citation.	50
Table 3L: showing spatiotemporal resolution and general logic of tools (citation in table 3J) -----	51
Table 3M: showing economic and technological assessment parameters(citation in table 3J) -----	52
Table 3N: showing estimated O&M costs for fixed tilt land-based PV systems -----	60
Table 3O: showing a comparison of CAPEX: Floating vs. land-based photovoltaic -----	61
Table 3P: showing assumptions used for LCOE forecast in Zambia (Source: CESI, 2020) -----	63
Table 3Q: showing LCOE for PV power plants – Zambia (source: CESI, 2020) -----	64
Table 3R: showing LCOE for wind power plants (source: CESI, 2020) -----	65
Table 3S: showing specific investment costs (CAPEX) of the transmission facilities (CESI, 2020) -----	65
Table 4A: showing Balanced Score. -----	73
Table 4B: showing FPV Attribute Score. -----	73
Table 4C: showing Wind Attribute Score. -----	73
Table 5A: showing the identification of hydro sites under study -----	75
Table 5B: showing the FPV stage 1 screening criteria -----	84
Table 5C: showing defined screening and filtering for onshore wind -----	85
Table 5D: showing the combined stage 1 screening outcome for both FPV and onshore wind sites -----	86
Table 5E: showing balanced scoring and ranking matrix table -----	87
Table 5F: showing floating PV scoring and ranking matrix table -----	88
Table 5G: showing onshore wind scoring and ranking matrix table -----	89
Table 7.1A: showing network compensation equipment -----	103
Table 7.1B - showing power flow results before addition of network compensating equipment. -----	103
Table 7.1C: showing line flows before addition of network compensating equipment. -----	104
Table 7.1D: showing the different energy optimization cases using OPF -----	108

Table 7.1E: showing cost function coefficient for the different generators.	108
Table 7.1F: showing IEEE 6 bus results statistics without VRES	110
Table 7.1G: showing IEEE 6 bus results statistics with VRES	110
Table 7.1H: showing lines flows after VRES integration	111
Table 7.1I: showing optimal power flow results for 6 different dispatch scenarios	113
Table 7.2A: showing the HVA table for Kafue Gorge Upper	117
Table 7.2B: showing E.O.M Upper reservoir rule levels for KGU	118
Table 7.2C: showing rating parameters of Kafue Gorge Upper generation plant	119
Table 7.3A: showing the albedo and U-value of the four different configurations	127
Table 7.3B: showing summary of system performance on average from January to December	131
Table 7.5.2A: showing cost and energy production distribution.	153
Table 7.5.3A: showing renewable fraction and system costs	164
Table 7.5.3B: showing system operation results	164
Table 7.5.3C: showing storage system operation results	164

List of Symbols, Abbreviations and Acronyms

AC:	Alternating Current
CEC:	Copperbelt Energy Corporation
DC:	Direct Current
ERB:	Energy Regulation Board
FPV:	Floating Photovoltaics
GETFIT:	Global Energy Transfer Feed-in Tariff
GW:	Gigawatt
GWh:	Gigawatt Hours
HFWDD:	Hydro-FPV-Wind Daily Dispatch
HOMER:	Hybrid Optimization of Multiple Energy Resources
JICA:	Japan International Cooperation Agency
KW:	Kilowatt
KWh	Kilowatt Hours
LCOE:	Levelized Cost of Energy
MCDM:	Multi Criteria Decision Making
MOE:	Ministry of Energy
MPP:	Maximum Power Point
P:	Active Power
PSAT:	Power System Analysis Toolbox
PV:	Photovoltaic
PVSYST:	Photovoltaic System Software
Q:	Reactive Power
REFIT:	Renewable Energy Feed-in Tariff
TWh:	Terawatt Hour
VRES:	Variable Renewable Energy Sources
W _P :	Watt Peak
WSM:	Weighted Sum Method
ZESCO:	Zambia Electricity Supply Corporation Limited
£:	Pound Sterling Currency Symbol
%:	Percentage
\$:	United States Dollar Currency Symbol

CHAPTER ONE: INTRODUCTION

This chapter outlines the context of the study topic and its relevance to the author and stakeholders. The chapter's progressive structure is as follows: [section 1.1](#) gives the high-level background, [section 1.2](#) defines the problem statement of the research and authors motivation, [section 1.3](#) asks three pertinent research questions, [section 1.4](#) describes the study outcomes, [section 1.5](#) defines a stepwise research methodology, [section 1.6](#) lists the research items in scope and those out of the scope and lastly the dissertation structure is defined in [section 1.7](#).

1.1 Background

Floating photovoltaics (FPV) panels, also known as “floatovoltaics”, initially gained practical popularity in Japan, motivated mainly by constraints in land utilization for new power generation plants. These took advantage of unused water bodies (i.e. reservoirs and freshwater ponds). Nevertheless, as the photovoltaic (PV) panel efficiency increased to 21% from 14% and the price of PV modules dropped by 75% between 2010 and 2017, a new market in FPV quickly came into fruition ([Thi, 2017](#); [Trapani and Redon, 2015](#); [Ferrer Gisbert, 2013](#)).

The interest in floating PV has significantly evolved to include the hydropower industry. This is because of the presented opportunity of installing (or retrofitting) floating PV on the hydro reservoir which has an abundant water surface area. To put this into global perspective, more than a hundred floating photovoltaic plants had been installed and commissioned between 2015 to 2018, with a total installed capacity of approximately 600 MW ([Mesbahi, 2018](#); [Tsanova, 2018](#)). Even though the FPV technology deployment at large scale was initially pioneered by Asian countries (i.e. Japan, China, Thailand, South Korea), interest has also spread to Europe, North and South America. Therefore, Sub Saharan African (SSA) countries could also follow suit and embrace this technology to complement land-based photovoltaics.

With the advancement in photovoltaics technology (coupled with enhanced mooring and anchoring techniques), the potential of large-scale hydro-connected PV (both land and floating) is highly promising ([Farfan, J. and Breyer, C., 2018](#)). For instance, the Longyangxia power plant in China, is a hybrid of a 1280 MW hydropower and 850 MW solar photovoltaics land-based plant as a single source energy generation system. This generation mix offers a temporal complementarity and thus the variable solar power is smoothed by the stable and dispatchable hydro. The hydropower output is throttled upwards or downwards depending on whether the PV output is low or high respectively, thereby meeting the network power dispatch

curve by an improvement in reliability and enhancement in total energy generation (Ming et al., 2018).

Research (Farfan and Breyer, 2018; Spencer, 2018) has revealed the water-based configuration of photovoltaic systems to be mutually beneficial: Along with providing such benefits as reduced evaporation and algae growth, it can lower PV operating temperatures and potentially reduce the costs of solar energy generation. These benefits can be applicable to Zambia as well.

With approximately 3000 sunshine hours per annum and an average solar insolation of 5.5 kWh/m²/day, Zambia has good potential for photovoltaic and solar thermal applications (IRENA, 2013), this, coupled with 13 operational hydro power plants (~2380 MW), which accounts for about 85% of total installed generation (~2800 MW), makes the country better suited for a generation mix. Further, a recent study conducted by the World Bank (2018) and DNV-GL revealed that there was great wind resource potential (~6 to 11 m/s) for utility scale wind power in some parts of the country (i.e. Serenje, Luangwa, Muchinga etc.) at heights between 80 and 200 m above sea level (A.S.L). This culminated into the commissioning and validation of a mesoscale wind atlas for Zambia with accurate wind measurements taken from eight meteorological masts for a period of 2 years (World Bank, 2015; World Bank, 2018).

In line with the Zambia energy policy (2019), this study will encourage all stakeholders involved in the production of electricity to promote the alternative use of renewable energy practices such as floating photovoltaics and onshore wind that will increase electricity capacity in the country. However, there is need to develop a clearer framework of regulations and policies related to these technologies that could potentially help to minimize financial risks and encourage investment. Consequently, this could contribute to promote safe and sustainable electricity generation for economic growth and development which is vital in achieving the Zambia Vision 2030 which aims to make Zambia a prosperous middle-income nation by the year 2030.

The increase in the understanding of natural variability of climate change and capacity to build better climate models such as global circulation models (GCM's) will help decision makers to enact well informed environmental sound policies that address current energy threats faced in Zambia and at the same time preparing for the future. Against this background, this study will help in the implementation of renewable energy such as floating photovoltaics and onshore wind to help increase electricity generation and supply.

Although there is growing interest in FPV, to date there has been no systematic assessment of technical potential in Zambia and Sub-Saharan Africa as a whole. This research provides the first national-level estimate of FPV and onshore wind technical potential using a combination of filtered, large-scale datasets, site-specific PV/wind generation models, and geospatial analytical tools, near hydro sites.

1.2 Problem Statement and Motivation

Zambia still faces significant challenges in her quest to become a middle-income nation by 2030. Some of these issues include low access to clean energy technologies, low electrification rates and limited infrastructure to transport electricity. National access to electricity averages thirty one percent with 4% of the rural and 67% of the urban population having access to electricity, this, leaves approximately twelve million people without access (CSO, 2019; USAID, 2018). Therefore, the households that are not electrified rely on other fuels for energy utilization (i.e. crop residues, wood fuels, charcoal and wood fuel for their heating and cooking, candles and kerosene for lighting).

Further, when compared to that of peer countries, Zambia's power consumption (~706 kilowatt-hour per capita) is below expectations relative to its social and economic potential. Other resource rich countries (i.e. Chile, Peru, Namibia and South Africa) have a per capita consumption in the range of about 1412 kWh to 2118 kWh, which is about two to three times higher than that of Zambia. With a population of about 17million people and a GDP of \$20.5 billion (2016), Zambia was ranked 18th in terms of economic growth prospects in Africa. Today, nearly 69 percent of Zambians have no access to electricity, however, those that have access (31 percent) mostly endure power outages during the drought seasons (USAID, 2018).

Zambia's current total installed capacity of approximately 2800 MW does not allow for much economic growth especially in drought prone years when there is a reduction in generation. This is because 85 percent of the installed capacity is hydropower which relies on availability of good water resource. The three major hydro plants (Kariba North, Kafue Gorge and Kariba North Extension) account for 81 percent electricity production. The reliance on hydropower has been attributed to a vast spread of water resource with estimated potential of 6000 MW. However, in the recent past, climate change has reduced the dynamics of this resource potential by making the electricity system vulnerable to droughts. The country has experienced 4 major droughts in the past fifteen years. The most recent droughts occurred in 2015-2016, 2016-2017

and 2018-2019 rainfall seasons. This exacerbated the load management strategies by ZESCO limited to conserve the water resource and, consequently a reduction in economic activity from mining and other commercial sectors (ZESCO, 2020; CSO, 2019; USAID, 2018).

Therefore, it is the motivation of the author to contribute to improving the livelihoods of all Zambians and that of neighbouring citizens by increasing the total energy generation and electricity access through the adoption of other renewable energy technologies like floating photovoltaics and onshore wind, consequently alleviating the energy poverty that the region faces. Moreover, Zambia has the potential to earning foreign exchange through the export of power to these countries and mitigate a chronic trade deficit the country is grappling with.

1.3 Research Question

Threats to Zambia's electricity system have been highlighted in the preceding sections. There was a need to better understand the extent to which a dry year can affect the electricity system, specifically the impact on the cost of generating electricity. Given the risks of having a hydro-dominated supply system, there was a need to assess other supply options such as other renewable energy technologies (i.e. floating photovoltaics, onshore wind).

Consequently, this research sought to answer the following three questions:

1. Which hydro sites in Zambia are suitable for cost-effective floating photovoltaic (FPV) and onshore wind integration?
2. How can we best assess the technical and economic feasibility for potential FPV and onshore wind utility scale installations near hydro sites?
3. Is it cost effective and technically feasible to integrate the Zambian hydro sites with floating photovoltaics and onshore wind?

The above questions formed the cornerstone of data collection and progression of the research.

1.4 Aims and Objectives

The expected outcomes of this study are:

- Create a site appraisal method to rank possible hydro sites for potential retrofitting of FPV and addition of onshore wind in Zambia
- Develop methodology for scoping of case study design.
- Apply the design methodology on an actual site.

1.5 Methodological Approach

The project research methodological approach is as shown below:

- Step 1 - review relevant literature, previous work done, justify the choice of research methods and selection of software modelling tools.
- Step 2 - Establish and define a site assessment, screening and ranking methodology.
- Step 3 - Apply the site assessment, screening and ranking methodology to Zambia, cataloguing of sites and making a case study selection based on step 2 above.
- Step 4 - Define and document a scoping of design study methodology to be applied to case study site investigations which will provide answers to key questions with respect to technical and economic feasibility of the energy system (hydro + FPV + Wind). The developed method aims to:
 - Assess the technical parameters of the local grid.
 - Assess current generation situation considering hour by hour basis throughout the year.
 - Assess floating photovoltaics and onshore wind potential and ascertain how much of the hydro generation profile matches with FPV and wind.
 - Assess storage potential (implied by throttling down hydro in presence of wind and FPV).
 - Maximise daily energy production within grid constraints using optimal dispatch strategy and ascertain the levelized cost of energy of the system.

The above approach will optimize the daily-seasonal generation of the hybrid energy system while balancing the specified system load characteristics within the constraint of the local grid. Consequently, the following pertinent questions will be answered:

- i. What complementary FPV and wind would fit without extra upgrades and additional energy storage devices?
 - ii. By how much real power contribution from floating PV or/and wind would make the system cost optimal?
- Step 5 - Apply the scoping design case study methodology to the case study site and produce results which answer the key questions in step 4.
 - Step 6 - Discussion of the outcomes and wider implications of the findings of the site assessment and scoping design study methodologies.

1.6 Scope Statement

Scope Statement: The project involves the initiating, planning, research methodology devising and case study designing of a hydro-connected floating photovoltaics (FPV) renewable energy system with onshore wind potential in Zambia.

The project scope includes:

- Hydro site appraisal for FPV + wind resource potential in Zambia.
- Development of a multi-criteria decision making (MCDM) methodology for site assessment and ranking in Zambia.
- Electrical design and analysis of floating photovoltaic system.
- Electrical grid impact analysis (grid code network parameter assessment).
- Development of a generation dispatch strategy.
- Economic analysis of the energy system and how it competes with other technologies.
- Optimal placement of wind turbine
- Geographical information system mapping of sites and attributes
- Hydro reservoir water saving potential by FPV installation

The project scope excludes:

- Power tracking of PV modules
- Bathymetry and topography study, soil study, FPV mooring and anchoring design.
- Mechanical design of FPV & wind turbines, detailed electrical design of wind turbines.
- Short circuit analysis and protection grading.
- Grid connection design of actual primary equipment (i.e. transformers and associated switchgear).
- Site geotechnical analysis, environmental impact analysis.
- Carbon saving analysis.

1.7 Thesis Structure

Having tackled the study parameters in this chapter (i.e. high-level background, threats faced to the existing electricity system, methodological approach, aims, scope statement, motivation and relevance of the research), the remainder of the thesis is structured as follows:

Chapter two gives a detailed overview of the Zambia power sector with emphasis placed on the electrical demand and demand forecast, generation fleet and the status of variable

renewable energy sources and future generation plan. Further, it addresses the renewable energy policies (i.e. REFiT and GETFiT) aimed at promoting the integration of renewables.

Chapter three reviews the literature and the theoretical background relevant to the research topic. It explains some underlying concepts in understanding the study topic pertaining to floating photovoltaics, onshore wind, grid impact assessment, renewable energy system integration, optimal/economical dispatch control of the variable renewable energy systems (VRES) with hydro. Additionally, the choice and justification of research methods is also made, including the selection of modelling software.

Chapter four describes the development of a site assessment, screening and ranking methodology employed in this study. This ranged from site identification, filtering and ranking of sites based on assigned relative weight and attribute suitability scores as adopted from literature, industry practice and stakeholder engagement.

Chapter five describes the application of the site assessment, screening and ranking methodology to Zambia and case study selection. Furthermore, the chapter tackles the data collection process, examines the uncertainties introduced in the assumptions made when building the multi-criteria decision-making (MCDM) models. Thereafter, the limitations in the methods and tools used are highlighted.

Chapter six defines a scoping design study methodology.

Chapter seven includes the application of the scoping design methodology to a case study for one of the hydro sites.

Chapter eight examines and discusses the results of the detailed case study design and formulated models. It also summarizes the project research outcomes, study limitation and proposes further work to be done. Lastly, the chapter draws a conclusion of the research by referencing the key results and answering the research question in [section 1.3](#).

CHAPTER TWO: POWER SECTOR REVIEW & RENEWABLE ENERGY POLICY IN ZAMBIA

This chapter gives an overview about Zambia's power sector and the underlying policies (REFiT and GETFit) in support of renewable energy penetration. [Section 2.1](#) looks at the snapshot of the country's power sector by highlighting the key players and resource potential. [Section 2.2](#) describes the power system in detail by focusing on the current demand, demand forecast, current generation system, variable renewable source generation plan and the status of the power transmission network. [Section 2.3](#) describes the main policies that have been developed to promote and support renewable energy projects.

2.1 Overview

The electricity sector in Zambia is overseen by the Ministry of Energy (MOE), which provides policy guidance, and it is dominated by the vertically integrated utility company ZESCO Limited (ZESCO). The utility is fully owned by the Government of the Republic of Zambia (GRZ) through the Industrial Development Corporation (IDC), the holding company for most of state-owned enterprises in Zambia. ZESCO owns and operates over 80% of the generation, transmission, and distribution assets in the country and supplies electricity to all grid-connected consumers. On November 21, 1997, the Copperbelt Energy Corporation (CEC) and ZESCO entered into a power supply agreement (PSA) where the latter was supplying to the former at wholesale to supply the mining companies on the Copperbelt. However, this deal came to an end on 31 March 2020, and with the introduction of a statutory instrument No 57 declaring all CEC's transmission and distribution lines as "Common Carrier", ZESCO had taken up the role of supplying the mining companies on the Copperbelt using CEC infrastructure. Other Independent Power Producers (IPPs) operate in the electric power sector under long-term Power Purchase Agreements (PPAs) with ZESCO: Maamba Collieries Limited (MCL), Itezhi-Tezhi Power Corporation (ITPC), Ndola Energy Company Limited (NECL) and Lunsemfwa Hydro Power Company Ltd (LHPC) ([CESI, 2020](#)). The market structure in Zambia can be described as de facto, single buyer model as illustrated in [figure 2A](#) below;

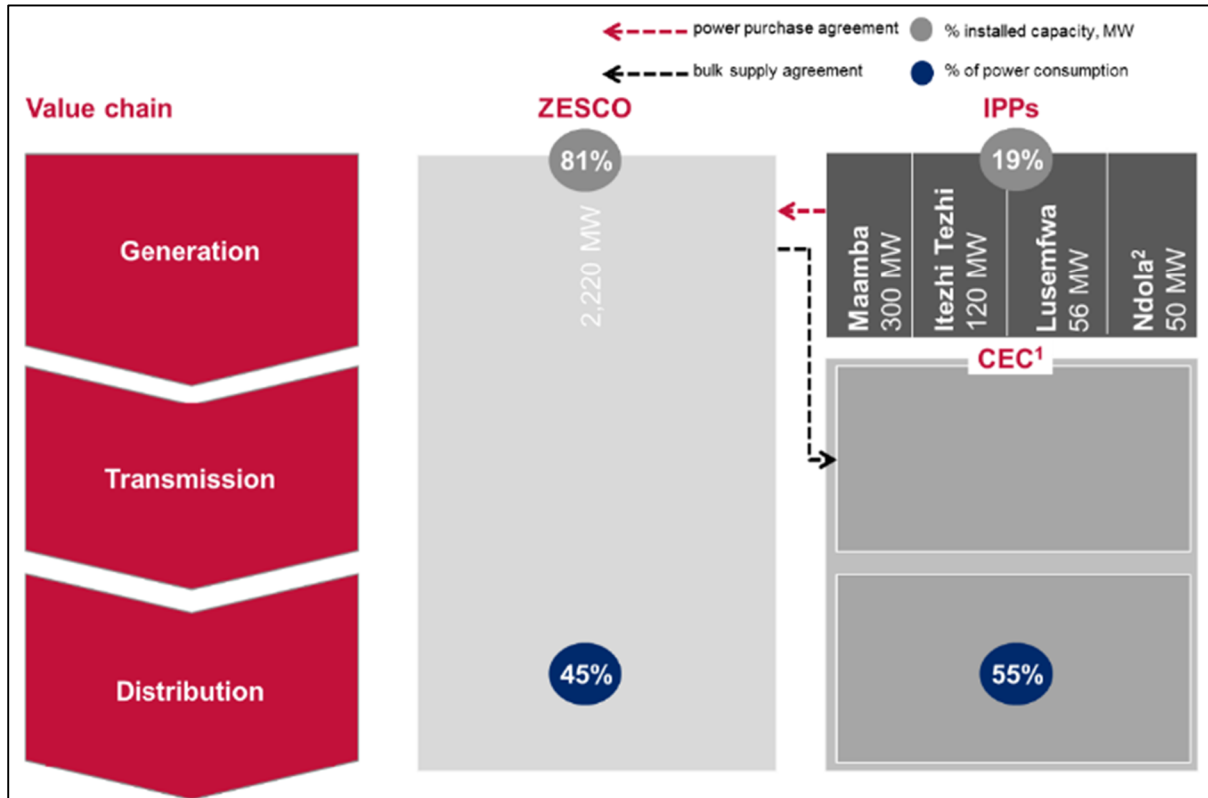


Figure 2A: showing the single buyer market model (Source: ERB, 2018; USAID, 2018).

1 CEC has 80MW generation capacity

2 excludes 55MW that came online in 2017

The electricity sector also includes the independent Energy Regulation Board (ERB) created under the Energy Regulation Act of 1995 to balance the needs of the consumers with the need of the undertakings. It is responsible for licensing, tariff setting and quality of supply for all segments of the electricity sector. Furthermore, about the rural areas of the Country, the Rural Electrification Authority (REA) is the institution responsible for providing electricity infrastructure to all rural areas using appropriate technologies to increase access to energy, productivity and quality of life (ERB, 2019).

Zambia is an active member of the Southern African Power Pool (SAPP), the cooperation of the national electricity companies in southern Africa with the scope to optimize the use of available energy sources in the region and enhance energy exchange between countries facilitating the development of a competitive electricity market in the Southern African Development Community (SADC) (CESI, 2020).

Historically, the GRZ focused on the electricity production from hydropower which is the most important energy source for the Country. However, the energy crisis of 2015/2016 pushed the GRZ to diversify the generation mix. With Vision 2030 and National Development Plans, the

GRZ is focused on diversifying its energy mix with renewable sources other than the hydroelectric source to complement the large base of hydro resources development. A diversified mix of energy resources allows ensuring the security of supply and contributes to mitigate climate change. In this regard, the GRZ through the MOE launched the initiative “REFiT Strategy” to accelerate private investments in small- and medium sized renewable energy projects in order to open the power sector and more so develop a renewable energy subsector to supplement the large hydro energy sources which have been negatively affected by climate change (Francesco et al., 2020).

Zambia is rich in renewable energy resources; the identified potential includes 6,000 MW from hydropower, 5.5 kWh/m²/day (annual average daily radiation) from solar source, average wind speed at 130 m between 7 and 8 m/s, 80 hot springs to be exploited for geothermal production. This potential can be exploited to meet the growing internal demand (expected compound annual growth rate of 3.8% in the period 2019-2030) and increase/decrease the export/import with the neighbouring countries (IRENA, 2013; World Bank, 2018).

The existing power generation capacity is about 2.9 GW. Hydropower plays an important role in the existing Zambian generation fleet with about 84% of total installed capacity and it will continue in the future; about 13% of total capacity is from coal and fuel oil power plants while 2.6% is from PV power plants (ERB, 2019; Francesco et al., 2020).

2.2 Power System Outlook

This section gives a prospective of the supply and demand balance in the country and the underlying short/long term gaps in view of the 2030 target of transforming Zambia into a middle-income nation.

2.2.1 Demand and Demand Forecast

According to the ERB’s power sector report (2018), the electricity consumption per economic sector for 2017 and 2018 is given in the [figure 2B](#) below. The 2019 – July 2020 period also has a similar profile to the latter year.

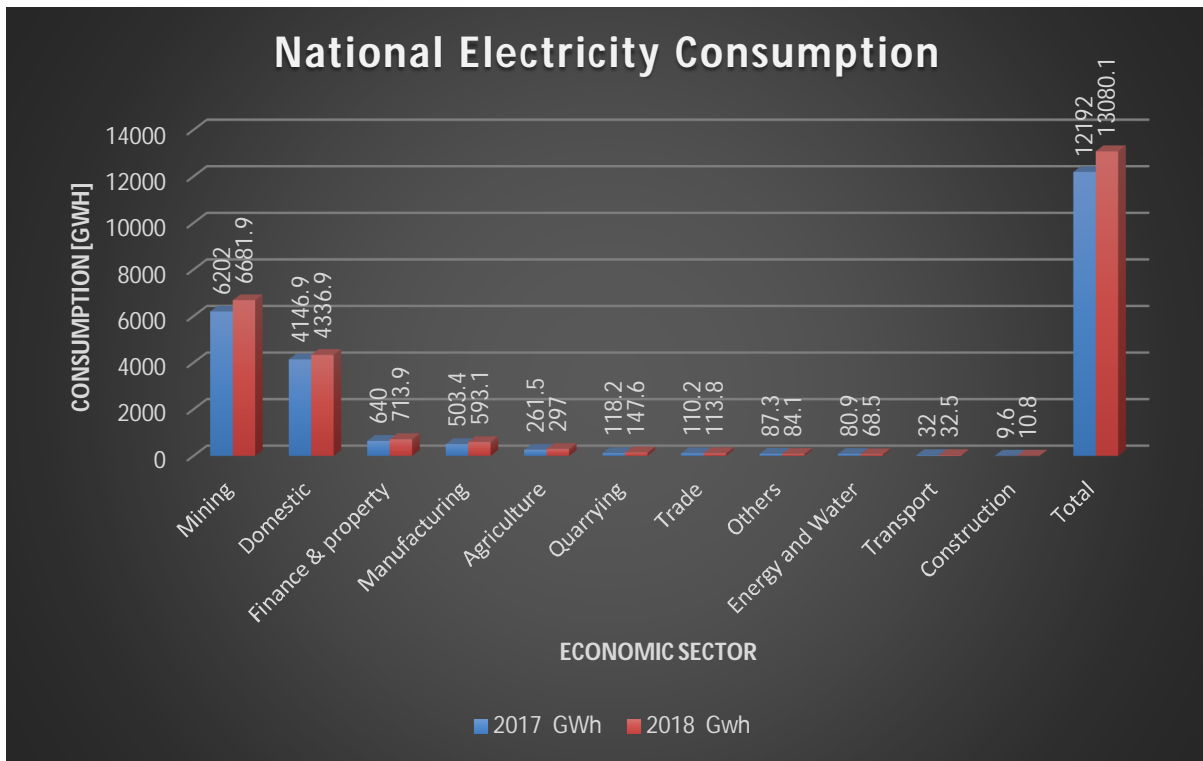


Figure 2B: National electricity consumption in GWh per economic sector (Source: ERB, 2018)

Further, based on the inputs from the Zambia power sector masterplan (2010) and the Power Africa road map (2016), complementary demand forecast modelling and analysis was done by JICA and USAID (2018) as illustrated in figure 2C below.

Type of scenario		Scenario name	Demand forecast in 2030, MW	CAGR ³ , %	Year in which scenario was developed
Domestic demand	Scenarios used by the Ministry of Energy based on the 2010 roadmap	JICA low	3,544	3.7	2010
		JICA base	4,066	4.3	
		JICA high	5,406	5.7	
Domestic demand and exports	Most recent alternative scenarios	Historical, 2010-2015 ²	3,591	3.5	2015
		Updated JICA high (2016 peak as a base) ²	4,696	5.7	2017
Domestic demand and exports		Power Africa Roadmap ¹	6,390	6.7	2015

Figure 2C: perceived demand by 2030 (Source: USAID, 2018)

1 Considers allowance for exports and internal demand

2 For true reflection of demand forecasts into capacity requirements, a reserve margin needs to be added to the two scenarios.

3 Compound Annual Growth Rate

It’s worth noting that demand increase is not expected to take up a smooth trajectory, but rather evolve in step changes dependant on prospectus demand (i.e. new mining projects), thus putting more strain on the short-term demand and supply balance.

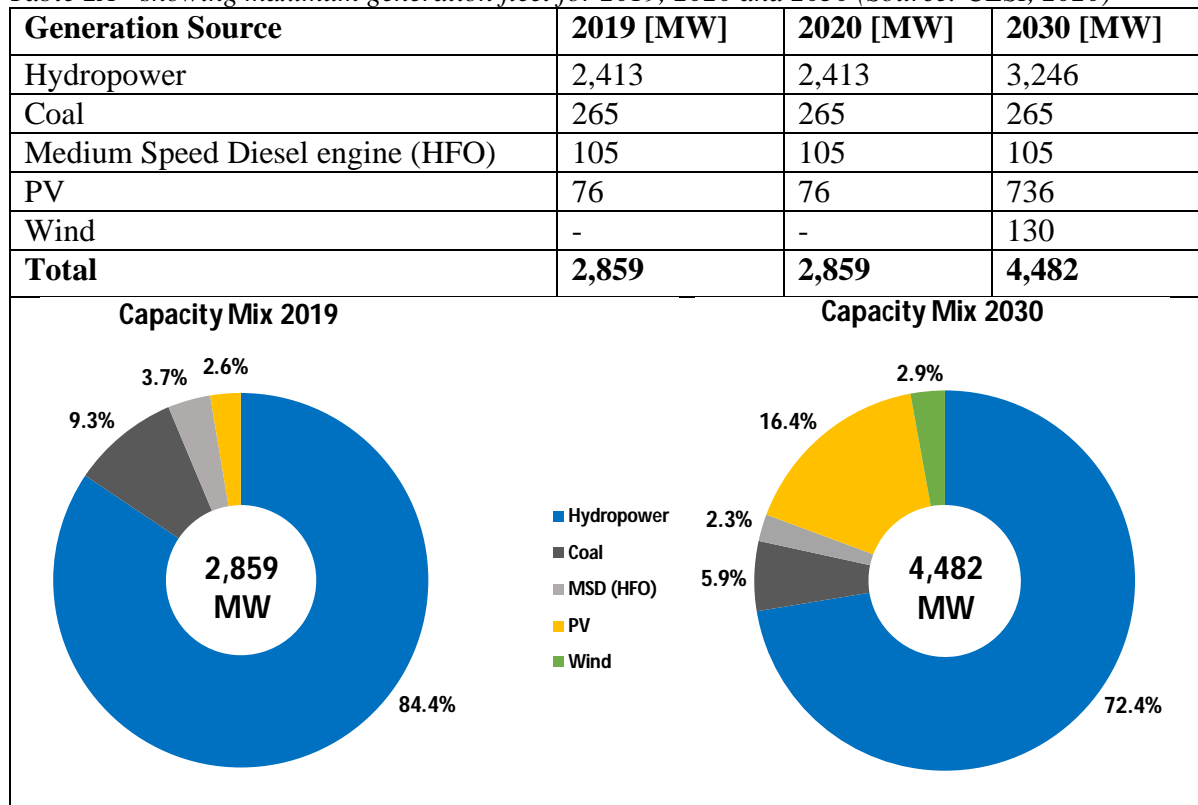
2.2.2 Power Generation System

This section gives a description of the current and forecasted generation fleet to cover the demand at the target year 2030, highlighting the existing power plants that will still be in service and the additional capacity already foreseen by the national authorities (power plants under construction, committed or with high probability to be built).

2.2.2.1 Generation Fleet

Table 2A below shows the maximum power of the generation fleet available in 2020, and the generation fleet expected to be committed in 2030. The maximum capacity available as of August 2020 was 2,859 MW, about 13% from conventional thermal power plants and 87% from renewable sources (~85% from hydropower plants and 2.6% from PV power plants). In the mid-term an increase of hydro available capacity is foreseen, the most important source in the country, together with new wind and PV power plants (CESI, 2020).

Table 2A - showing maximum generation fleet for 2019, 2020 and 2030 (Source: CESI, 2020)



Further, the generation expansion plan for 2019 to 2030, according to the committed generation is illustrated in figure 2D (ZESCO, 2020; CESI, 2020).

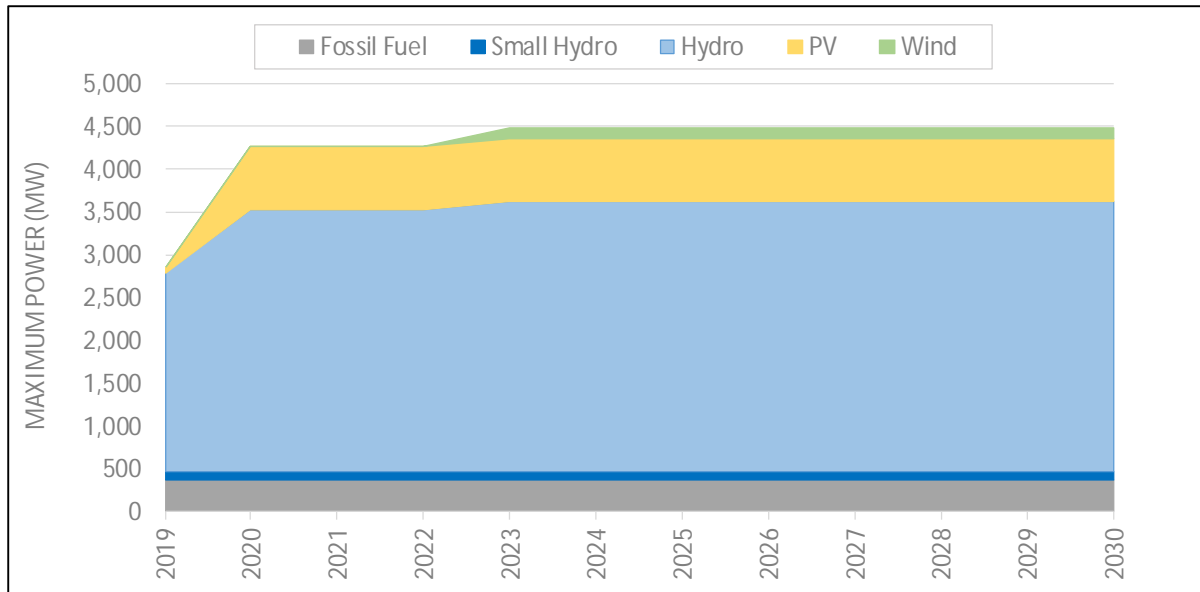


Figure 2D: showing generation expansion plan 2019 – 2030 (Source: CESI, 2020)

2.2.2.2 Hydropower Generation

Currently hydropower plants play an important role to cover the annual demand in Zambia, with an overall installed power of 2,413 MW, of which 91% are from reservoir plants and the remaining 9% from Run-of-River (RoR) power plants. Hydroelectric installed capacity accounts for 85% of the overall Zambian installed capacity. Within the year 2023 about 850 MW of run-of-river plants should come into service, while about 20 MW should be retired.

The majority of the installed capacity and generated energy is concentrated along Zambezi river and its affluent Kafue river. After feeding the 108 MW RoR plants installed at Victoria Falls, the Zambezi flows into the Kariba reservoir, that feeds the Kariba North Bank (720 MW) and the Kariba North Bank Extension (360 MW), owned by Zambia, and the Kariba South Bank (1,050 MW), owned by Zimbabwe. After feeding the Itzhi-Tezhi reservoir power plant (120 MW), Kafue river flows to the Kafue Gorge Upper reservoir (990 MW) and into the 750MW Kafue Gorge Lower RoR plant currently under development to be commissioned in the fourth quarter of 2020. The overall production of the power plants on the Kafue river accounts for 58% of the expected overall Zambian hydroelectric production, considering average hydrological conditions, with the Kafue Gorge Upper alone accounting for 38%. Victoria Falls RoR plant and the Kariba plant account for 35% of the total Zambian hydroelectric production. The relevance of mentioned plants in terms of generated energy and installed power clearly emerges also from Figure 2E, while Figure 2F shows modest capacity

factor for the under construction Kafue Gorge Lower plant and a meager (15%) for the existing Kariba North Extension plant, likely used more as peaking power plants than baseload power plants.

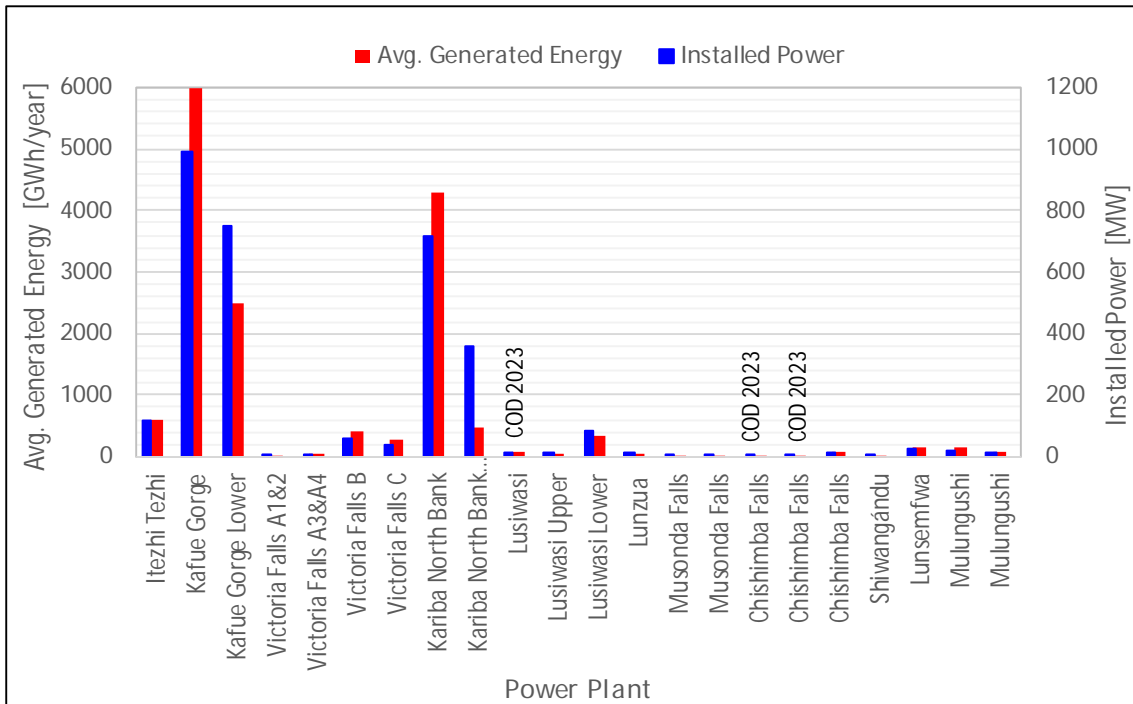


Figure 2E: Installed capacity and expected yearly average generated energy for hydropower plant, under average hydrological conditions (COD: Commercial Operating Date) [Source: CESI, 2020]

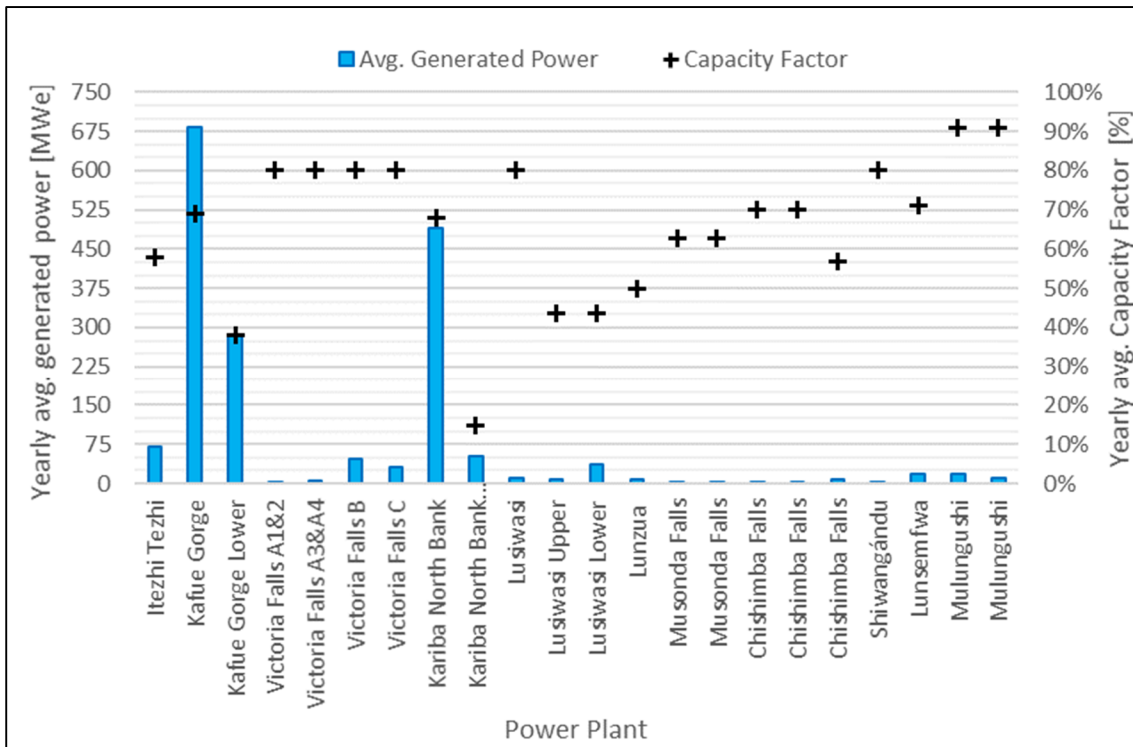


Figure 2F: Average generated power and Capacity Factor for hydropower plant under average hydrological conditions (Source: CESI, 2020)

2.2.2.3 Variable Renewable Energy Sources

Wind farms and solar power plants are generation units with power production dependent on non-controllable sources (wind and solar radiation). Their power production is affected by the variability of primary sources and by the uncertainty of their forecasting. Therefore, this type of generation can be classified as variable RES power plants. Zambia has currently 76 MW utility scale solar photovoltaic installed and no utility scale wind turbines/plants.

2.2.2.3.1 Solar Generation Potential

The World Bank under a project covering biomass, solar and wind mapping funded by the Energy Sector Management Assistance Program (ESMAP) developed a solar resource model for Zambia that was refined by integrating fields measurements performed on six selected sites shown in Figure 2G and table 2B, over a period of two years. The model results are represented in Figure 2G, and they show a generally high solar resource, especially for the south-western part of Zambia, where average value of global horizontal irradiation (GHI) exceeds 2,000 kWh/m²/year (CESI, 2020).

Table 2B: showing the location of selected sites for solar resource (Source: World Bank, 2019)

No.	Site name	Nearest town	Latitude [°]	Longitude [°]	Altitude [m a.s.l.]	Measurement station host*
1	Lusaka UNZA	Lusaka	-15.39463°	28.33722°	1263	UNZA
2	Mount Makulu	Chilanga	-15.54830°	28.24817°	1227	ZARI/ZMD
3	Mochipapa	Choma	-16.83828°	27.07046°	1282	ZARI/ZMD
4	Longe	Kaoma	-14.83900°	24.93100°	1169	ZARI
5	Misamfu	Kasama	-10.17165°	31.22558°	1380	ZARI/ZMD
6	Mutanda	Mutanda	-12.42300°	26.21500°	1316	ZARI/ZMD

*Zambia Meteorological Department (ZMD), Zambia Agriculture Research Institute (ZARI) and School of Agricultural Sciences at University of Zambia (UNZA)

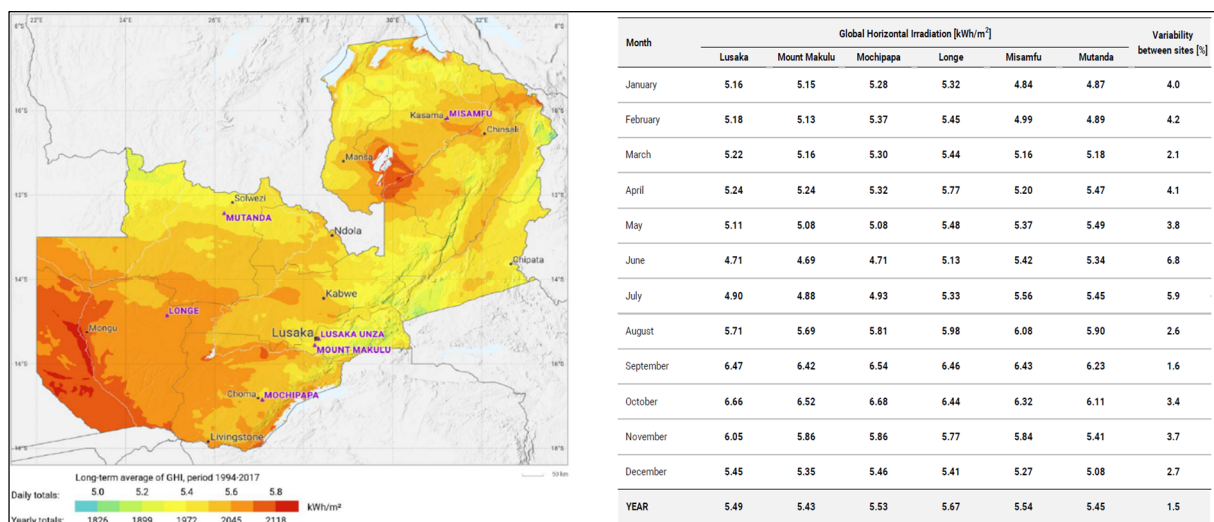


Figure 2G: showing the distribution of global horizontal irradiation in Zambia and 6 candidate sites (Source: World Bank, 2019)

2.2.2.3.2 Wind Generation Potential

Zambia is still in the early stages of exploring the resource potential for wind power: to date there are no utility scale wind turbines operating in the country and there is only one candidate project, the Access Power Wind Project in Pensulo, Serenje District, with a nominal capacity of 130 MW that should come online in 2023. The World Bank commissioned a DNV GL mesoscale wind atlas for Zambia, to be validated with wind speed measurements taken at eight meteorology masts over a period of two years. Figure 2H shows the mesoscale wind speed map at 80 m AGL, as simulated by the DNV GL Wind Mapping System. Figure 2I shows the location of the installed met masts (Francesco et al., 2020). The measured wind data from these masts has therefore, revealed great wind potential in Zambia, with wind speeds ranging between 6 to 11 m/s for utility scale wind power in some parts of the Country.

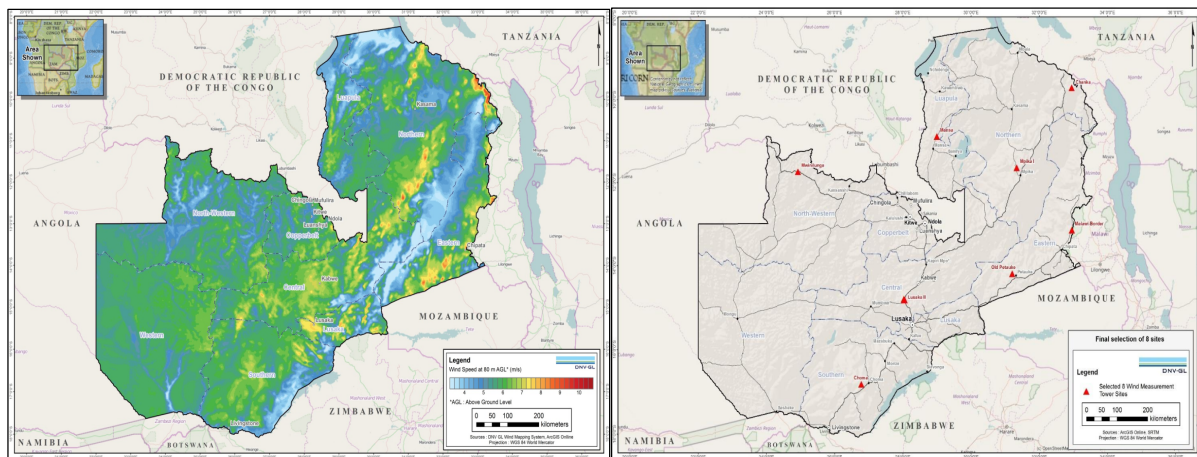


Figure 2H: showing mesoscale wind speed at 80m AGL Figure 2I - showing location of installed met masts.

2.2.3 Power Transmission Network

The main actors of the power transmission system are:

- ❖ ZESCO: a vertically integrated power utility that generates, transmits, distributes and supplies electricity in Zambia, fully owned by the Government of the Republic of Zambia. ZESCO operates the electricity grid and is responsible for much of the country's power generation.
- ❖ Copperbelt Energy Corporation Plc (CEC) is an independent transmission company that purchased power from ZESCO and supplied the mines, smelters and refineries in the Copperbelt Province through its own transmission and distribution network before March 31, 2020 when the PSA was in full effect. CEC grid is interconnected also with the Democratic Republic of Congo (DRC).

2.2.3.1 Network Composition

Figure 2J reports the planned and existing transmission system in Zambia. The transmission grid comprises transmission lines and substations at 330 kV, 220 kV, 132 kV, 88 kV and 66 kV voltage levels. The 330 kV system is the backbone of the grid; it connects the greater hydro power stations located in the southern part of the country with the biggest load centers in Lusaka and Central provinces up to the Copperbelt region. Furthermore, it allows the strong connection of the eastern regions of the country.

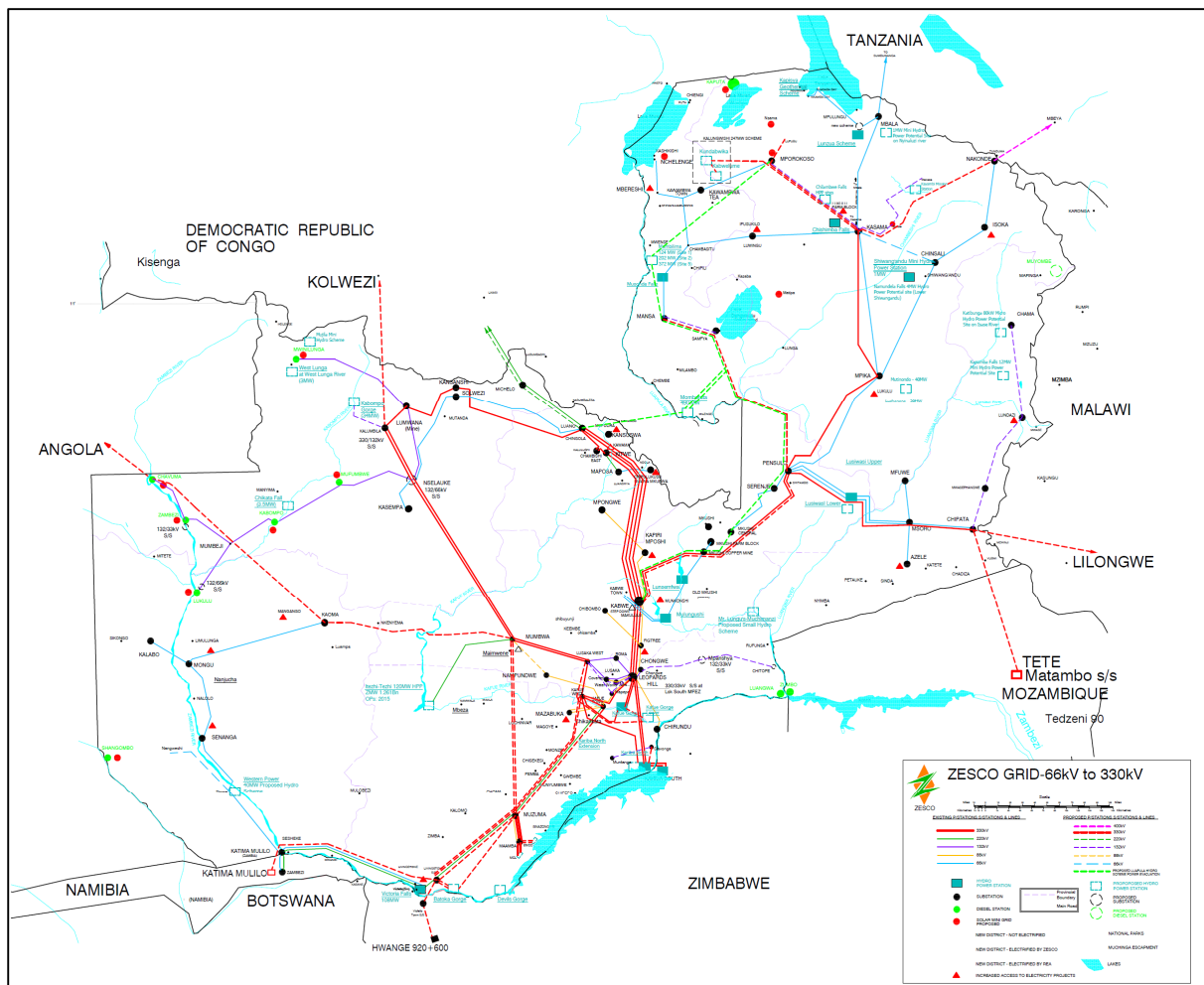


Figure 2J: showing Planned and existing transmission system in Zambia. (Source: ZESCO)

2.2.3.2 Interconnection with Neighbouring Countries

Concerning the interconnections with the neighboring countries, the current grid is interconnected with Democratic Republic of Congo, Namibia, Malawi and Zimbabwe by means of:

- ✓ 1x220 kV AC overhead line Luano (Zambia) – Karavia (DRC);
- ✓ 2x220 kV AC overhead line Michelo (Zambia) – Karavia (DRC);

- ✓ 1x220 kV AC overhead line Sesheke (Zambia) – Zambezi (Namibia). This interconnection allows for power exchange up to the central Namibia by means of the 350 kV HVDC link between Zambezi and Gerus stations in Namibia (Caprivi Link Interconnector, 350 MW);
- ✓ 2x330 kV AC overhead line Kariba North (Zambia) - Kariba South (Zimbabwe);
- ✓ 1x33 kV AC overhead line Chipata (Zambia) - Lilongwe (Malawi). A 5-years PPA, take or pay, for 20 MW export from Zambia to Malawi was signed between ZESCO and ESCOM at the end of the year 2018. This PPA is just a pilot start and additional export is expected in the coming years.

Important interconnection projects are expected in the next years in SAPP to improve market integration, security of supply and the use of sources. Zambia is in a strategic geographic position; in the center of SAPP, it borders with eight countries that are member of SAPP and is involved in important interconnection projects (ZESCO, 2020; SAPP, 2017).

The map of the existing and planned interconnections, together with the net transfer capacities (NTCs) expected by 2023, is in figure 2K.

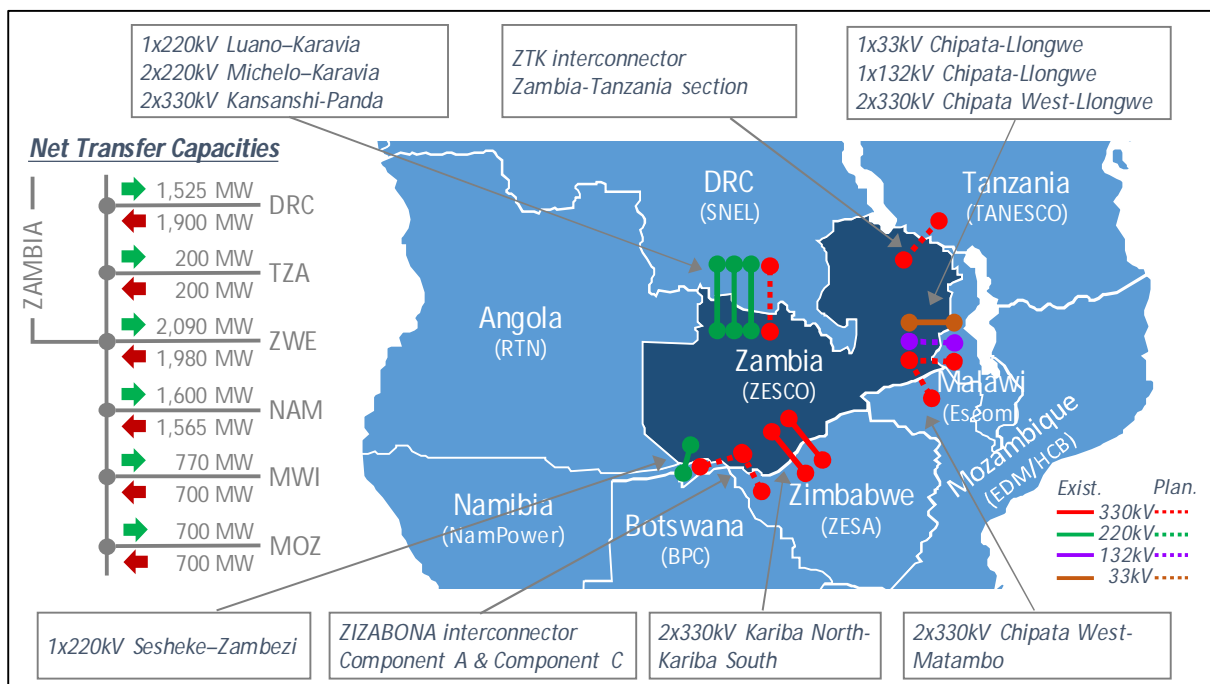


Figure 2K: showing net transfer capacities and interconnections expected in the long-term between Zambia and the interconnected countries (Source: ZESCO, 2020; SAPP, 2017; CESI, 2020).

Zambia, with ZESCO Limited, Copperbelt Energy Cooperation and Lunsemfwa Hydro Power Company, is an active member of the Southern African Power Pool (SAPP); the cooperation of the national electricity companies in Southern Africa with the scope to facilitate the development of a competitive electricity market in the Southern African Development

Community (SADC). All the interconnections between the SAPP countries are highlighted in figure 2L.

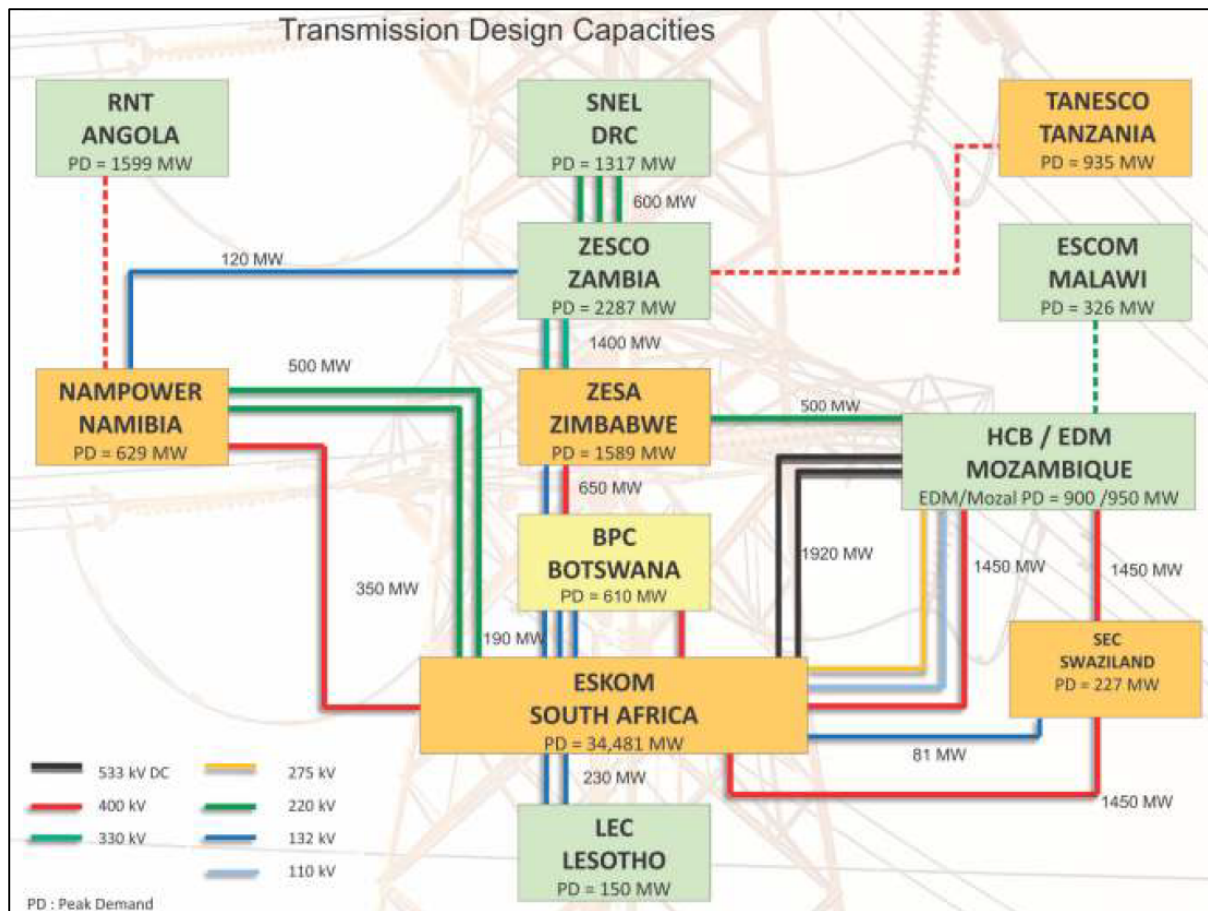


Figure 2L - showing planned and existing interconnections within the SAPP system (Source: SAPP, 2017)

2.3 Renewable Energy Policies (REFiT & GETFiT)

The aim of the Renewable Energy Feed in Tariff (REFiT) policy strategy is to support and encourage to a great extent private participation in renewable energy generation for increased access to clean energy in line with the country's energy policy (REFiT, 2016). The renewable energy sources covered under this program include solar energy, biomass, waterpower, wind power and geothermal energy. Further, only small-scale renewable energy systems are covered in the program as illustrated in table 2C.

Table 2C: showing procurement limits per technology (REFIT, 2016)

#	Procurement Limits per Technology
1	10 MW for micro generation projects
2	50 MW for technologies other than hydropower (20 MW maximum per project)
3	100 MW for hydropower (20 MW maximum per project)

The REFiT program was developed by the ministry of energy (MOE) with support from USAID through the Southern African Trade Hub (SATH). It was approved by Cabinet and launched in October 2017. With the support from the Development Bank of Germany, the REFiT program is being implemented through the Global Energy Transfer Feed-in-Tariff (GETFiT). Consequently, the MOE announced the results for the first round of 6 international bidders who were awarded the solar photovoltaic tender in April 2019 to generate 120 MW of power.

The second round of policy implementation involved the small hydro tender of up to 100 MW. For this phase, the MOE had received pre-feasibility study rights from prequalified developers for the REFiT/GETFiT 100 MW small hydropower tender.

2.4 Summary

With Zambia's increase in forecast demand between 2020 and 2030, a robust expansion plan for the power transmission network, strong network backbone through regional interconnection (SAPP), introduction of renewable policy and regulatory framework (REFiT and GETFiT), a good renewable energy potential, together with the decreasing levelized cost of electricity (LCOE) from wind and photovoltaic technologies (competitive in the mid- and long-term with the cheapest technologies) will allow attractive prospects for private investors. Technical investigations are needed to identify possible criticalities both about the operation of the power system and the network reinforcements needed to the connection of new VRES power plants in accordance with the security criteria adopted by the system operator.

The next chapter gives a detailed literature review of the research study.

CHAPTER THREE: LITERATURE REVIEW

This chapter introduces the concepts of literature that are in line with the subject of integrating floating photovoltaics and onshore wind to the Zambian national grid in the presence of dispatchable hydro generation. The topics in the subject matter were strategically selected to enable comprehensive research in the area of economical dispatch of grid integrated hybrid energy systems, that would lead to devising site suitability assessment and scope design methodologies and eventually their respective application on a specific case study. The high-level literature review is structured as follows: [Section 3.1](#) looks at the emerging technology of floating photovoltaics (including previous work), [section 3.2](#) addresses the potential of hydro-connected floating PV systems, [section 3.3](#) describes the relevant onshore wind turbine technology for grid integration, [section 3.4](#) defines a methodology and justifies the selection of the analysis software (i.e. power system, renewable energy simulation and optimization tools), [section 3.5](#) illustrates key literature on the impacts of integrating variable renewable energy sources on the grid, [section 3.6](#) reviews the dispatch of different combinations of hybrid systems (i.e. hydro, wind, PV) and finally [section 3.7](#) looks at the cost of energy with respective to global and local perspectives. A summarizing statement about the chapter is given in [section 3.8](#).

3.1 Floating Photovoltaics (FPV) Technology

Literature review on technology evolution, design aspects, previous works related to the pre-feasibility analysis and performance of floating photovoltaics is discussed in this section.

3.1.1 Overview

The advent of floating photovoltaics (FPV) has been driven mainly by efficiency loss at high operating temperatures, land scarcity for projects, decarbonization and energy security targets. With the reduction in the PV levelized cost of energy (LCOE) in the recent past coupled with technological development in PV modules, floating PV has demonstrated large-scale market potential globally ([Oliveira-Pinto, S. and Stokkermans, J., 2020](#)).

To the author's best knowledge, there has been a significant challenge in assessing the performance of FPV projects due to the scarcity of suitable simulating tools for estimating the energy yield factoring in the cooling effect that different technologies offer. However, research ([Liu et al., 2018](#)) was able to relate different U-values ($\text{W/m}^2\text{K}$) to the typology of the FPV structure (i.e. large footprint, small footprint and free standing).

3.1.1.1 Floating PV Typical Components

The typical components of a floating PV system, figure 3A, comprise of a floating structure, mooring and anchoring, solar panel and support system, inverter and cabling that transfers generated energy from FPV system to a land-based substation or transmission network (World Bank Group, ESMAP, SERIS, 2019; Nguyen, 2017).

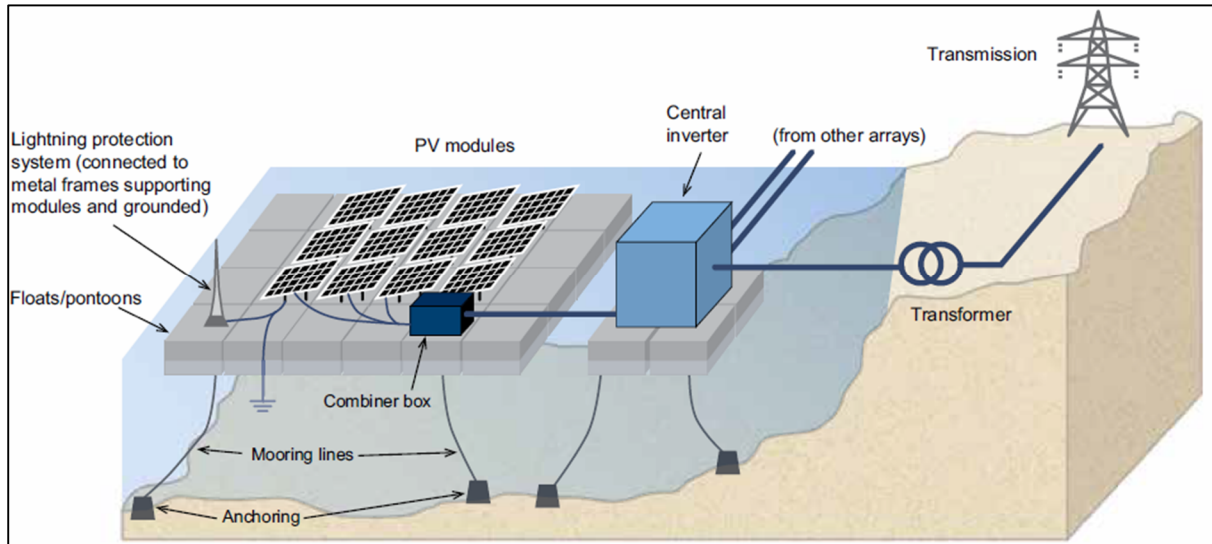


Figure 3A: showing the typical representation of a large floating PV system (Source: SERIS, 2019)

Table 3A summarizes the functions of some of the components shown in figure 3A.

Table 3A: showing description of typical components of FPV system (Oliveira-Pinto, 2020)

#	Component	Description and Function
1	Floats/pontoons	Provides support to the PV modules, which are normally fixed tilt.
2	Mooring/Anchoring	Hold the floating structure in position and can adjust to water level fluctuations while maintaining original azimuth orientation.
3	PV System	Includes PV modules that are photovoltaic generation equipment, PV arrays, inverters(string for small scale and central for large scale), combiner box, lightning protection to protect the modules from lightning strikes, transformer for voltage conditioning/regulation, transmission line to transfer energy to intended demand/load.
4	PV Modules	Uses photovoltaic effect to convert solar radiation into electricity.
5	Cabling	Transfers the PV generated power to the transmission line.

3.1.1.2 Different Floating PV Technologies

The most commonly used floating PV technologies and other emerging innovative solutions(i.e. membranes) are summarized in table 3B based on research (Sahu et al., 2016; Oliveira-Pinto, S. and Stokkermans, J., 2020).

Table 3B: showing the description of commonly applied floating PV technologies in reservoirs





#	Floating PV Technology	Summary Description
1	Membrane 	<ul style="list-style-type: none"> ▪ Aquaculture based mooring system. ▪ Buoyant ring produced from welded high-density polyethylene piping. ▪ Direct contact of membrane with water makes cooling possible. ▪ Low transport volume required for membrane (convenient for logistics). ▪ Hydro-elastic thin polymer membrane. ▪ Specialist produced membrane (Norway). ▪ Smaller membrane sections welded in controlled environment.
2	Galvanised Steel 	<ul style="list-style-type: none"> ▪ Low manufacturing cost. ▪ Convection based cooling. ▪ Module inclination adjustable. ▪ Technology employs utilization of local and cheap materials. ▪ Reservoir/pond/dam bank anchoring is typically employed.
3	High Density Polyethylene (HDPE) 	<ul style="list-style-type: none"> ▪ Cooling based on convection. ▪ Individual (sometimes modular) floaters used. ▪ Adjustment of the tilt inclination angle not possible. ▪ Anchoring involves utilizing the bank of the reservoir. ▪ Blow moulding fabrication process. ▪ Mass production possible with floating modules. ▪ Costly logistics (25 truckloads for 1MWp).
4	One or two axis tracking 	<ul style="list-style-type: none"> ▪ Convection type cooling. ▪ Module inclination adjustable. ▪ Azimuth angle adjustable. ▪ Has several moving parts. ▪ Expensive to maintain because of moving parts. ▪ Manufacturing cost low. ▪ Imposed strain on moving mechanism parts in turbulent and high wind velocities.

Table 3C gives examples of suppliers for each technology type tackled in table 3B. Other technologies with lower maturity level to the technologies in table 3C but not tackled in detail include submerged and concentrated photovoltaics.

Table 3C: showing example of supplier for each technology type in table 3B (World Bank, 2019; Correia et al., 2019; Oliveira-Pinto, S. and Stokkermans, J., 2020)

Detail	Technology Type			
	Membrane	Galvanised Steel	HDPE	1/2 axis tracking
Country of origin	Norway	USA	China	Portugal
Example of supplier	Ocean sun	4C Solar	Sungrow	Solarisfloat
Location of complete FPV projects	Singapore, Norway	Chile, Maldives, Singapore	Worldwide	Portugal
Purpose	Freshwater	Freshwater bodies	Freshwater	Freshwater
Peak Power	500kWp/island, with 72m diam.	Not available	1 PV module per float	67kWp/island
FPV capacity installed (Total)	0.1MWp	<5MWp	500MWp	<5MWp

3.1.1.3 Global Market for Floating PV

With a global footprint of more than 400,000 square kilometres (km²) of man-made reservoirs, signifying a theoretical floating PV potential of approximately a terawatt scale without putting mooring and anchoring into consideration. The conservative global estimate of floating PV on available man-made water bodies exceeds the 2017 global cumulative PV installed capacity of 400GWp (World Bank & SERIS, 2019). Table 3D illustrates the distribution of this conservative estimate (assuming 10 percent of the water surface areas is used for floating PV deployment and considering global irradiance data on key water bodies).

Table 3D: shows FPV generation potential in man-made freshwater reservoirs, by continent (Source: SERIS, 2019)

Continent	Total surface area available (km ²)	Number of water bodies assessed	FPV potential (GWp)			Possible annual energy generation (GWh/year)		
			Percentage of total surface area used			Percentage of total surface area used		
			1%	5%	10%	1%	5%	10%
Africa	101,130	724	101	506	1,011	167,165	835,824	1,671,648
Middle East and Asia	115,621	2,041	116	578	1,156	128,691	643,456	1,286,911
Europe	20,424	1,082	20	102	204	19,574	97,868	195,736
North America	126,017	2,248	126	630	1,260	140,815	704,076	1,408,153
Australia and Oceania	4,991	254	5	25	50	6,713	33,565	67,131
South America	36,271	299	36	181	363	58,151	290,753	581,507
Total	404,454	6,648	404	2,022	4,044	521,109	2,605,542	5,211,086

By the end of 2018, floating PV installations had reached 1.3GWp of installed global capacity as shown in figure 3B. As technologies mature and the LCOE continues to drop, FPV deployment is perceived to most likely accelerate (World Bank Group, ESMAP, and SERIS 2019).

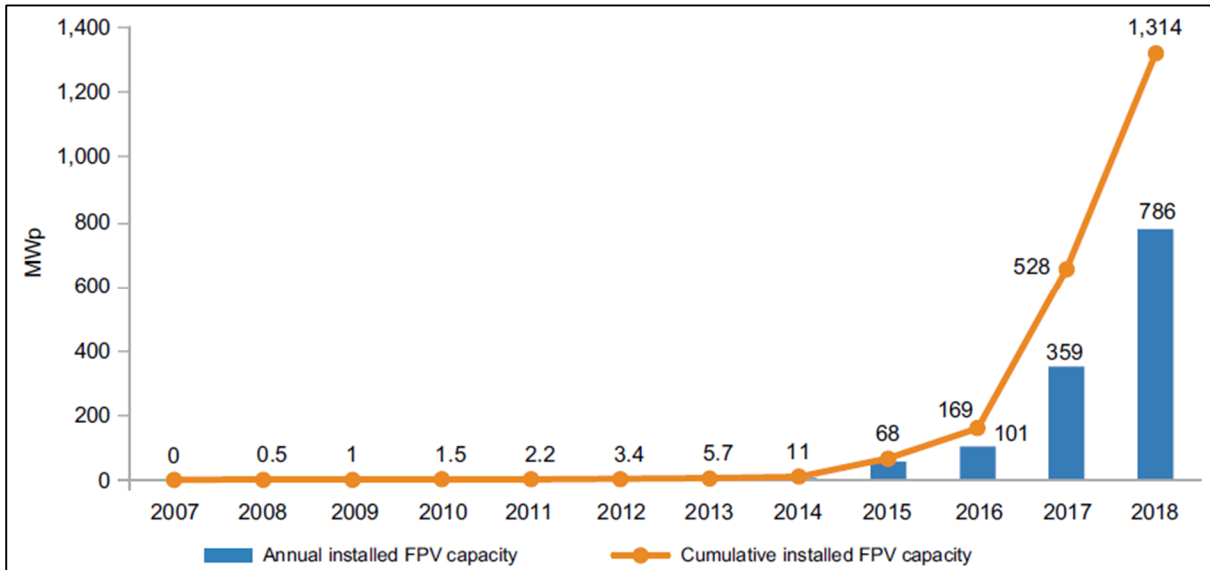


Figure 3B: showing annual additions and global installed capacity of FPV (Source: World Bank, SERIS, 2019)

China had become the market leader of FPV systems since 2017, with the deployment of a few large-scale FPV systems (i.e. 950MW installed capacity in 2018, approximately equal to 73 percent of the global total as illustrated in figure 3C). Beginning of 2019, the remainder of the installed capacity was distributed among Japan (16%), China and Taiwan (2%), South Korea (6%), United Kingdom (1%), while 2% represented the rest of the world. Though, more than 30 countries had floating PV projects under development (World Bank, ESMAP, and SERIS 2019).

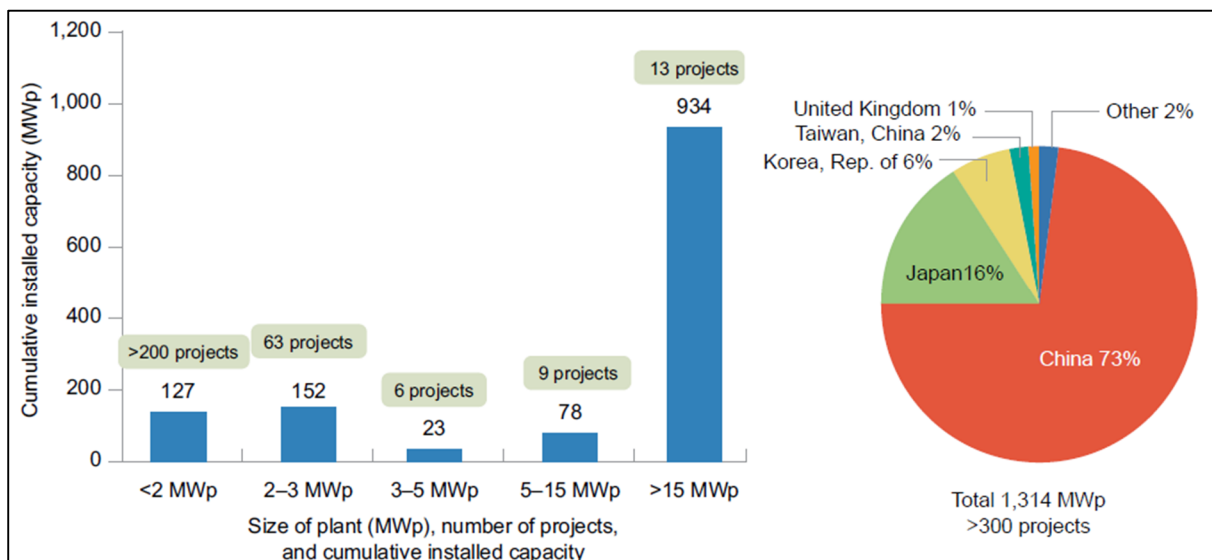


Figure 3C: showing size distribution of FPV as of December 2018 (Source: World Bank, SERIS, 2019)

3.1.1.4 Floating PV Pros & Cons

The key drivers for massive growth in floating PV are the land utilization conflicts with other activities (i.e. agriculture and tourism), receding water levels in hydro reservoirs, PV

cell/module efficiency loss at operating high temperatures. To put the land utilization factor into perspective, some projects are in hilly (high slope), unstable terrain and remote areas, thus adding to the project investment cost in the level of site preparatory earthworks. Therefore, such additional costs coupled with the ever-increasing land acquisition cost make such projects uneconomical and financially unattractive to investors.

Scholarly analyses (Sahu et al., 2016; Rosa-Clot et al., 2018) have highlighted more benefits than disbenefits of floating PV on man-made reservoirs, thus contributing to the attractiveness of the technology. The pros and cons of floating PV are summarized in table 3E below:

Table 3E: illustrating pros and cons of floating PV technology applications

Floating PV Advantages	Floating PV Disadvantages
<p>FPV on Hydro Reservoir</p> <ul style="list-style-type: none"> ✓ FPV (with high solar resource) complements hydro in dry season, thus reducing seasonal fluctuations (Liu et al., 2018). ✓ Variable PV compensated by dispatchable hydro (Liu et al., 2018). ✓ Proximity to existing infrastructure and grid connection (Rosa-Clot et al., 2017). ✓ Virtual storage capability - use PV when available during the day and ramp down on hydro for use in evening peaks (SERIS, 2019). 	<ul style="list-style-type: none"> ❖ Possibility of biofouling on floating structure (Liu et al., 2018). ❖ Reliability issues under humid and corrosive conditions (Liu et al., 2018). ❖ Poorly documented environmental impact (Sahu et al., 2016). ❖ No clear policy or regulatory framework since the technology is new emerging (SERIS, 2019). ❖ Guidelines required for insurances purposes non-existent. ❖ Cost premium likely in some saline conditions of installed modules for warranty (Sahu et al., 2016). ❖ PV modules experience turbulence from high waves and velocity and compromise support structure (Sahu et al., 2016). ❖ While land based mounting installations last for 30 to 40 years, floaters typically last for 25 years. ❖ System more vulnerable to violent weather events like storms (Sahu et al., 2016). ❖ Degraded floats prone to corrosion easily (Liu et al., 2018). ❖ Station keep design to withstand extreme weather events and water depth variations, thus adding complexity. ❖ Competes with other water-based activities and sports (i.e. tourism, fishing, boat cruise) (Sahu et al., 2016).
<p>Other</p> <ul style="list-style-type: none"> ✓ Algae growth reduction (Rosa-Clot et al., 2018). ✓ Reduction in shading effect since the location is usually in open space (Liu et al., 2018). ✓ Cost saving by eliminating need to rent land or earthworks for preparation (Cazzaniga et al., 2018). ✓ Module cleaning made easy due to readily available water (Trapani and Millar, 2013). ✓ Evaporation reduction of water body surface (Cazzaniga et al., 2018). ✓ Energy yield enhanced due to cooling effect [temperature difference between air and water] (Choi et al., 2016). ✓ Existing modules compatible (no need for customization). ✓ Reflectivity (albedo) of the water increases incident radiation thus improving energy yield (Rosa-Clot et al., 2017). ✓ Simplified installation process not requiring heavy equipment (assembly of floating structure easily done at the location) (Rosa-Clot et al., 2018). 	

3.1.2 System Design

This section elaborates on the literature design attributes of a photovoltaic system. It highlights the mathematical model formulation of a photovoltaic cell, describes different modules commonly used, interconnection of cells and modules and the basic protection options employed for different system configuration. Further, the cable management strategy on water is also tackled.

3.1.2.1 PV Technology

A photovoltaic plant instantaneously and directly transforms the input solar energy (electromagnetic radiation) into electrical energy output without any fuel utilization. The intensity of this solar electromagnetic radiation incident on a square meter surface [$1\text{kW}/\text{m}^2$] is called “solar irradiance” (ABB Group, 2016; World Bank, 2019).

3.1.2.1.1 PV Cell Equivalent Circuit and Model

According to research (Sabley, M. and Adhau, S., 2014), a solar photovoltaic cell comprises of a semiconductor p-n junction. When exposed to solar radiation, a direct current (DC) is generated (also called the photocurrent). This photocurrent varies linearly with the solar insolation. The equivalent circuit of an ideal photovoltaic cell can be treated as a current source in parallel with a diode. Figure 3D illustrates the solar cell equivalent circuit with a current source, diode, parallel (R_{sh}) and series (R_s) resistance.

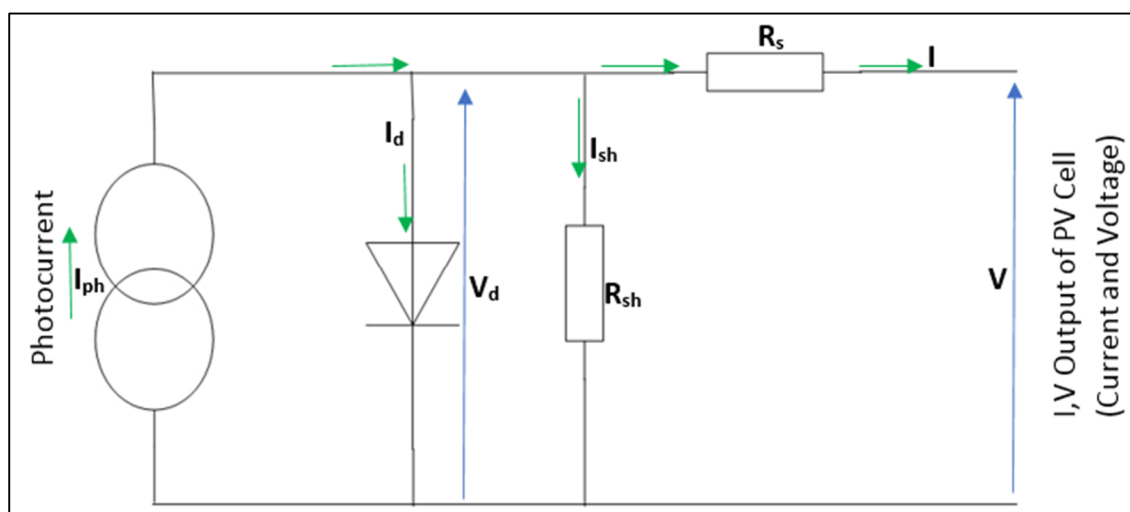


Figure 3D: showing equivalent circuit of photovoltaic cell

The p-n junction of the solar cell in figure 3D is represented by a diode. The voltage drop is represented by series resistance, while the leakage current is denoted by the parallel resistance.

The magnitude of parallel resistance is very large compared to the series resistance. The mathematical model formulation is described below;

Applying KCL:

$$I_{ph} - I_d - I_{sh} - I = 0, \text{ where } I_{sh} = V_d/R_{sh} \quad (1)$$

The PV cell output current:

$$I = I_{ph} - I_d - (V + IR_s)/R_{sh} \quad (2)$$

$$\text{But diode current, } I_d = I_o(e^{(V + IR_s)/nV_T} - 1) \quad (3)$$

Where I_o is the reverse saturation current, n is the ideality factor, “ n ” is a parameter which is dependent upon the material and it has a value equal to 2 for silicon and it has values which are different for other semiconductor materials V_T is the volt equivalent of temperature.

$$V_T = kT/q = T/11600, \text{ where } k \text{ is the Boltzmann constant, } q \text{ is the electron charge, } (4)$$

$$\text{But reverse saturation current, } I_o = KT^m(e^{-V_{GO}/nV_T}) \quad (5)$$

Where K is a parameter dependent on dimensions on PN junction, V_{GO} is the band gap energy in electron volts, m is parameter dependent on material ($m=1.5$ for Si), T is temperature in degree kelvin.

$$I = I_{ph} - I_o(e^{(V + IR_s)/nV_T} - 1) - (V + IR_s)/R_{sh} \quad (6)$$

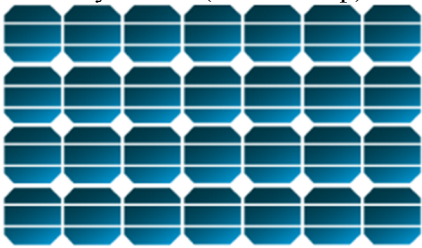
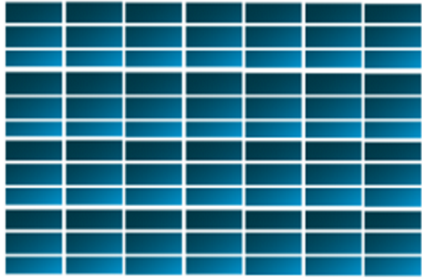
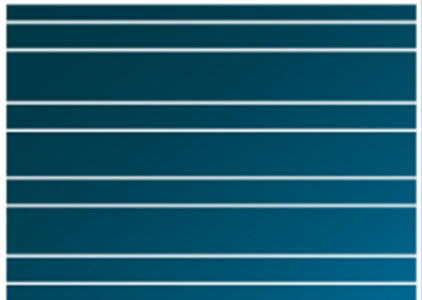
$$\rightarrow I = I_{ph} - KT^m(e^{-V_{GO}/nV_T}) (e^{(V + IR_s)/nV_T} - 1) - (V + IR_s)/R_{sh} \quad (7)$$

$$\rightarrow I = I_{ph} - KT^m(e^{-11600*V_{GO}/nT}) (e^{(V + IR_s)*11600/nT} - 1) - (V + IR_s)/R_{sh} \quad (8)$$

3.1.2.1.2 PV Modules Types

A photovoltaic module consists of many solar cells connected series and parallel to give the desired voltage and current characteristics (ABB Group, 2016). There are basically three types of PV modules commonly used and the description of these is summarized in [table 3F](#).

Table 3F: describing the three types of photovoltaic modules (ABB Group, 2016)

#	Module Type	Brief Description
1	Monocrystalline (ABB Group) 	<ul style="list-style-type: none"> ✚ Single crystal modules made from high purity silicon. ✚ Single crystal Ingot is cylindrical in form, length of 200cm, diameter of 13-20cm. ✚ These cells have high efficiency (16-16.5%, with high performance modules reaching 20 to 22%). ✚ In 2016, the price of these modules was about 0.7 €/W. They have a homogeneous dark blue colour.
2	Polycrystalline (ABB Group) 	<ul style="list-style-type: none"> ✚ Crystals aggregate taking different directions and forms. The ingot is formed by melting and casting the silicon into a mould which is parallelepiped shaped. ✚ The resulting wafers are square shape with striation thickness of 180 - 300µm. ✚ These are low in efficiency (15-16%) compared to monocrystalline. With 18-20 for high performance. ✚ In 2016, the price of these modules was about 0.67 €/W. This is also made of silicon.
3	Thin film module (ABB Group) 	<ul style="list-style-type: none"> ✚ Semiconductor deposited on supports such as aluminium, polymers, glass as gas mixtures, giving such a mixture a physical consistency. ✚ While silicon is hundreds µm in thickness, thin film is only a few µm (material saving). ✚ The used materials are mostly cadmium telluride (CdTe), amorphous silicon (a-si), indium diselenide and alloys of copper (CIGSS, CIGS, CIS), gallium arsenide (GaAs). ✚ a-si has low efficiency (7-8%) and costs 0.52-0.56€/W.

3.1.2.1.3 Series & Parallel Interconnection

For PV cells to be used in power applications, the output power must be enhanced by increasing the current and voltage (>> than cell voltage of 0.6V). Therefore, many PV cells need to be connected in parallel and series to arrive at a module. Connecting cells in series increases the overall output voltage and is achieved as shown in figure 3E for two identical cells (i.e. by connecting the negative terminal of one cell to the positive terminal of the other).

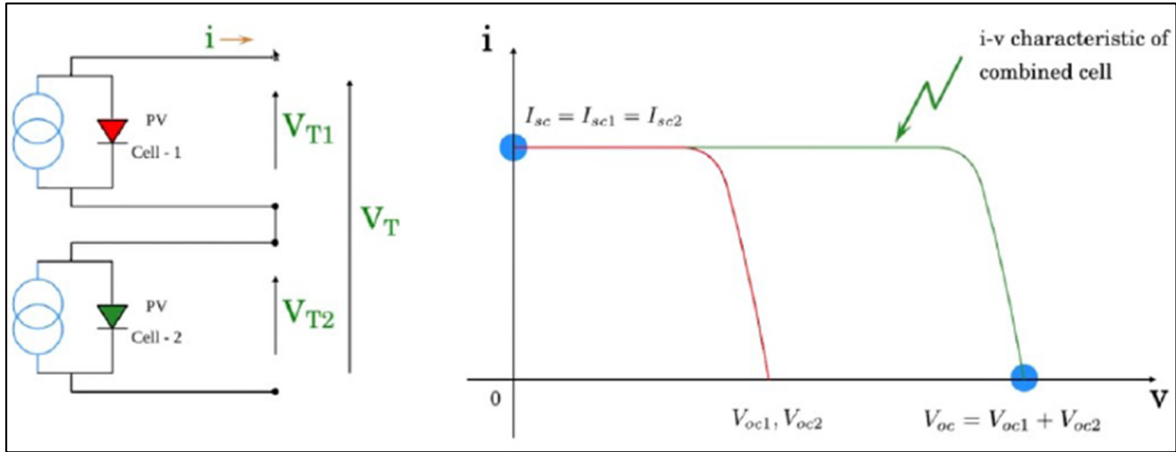


Figure 3E: showing IV characteristics of connecting two identical cells

Connecting cells in parallel increases the overall output current and is achieved by connecting the negative terminals of the cells together and the positive terminal also connected as illustrated in figure 3F for two identical cells.

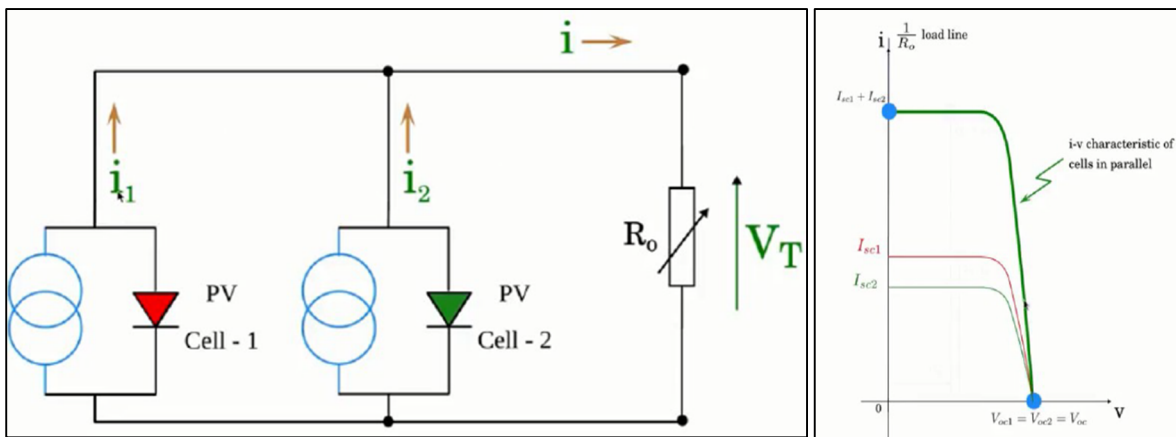


Figure 3F: showing two identical cells connected in parallel

In practice, the cells are never identical at every instance (i.e. due to shading) and this changes the output characteristics of the system. The next section addresses how to improve the efficiency and protect cells or modules in the event of shading.

3.1.2.1.4 Protecting Cells & Modules

In practice cells usually have non identical characteristics, therefore, a weaker cell operates as a sink while a stronger cell operates as a source (for cells connected in either series or parallel or combination of both). Sinking reduces the efficiency of the system due to the resistive dissipation of energy. Research (ABB Group, 2016) has shown that introduction of a bypass diode in series for parallel connected system and in parallel for series connected system protects the modules and cells from overheating.

When modules are interconnected (to get the required PV array combination), its common practice and economical to connect 1 bypass diode across each module in a series string and 1 bypass diode in series for each parallel string, thus, protecting the entire system in the event of shading.

3.1.2.2 Management of System Cables on Water

According to [SERIS \(2019\)](#), cable route planning and management for floating PV systems requires careful consideration due to the variations in the water level of the reservoir. As such, enough slack must be left to accommodate depth variations and movement of the floating island by wind or turbulent action. Else, the tension developed in the cables would cause them to rupture and snap. The design of the floating island must be such that the slack of cable does not touch the water and is fastened with stainless steel clamps or UV-resistant cable ties. Most large FPV applications will have cables routed to the onshore substation from transformers and inverters floating on the photovoltaic island. These cables can be submarine or floating type, although the cost of the former option would be much higher ([World Bank, 2019](#)).

3.1.3 Analysis of Energy Yield

This section reviews some factors from literature that affect the energy yield of floating photovoltaic systems (i.e. various environmental factors, system component design partly covered in previous section). Further, the different types of losses that appear on a loss diagram are described in detail. Research ([SERIS, 2019](#)) reveals how yield analysis of an energy system must be able to predict the expected electricity output by utilizing validated irradiance data from different datasets. This is because a good analysis is only as good as the quality of the data, and the simulation software of choice uses this data to estimate the expected energy output at a given location.

3.1.3.1 Insolation and Irradiance on Solar Modules

The weather data from the meteorological stations or satellite datasets provide solar irradiation inputs for yield analysis (i.e. direct normal radiation – DNI, diffuse horizontal irradiation and global horizontal irradiation – GHI). Some of the validated datasets for irradiance data with wide geographical coverage include Merra2, Meteonorm, 3Tier and Solargis ([World Bank, 2019](#)).

3.1.3.2 Soiling

The loss attributed to reduction in absorbed irradiation on the solar module due to accumulation of dirt like bird droppings and dust is called “soiling”. PV cells with soil exhibit shading and in extreme cases lead to hot spots which eventually contributes to module degradation (Oliveira-Pinto, S. and Stokkermans, J., 2020).

According to Lumby (2015), a loss factor less than 4 percent is evident in places which usually have snow resting on the modules for a period of time, however deserts can have values as high as 15 percent. Soiling is a function of surrounding activity on the environment (i.e. industry, agriculture), module cleaning frequency, tilt angle of the system, among others. Soiling in Morocco was analysed to reach up to 2 Wh/Wp (Dahlioui et al., 2019). There has been little research on soiling of floating PV systems and thus typical values of 2 percent are used in most simulation software [i.e. PVSYST] (PVSYST, 2020).

3.1.3.3 Shading Losses

Floating PV systems are less prone to shading losses due to buildings or trees as compared to rooftop or ground mounted systems. The low tilt angle for FPV implies a reduction in interrow shading. However, shading adjacent to banks or far horizons may occur, particularly in hilly or high slope areas. Therefore, it is imperative to conduct shading analysis in the planning and design phase of a project. Seasonal or diurnal shading may also occur due to noticeable water level variations. Poorly designed system layout may also exhibit shading from central inverters on the floating island (SERIS, 2019).

3.1.3.4 Temperature Dependent Losses

At the module standard test conditions of 25°C operating temperature, 1kW/m² irradiance, the temperature coefficient of the module determines the power deviation at non-standard conditions (i.e. actual installation or non STC). Since the large share of market potential for floating PV is in hot locations, the modules are thus exposed to high operating temperature which translate to high temperature dependent losses (and high energy generation loss factor). Accurate yield analysis must therefore, factor in the cooling effect from the wind or surrounding water body. The low air temperature on water and high wind speed improve the ventilation of the PV modules on the floating island. A simple and common model relates the cooling effect to the heat-loss coefficients (U-values), whereby the module temperature is reflected as air temperature and incident irradiance (SERIS, 2019).

3.1.3.5 Mismatch, Cabling and Inverter Losses

Research (Lappalainen, 2017; Wurster, 2014) has revealed mismatch losses to occur as a result of partial shadows caused by different current-voltage characteristics of interconnected photovoltaic cells for a series or parallel string or combination of both. Even though several studies about mismatch losses can be found in literature (Olivares, 2017; Dahlioui, 2019), there has not been much research for floating PV. As a result, (Oliveira-Pinto, S. and Stokkermans, J., 2020) assumed such losses to be 1 percent by treating the dynamic behaviour of assessed freshwater bodies as smooth.

Accurate loss estimation in cables considers the material type, cross section, length and the installation layout. According to SERIS (2019), the selection cables for PV systems must be able to hold losses in the range 0.5 to 2 percent. However, for floating PV, it is imperative to consider, distance to shore, routing schemes of cable, dimensions of island, location of inverters and transformers (i.e. on floating island or land). Such losses usually depend on system design and are similar for both FPV and land-based installations (World Bank, 2019).

Estimation of losses (and efficiency) for inverters usually references manufacturer's datasheet and assumes static maximum power point tracking (MPPT) for a defined temperature operating range. Though, the efficiency for dynamic MPPT may be lower in practice due to high fluctuations in operating conditions. Research (SERIS, 2019), revealed that both FPV platform movement and cloud movement lead to shift in the MPPT not followed by the system inverters.

3.1.3.6 Water Surface Albedo

Scholarly analyses (Lumby, 2015; Trapani, 2014) relate the percentage of ground reflected global irradiation received by photovoltaic modules to the "albedo value". This value is highly dependent on the specific site and increases in value the brighter the surface gets. For instance, fresh snow has an albedo value of 80 percent, while fresh grass has a value of 26 percent. Dvoracek et al. (1990) developed an albedo coefficient estimation model for different water surfaces. This model involved characterising a water surface (or body) through the sun's heights, colour and roughness coefficient. Recent study (Liu et al., 2018) at Singapore's test bed recorded water albedo values ranging from 5 to 7 percent, compared to 13 percent measured for a rooftop application.

3.1.3.7 Long-Term Degradation Rates

Research (SERIS, 2019) has revealed aquatic setting of floating PV to exhibit induced degradation of PV modules due to high humidity potential. As such, electrical component degradation for land-based system may differ from rates for a floating island. Further, in order to obtain a more pragmatic value of long term levelized cost of energy and energy yield, adjustment of degradation rates is thus inevitable.

3.1.3.8 Optimal Tilt Angle

Yadav and Chandel (2013), were able to show the correlation between optimal tilt angle to the local climate conditions, sun position, local geographical attributes and latitude. Research (Oliveira-Pinto, S. and Stokkermans, J., 2020) was able to show the high dependency of PV system inclination (or tilt angle) on energy production. According to Babatunde (2018), the latitude of the site normally guides with setting the theoretical optimum tilt angle. Yet, other parameters as shading, seasonal distribution of irradiation and soiling also play an important role in determining the tilt angle for a specific location. Lumby (2015) and Babatunde (2018), revealed that high inclination angles resulted in increased self-shading but less soiling. Many different approaches to arithmetically determine the optimum angle of a PV module have been tackled in literature (Yadav and Chandel, 2013).

3.1.3.9 Cooling Effect

Energy yield enhancement by the cooling effect of the module is considered one key aspect of floating PV (Rosa-Clot et al, 2018). Research by Liu et al., (2018) comparing FPV and reference land-based systems revealed that installation and configuration of the PV module coupled with the technology employed for module floating island dictated the extent of the cooling effect. Lower temperatures were recorded for all floating PV systems compared to the reference land-based system. Further, the comprehensive data about system performance operating conditions enabled Liu et al., (2018) the characterization of floating structures (table 3G) based on cooling effect and module temperature results (large footprint: high density polyethylene floaters partially blocking water surface , free standing: modules with reduced footprint in water and thus good cooling by convection, and small footprint: installation of modules done close to water surface and providing small coverage on water).

Table 3G: showing characterization of floating structures using the heat loss factor (Liu et al., 2018)

#	Floating PV Typology	Average heat loss factor (W/m ² K)
1	Large footprint	~31
2	Small footprint	~35
3	Free standing	~46

Research (Cornaro et al., 2018) was able to account for the cooling effect by adjusting the U-value (or heat loss factor W/m²K) in PVSyst, thus defining the transfer of heat between the surroundings and the PV module. The concept was defined in detail by (Skoplaki and Palyvos, 2009) using the energy balance as:

$$U \times (T_{\text{module}} - T_{\text{ambient}}) = G_{\text{irradiation}} \times \alpha \cdot \tau \times (1 - \eta(T) / \alpha \cdot \tau) \quad (9)$$

Where U is the heat loss factor in W/m²K, T_{ambient} and T_{module} are the ambient and module temperature respectively in degree kelvin, α is the percentage of solar spectrum absorbed, τ represents the glazing transmittance, G_{irradiation} is the PV module irradiation in W/m², $\eta(T)$ is the temperature dependent module efficiency. Equation 9 therefore, describes the PV module thermal characteristic denoted by an energy balance equation between the solar cell's heat losses (due to irradiation incident on surface) and the ambient temperature of the specific location (Oliveira-Pinto, S. and Stokkermans, J., 2020).

3.1.3.10 Performance Ratio

Research (Moraitis, 2018 and Reich et al., 2012) defines performance ratio (PR) as the effectiveness of a PV plant to produce energy. This ratio is widely used in literature to compare different photovoltaic plants over a period of time (Lumby, 2015; Reich et al., 2012). Reich et al. (2012) quantified the PR as the reciprocal of ratio between the reference yield (Y_r) and the final yield (Y_f).

$$1/\text{PR} = Y_r/Y_f \quad (10)$$

By dividing the measured power output of the system, P_{output}(kWh) and the time interval τ_k , to the rated power of the system P_{rated}(kWp) we obtain the final yield. At standard test conditions, the reference irradiation G_{reference} is 1kW/m², thus, the ratio between the total plane irradiation G_{POA} to the STC reference is the reference yield (Reich et al., 2012) denoted as:

$$Y_f = \sum_k (P_{\text{output}} \times \tau_k) / P_{\text{rated}} \quad (11)$$

$$Y_r = \sum_k (G_{\text{POA}} \times \tau_k) / G_{\text{reference}} \quad (12)$$

3.2 Hydro-Connected FPV Potential

Research (Farfan, J. and Breyer, C., 2018) mapped the electricity generation potential in terawatt-hour (bottom) and the installation capacity potential in gigawatt (top) by floating photovoltaics for water bodies (reservoirs) with capabilities of hydropower (irrespective of whether it is the secondary or primary purpose of the reservoir).

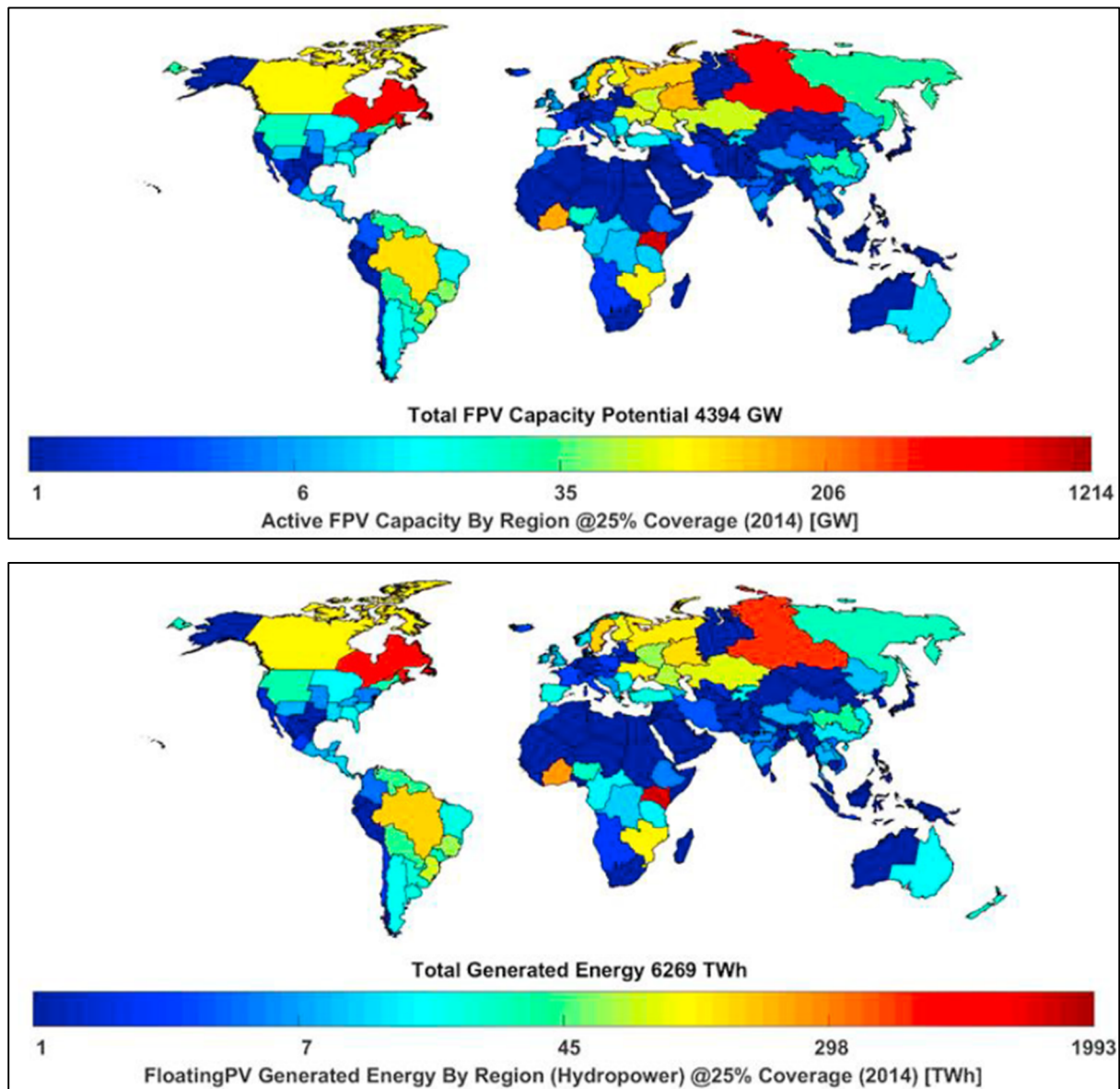


Figure 3F: showing FPV capacity potential in GW (top) and electricity generation potential TWh (bottom) covering twenty five percent of the hydropower reservoir water surface (Source: Farfan, J. and Breyer, C., 2018).

Table 3H shows a sample space of high-resolution review by comparing the percentage of the water surface area required to match the hydropower capacity for some plants in the following countries; Zambia, India, Turkey, Egypt, Brazil, Venezuela, Ghana and Malaysia.

Table 3H: showing estimated power generation and reservoir size to match hydropower capacity (Authors compilation and SERIS, 2019)

Dam/reservoir	Country	Reservoir size (km ²)	Hydropower (GW)	Percentage of reservoir area required for FPV to match dam's hydropower capacity (%)
Bakun Dam	Malaysia	690	2.4	3* /6
Lake Volta	Ghana	8,500	1.0	<1* /<1(0.2)
Guri Dam	Venezuela	4,250	10.2	2* /4
Sobradinho Lake	Brazil	4,220	1.0	<1* /<1(0.4)
Aswan Dam	Egypt	5,000	2.0	<1* /<1(0.68)
Attaturk Lake and Dam	Turkey	820	2.4	3* /5
Narmada Dam	India	375	1.5	4* /7
Kafue Gorge Upper Dam	Zambia	70	0.99	14* /24
Kariba North Bank Dam	Zambia	4354	1.08	<1* /<1(0.42)
Itezhi-tezhi Dam	Zambia	113	0.12	1* /2

Note: *means percentage without mooring consideration (1MW = 0.01km²), with mooring 1MW ~ 0.017km²

3.3 Onshore Wind Turbine Technology

There exists a lot of literature relating various aspects of wind turbine technology, however, much of it is outdated owing to the continuous evolution in technology. This section reviews the mainstream technology for onshore wind based on network integration. Section 3.3.1 briefly looks at the overview from literature with main focus on the doubly fed induction generator (DFIG) based wind turbines, while the basic wind turbine model formulation is tackled in Section 3.3.2.

3.3.1 Overview

Studies (Serrano-González and Lacal-Aránegui, 2016) have shown the evolution of wind energy technology towards bigger machines (power generators, longer blades and taller towers). To put this in perspective, the wind turbine size (in term of rated power, hub height and rotor diameter) had increased to 2.1 MW rated power, 87.7 m hub height and 92.7 m rotor diameter on average at the beginning of 2015, from 300 kW power, 30 m hub height and 30 m rotor diameter in the late 1980's. This evolution in technology has been multifaceted by innovative solution development to minimize cost while dealing with reliability issues, grid code adherence, and the scaling up process to attain carbon neutrality. According to Jin et al. (2014) and the global wind energy council, the last two decades had witnessed wind renewable resource become the most successful and largest deployment achieving global cumulative capacity of 370 gigawatt at the beginning of 2015.

Research (Hughes et al., 2008) reviewed many types of wind turbines (i.e. hybrid configuration, direct drive or gearless configuration, geared turbine with doubly fed induction generator), but classified the DFIG to have had mainstream and advanced technological development owing to its low mechanical stress, low power consumption and high energy efficiency. With the continuous rise in the penetration of variable renewable energy sources (i.e. wind) it has become pertinent to evaluate the impact of the DFIG on system reliability and stability (Liu et al., 2013; Jiang et al., 2011; Feng et al., 2015; Vittal et al., 2012).

Further research by Swarna et al. (2015), revealed the ability of DFIG's to deliver reactive power support at the wind machine terminals during scenarios when the machine was curtailed with active power generation.

3.3.2 Wind Turbine Model Formulation

According to Engin (2013) and Orlando et al. (2008), the operational curves characterizing the wind turbines are given as output power versus the wind speed at respective hub height. The configuration of a wind farm is such that the wind turbines could be connected in parallel (parallel strings of different or same wind turbine type) to match the current requirements of the system but never in series. The annual energy density for wind is defined as:

$$P_{\text{WTED}} = 0.5 * C_P * \rho_{\text{air}} * V^3 \quad (13)$$

Where P_{WTED} is the wind turbine power density, C_P is the capacity coefficient, ρ_{air} is the density of air, V is the wind speed (Engin, 2013). According to Salameh (2011), if we have an assumed annual energy demand of $D_{\text{ave,year}}$, the wind turbine diameter D_{WT} can be determined using equation 14 making it easy to define the type of turbine by inputting the characteristics parameters (i.e. diameter).

$$D_{\text{WT}} = (D_{\text{ave,year}} / (\text{hours/year} * P_{\text{WTED}} * \pi * 0.25))^{1/2} \quad (14)$$

Therefore, power output of the turbine array at any given time is given as:

$$P_{\text{WT}}(t) = 0.5 * C_P * \rho_{\text{air}} * V^3(t) \quad (15)$$

3.3.3 Wind Energy in Zambian Context

According to the World Bank's wind resource mapping study, Zambia has great resource potential with validated datasets at eight meteorological wind masts (i.e. located in Choma,

Mwinilunga, Lusaka, Mpika, Chanka, Petauke, Mansa & Malawi) at 80 m above ground level. Further, energy analysis conducted by DNV GL at these sites using a generic 4 MW turbine, 140 m rotor diameter and hub height of 130 m yielded promising results ([World Bank, 2018](#)).

3.4 Selection of Software Analysis Tools

This section justifies the selection of software tools used in the analysis that follows in the coming chapters by reviewing literature on power system tools, renewable energy simulation tools and optimization tools. [Section 3.4.1](#) reviews the various power and energy system modelling tools, while selection of renewable energy simulation and optimization tools is tackled in [section 3.4.2](#).

3.4.1 Power System Modelling

The interactions between the demand from consumers (i.e. load), generation (both conventional and variable renewable sources) and the transmission/conversion equipment (i.e. used to transfer energy/power from the source to the end user) is modelled by Power/Energy System tools. The significance of such tools globally has risen in the recent past due to the desire to attain carbon neutrality by integrating variable renewable energy sources (VRES) onto the grid. Additionally, all new power projects or perceived increased demand dictates some sort of modelling to ensure grid code adherence to network parameters and power quality.

On the energy production side, VRES introduces stochastic tendencies in the power flow patterns on the network. On the load side, the desire to decarbonize the heating and transport has put a strain on the grid by a forecasted increased demand. This is because fossil fuel boilers and combustion engines are to be replaced with heat pumps and electric motors respectively. Additionally, the inclusion of energy storage technologies complicates the electrical grid by introducing more network users which are “both generators and consumers of energy” ([Brown et al., 2017](#)).

Moreover, the computational burden of power system dynamic analysis is as cumbersome for large networks as it is for small networks. Consequently, for research students to bridge the gap between theoretical and practical issues pertaining to the powers system, software modelling tools for educational purpose are fundamental. These tools usually have user-friendly interfaces and some even have graphic visualizations in interpreting simulation results ([Vanfretti, L. and Milano, F.,2007](#)).

Most tools used for power system analysis and modelling were developed before there was much talk of decarbonizing the load (i.e. electrification of heating and transport) or grid integration of VRES. As such, they typically focused on single-time period network flow analysis (Brown et al., 2017). Some of these tools include commercial tools like PSS/E, PowerWorld, NEPLAN, PSS/SINCAL, Digsilent-Powerfactory, ETAP, SIMARIS, SIMSCAPE, MILSOFT and PSAF, and free and open source software (FOSS) tools like PSAT, PYPSA, PYPOWER, pandapower and MATPOWER (Brown et al., 2017; Zahurul Islam, 2019; Richard Lincoln, 2017; Zuo et al., 2015; Vanfretti, L. and Milano, F., 2007; Zimmerman, R.D., et al., 2010; Gonzalez-Longatt et al., 2014; Bica et al., 2008; Makoka et al., 2013). However, some FOSS tools like PSAT and MATPOWER require a licensed MATLAB platform for full functionality. The development and deployment of FOSS has made it possible for anyone around the world to obtain research and educational tools, thereby creating a collaborate and interactive community of learners/users. Most FOSS projects are successful because of the freedom that users and learners have to enhance and optimize the source code (Stallman, 2002).

Furthermore, software tools like DigSilent and PSAT have had software upgrades over time to include modelling of VRES (i.e. detailed turbo-generators, wind and solar photovoltaic modelling). Further, these tools also have optimization capability for minimizing network operating costs using optimal power flow cost function features (Princy et al., 2018; DIGSILENT GmbH, 2020).

Other energy system tools incorporate a subset of many attributes for operation, optimization and modelling. For instance, infrastructure capacity optimization over stochastic weather conditions and load characteristics. Further, optimization of demand side management, storage, conventional generator unit commitment (i.e. hydro) places emphasis on multiple time periods in order to give a true representative picture of reality. Some of these include urbs, PRIMES, calliope, PLEXOS, PowerGAMA, MOST, OSeMOSYS, TIMES, oemof and minipower. However, the drawback with some of these tools is the oversimplification of electrical network layouts for detailed grid analysis (Pfenninger, S., 2017; Greenhall et al., 2012; Murillo-Sánchez, 2013; Howells et al., 2011; Hilpert et al., 2017; Energy Exemplar, 2017; Svendsen and Spro, 2016; Brown et al., 2017; Dorfner et al., 2016).

Having looked at an overview of the power system tools; the remaining sections are outlined as follows: Section 3.4.1.1 compares the different tools in terms of technical and economic

features (i.e. grid analysis and economic analysis). Section 3.4.1.2 highlights the research selection criteria and proposes some tools viable to help attain the first objective of the scope design methodology (i.e. assessing of the local grid and optimization within grid constraints).

3.4.1.1 Comparison of Power System Analysis Tools

The assessment of some of the FOSS and commercial modelling tools was done by comparing some embedded economic and grid analysis features. Under grid assessment the following attributes were tackled: Simple power flow (SPF), continuation power flow (CPF), Optimal power flow (OPF) and dynamic analysis (DA). The Economic assessment features included: investment optimization (IO), linear OPF (LOPF), non-linear OPF (NLOPF), transport model (TM), multi-period optimization (MPO) and security constrained linear OPF (SCLOPF). Table 3I defines some of these terms in detail while table 3J shows the simplified attribute comparison by stating whether it exists or not (i.e. YES or NO assessment).

Table 3I: defines some of the grid and economic analysis features

Term	Citation	Definition
DA	<i>Sultan et al., 1998</i>	Dynamic analysis involves the evaluation of the performance of the power system in real-time in relation to the evolving and changing generation, loading, and external environment (i.e. faults and disturbances). The modelling and analysis tools tackle stability, reliability and efficiency as performance benchmarks.
SPF	<i>Fnaiech, 2015</i>	Simple power flow involves the determination and calculation of all bus voltages of the electrical power network. Each bus is associated with four quantities: voltage magnitude, voltage angle, real power and reactive power. Unknown and known quantities are also specified at each bus for the SPF problem formulation.
CPF	<i>Fnaiech, 2015</i>	Maximum loading determination is a cardinal issue in voltage stability analysis problem. When operating near the critical (stability) limit convergence issues arise with conventional SPF programs. CPF overcomes this problem and consequently, all probable loading settings of the network remain well conditioned. CPF achieves this by using a series of predictor and corrector steps in its computation of the voltage profile at the point of collapse.
OPF	<i>Khan and Singh, 2017</i>	OPF is critical for system planning and operations. It is used for state optimization of a network under constrained conditions (i.e. reactive power limits, transmission line thermal limits, minimizing losses, optimization of reactive power).
TM	<i>Sola et al., 2018</i>	TM constitute energy prediction capabilities of transport-based models (macro/micro simulation). These use consumption energy data that has been aggregated to make predictions about consumption of transportation energy with low temporal and spatial resolution.

IO	<i>Cornuejols, 2006</i>	IO considers resource investment problem guided by upper and lower bounds. According to the adopted mathematical algorithm, the optimization tools search for a distinctive modelling space to find the maxima of minima of the IO objective function.
MPO	<i>Fazlollahi, 2015</i>	MPO involves energy system optimization by factoring in multi-interval analysis of the parameters of the objective function.
LOPF	<i>Hörsch, 2018</i>	An LOPF algorithm optimizes the dispatch of generators in network branches which have a constraint on loading by linearizing the AC load flow equations.
NLOPF	<i>Nejdawi, 2000</i>	NLOPF describes an interior point dynamic OPF algorithm for energy intensive consumers that are able to reschedule energy demand after meeting the daily production target so as to reduce the electricity bill.
SCLOPF	<i>Brown et al., 2017</i>	SCLOPF is developed from LOPF by inclusion of other branch constraints that ensure a no-overload condition even after certain selected branches have an outage.

Table 3J: shows the comparison of different grid and economic analysis features

SOFTWARE TOOL NAME	VERSION	FOSS	ECONOMIC ASSESSMENT										GRID ASSESSMENT			CITATION	
			Linear OPF	Nonlinear OPF	SCLOPF	Transport Model	Investment Optimization	Multi-period Optimization	Unit Commitment	Simple PF	Continuation PF	Dynamic Analysis					
1 calliope	0.5.2	Yes	No	No	Yes	Yes	Yes	Yes	Yes	Yes	No	No	No	No	No	No	Pfenninger, S., 2017
2 Digsilent	2019	No	Yes	Yes	No	No	No	No	No	No	Yes	Yes	Yes	Yes	Yes	Yes	PowerFactory, 2020
3 MATPOWER	6.0.	Yes	Yes	Yes	No	Yes	Yes	No	No	No	Yes	Yes	Yes	Yes	Yes	No	Zimmerman et al., 2010
4 minipower	4.3.10	Yes	Yes	No	Yes	Yes	Yes	No	No	No	Yes	No	No	No	No	No	Greenhall et al., 2012
5 MOST	6.0.	Yes	Yes	Yes	Yes	Yes	Yes	No	No	No	Yes	Yes	Yes	Yes	Yes	No	Murillo-Sánchez, 2013
6 NEPLAN	5.5.8	No	Yes	Yes	Yes	Yes	Yes	No	No	No	Yes	Yes	Yes	Yes	Yes	Yes	Neplan AG, 2020
7 oemof	0.1.4	Yes	No	No	Yes	Yes	Yes	Yes	Yes	Yes	Yes	No	No	No	No	No	Hilpert et al., 2017
8 OseMOSYS	2017	Yes	No	No	No	Yes	Yes	Yes	Yes	Yes	No	No	No	No	No	No	Howells et al., 2017
9 pandapower	1.4.0	Yes	Yes	Yes	No	Yes	Yes	No	No	No	Yes	Yes	Yes	Yes	Yes	No	Thurner et al., 2018
10 PLEXOS	7.4	No	Yes	Yes	Yes	Yes	Yes	Yes	Yes	Yes	Yes	Yes	Yes	No	No	No	Energy Exemplar, 2020
11 PowerGAMA	1.1	Yes	Yes	No	Yes	No	Yes	No	No	No	Yes	Yes	Yes	No	No	No	Svendsen, 2016
12 PowerWorld	21	No	Yes	Yes	Yes	Yes	Yes	No	No	No	Yes	Yes	Yes	Yes	Yes	Yes	PowerWorld, 2020
13 PRIMES	2017	No	Yes	No	No	Yes	Yes	Yes	Yes	Yes	Yes	Yes	Yes	No	No	No	e3mlab, 2020
14 PSAT	2.1.11	Yes	Yes	Yes	No	No	No	No	No	No	Yes	Yes	Yes	Yes	Yes	Yes	Milano F., 2007
15 PSS/E	33.12	No	Yes	Yes	No	Yes	No	No	No	No	No	Yes	Yes	No	No	Yes	Siemens AG, 2020
16 PSS/SINCAL	14.5	No	Yes	No	No	No	No	No	No	No	Yes	Yes	Yes	No	No	Yes	Siemens AG, 2020
17 PYPOWER	5.1.2	Yes	Yes	Yes	Yes	No	Yes	No	No	No	Yes	Yes	Yes	No	No	No	Lincoln R., 2017
18 PyPSA	0.11.0	Yes	Yes	No	Yes	Yes	Yes	Yes	Yes	Yes	Yes	Yes	Yes	No	No	No	Brown et al., 2017
19 TIMES	2016	No	Yes	No	Yes	No	Yes	Yes	Yes	Yes	Yes	Yes	Yes	No	No	No	Richard, 2016
20 urbs	0.7	Yes	Yes	No	Yes	No	Yes	Yes	Yes	Yes	Yes	Yes	Yes	No	No	No	Dorfner et al., 2016

3.4.1.2 Selection Criteria of Power System Tools

Figure 3G below shows the flow chart selection criteria for software tools in table 3J. The power or energy system analysis tool must meet a minimum of the key features indicated below to be able to perform detailed economic and grid analysis as required in the scope design methodology.

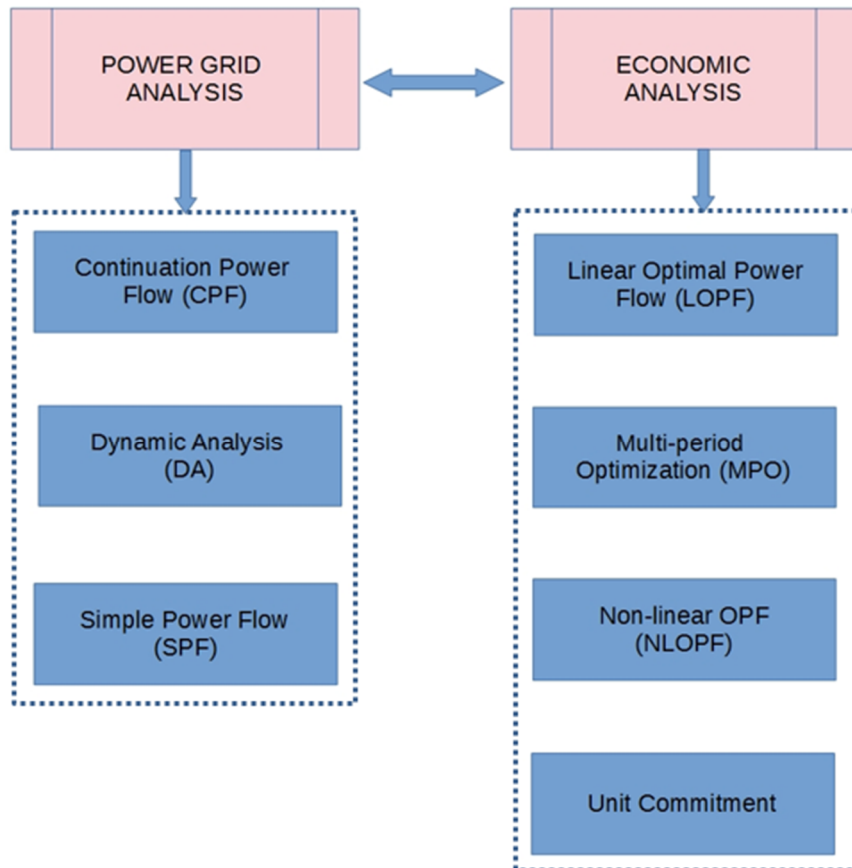


Figure 3G: showing the power/energy system software selection criteria

3.4.2 Renewable Energy Simulation and Optimization Tools

The specific aims of this section are to: (i) Document and categorize the capabilities of different renewable energy modelling and analysis tools for site potential assessment (using online tools), renewable energy configuration and optimization (using hybrid and optimization tools) and specialized photovoltaic analysis tool (to ascertain best tool to emulate floating photovoltaics), and (ii) develop a simple flowchart selection criteria for online tools, multi-source configuration/optimization tools and photovoltaic analysis tools suitable and in line with the project design scope.

This will be achieved through:

- Tabulation and categorization of different renewable energy modelling and analysis software.
- Development of a simple tool selection process using tables and a flowchart.
- Demonstration of the selection through the project case study (and initial assessment of potential project sites using online tools).

This write-up tackles different software tools used for modelling and analysing solar renewable energy systems (i.e. PV, wind and dispatchable hydro). The remaining section are structured as follows: [Section 3.4.2.1](#) reviews the online software tools for wind and photovoltaics. [Section 3.4.2.2](#) reviews 13 different types of renewable energy modelling tools. [Section 3.4.2.3](#) describes the devised selection methodology while [section 3.4.2.4](#) illustrates selection criteria for the tools used in the research of the hydro-floating photovoltaics and wind.

3.4.2.1 Online Software Tools

Renewable Energy Online Software Tools (REOST) were used in the initial assessment of each site's renewable energy source (RES) potential (i.e. power and annual energy output from validated datasets). The RES output formed the input to the screening and filtering models of all candidate sites. Two online software platforms were selected and used in a complimentary fashion, these are Renewables Ninja and Global Atlas for Solar and Wind. The choice was based on dataset validation and wide coverage ([Pfenninger, S. and Staffell, I., 2016](#); [GSA, 2020](#); [GWA, 2020](#)).

3.4.2.2 Renewable Energy Modelling Tools

Given the significance of renewable energy integration in conventional and standalone systems, it's imperative to choose the right modelling and analysis tool in the planning phase of such an undertaking. As such different features of several modelling tools must be compared and analysed to fit the problem statement before a decision could be made on the specific tool(s) to use. Some of these features include energy supply variations, embedded, storage technologies, market models, emissions support, types of loads, climate context (meteo data source), user interactions and expectations. For instance, a generic model for renewable energy planning at community level is described in ([Huang et al., 2015](#); [Lyden et al, 2018](#)). There are many validated and world-renowned energy modelling tools developed over the years to meet different system configurations and demand scenarios. Eleven (11) of such tools are discussed in detail below:

DIETER: Dispatch and Investment Evaluation Tool with Endogenous Renewables. DIETER was developed to study the investment cost optimization of project consisting of demand side management, energy storage, power generation and dispatch requirements. The model is implemented using the GAMS (general algebraic modelling system) (Schill et al., 2017).

HOMER: Hybrid Optimisation of Multiple Energy Resources. HOMER is a modelling, simulation and optimization tool. It is a global standard for micro-grid design optimization in all sectors (i.e. island utilities, military bases, village power, grid-tied systems). This is a design and evaluation tool in terms of financial technical aspects of on-grid and off-grid energy systems. HOMER runs system simulations by making energy balance for each time step (Lambert et al., 2006; Sen, R. and Bhattacharyya, S.C., 2014).

IHOGA - Improved Hybrid Optimisation by Genetic Algorithms. iHoga can model systems based on water consumption from reservoir, electrical energy or hydrogen consumption. The tool can optimize and simulate systems of any size, connected to AC grid, with or without demand consumption. iHoga includes simulation, multi-objective optimization in time intervals of up-to one minute, probabilistic and sensitivity analysis. (Fadaeenejad et al., 2014; Ringkjøb et al, 2018).

PVSYST: Photovoltaic systems. This tool is used for detailed sizing, studying and analysis of photovoltaic systems. PVSyst includes general solar energy tools, extensive system component and meteorological databases. It also deals with DC-grid, standalone, grid-connected and pumping systems. The software has four main features which include tools, databases, preliminary design and project design. Further, PVSyst incorporates PV array, plane orientation, battery pack, inverter model etc. to run the simulations (Umar et al, 2018; PVSYST, 2020; Ajgaonkar et al., 2019).

REMIx: Renewable Energy Mix. REMix is a linear cost minimizing model widely used in Europe for energy systems with high share of variable renewable sources (VRES). It is also used to assess hourly dispatch and capacity expansion of VRES. REMix consists of two main elements: Optimization model (REMIx-OptiMo) and analysis tool for energy data (REMIx-EnDAT) (Scholz et al., 2017; Gils et al., 2017).

Renpass: Renewable Energy Pathways Simulation System. Renpass can make simulations of different energy transition pathways with high regional and temporal resolution. The model

makes quarter hour calculations of the configured system network (Wiese F, 2015; Wiese et al., 2014).

RETScreen: Renewable Energy Technologies Screen. RETScreen is Clean Energy Project Analysis Software. This tool enables decision makers and professionals to assess and identify potential renewable energy, energy efficiency, cogeneration projects and energy performance of power plants, buildings and factories. The first version of RETScreen was published on 30 April 1998. This tool can perform energy analysis, feasibility, cost analysis, financial analysis, emission analysis, risk/sensitivity analysis (Lee et al., 2012; RETScreen, 2020).

SAM: System Advisor Model. The SAM tool is technical-economic model that provides renewable energy decision support for policy analysts, researchers, technology developers, engineers and project managers (SAM, 2020; Blair et al., 2014; Blair et al., 2013).

SWITCH: Solar, Wind, Transmission, Conventional generation and Hydroelectricity. The SWITCH model was initially published for California but has been refined and expanded to other regions (i.e. China, Chile, Nicaragua). This is a capacity expansion tool that invests in new systems assets (i.e. transmission and generation). It also provides demand side options including storage and electric vehicles with high resolution planning and assessment capabilities (Nelson et al., 2012; SWITCH, 2020).

Temoa: Tools for Energy Model Optimisation and Analysis. Optimizing of an energy system is the core component of this modelling tool. Temoa minimizes the present cost of energy by utilizing and deploying energy commodities and technologies to meet end user demand over time (DeCarolus et al., 2010; Hunter et al., 2013).

WITCH: World Induced Technical Change Hybrid model. The WITCH model was developed to help understand the socio-economic consequences of climate change. Some of the model sample inputs include population, resource use, climate policies, GDP etc. WITCH balances a bottom down input component of the energy sector and top down hybrid optimization structure (Emmerling et al., 2016; Carrara, 2017).

3.4.2.3 Methodological Approach

The methodology is adopted from research by Lyden et al. (2018) and Ringkjøb et al. (2018). Most of the tools presented here are designed for sub hourly and hourly timestep modelling. These tools can be applied to regional, residential, industrial, national, and community scale

systems containing, demand side management, storage, off-grid, grid tied for use at the planning phase of a project. Other system design tools have been considered outside the scope of this write-up. Further, it is now common to use modelling tools in conjunction with other tools (i.e. modelling hydro potential in iHOGA and exporting output file to HomerPro, modelling of photovoltaics in PVSyst and exporting the energy delivered to grid output file to HomerPro) or powerful multi-paradigm tools such as MATLAB (Bava & Furbo, 2017; Irigoyen Tineo, A., 2017), mainly to support customized and advanced optimization control strategies.

The software capabilities tables were developed for the 11 renewable energy modelling tools that define:

- i. List of modelling tools, tool developer, tool availability, relevant software and citation (Table 3K).
- ii. Spatiotemporal resolution and general logic of tools (Table 3L).
- iii. Economic and technological assessment parameters (Table 3M).

These tables formed the cornerstone of the tool selection process (described in section 3.4.2.4) by providing an assessment benchmark of what each tool “can do” with reference to the project scope and objectives.

Figure 3H below illustrates the flowchart summarizing the methodology and categorisation followed in this report.

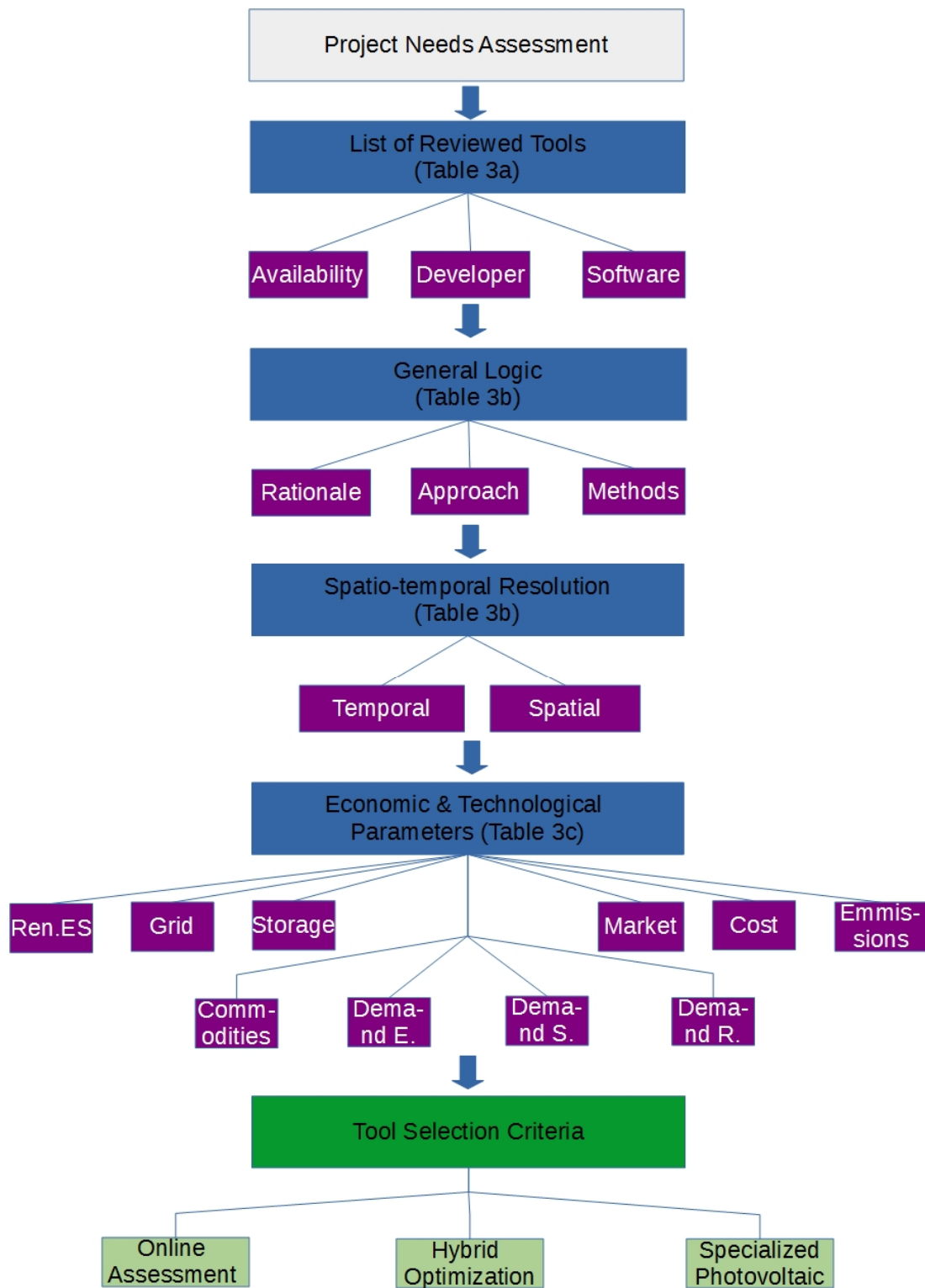


Figure 3H: showing flowchart summarizing the methodology and categorisation

Table 3K: showing a list of modelling tools, tool developer, tool availability, relevant software and citation.

#	Tool Name	Availability	Developer	Underlying Software	Citation
1	DIETER	Open source	DIW Berlin - Alexander Zerrahn & Wolf-Peter Schill	GAMS+Solver	Schill et al., 2017
2	HOMER	Commercial	NREL – Peter Lilienthal	Stand-alone	HOMER, 2020
3	iHOGA	Free/Commercial	Dr. Rodolfo Dufo-López - University of Zaragoza	Stand-alone	Fadaeenejad et al., 2014
4	PVSYST	Commercial	Andre Mermoud and Michel Villoz	Windows	Umar et al, 2018
5	REMix	NA	DLR	GAMS	Scholze et al., 2017
6	Renpass	Open source	Frauke Wiese & Gesine Bökenkamp	MySQL, R, RMySQL	Wiese F, 2015
7	RETScreen	Free	Natural Resources Canada	Windows with .NET	RETScreen, 2020
8	SAM	Free	U.S. Department of Energy and NREL	Stand-alone	SAM, 2020
9	SWITCH	Open source	Fripp, Johnston & Maluenda	Python	SWITCH, 2020
10	Temoa	Open source	NC State University - K. Hunter et al.,	Python+Solver	DeCarolis et al., 2010
11	WITCH	Upon request	FEEM	GAMS	Carrara, 2017

Note: NA - Not available except for collaboration/cooperation with masters and PhD students

3.4.2.3.1 Logic (general)

Rationale

Electricity and Energy tools are usually developed and aligned with a specific problem statement. The 11 renewable energy models under review can thus fit into the three categories below (linked to the rationale):

Operations-decision-support (ODS): Tools developed to optimize the dispatch/operation of energy(or electricity) systems.

Investment-decision-support (IDS): These tools optimize the invest strategies of different electricity/energy systems.

Scenario (Sc): Such tools for instance evaluate the policy impacts by evaluating future long-term scenarios in the electricity/energy sector (Ringkjøb et al. 2018).

Methods

The applied methods in electricity/energy models are generally divided into three categories; equilibrium, simulation or optimization tools (Ringkjøb et al. 2018).

Approach

Two approaches are followed by most energy modelling tools; these are the bottom-up (also called engineering approach) or the top-down approach. Bottom up tools are based on describing the energy system with high level of technological detail while the latter incorporates long term changes in macro-economic relationships (Ringkjøb et al. 2018).

3.4.2.3.2 Spatiotemporal resolution

Spatiotemporal resolution sets practical limits to which process can be modelled within acceptable tolerance of uncertainty. This is particularly important in systems with high share

of variable renewable energy sources. Time intervals can vary from many decades in equilibrium models to milliseconds in power system analysis tools. Some models have time-step given as input data while in others it is fixed.

Table 3L: showing spatiotemporal resolution and general logic of tools (citation in table 3J)

#	Tool Name	Rationale	Methods	Approach	Temporal resolution	Modelling horizon	Geographical reach
1	DIETER	IDS , ODS	LP	Bottom-up	Hourly	1 year	Calibrated to Germany
2	HOMER	IDS , ODS	S , O	Bottom-up	Minutes	Muliti-year	Local
3	iHOGA	IDS , ODS	HO	Bottom-up	Hourly	Yearly	Local
4	PVSYST	ODS , Sc	S, O	Top down	Hourly	Yearly	Global/User defined
5	REMIx	IDS , ODS	LP	Hybrid	Hourly	1 year	National (Europe)
6	Renpass	ODS , Sc	S(In), O(Op)	Bottom-up	Hourly	1 year	Regional/National (W.E)
7	RETSscreen	IDS , Sc	S	Hybrid	M/Y/D	100years max	Single system (Global)
8	SAM	IDS	S	Bottom-up	Sub-hourly	1 year	Single system
9	SWITCH	IDS , ODS	MIP	Bottom-up	Hourly despatch	User defined(2050)	Regional/National
10	Temoa	Sc	LP	Hybrid	Yearly/User defined	User defined)	Regioanal /User defined
11	WITCH	Sc, IDS	E , NLP	Hybrid	5 years	150 years	Global/User defined
<i>Rationale: IDS - Investment decision support, ODS - Operation decision support, Sc - Scenario</i>							
<i>Methods: LP - Linear programming, S - Simulation, O - Optimization, HO - Heuristic optimization, E - Equilibrium</i>							
<i>MIP - Mixed interger programming, NLP - Non-linear programming</i>							
<i>Temporal resolution: M/Y/D - Monthly/yearly/daily</i>							
<i>Geographical reach:W.E -Western Europe, Tools have validated satellite dataset to enable global reach with less resolution</i>							
<i>Most tools have provision to import local meteorological data of specific site</i>							

3.4.2.3 Economic and technological characteristics

The economic and technological parameters under review for the 11 modelling tools are; renewable energy sources, grid, storage, commodities, demand elasticity, demand response, demand sector, embedded market structure, costs for financial analysis, emissions support. These parameters under study are in line with other research (Lyden et al., 2018; Ringkjøb et al. 2018). Table 3M highlights these parameters in a summarized manner.

3.4.2.4 Selection Criteria of Renewable and Optimization Tools

The section describes the renewable energy tool selection criteria for the “hydro-connected floating photovoltaic with onshore wind potential” project. This is divided into 3 categories (i.e. online, hybrid/optimization and photovoltaic analysis tools). The figure 3I summarizes this selection process.

Table 3M: showing economic and technological assessment parameters(citation in table 3J)

#	Tool Name	Ren. ES	Grid	Storage	Commodities	Demand E.	Demand S.	Demand R.	Market	Costs	Emissions
1	DIETER	WP, SP	None	B, H, PHS, CAES	Electricity	Inelastic	Aggregated	Yes	Spot	I, F, CO2, B, O&M	-
2	HOMER	All	I/E	CAES, B, H	Electricity, Heat	Inelastic	Aggregated	No	S/D	I, F, CO2, O&M	Any pollutant
3	iHOGA	WP, SP, HP	I/E	H, B	Electricity, H2	Inelastic	Aggregated	No	S/D	I, F, CO2, O&M	CO2
4	PVSYST	SP (land & floating)	AC/DC Grid	Grid storage	Electricity	-	-	No	S/D	I, O&M, UD	CO2
5	REMIX	All	NTC, DC	All	Electricity, H2, Heat	Inelastic	Aggregated	Yes	S/D	I, F, CO2, O&M	CO2
6	Renpass	WP, SP, HP, ROR, GT	NTC	PHS, CAES, B	Electricity	Inelastic	Aggregated	No	Spot	I, F, CO2, O&M	CO2
7	RETScreen	All	C, IS, O(I/E)	B	Electricity, Heat	Inelastic	B/I	No	S/D	I, F, CO2, O&M, T	GHG
8	SAM	SP, ST, CSP, WP, GT	None	B, TES	Electricity	Inelastic	Aggregated	No	None(PPA)	I, F, O&M, T	None
9	SWITCH	All	CACPF	All	Electricity, Transport	E/I	Aggregated	Yes	S/D	I, F, O&M	CO2
10	Temoa	All	NTC	All	Any commodity	Inelastic	B/T/I	No	S/D	I, F, O&M	Any pollutant
11	WITCH	HP, WP, SP, CSP	NTC	TES, B	Any commodity	Elastic	Aggregated	Yes	S/D + CO2M	I, F, CO2, B, O&M	Any pollutant
Abbreviations & Notes:											
Ren. ES: - Renewable Energy Sources, WP - Wind Power, SP - Solar Power, HP - Hydro Power, ROR-Run of river, GT-Geothermal, CSP-Concentrated solar power, ST-Solar thermal											
Grid: I/E - Import/Export, NTC - Net transfer capacity, DC - Direct current, C-Central, IS-Isolated, O-Off-grid, CACPF-Constrained AC power flow for production cost modelling											
Storage: B - Battery, CAES-Compressed air energy storage, PHS - Pumped hydro storage, H-Hydrogen, TES - Thermal energy storage, Grid storage in PVSYST has 3 scenarios(i.e. storage for enhancing the self-consumption of the PV system owner, a storage for ensuring peak shaving, a storage for the continuity of the user's electricity feeding)											
Commodities: H2 - Hydrogen											
Demand E: -Demand Elasticity, E/I - Elastic/inelastic											
Demand S: -Demand Sectors, B/I - Building and industry											
Demand R: -Demand Response											
Market: S/D - Supply/Demand, PPA - Power purchase agreement, CO2M - Carbon dioxide market											
Costs: I - Investment, F - Fuel, CO2 - Carbon, B - Balancing, O&M - Operations & maintenance, T - Taxes, UD - User defined costs											
Emissions: CO2 - Carbon dioxide, NOx - Oxides of nitrogen, SO2 - Sulphur dioxide, GHG - Greenhouse gases											

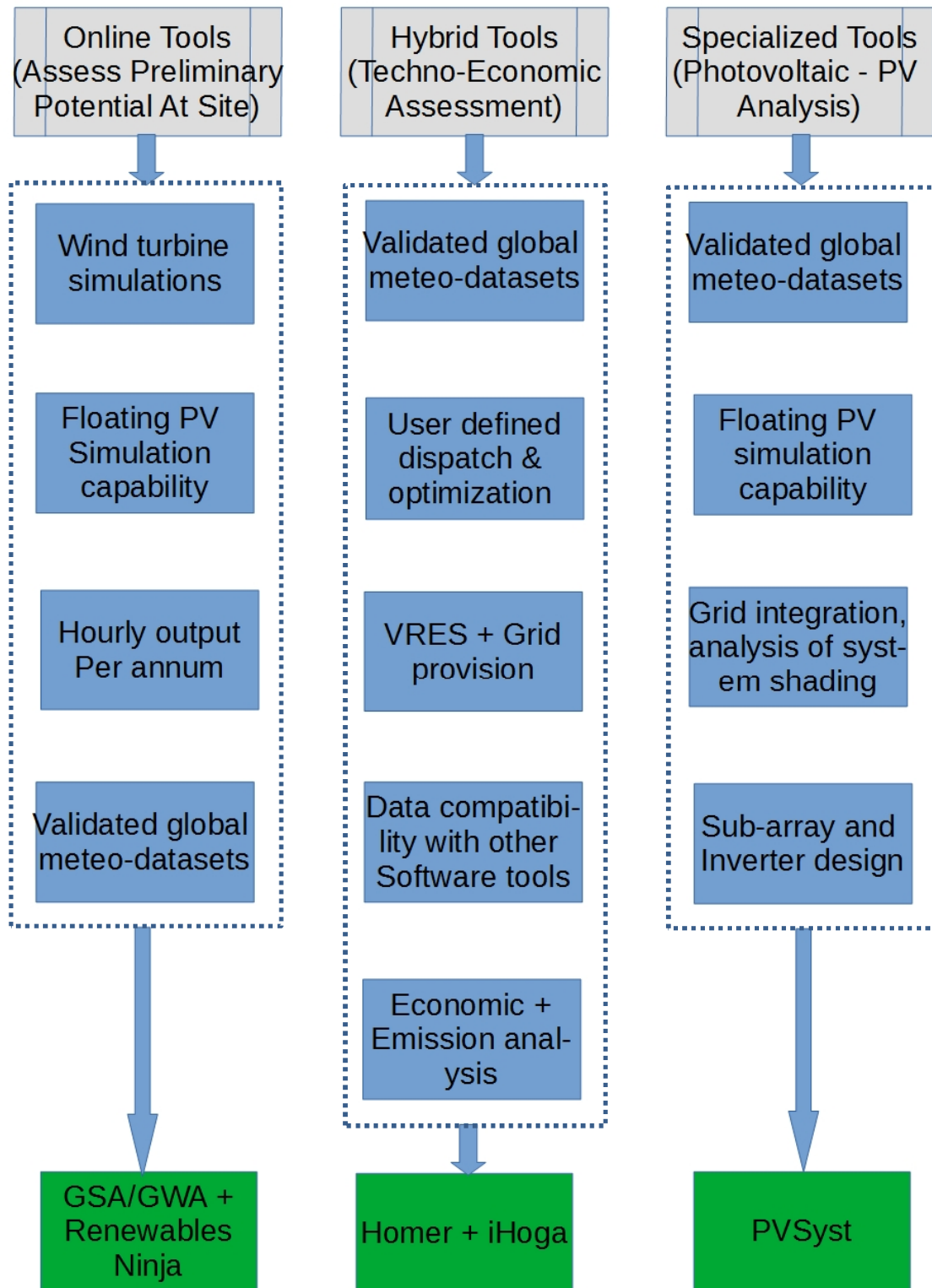


Figure 3I: showing the renewable energy modelling tool selection criteria

3.5 Grid Integration of Variable Renewables

This section looks at the various studies from literature on the integration of variable renewable energy sources (VRES). [Section 3.5.1](#) looks at the overview of integration and defines the pertinent parameters. [Section 3.5.2](#) describes the impact of integration on the voltage profile. [Sections 3.5.3](#) and [3.5.4](#) tackle the aspect of losses and network optimal power flow-based optimization respectively.

3.5.1 Overview

The inherent variability and uncertainty in variable generation technologies add to the variability and uncertainty in the electric power system and can have significant effects on the system operation. Variability is the expected change in generation-demand balance (e.g. load changing throughout the day and wind and solar power resource changes) while uncertainty is the unexpected change in generation and demand balance from what was forecasted (e.g. a contingency or a load or variable generation forecast error). The increasing penetration of wind and photovoltaic technologies make it necessary to understand network parameters and grid code constraints to preserve the reliability, integrity and efficiency of the electric power system ([CESI, 2020](#)).

One of the challenges in modern power systems is the large-scale integration of variable renewable energy sources such as wind and photovoltaics. This because of the complexities in the interaction of the reactive and active power flows in the network, based on the connection characteristics and network design, consequently impacting network voltage profile, losses and dispatch operating costs.

3.5.2 Impacts on Voltage Magnitude Profile

Research ([Widen et al., 2010](#); [Walla et al., 2012](#); [Shalwala, 2012](#)) has presented impacts on voltage profile on the existing electrical grid caused by integration of variable renewable energy sources (i.e. photovoltaics). Studies in Sweden attempted to establish the maximum penetration of PV and impacts on voltage profile for distributed generation ([Widen, 2010](#); [Walla et al., 2012](#)). These studies for three grids under consideration showed voltage increase at the integration bus (one grid experienced maximum voltage violations at buses in the proximity of the point of common connection, while the other two grid showed voltage rise without any voltage violations). [Walla et al. \(2012\)](#) showed that maximum variable renewable

energy source (VRES) penetration was not only determined by impact on voltage profile and magnitude, but also by other parameters (i.e. losses and loading capability of the line). Other research ([Shah et al., 2015](#); [Katiraei, 2011](#); [Schoene et al., 2013](#)) revealed that the impact on voltage profile related to integration of variable renewables was highly dependent on configuration of the existing electrical grid. Studies ([Willis, 2004](#); [Bollen and Hassan, 2011](#)) showed that feeders with long transmission lines experienced lower voltages compared to the sending end voltage. Thus, integration of photovoltaics (or wind or both) improves the voltage magnitude profile along such feeders.

3.5.3 Impact on Network Power Losses

Scholarly analyses ([Widen, 2010](#); [Solanki et al., 2012](#)) presented the effects of integrating photovoltaics at different penetration levels on the electrical network losses. Research by [Willis \(2004\)](#) demonstrated the impact of losses on the distribution grid's cost of operation. Further, studies by [Widen \(2010\)](#) revealed an increase in network losses at high VRES penetration levels and a decrease at lower penetration. [Solanki et al. \(2012\)](#) demonstrated and correlated the rise in network losses in a radial grid with the reverse power flow which increased the loading capacity and consequently the current squared losses (and has potential to interrupt supply by causing maloperation of non-directional protection devices on the network).

3.5.4 Optimal Power Flow Based Optimization.

A lot of research has gone into the optimization of network operating costs and loss reduction by the economic dispatch of different generators on the power network. For instance, scholarly analyses ([Durvasulu, V. and Hansen, T.M., 2018](#); [McLarty et al., 2019](#); [Đurović et al., 2012](#); [Princy et al., 2018](#)) have demonstrated how to relate and optimally reduce fixed, proportional and quadratic cost relationships of different generating units ranging from conventional thermal, hydro and variable renewable energy sources. Coal power plants follow the quadratic cost function with unique input-output characteristics (i.e. fuel feed cost). However, photovoltaics and wind have an almost free input cost due to the nature of fuel used (wind and solar). The main operational cost aspect is operation and maintenance, which is often a small percentage of the investment cost.

3.6 Dispatch of Hybrid Energy Systems

Attaining carbon neutrality towards the fight against climate change has been the main motivator behind global interest in production of energy from renewable energy sources - RES (i.e. solar, wind, marine, geothermal) (Shah et al., 2015; Ming et al., 2018). However, high penetration of variable renewable energy sources (VRES) into conventional electrical network grids amplifies the concerns about system stability and security (Ding et al., 2016). Scholarly analyses (Ming et al., 2018; Chen et al., 2016) found a balance of dispatchable and non-dispatchable power sources (i.e. hydro-solar operation) to be economical and thus promoting the integration of more renewables.

Energy systems which provide a mix of two or more power sources (called Hybrid systems) have been widely adopted in many countries due to the benefit of increased energy supply balance and enhanced system efficiency (Deshmukh, M.K. and Deshmukh, S.S., 2008; Paska et al., 2009). Typical hybrid systems include hydro-photovoltaic (Campana et al., 2013; Glasnovic, 2009), hydro-thermal-wind (Chen et al., 2017), hydro-wind (Bayón, 2016; Portero et al., 2015) and hydro-solar photovoltaic-wind systems (Wang et al., 2017; Liu et al., 2016). Research (Shabani, 2018) has found the mix of solar and hydro to be widely used because of the rapid regulation capability of hydro and the vast spread of solar as a largest global renewable energy resource. Therefore, regions such as Sub-Saharan Africa (i.e. Zambia) that are rich in both solar and hydro renewable resources are well suited in the deployment and development of hydro-solar hybrid systems.

Scholarly analyses regarding the optimal mix of renewable resources involving hydro-solar PV and wind systems mostly focus on the resource time complementarity (Beluco et al., 2012; Francois et al., 2016; Kougias et al., 2016), management of plant operations (Jurasz, 2017; Liu, 2016; Ming et al., 2018), and system configuration optimization (Glasnovic, 2009; Kougias et al., 2016; Fang et al., 2017; Jurasz, 2017). Research by Beluco et al. revealed a decrease in customer power interruptions as attributed to the photovoltaics-hydro temporal complementarity. A case study conducted by Francois et al in Italy showed a decrease in the variability in energy balance due to the mix of solar energy and run-of-river hydro. Further research by Kougias et al. revealed that optimizing the photovoltaic system tilt and azimuth of an installation improved the small hydro-photovoltaic output time complementarity.

Most research on hybrid systems involving hydro-photovoltaics-wind aims at enhancing system flexibility and reliability by optimally coordinating the available resource(s). However, such scholarly analyses rarely incorporate the stochastic attributes of wind and PV power in the modelling, and thus introducing errors in the process (Chen, 2012; Yang et al., 2013; Yang et al., 2017). Research (Wei and Liu, 2019) has handled the uncertainties of VRES by using stochastic and deterministic programming. Further, research by Wei et al. (2017) and Liu et al. (2016) revealed that while the inclusion of the spinning reserve to the dispatch model (deterministic) enhanced system security, the flexibility and the economy of the system were limited. Dong et al. (2015) and Zou (2015) showed that by adopting a multi-scenario viewpoint, an optimization problem that was stochastic in nature was converted to a deterministic one. The trade off, however, is the inaccuracy in the optimization due to scenario loss reduction in operations brought about by computation of system efficiency (Wei and Liu, 2019).

Of late, economical dispatch has employed robust optimization techniques due to its efficacy in excluding both massive datasets for sampling variables and precise probability distribution models (Yixin et al., 2018). The randomness of VRES necessitates accustoming between the actual and base generation of a hybrid energy system. The prediction of VRES introduces error in the model creating an imbalance in power. Therefore, this has accentuated the introduction of an adjustment strategy in some energy systems (Wang et al., 2018; Reddy, 2017). Research (Reddy, 2015) has devised a real-time method between two consecutive scheduling intervals that incorporates uncertainty and variability cost of RES. This has been treated as a penalty cost for VRES (i.e. wind and PV) energy curtailment in other research (Wei and Liu, 2019).

3.7 The Cost of Variable Renewable Energy

This section reviews the cost of variable renewable energy sources (floating photovoltaics, ground mounted and wind) in the global context and perceived Zambian context. Section 3.7.1 looks at the global wind and photovoltaic cost trend from 2010 to 2018. Section 3.7.2 address the cost of floating photovoltaics by reviewing installed and planned projects from key players in industry. Section 3.7.3 compares the capital cost involved in ground mounted and floating PV systems. Section 3.7.4 looks at the perceived costs of wind and photovoltaics 10 years in the future (2020 to 2030). Integration of additional generation usually requires investing in network reinforcement, therefore, section 3.7.5 looks at grid reinforcement costs.

3.7.1 Cost Overview

Costs for solar and wind technologies continue falling in the last years, increasing the competitiveness of VRES with fossil fuel technologies and other renewable energy sources. The cost reductions of utility-scale PV projects continue to be driven by falling PV module prices and balance of system (BOS) costs. The electricity cost from onshore wind projects likewise continue to decrease thanks to the reductions in total installed costs, as well as the improvements in turbine design and manufacturing (higher hub heights and larger swept areas collect more electricity from a given resource than older technologies) able to improve the turbine performance increasing the capacity factor. Furthermore, the introduction of auction mechanisms to develop VRES projects fostered the fast decrease of the electricity costs from wind and PV sources (CESI, 2020).

The reduction of the electricity cost from utility-scale PV and onshore wind projects in the last years is well highlighted in the figures 3J and 3K. The figures show the results of IRENA calculations carried out on a world-wide database of onshore wind and PV projects in the period 2010-2018; the global weighted average installed costs, the capacity factors and the levelized costs of electricity (LCOE) for solar PV and onshore wind projects are showed (CESI, 2020).

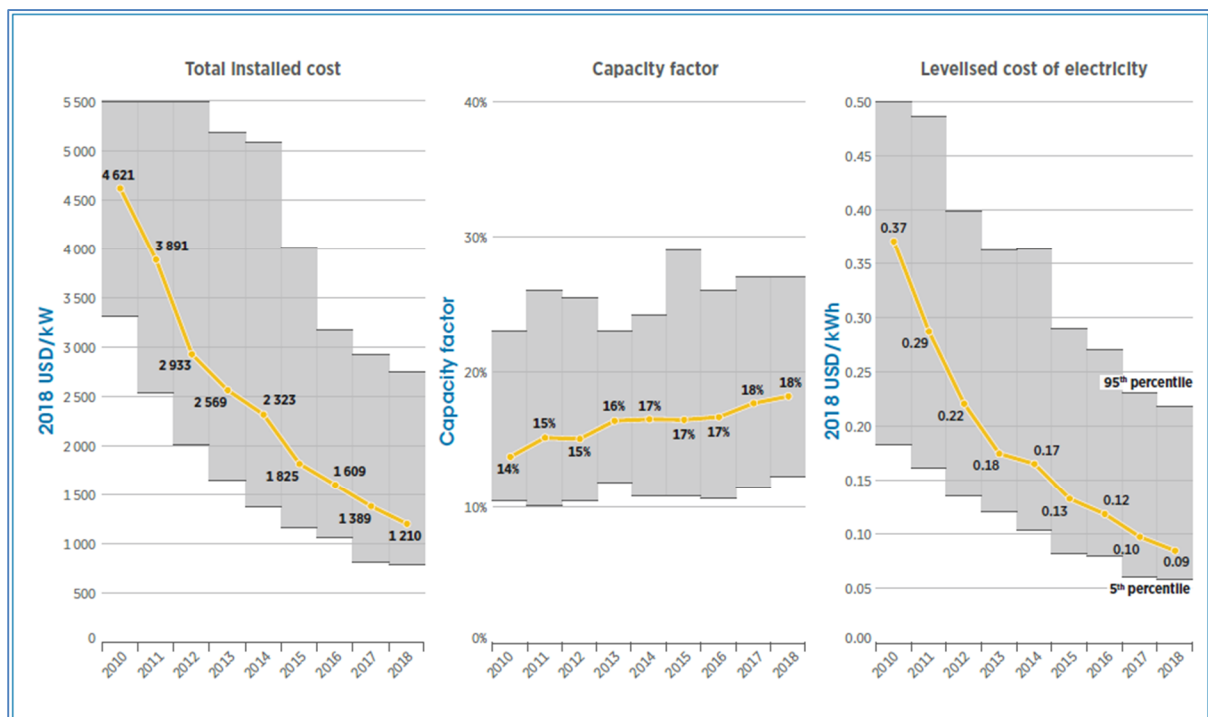


Figure 3J: showing Global weighted average total installed costs, capacity factors and LCOE for solar PV; world data 2010–2018 (Source IRENA, 2019)

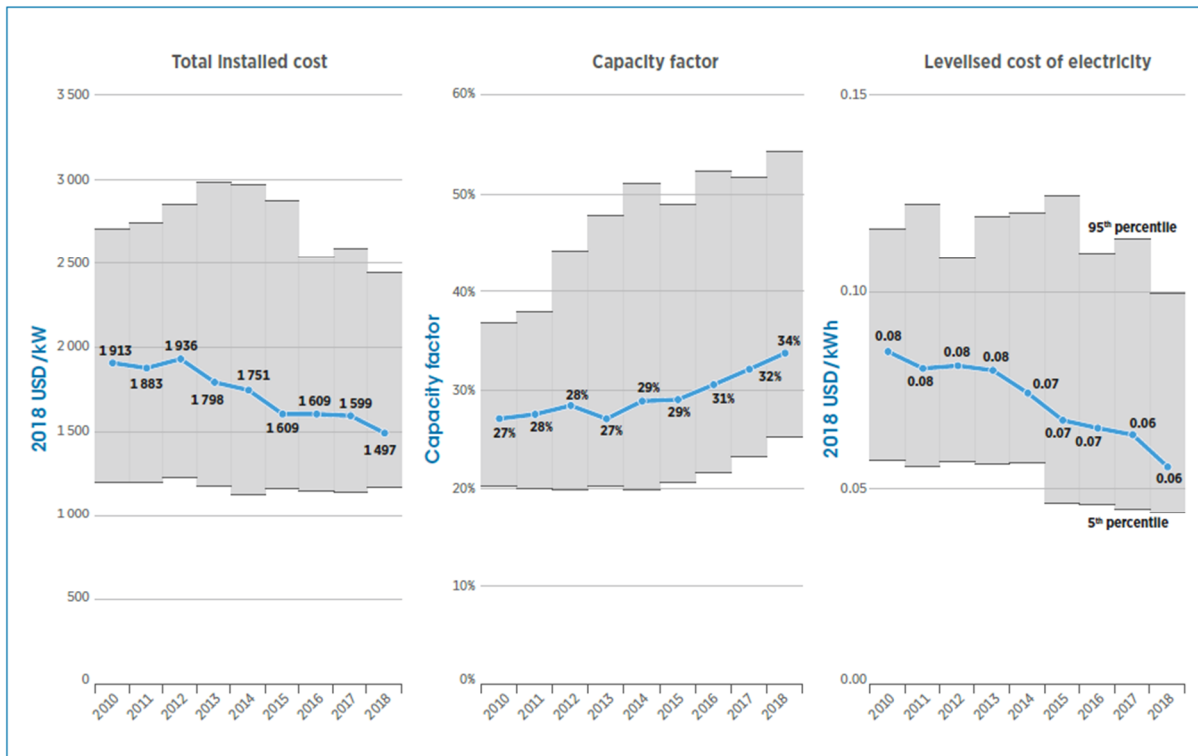


Figure 3K: Global weighted average total installed costs, capacity factors and LCOE for onshore wind; world data 2010–2018. (Source IRENA, 2019)

3.7.2 The Cost of Floating PV

Cost data (CAPEX and OPEX) remains difficult to access for floating PV systems partly because the technology is not as widespread or common as land-based systems.

Capital Expenditure (CAPEX)

The capital costs for land-based PV systems are slightly lower than floating PV, owing to the need for mooring, floats, more resilient electrical components in the latter. However, owing to better economies of scale, the cost of floats/pontoons is perceived to drop over time. The CAPEX for most FPV installations ranged between \$0.8 to \$1.2 per Wp in 2018, depending on system size, depth of water body, fluctuation in depth and project location (World Bank, 2019). The distribution and comparison of FPV investment costs for China, Japan, UK, India and Portugal is shown in the figure 3L.

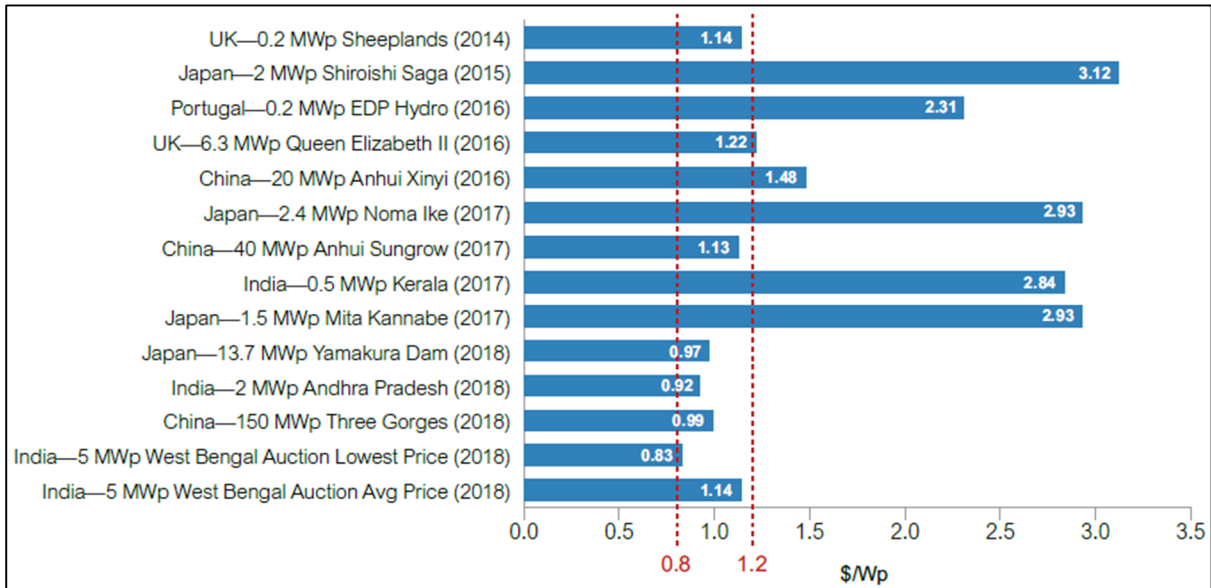


Figure 3L: showing Investment costs of FPV in 2014–2018 (realized and auction results) (source: World Bank and SERIS, 2019)

Operation & Maintenance

The key operating costs of land based and FPV systems are identical: inverter replacement costs, insurance, rental or leasing of space (most applicable to land systems), and operation and maintenance. According to SERIS (2019), O&M costs vary depending on the adopted investment strategy of the owner. Further, these costs are comparable over the lifetime of a project for both FPV and land-based systems, even though the former in some circumstances can have additional costs due to the need for divers or use of boats. This is balanced against the cost saving from the availability of cleaning water and the infrequent soiling from dust of FPV systems (i.e. solar panels). Another aspect that adds to maintenance cost for FPV systems is the safety measures for personnel working on or under water (World Bank, 2019). Estimation of O&M costs remains a difficult task as evidenced by the different assumptions used by leading developers and institutions in renewable energy as illustrated in table 3N. The key factors that contribute to this variation are labour cost, investment strategy, projects environment.

Table 3N: showing estimated O&M costs for fixed tilt land-based PV systems (source: NREL, 2017; Lazard, 2018; Fraunhofer, 2018)

Utility-scale fixed tilt	O&M (\$/Wp/year)	Geographic focus
NREL (September 2017)	0.0154	United States
Lazard v12.0 (November 2018)	0.009	United States
Fraunhofer ISE (March 2018)	2.5% of CAPEX	Germany

3.7.3 CAPEX of Floating vs Land PV

Even though this section compares the capital expenditure cost of FPV and land-based PV (or ground mounted), the former technology complements the latter and serves a different purpose and need altogether. For instance, FPV reduce seasonal fluctuations of hydropower generation when retrofitted on hydro reservoirs. Thus, FPV must not be put forward as a competitor to land based PV systems (SERIS & World Bank, 2018). In the third and fourth quarter of 2018, the capital expenditure of large-scale projects ranged from \$0.7 to \$0.8 per Wp. Table 3O and figure 3M below illustrate the capital expenditure of 50 MWp floating PV installation (hypothetical case) as compared to a land-based system of similar capacity, same module and inverter costs, at the same location and both with fixed inclination. The balance of system (BOS) mounting structures costs are lower for land-based systems than for floating PV. The total CAPEX for FPV is about 10 cents higher than land-based systems on a watt peak basis. The cost of FPV float structures is perceived to reduce with high economies of scale and increased competition (SERIS, 2019).

Table 3O: showing a comparison of CAPEX: Floating vs. land-based (ground-mounted) photovoltaic projects (source: World Bank and SERIS, 2019)

CAPEX component	FPV 50 MWp (\$/Wp)	Ground-mounted PV 50 MWp (\$/Wp)
Modules	0.25	0.25
Inverters	0.06	0.06
Mounting system (racking)*	0.15	0.10
BOS**	0.13	0.08
Design, construction, T&C	0.14	0.13
Total CAPEX	0.73	0.62

Note1: *For FPV, the mounting system includes a floating structure, and anchoring and mooring system.

**Including monitoring system. BOS = balance of system; T&C = testing and commissioning;

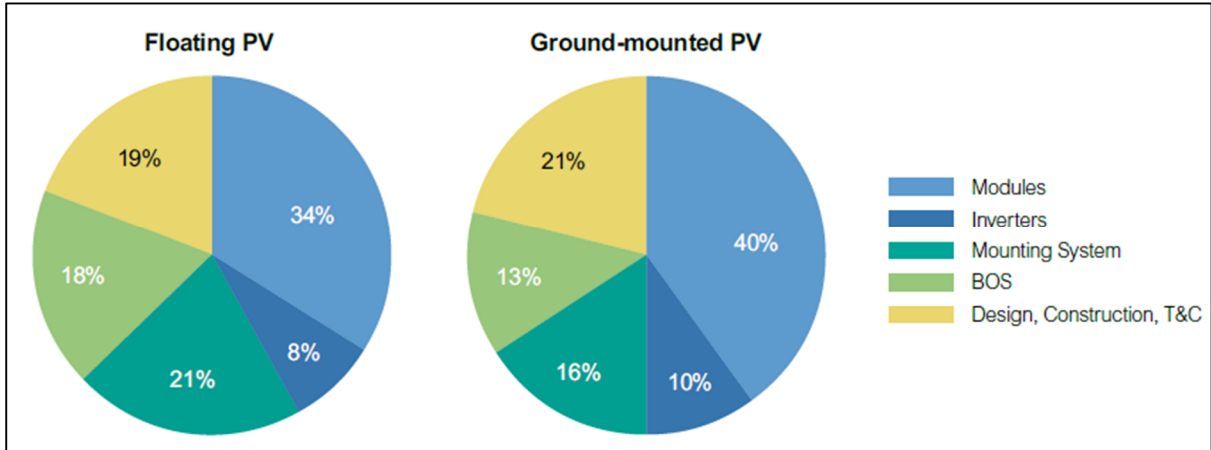


Figure 3M: showing CAPEX of floating vs. land-based (ground-mounted) photovoltaic systems, by component (source: World Bank and SERIS, 2019).

3.7.4 Perceived Costs of VRES in Zambia

The electricity costs from VRES projects are specific for the analysed country because they depend by several aspects regarding the potential of solar and wind in the country, the economic conditions and the environmental issues. Therefore, an assessment of the levelized costs of electricity from wind and photovoltaic technologies in Zambia has been carried out proving an indication of their competitiveness. Capacity factors of wind and PV power plants have been considered together with the investment costs, operating costs and lifetime of these technologies to provide a qualitative assessment of LCOE to be adopted as reference in the cost-benefit analysis of VRES integration. International standards (i.e. EU, IRENA, SERIS, World Bank, NREL) and the experiences of RES4Africa’s partners on southern Africa regions have been used as reference (CESI, 2020).

LCOE is usually defined as the total cost for the construction and operation of a power plant over an assumed lifetime divided by the expected energy production over the same period; both of which are discounted back to a common year using a discount rate that reflects the average cost of capital. Hence, the formula used for calculating the LCOE of renewable energy technologies is (CESI, 2020):

$$LCOE = \frac{\sum_{t=1}^n \frac{I_t + O\&M_t}{(1+r)^t}}{\sum_{t=1}^n \frac{E_t}{(1+r)^t}} \tag{16}$$

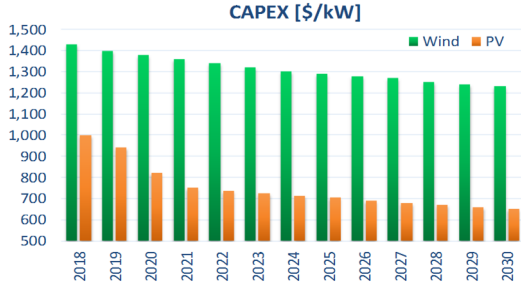
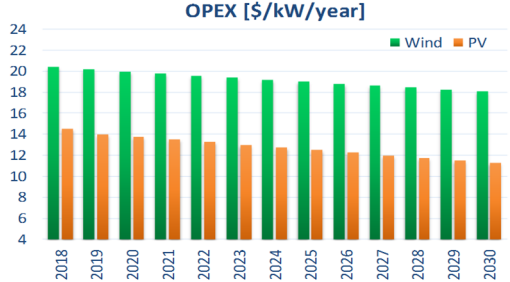
where:

- I_t is the investment expenditure in year t ;
- $O\&M_t$ is the operation and maintenance expenditure in year t ;
- E_t is the energy produced in year t ;
- r is the discount rate;

- n is the plant lifetime;

The forecast of LCOE from wind and PV power plants was recently performed by [CESI \(2020\)](#) considering the assumptions in the [table 3P](#):

Table 3P: showing assumptions used for LCOE forecast in Zambia (Source: CESI, 2020)

#	Assumption Details
1	<p><i>Capital and Operating Costs (CAPEX & OPEX)</i></p> <p>The values for investment costs (CAPEX) and O&M costs (OPEX) of each technology, specific to one installed kW, have been assumed considering the results of the GET FiT Round 1, international standards and the experience of RES4Africa’s partners in southern Africa regions. Figures below shows the forecast of CAPEX and OPEX for wind and PV technologies in the period 2019-2030. About CAPEX, the reduction of wind projects costs was assumed quite linear over the planning period, while an important reduction was assumed in the short-term (2020-2021) for PV technology. This last is the effect of GET FiT Round 1 in which 120 MW PV capacity was committed with a weighted average LCOE equal to 4.41 \$c/kWh (the lowest bid was 3.99 \$c/kWh). The CAPEX and OPEX forecast from 2018 to 2030 is shown below;</p> <div style="display: flex; justify-content: space-around;">   </div>
2	<p><i>Operating Hours</i></p> <p>Starting from the average capacity factors of wind and PV generation calculated from wind speed and solar radiation measures with state-of-art technologies, technological developments able to improve the power plants performance increasing the capacity factor have been assumed in the long-term. From the wind side, CESI considered improvements in turbine design and manufacturing, such as higher hub heights and larger swept areas, while bi-facial photovoltaic panels have been introduced for new PV power plants.</p>
3	<p><i>Power plant lifetime and PPA duration</i></p> <p>The power plant lifetime for wind and PV power plants is commonly considered equal to 25 years. However, the duration of Power Purchase Agreements (PPAs) to be put in place with independent power producers was conservatively used for the evaluation of the discounted cash flow and the total energy produced; this is because the PPA duration is the period in which the remuneration is granted. Therefore 20 years have been assumed for the discounted cash flow both for PV and wind projects.</p>
4	<p><i>Discount Rate</i></p> <p>The discount rate, which considers both cost of debt and cost of equity, has been assumed equal to 10%.</p>

Note1: Global Energy Transfer Feed in Tariff (GET FiT) is an initiative designed to assist the Government of the Republic of Zambia in the implementation of its Renewable Feed in Tariff (REFiT) Strategy. GET FiT aims to support small- and medium-scale Independent Power Producer projects up to 20 MW and procure the 200 MW of PV and small hydro energy projects in the Country (Source: CESI, 2020).

Based on the above information and assumptions, the expected LCOE has been calculated for each year in the period 2018-2030. Figure below shows the LCOE from wind and PV projects with commercial operating date (COD) between 2018 and 2030 ([enel, 2020](#); [Francesco et al., 2020](#)).

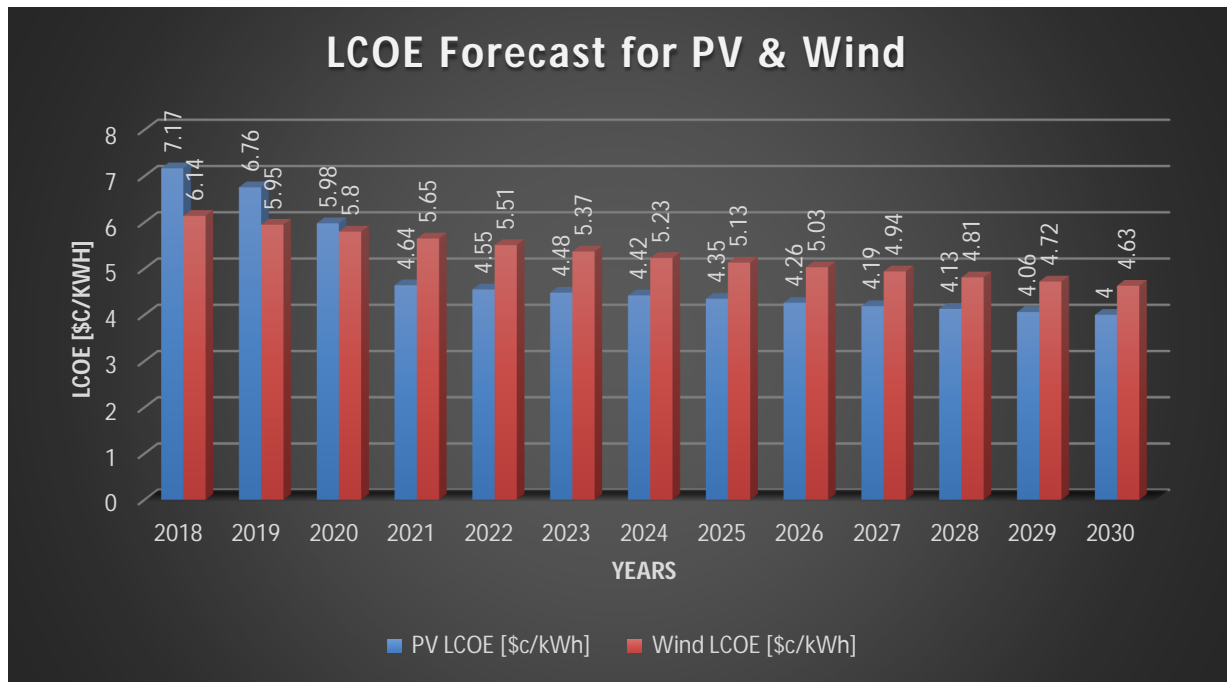


Figure 3N: showing comparison between annual LCOE for wind and PV technologies (source: CESI, 2020)

Detailed data and results about the forecast of LCOE for new wind and PV projects are highlighted in the [table 3Q](#) and [3R](#):

Table 3Q: showing LCOE for PV power plants – Zambia (source: CESI, 2020)

Year	CF [%]	EOH [h/yr]	CAPEX [\$/kW]	OPEX [\$/kW/yr]	LCOE [\$/kWh]
2018	21.0	1,840	1,000	14.5	7.17
2019	21.0	1,840	940	14.0	6.76
2020	21.0	1,840	820	13.8	5.98
2021	25.0	2,190	750	13.5	4.64
2022	25.0	2,190	735	13.3	4.55
2023	25.0	2,190	725	13.0	4.48
2024	25.0	2,190	715	12.8	4.42
2025	25.0	2,190	705	12.5	4.35
2026	25.0	2,190	690	12.3	4.26
2027	25.0	2,190	680	12.0	4.19
2028	25.0	2,190	670	11.8	4.13
2029	25.0	2,190	660	11.5	4.06
2030	25.0	2,190	650	11.3	4.00

Note1: CF – capacity factor, EOH – equivalent operating hours, CAPEX – capital expenditure, OPEX – operating expenditure, LCOE – levelized cost of energy

Table 3R: showing LCOE for wind power plants (source: CESI, 2020)

Year	CF [%]	EOH [h/yr]	CAPEX [\$/kW]	OPEX [\$/kW/yr]	LCOE [\$/kWh]
2018	35.0	3,066	1,430	20.4	6.14
2019	35.4	3,103	1,400	20.2	5.95
2020	35.8	3,140	1,380	20.0	5.80
2021	36.3	3,176	1,360	19.8	5.65
2022	36.7	3,213	1,340	19.6	5.51
2023	37.1	3,250	1,320	19.4	5.37
2024	37.5	3,287	1,300	19.2	5.23
2025	37.9	3,324	1,290	19.0	5.13
2026	38.4	3,360	1,280	18.8	5.03
2027	38.8	3,397	1,270	18.6	4.94
2028	39.2	3,434	1,250	18.4	4.81
2029	39.6	3,471	1,240	18.2	4.72
2030	40.0	3,508	1,230	18.1	4.63

Note1: CF – capacity factor, EOH – equivalent operating hours, CAPEX – capital expenditure, OPEX – operating expenditure, LCOE – levelized cost of energy

3.7.5 Grid Reinforcement Costs

The cost-benefit analysis for the VRES (i.e. wind and solar PV) integration in an electric power system must consider the cost of additional grid reinforcements that could be needed for the optimal economic exploitation of VRES technologies. The cost of a grid reinforcement includes both the investment cost (CAPEX) and the operational cost (OPEX). No information was provided by the national utility (ZESCO) for the unitary investment costs and O&M costs for new transmission assets (lines and transformers). However, based on literature and the experience of international sources (CESI, 2020; IRENA, 2019; World Bank, 2019), standard investment costs for lines and transformers are adopted as shown in table 3S. The operation and maintenance costs are equal to 1.5 percent of the overall CAPEX of the grid reinforcement. Furthermore, a discount rate of 10 percent and a lifetime of the new transmission assets equal to 40 years will be applied in the economic analyses.

Table 3S: showing specific investment costs (CAPEX) of the transmission facilities (CESI, 2020)

Transmission Facility	Unit	Specific investment costs
AC 400 kV overhead line, double circuit	[k\$/km]	425
AC 400 kV overhead line, single circuit	[k\$/km]	360
AC 330 kV overhead line, double circuit	[k\$/km]	350
AC 330 kV overhead line, single circuit	[k\$/km]	300
AC 220 kV overhead line, double circuit	[k\$/km]	250
AC 132 kV overhead line, double circuit	[k\$/km]	180
600 MVA 400/330 kV transformer	[k\$]	6,000

Transmission Facility	Unit	Specific investment costs
400 MVA 400/330 kV transformer	[k\$]	4,000
400 MVA 400/220 kV transformer	[k\$]	4,000
400 MVA 330/220 kV transformer	[k\$]	4,000
350 MVA 330/132 kV transformer	[k\$]	3,800
200 MVA 330/132 kV transformer	[k\$]	2,800
90 MVA 220/132 kV transformer	[k\$]	1,800

3.8 Literature Review Summary

The literature review on renewable technologies, grid integration of VRES, dispatch of generators and associated cost of energy illustrates the massive potential of a hydro-connected floating PV energy system with onshore wind, due to technological advancement and the continuous decrease in the levelized cost of energy for photovoltaics and wind systems. This is true for both small-scale and large-scale projects between hydro and photovoltaics (floating or land based), hydro and wind, and a combination of all three technologies. For instance, the Longyangxia power plant in China, is a largescale hybrid of a 1280MW hydropower and 850 solar photovoltaics land-based plant as a single source energy generation system. This generation mix offers a temporal complementarity and thus the variable solar power is smoothed by the stable and dispatchable hydro (Ming et al., 2018).

The next chapter defines a site assessment and screening methodology for hydropower sites with floating photovoltaic and onshore wind potential.

CHAPTER FOUR: SITE ASSESSMENT, SCREENING & RANKING METHODOLOGY

This chapter describes the development of a site assessment, screening and ranking methodology employed in this study. [Section 4.1](#) gives an overview and evolution on site assessment methods in literature. [Section 4.2](#) describes the proposed methodology for this study. [Section 4.3](#) illustrates the adopted criteria hierarchy structure based on different layers (i.e. economical, climate, topography, environmental). [Sections 4.4](#) defines three site attribute score tables for ranking based on extensive research (hybrid, floating photovoltaics and onshore wind), while [section 4.5](#) gives a summary about the chapter.

4.1 Overview

According to research ([Ali et al., 2019](#); [Harper et al., 2017](#); [Sunak et al., 2015](#); [Malczewski, 2004](#)), suitable site location assessment of VRES (i.e. wind and solar PV) makes use of geospatial parameters in aiding decision making. This mainly entails utilization of geographic information system (GIS) models for analysis (i.e. store, manage, capture, analyse, present and manipulate geographic or spatial data). Multi-Criteria Decision Making (MCDM) are usually paired with such GIS approaches to aid in devising a geospatial data interpretation and ranking methodology ([Malczewski, 2004](#)). Early literature in the development of variable renewable energy source (i.e. wind) models started in the late 1990s ([Voivontas et al., 1998](#); [Baban and Parry, 2001](#)).

The fight against climate change has aroused massive international interest in optimal siting of wind and solar photovoltaics in the recent past, leading to model formulation typically based on [figure 4a](#). Firstly, selection of input parameters ranging from social, environmental and technical is done ([Gigovic et al., 2017](#)). For instance, considering ideal wind sites typically includes high resource potential (i.e. capacity factor and average wind speeds); close to existing network for easy grid connection; close to good road network; far from settlements to prevent flicker and noise; far from protected zones (i.e. heritage land or national parks); not close to flight path (i.e. prevent radar interference near airports). Thereafter, the sites are scored against the input parameters to exclude unsuitable sites from further analysis (i.e. those near built-up areas or airports).

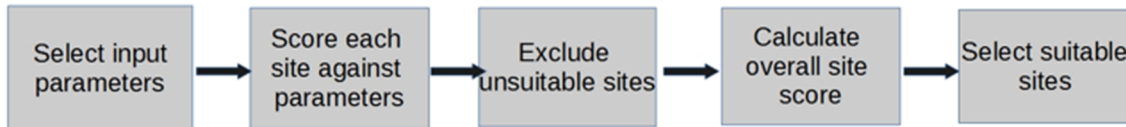


Figure 4A: showing typical structure of multicriteria decision method (source: Harper et al., 2017)

The sites that pass the screening stage and that have potential to be developed are then scored to assess suitability using the weighted sum method (WSM), equation 16 (Malczewski, 2004; Harper et al., 2017).

$$A_i^{WSM} = \sum_{j=1}^n w_j a_{ij} \text{ for } i = 1, 2, 3, \dots, N \tag{16}$$

Where 'w' is the relative parameter weighting, 'a' is the parameter score value, 'i' attribute layer.

4.2 Proposed Study Methodology

The methodology for site suitability assessment in this study was finalized after extensive literature review (Watson and Hudson, 2015; Höfer et al., 2016; Latinopoulos and Kechagia, 2015; Uyan, 2013) and stakeholder engagements (i.e. ZESCO Ltd, local experts). The developed flowchart-based methodology for the placement of FPV and onshore wind turbines near hydropower sites is shown in figure 4B.

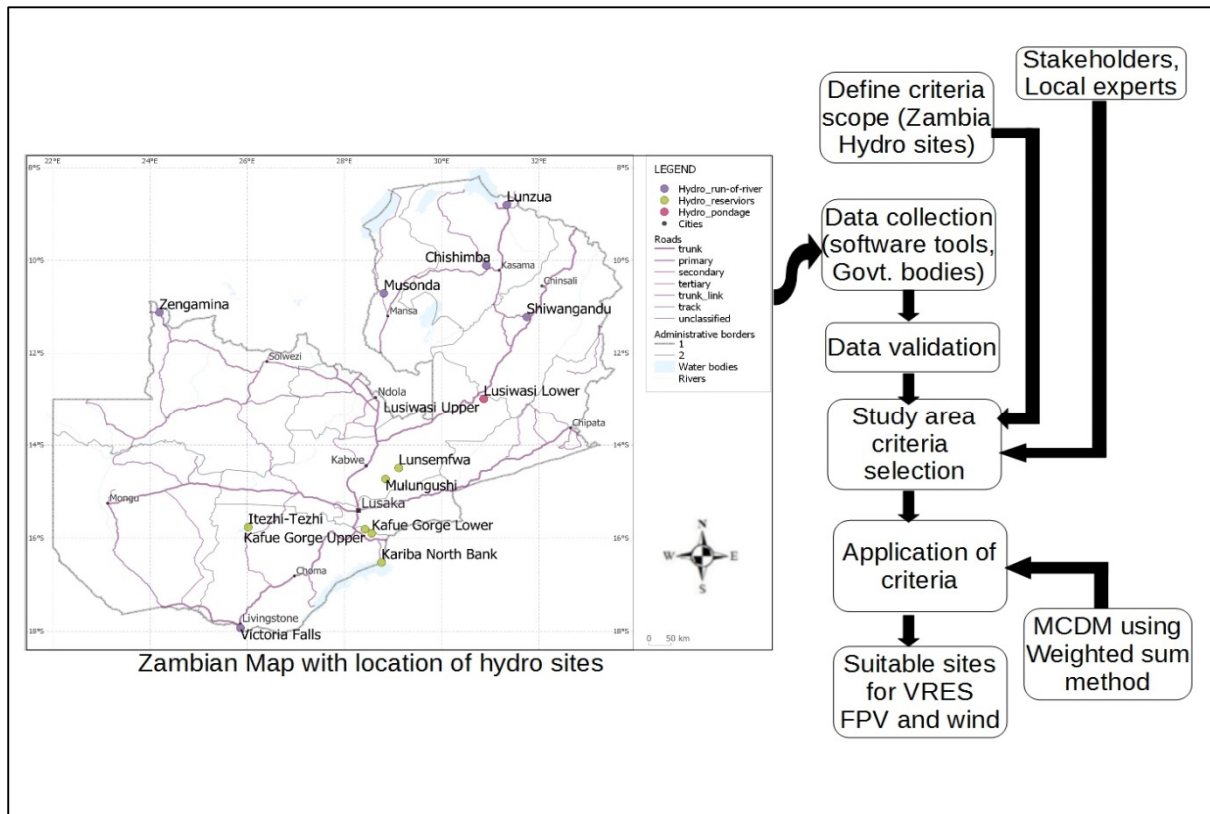


Figure 4B: showing proposed methodology flowchart of study area

The technical resource potential parameters for floating photovoltaics (capacity factor, surface area solar irradiance) and onshore wind (capacity factor and wind speed) are not the only deciding inputs to the site suitability model, rather, environmental, social and economic aspects are equally relevant in wind and solar farm placement. This is in line with other research (Anwarzai and Nagasaka, 2017; Latinopoulos and Kechagia, 2015; Van Haaren and Fthenakis, 2011; Uyan, 2013).

4.3 Criteria Hierarchy Structure

This section describes the criteria hierarchy structure for selection of optimal floating photovoltaic and onshore wind sites based on climate (solar irradiation and wind), landscape topography (elevation and slope), environmental (i.e. scenery and protection buffers etc) and economical layers (distance to demand, grid, roads etc).

4.3.1 Optimal FPV Site

The selection of potential floating PV sites utilized a two-stage approach namely stage 1 screening and filtering and stage 2 ranking and scoring as shown in figure 4C. The screening stage looked at the following input parameters; surface area, capacity factor, distance to grid and distance to protected zone.

The ranking and scoring stage included the relative weight (r.w.) distribution of the FPV potential (60% total r.w. comprising of “surface area” at 30% r.w. and “capacity factor” at 30%), energy export (20% total r.w. comprising of “distance to grid” at 10% r.w. and “capacity of grid” at 10% r.w.), ease of access (15% r.w. comprising land use, landownership and distance to road all with equal relative weight distribution) and demand (5% r.w. comprising of distance to demand centres).

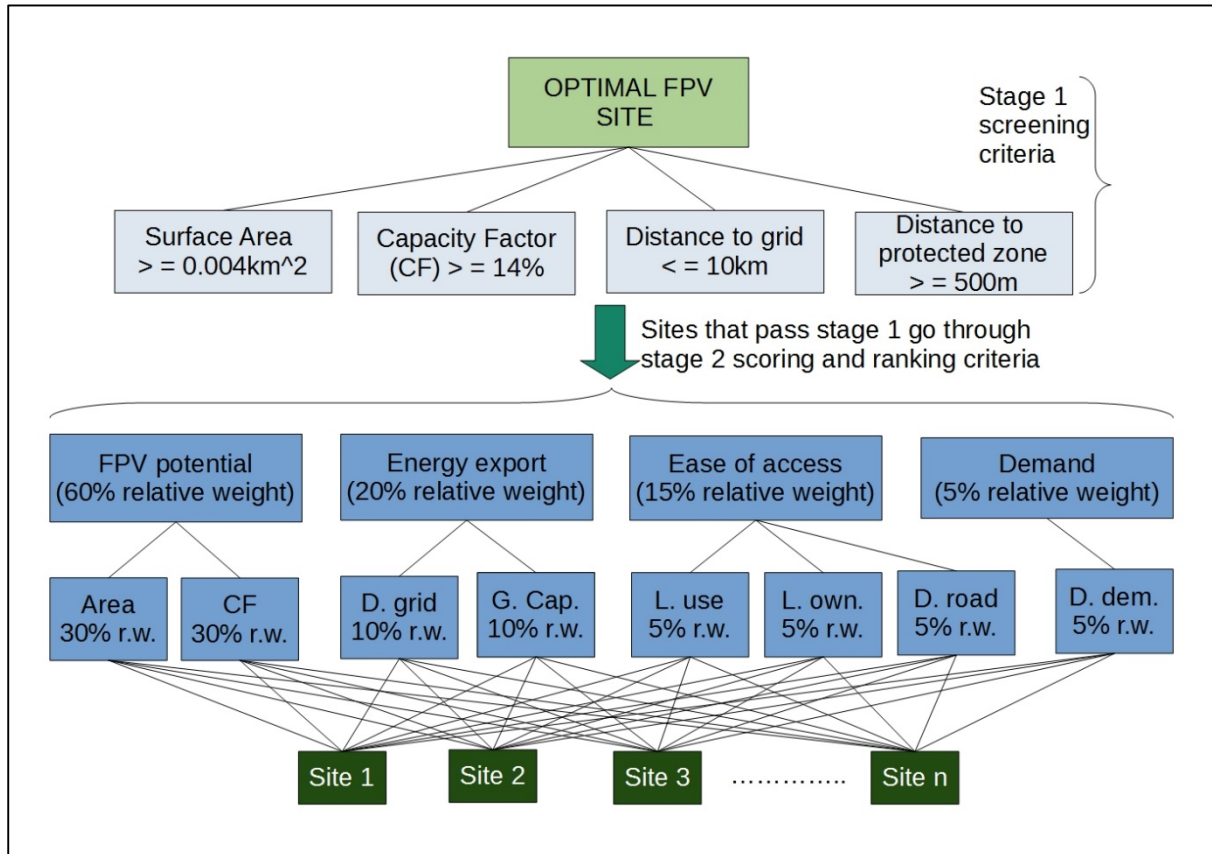


Figure 4C: showing 2 stage hierarchy structure for optimal floating photovoltaics site selection. Abbreviations: CF – capacity factor, D. grid – distance to grid, G. Cap. – capacity of grid, L. use – land use, L. own – land ownership, D. road – distance to road, D. dem. – distance to demand centre, r.w. – relative weight.

4.3.2 Optimal Wind Site

The selection of potential floating PV sites utilized a two-stage approach namely stage 1 screening and filtering and stage 2 ranking and scoring as shown in figure 4d. The screening stage looked at the following input parameters; flicker and noise due to proximity to settlements/buildings, security risk of installations (i.e. civil unrest or war as defined by the world bank and united nations), wind speed, capacity factor, distance to grid and distance to protected zone.

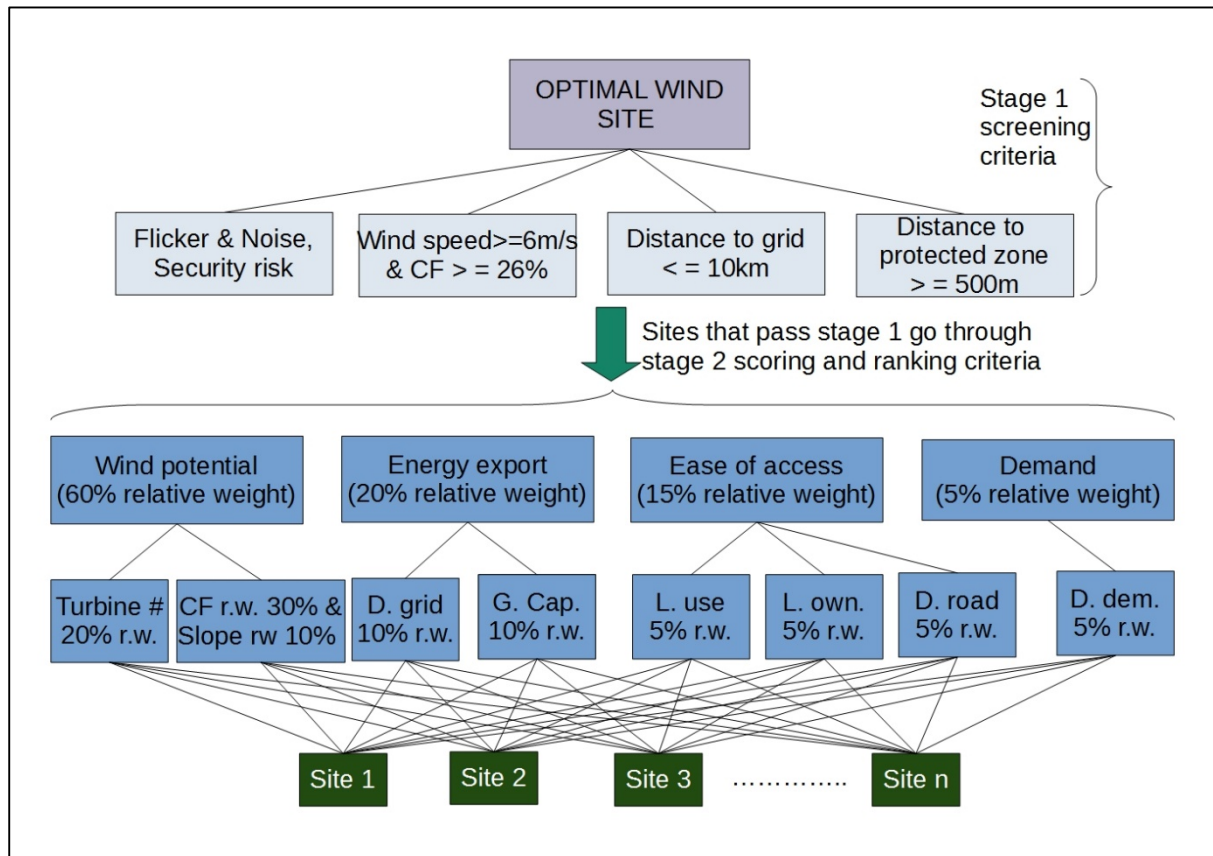


Figure 4D: showing 2 stage hierarchy structure for optimal onshore wind site selection.

Abbreviations: Turbines# - number of turbines, CF – capacity factor, r.w. – relative weight, D. grid – distance to grid, G. Cap. – grid capacity, L. use – land use, L. own – land ownership, D. road – distance to road, D. dem. – distance to demand centre, r.w. – relative weight.

Stage 2 scoring and ranking included the relative weight (r.w.) distribution of the wind potential (60% total r.w. comprising of “number of turbines” at 20% r.w. and “capacity factor” at 30%, terrain slope at 10%), energy export (20% total r.w. comprising of “distance to grid” at 10% r.w. and “capacity of grid” at 10% r.w.), ease of access (15% r.w. comprising land use, landownership and distance to road all with equal relative weight distribution) and demand (5% r.w. comprising of distance to demand centres).

4.4 Site Attribute Suitability Score

Adopted from extensive research (Höfer et al., 2016; Watson and Hudson, 2015; Uyan, 2013; Latinopoulos and Kechagia; Sunak et al., 2015; Jangid et al., 2016; Jankie, 2010; Chimres and Wongwises, 2016; Al Garni and Awasthi, 2017; Krewitt and Nitsch, 2003; Ho et al., 2015; Yue and Wang, 2006; Tanavud, 2004), three site attribute suitability tables were developed for the study and these include hybrid suitability (table 4A) looking at balanced parameters of wind and FPV, floating photovoltaics (table 4B) and onshore wind (table 4C). Since the solar

photovoltaics potential is more pronounced than wind in Zambia, the relative weight for FPV has been set higher than wind in [table 4A](#).

4.5 Summary

A site assessment appraisal and ranking methodology was developed for the potential of integrating floating photovoltaics and onshore wind on all hydropower plants in Zambia using multi-criteria decision-making (MCDM) approach. Further, three attribute suitability score tables were developed for single resource assessment (FPV or wind) and hybrid assessment (FPV and wind).

Whilst the methodology was developed for Zambia, the concepts can be internationally applied.

The next chapter applies the developed methodology on the actual hydro sites in Zambia which includes; initial screening and thereafter ranking suitable sites accordingly following the three attribute tables ([table 4A](#), [4B](#) and [4C](#)) developed.

Table 4A: showing Balanced Score.
 Table 4B: showing FPV Attribute Score.
 Table 4C: showing Wind Attribute Score.

Suitability score	Table 4a - Balanced Score Attribute Distribution				Energy Export (20% relative weight)		Ease of Access (15% relative weight)		Demand (5% rel. weight)	
	Wind potential (25% relative weight)	FPV Potential (35% relative weight)	Capacity Factor (%)	FPV distance to grid (km)	Wind distance to grid (km)	Grid capacity (MVA)	Land use	Land ownership	Distance to road (km)	Distance to demand (km)
High (100%)	>10	>10	>14	>2	0 - <15	>700	No current use	Customary / State	0-4	<=50
Medium (75%)	>5 - <10	>=7 - <14	-	>=5 - <2	>15 - <=30	<700 - >=400	-	-	4-8	50-100
Low (50%)	>=30 - <=35	>=14 - <20	-	>=7.5 - <5	>30 - <=45	<400 - >=100	-	-	8-12	100-150
Lowest (25%)	>=1 - <5	>=20 - <=30	-	<=10 - <7.5	>45 - <=60	<100 - >=1	Agriculture	Private	12-16	150-200
Unsuitable	0	<=26	>30	>10	>60	<1	Protected/sensitive land	-	-	>=200

Suitability score	Table 4b - Floating Photovoltaic (FPV) Attribute Score Distribution				Ease of Access (15% relative weight)		Demand (5% rel. weight)
	FPV Potential (60% relative weight)	Energy Export (20% relative weight)	Land use	Land ownership	Distance to road (km)	Distance to demand (km)	
High (100%)	>=10	>=2	No current use	Customary / State	0 - <=4	<=50	
Medium (75%)	>=1 - <10	>=5 - <2	-	-	>4 - <=8	>50 - <=100	
Low (50%)	>=0.1 - <1	>=7.5 - <5	-	-	>8 - <=12	>100 - <=150	
Lowest (25%)	>=0.004 - <0.1	<=10 - <7.5	Agriculture	Private	>12 - <=16	>150 - <=200	
Unsuitable	<0.004	>10	Protected/sensitive land	-	-	>200	

Suitability score	Table 4c - Onshore Wind Attribute Score Distribution				Ease of Access (15% relative weight)		Demand (5% relative weight)
	Wind potential (60% relative weight)	Energy Export (20% relative weight)	Land use	Land ownership	Distance to road (km)	Distance to demand (km)	
High (100%)	>10	>=2	No current use	Customary / State	0 - <=4	<=50	
Medium (75%)	>5 - <10	>=7 - <14	-	-	>4 - <=8	50-100	
Low (50%)	>=30 - <=35	>=14 - <20	-	-	>8 - <=12	100-150	
Lowest (25%)	>=1 - <5	>=20 - <=30	Agriculture	Private	>12 - <=16	150-200	
Unsuitable	0	<=26	Protected/sensitive land	-	-	>=200	

CHAPTER FIVE: APPLICATION OF SITE ASSESSMENT, SCREENING & RANKING METHODOLOGY

This chapter describes the application of the site assessment, screening and ranking methodology. This scope ranged from site identification, filtering and ranking of sites based on assigned relative weight and attribute suitability scores as adopted from literature, industry practice and stakeholder engagement. [Section 5.1](#) describes the data collection which included site identification and mapping. [Section 5.2](#) illustrates the screening and filtering process of sites. [Section 5.3](#) scores and ranks the potential sites according to three attribute suitability levels (hybrid, floating PV and onshore wind scoring). Furthermore, [section 5.4](#) examines the uncertainties introduced in the assumptions made when building the multi-criteria decision-making (MCDM) models and the limitations in the methodology application process. Thereafter, [section 5.5](#) gives a summary about the chapter highlighting key points and outcomes.

5.1 Data Collection & Mapping

This section outlines the data collection process which involved stakeholder engagement and information retrieval from websites and published reports (i.e. ZESCO website, energy sector report from energy regulation board - ERB, ministry of energy – MOE etc). [Section 5.1.1](#) identifies the sites (hydropower plant) for which the methodology is to be applied to. [Section 5.1.2](#) maps the photovoltaics potential using QGIS and includes the location of the hydro sites. [Section 5.1.3](#) maps the wind resource potential using global wind atlas (GWA) and DNV GL wind mapping system (WMS). [Section 5.1.4](#) maps the actual location of the FPV, and wind sites using google earth pro based on the QGIS and GWA inputs. [Sections 5.1.5](#) and [5.1.6](#) presents the actual floating PV and wind power output at the mapped sites respectively. [Appendix A](#) shows the detailed project data tables used for screening and ranking of sites for both floating PV and wind.

5.1.1 Site Identification

The sites of interest included 6 reservoir type, 2 pondage type and 6 run-of-river type hydro's as shown in [table 5A](#).

Table 5A: showing the identification of hydro sites under study

No.	HYDRO POWER STATION	COORDINATES	RATING (MW)	OWNER	RIVER	COUNTRY	TYPE	NOTES
1	Kafue Gorge Upper Power Station	15°48'25.0"S 28°25'16.0"E	990	Zesco	Kafue	Zambia	Reservoir	Grid
2	Kariba North Bank Power Station	16°31'20.0"S 28°45'42.0"E	1080	Zesco	Zambezi	Zambia	Reservoir	Grid
3	Kafue Gorge Lower Power Station	15°53'46.0"S 28°33'33.0"E	750	Zesco	Kafue	Zambia	Reservoir	Grid
4	Itezhi-Tezhi Power Station	15°45'55.0"S 26°01'05.0"E	120	Zesco/ITPC	Kafue	Zambia	Reservoir	Grid
5	Lusiwasi Upper Power Station	12°59'18.2"S 30°51'53.6"E	15	Zesco	Lusiwasi	Zambia	Pondage	Grid
6	Lusiwasi Lower Power Station	12°59'18.2"S 30°51'53.6"E	12	Zesco	Lusiwasi	Zambia	Pondage	Grid
7	Lunzua Power Station	8°48'06.4"S 31°20'18.3"E	14.8	Zesco	Lunzua	Zambia	Run-of-River	Grid
8	Musonda Power station	10°42'39.5"S 28°48'23.1"E	10	Zesco	Luongo	Zambia	Run-of-River	Grid
9	Chishimba Power station	10°06'29.8"S 30°55'02.7"E	6	Zesco	Luombe	Zambia	Run-of-River	Grid
10	Shiwangandu Power Station	11°13'10.25"S 31°45'0.61"E	1	Zesco	Munshya	Zambia	Run-of-River	Grid
11	Lunsemfwa Hydro Power Station	14°29'33.7"S 29°06'54.6"E	24	LHPC	Lunsemfwa	Zambia	Reservoir	Grid
12	Mulungushi Hydro Power Station	14°43'47.48"S 28°50'39.22"E	32	LHPC	Lunsemfwa	Zambia	Reservoir	Grid
13	Victoria Falls Power Station	17°55'52.5"S 25°51'37.9"E	108	Zesco	Zambezi	Zambia	Run-of-River	Grid
14	Zengamina Power Station	11°07'26.0"S 24°11'32.0"E	0.7			Zambia	Run-of-River	Off-Grid

5.1.2 Photovoltaics Parameter QGIS Mapping

This section shows the maps created in QGIS related to photovoltaic potential distribution in Zambia. The mapping was customized by including hydro sites using the world bank QGIS project file with selected datasets and layers for solar PV potential in Zambia (GSA World Bank). Further, all the data used for mapping spans from 1994 to 2017. Figure 5A shows the direct normal irradiation (DNI) distribution in kWh/m², figure 5B shows the diffuse horizontal irradiation (DIF) distribution in kWh/m², figure 5C shows the global horizontal irradiation (GHI) in kWh/m², figure 5D shows the global irradiation at optimum tilt (GTI) in kWh/m², figure 5e shows the monthly air temperature distribution in °C, figure 5F shows the optimum tilt angle(OPTA) in degrees to maximise yearly PV production and the photovoltaic electricity production (PVOUT) in kWh/kWp is shown in figure 5G.

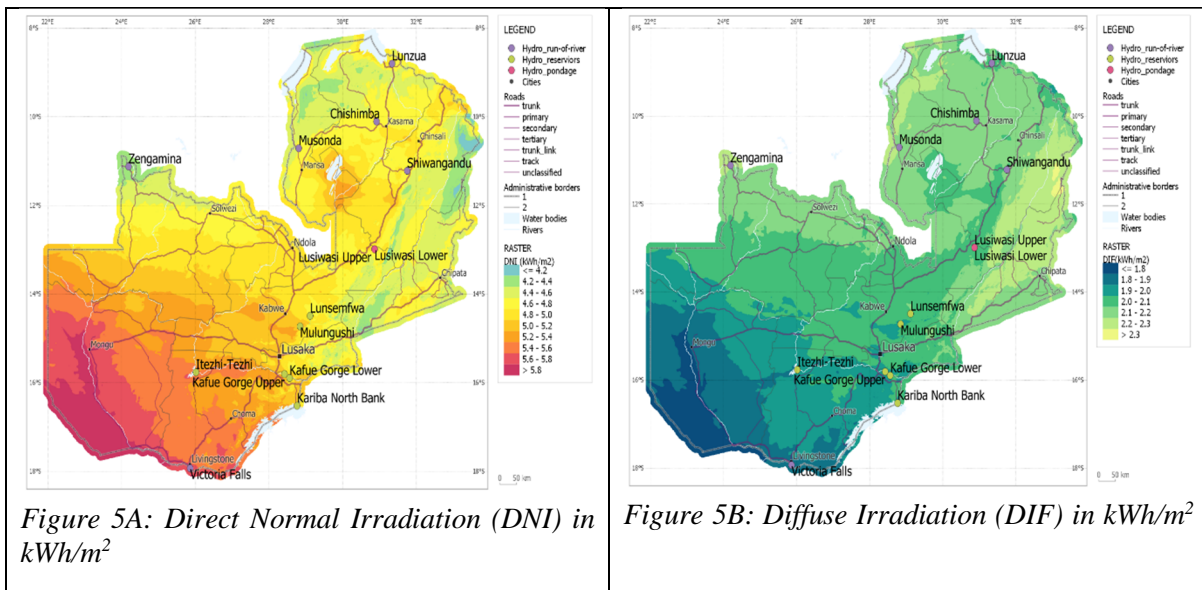


Figure 5A: Direct Normal Irradiation (DNI) in kWh/m²

Figure 5B: Diffuse Irradiation (DIF) in kWh/m²

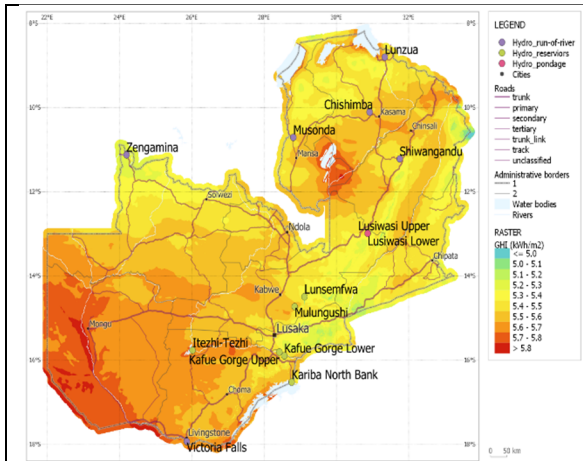


Figure 5C: Global Horizontal Irradiation (GHI) in kWh/m²

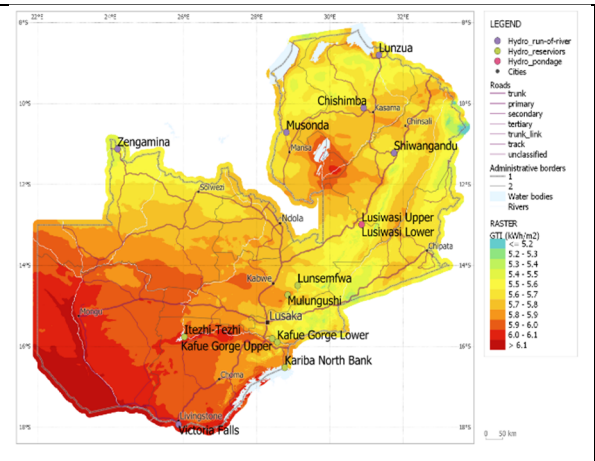


Figure 5D: Global Tilted Irradiation (GTI) in kWh/m²

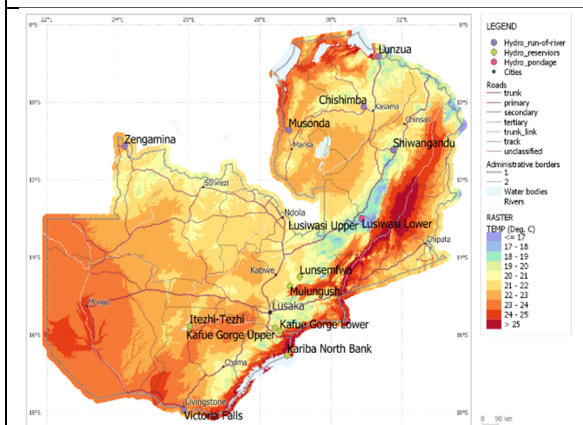


Figure 5E: Temperature Distribution in °C

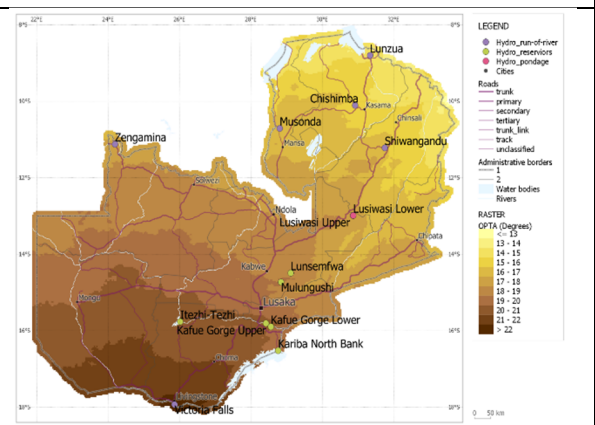


Figure 5F: Optimal Tilt Angle (OPTA) in degrees

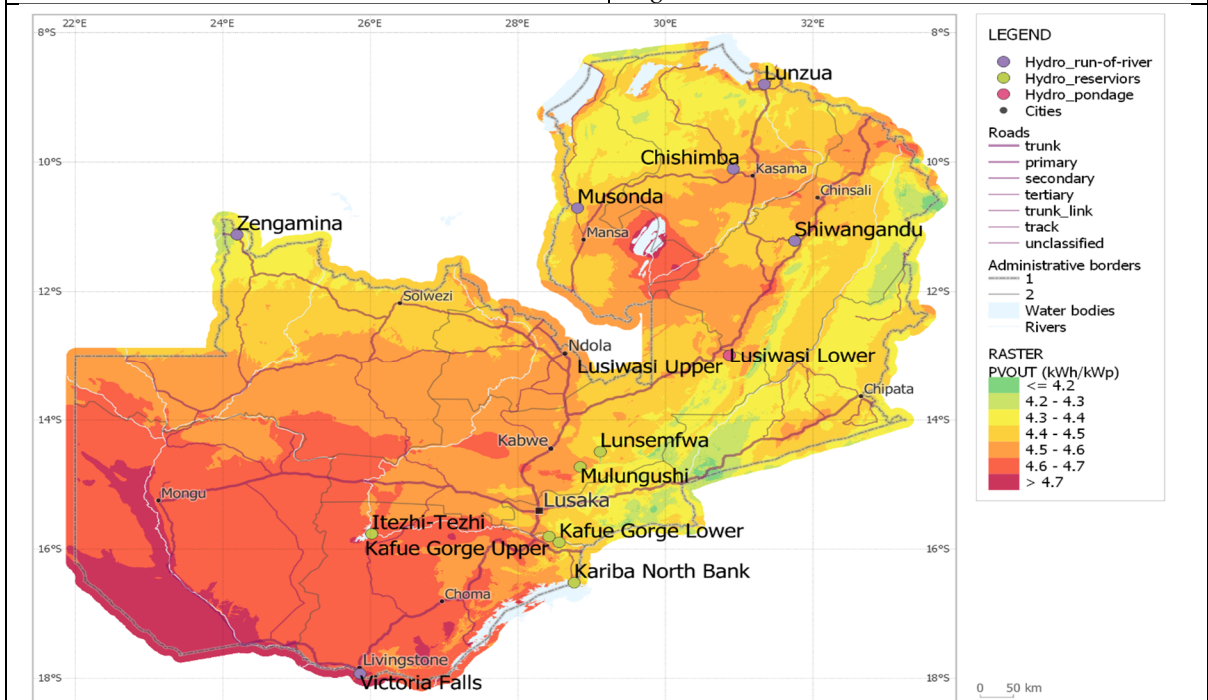


Figure 5G: showing hydro sites & long-term yearly average of potential photovoltaic electricity production (PVOUt) in kWh/kWp

5.1.3 Wind Parameter Mapping

This section shows the mapping of seasonal wind speed (figure 5N) and wind site assessment related parameters (slope – figure 5H, elevation – figure 5I, wetlands and bird area-figure 5H, roughness length – figure 5K, land tenure – figure 5L and electrical infrastructure – figure 5M).

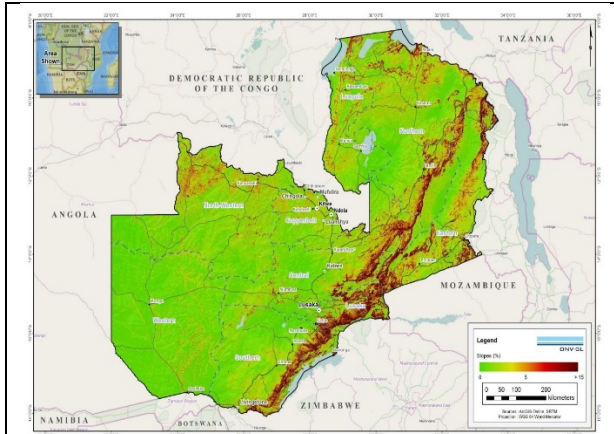


Figure 5H: showing average terrain slope distribution in Zambia (source: World Bank & DNV GL 2015)

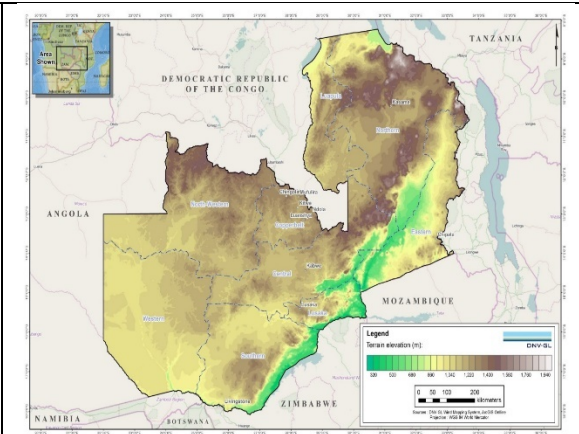


Figure 5I: showing terrain elevation distribution (source: World Bank & DNV GL 2015)

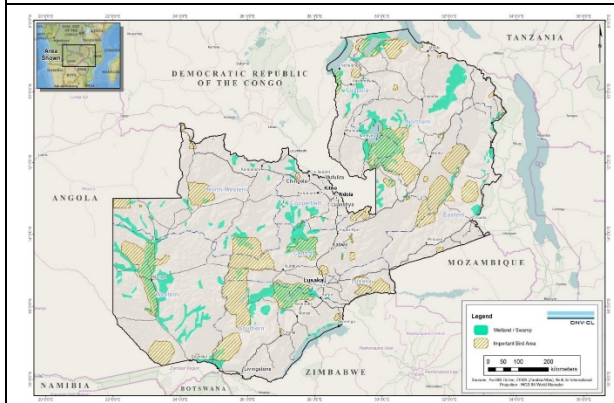


Figure 5J: showing wetlands & important bird areas (source: World Bank & DNV GL 2015)

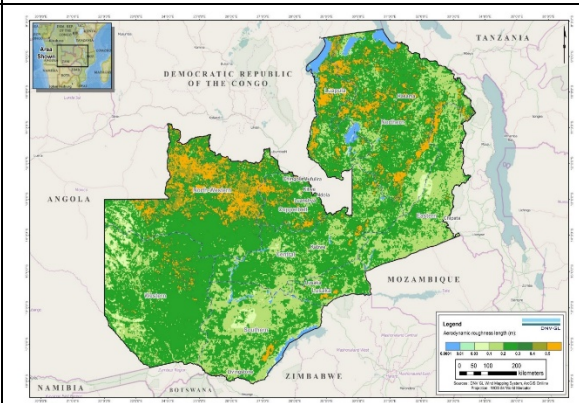


Figure 5K: showing aerodynamic roughness length (source: World Bank & DNV GL 2015)

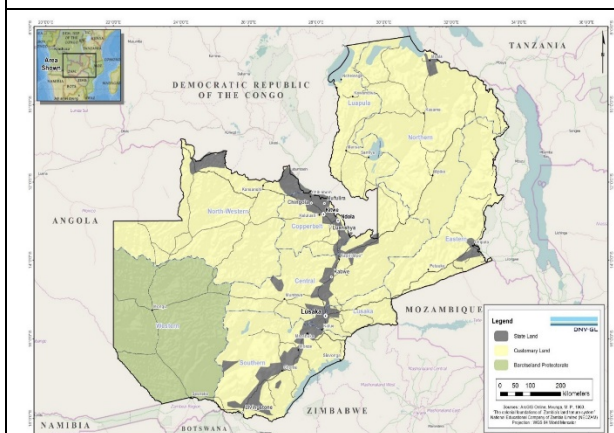


Figure 5L: showing the land tenure distribution (source: World Bank & DNV GL 2015)

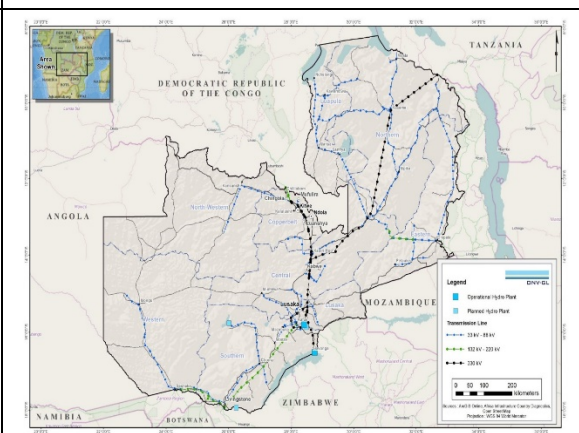
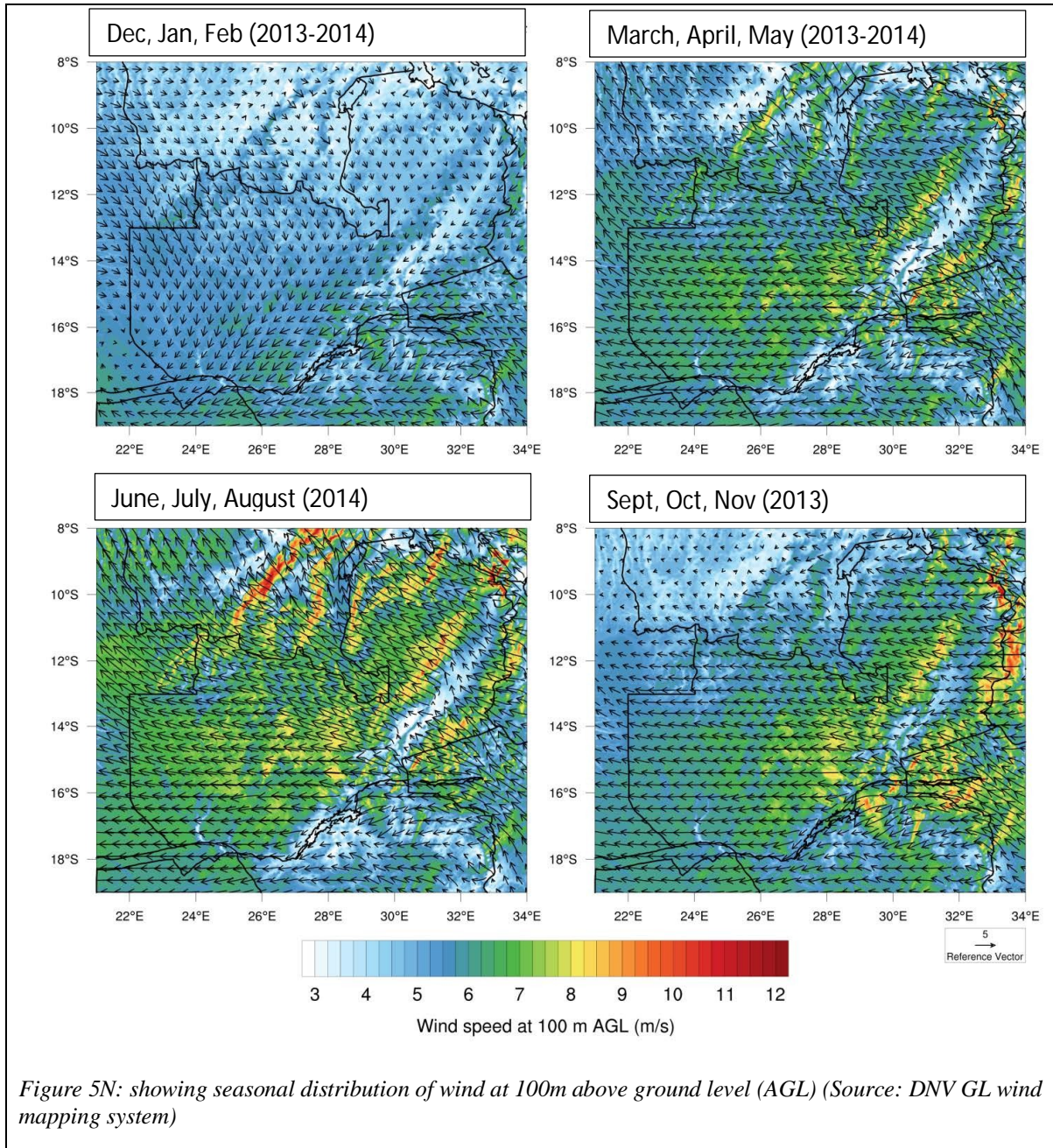


Figure 5M: showing power generation and transmission (source: World Bank & DNV GL 2015)



According to figure 5N, the wind speeds in Zambia are generally weak between December and February (upper left-hand map). Though, the situation is different for period between June and November, where the global wind atlas indicates average wind speeds of 7 to 8 m/s over much of the country between June and August, with high winds of 9 to 11 m/s over Nyika Plateau in the north, high mountains in northern parts of Zambia and Muchinga mountains.

5.1.4 Google Earth Pro FPV & Wind Site Mapping

Based on the resource assessment and mapping in sections 5.1.2 and 5.1.3, the actual floating PV and wind sites near the hydropower plant were mapped using google earth pro. However, only six sites (three FPV and three wind) are shown in figure 50 for illustrative purposes.

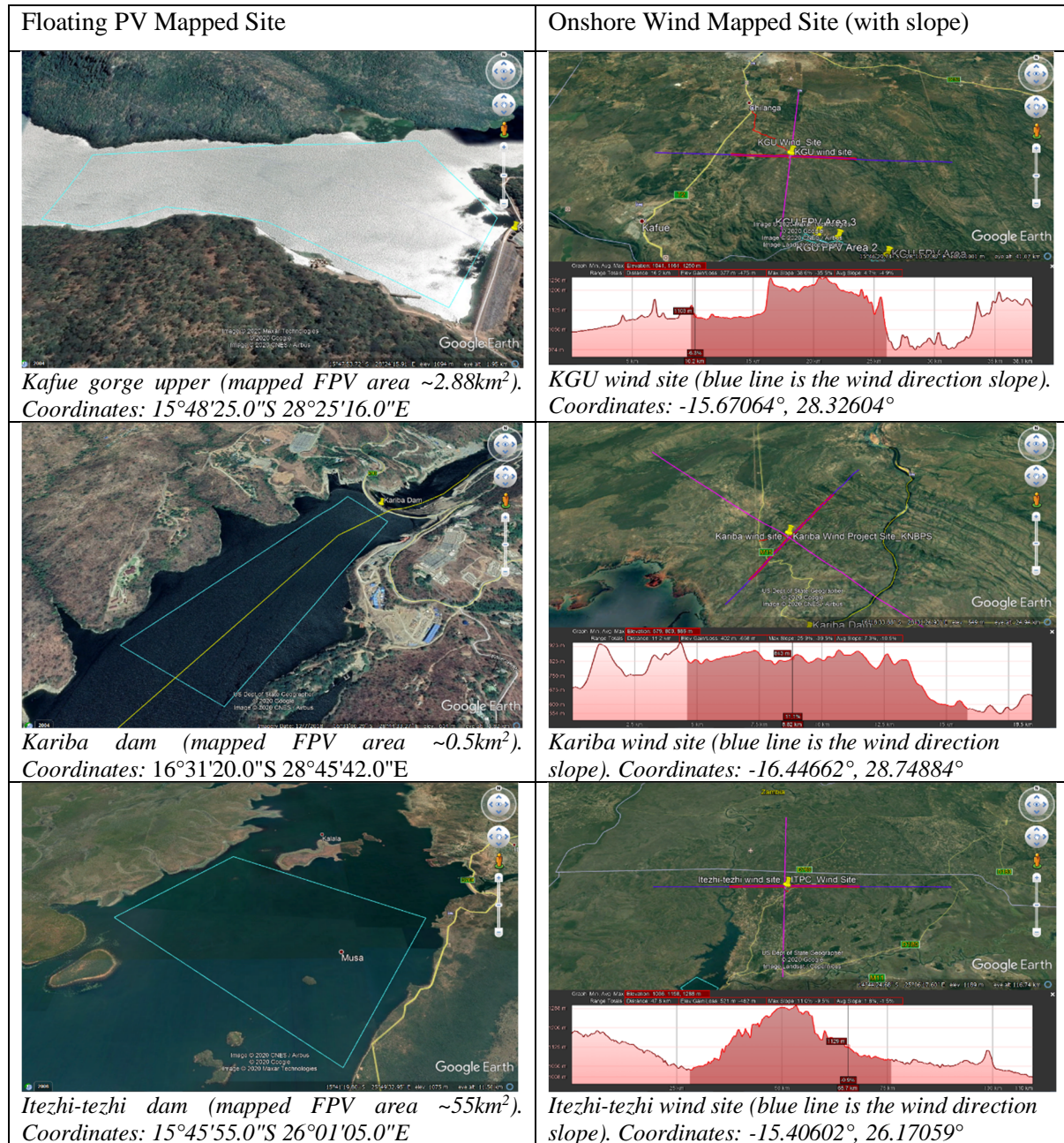


Figure 50: showing some mapped FPV and wind sites in google earth pro

5.1.5 Floating Photovoltaic Output Potential

This section illustrates the FPV output potential for all the sites under consideration. Four graphs are used to depict this site comparison, and these include the capacity factors of all potential sites as shown in figure 5P(obtained using renewables ninja), figure 5Q shows the optimal tilt angle of sites obtained using global solar atlas, figure 5R shows the summation of monthly totals of direct normal irradiation in kWh/m² and FPV output in kWh/kWp, while figure 5S shows the site generation potential in GWh.

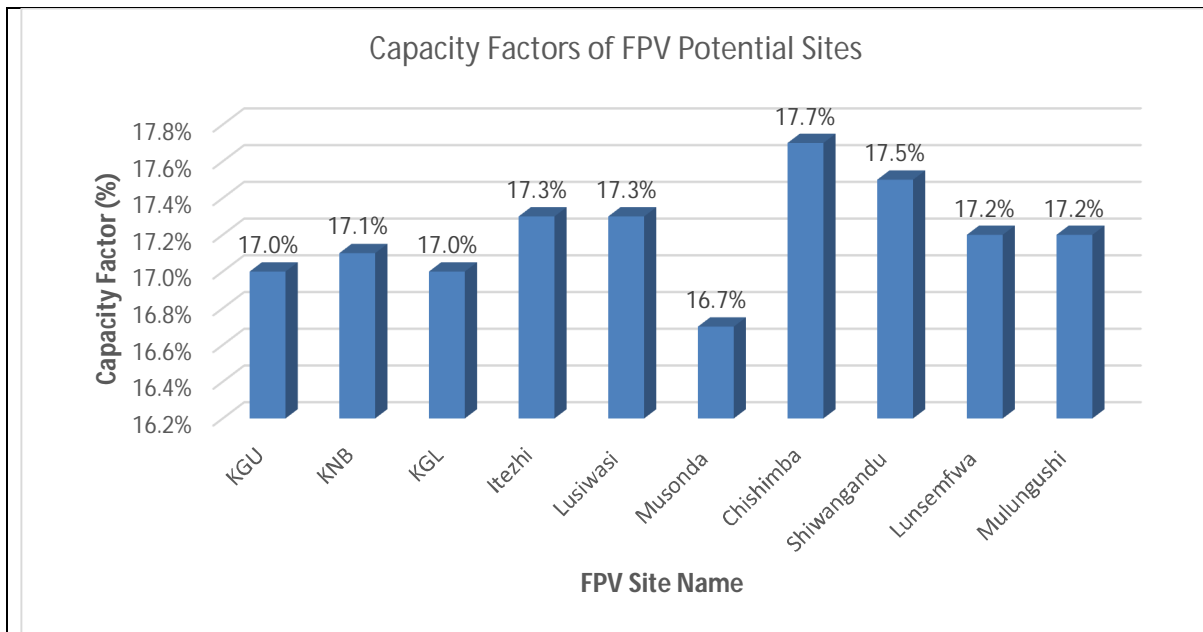


Figure 5P: showing site capacity factors for 2019 weather data from MERRA-2 dataset

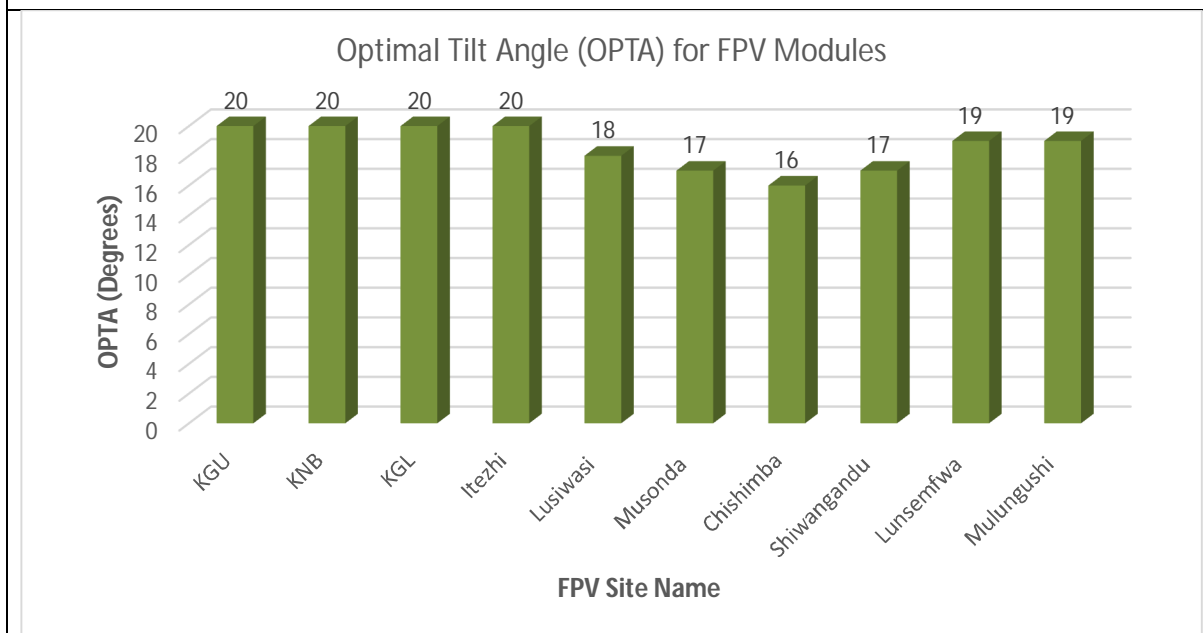


Figure 5Q: showing site optimal tilt angle based on the updated ESMAP for Zambia

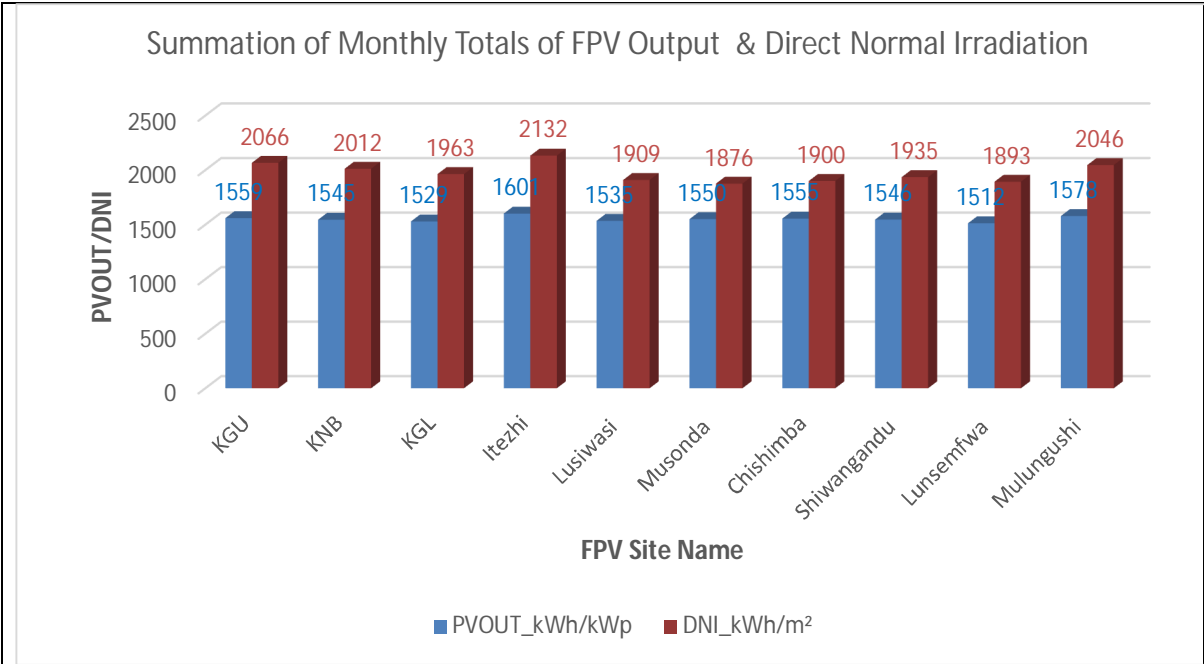


Figure 5R: shows the Summation of Monthly Totals of FPV Output (kWh/kWp) & Direct Normal Irradiation (kWh/m²)

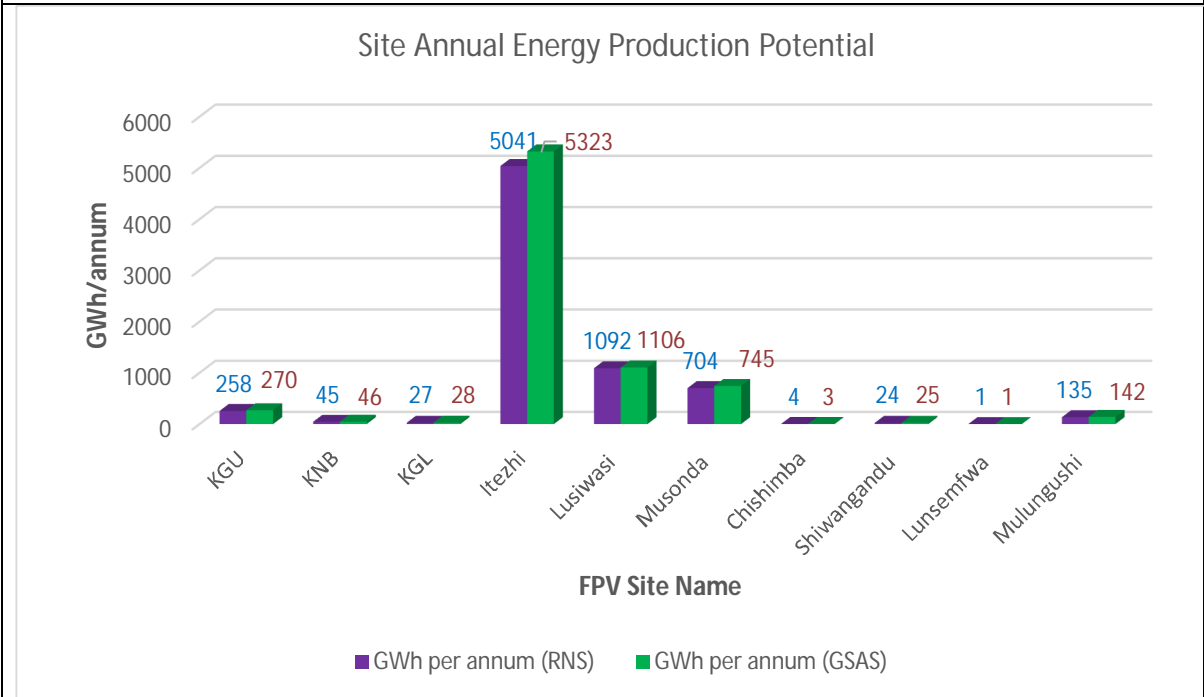
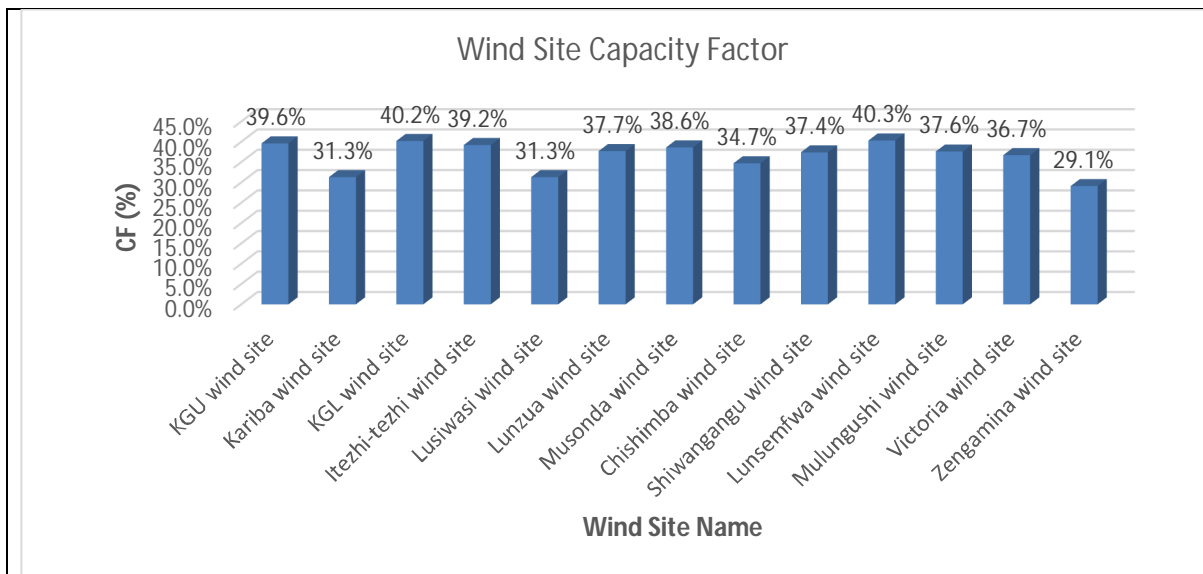


Figure 5S: showing the site energy production potential using renewables ninja and global solar atlas updated datasets.

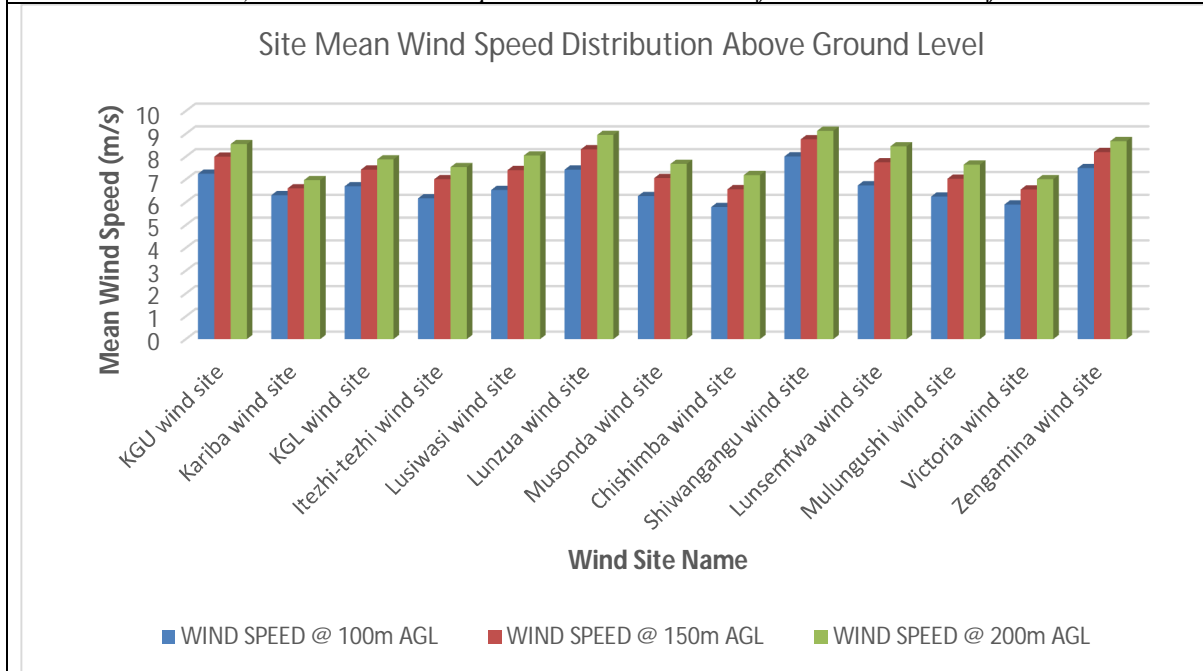
Where RNS – Renewable Ninja Simulation, GSAS – Global Solar Atlas Simulation. The GSAS has higher energy yield due to the temperature compensation capability in global solar atlas (except for Chishimba site which has a lower value of 3 compared to the RN value of 4).

5.1.6 Wind Output Potential

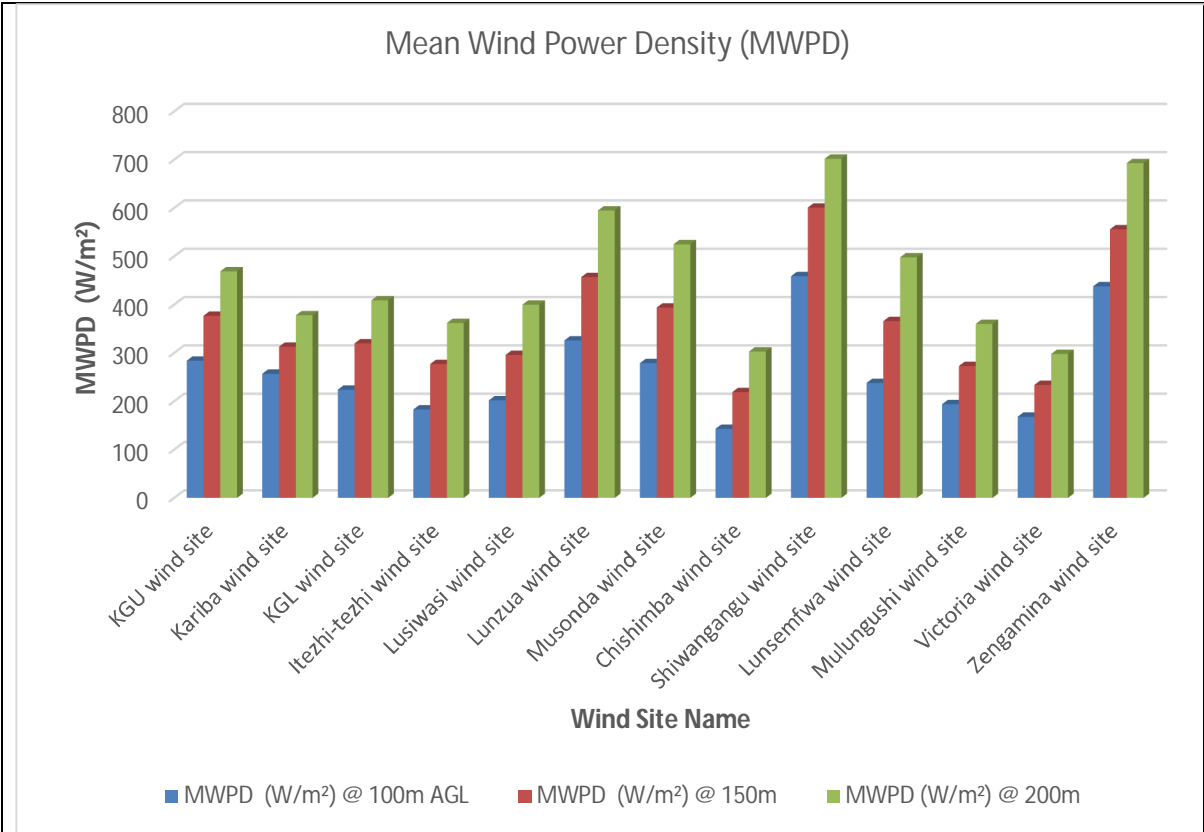
The wind turbine characteristics of the wind farm for each site was adopted from recent study conducted by the world bank and DNV GL titled “wind resource mapping in Zambia – 12month site resource report” (ESMAP and World Bank, 2018). Each site in the current study has 25 turbines and used the Siemens SWT DD 142 turbine model for simulations in renewables ninja (i.e. 4 MW power rating per turbine, 129 m hub height, 142 m rotor diameter). Figure 5T shows the wind potential output per site (i.e. wind capacity factor, mean wind speed distribution, mean wind power density and energy output in giga-watt hour).



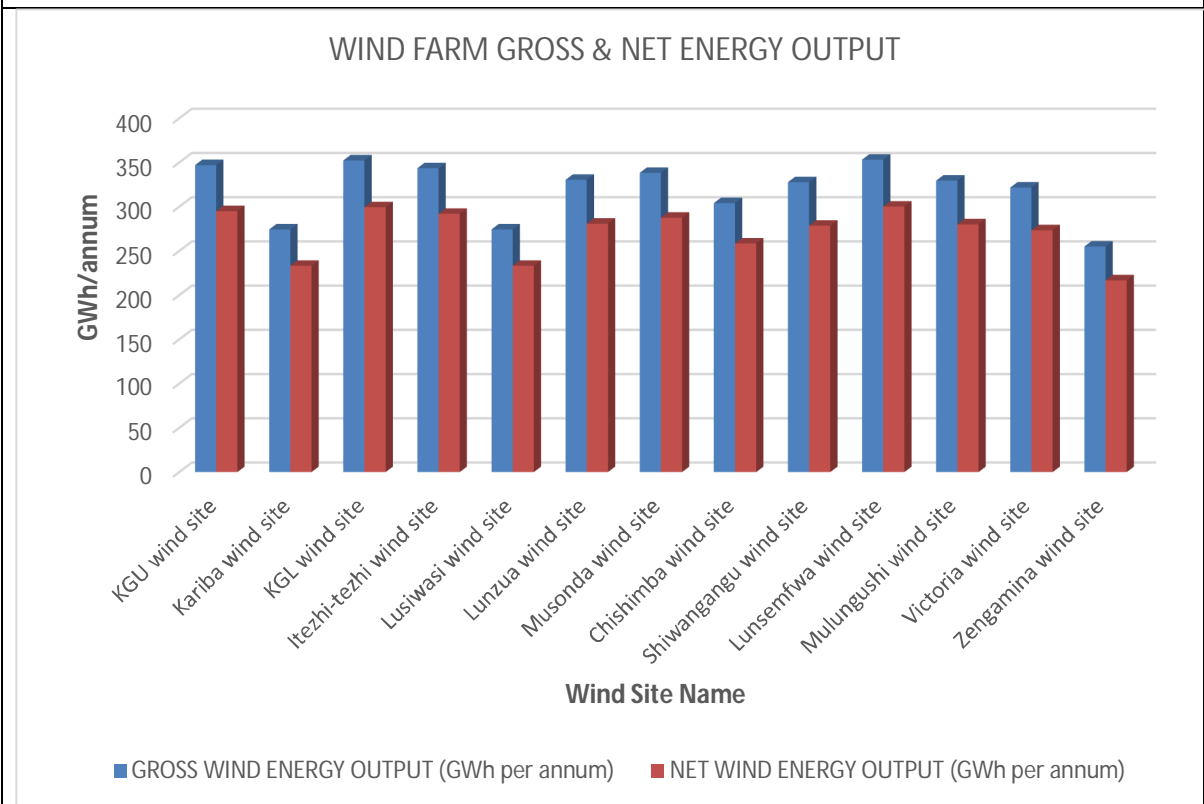
showing wind capacity factor using the Siemen SWT DD 142 turbine model (4MW rating, 129m hub height, 142m rotor diameter). Data based on the updated MERRA-2 dataset from Renewables Ninja.



showing mean wind speed distribution from global wind atlas (GWA). AGL – Above ground level



showing the mean wind power density at different heights above ground level from GWA



showing the wind farm gross energy output and the net energy output in GWh/annum at 85% assumed efficiency.

Figure 5T: showing wind potential output for each site

5.2 Stage 1 Screening

This section presents the screening and filtering criteria for floating PV and onshore wind.

FPV Stage 1 screening

Five criteria were defined in the FPV site screening process and these include surface area greater or equal to 4000 m², capacity factor greater or equal to 14 percent, distance to existing electrical grid less or equal to 10 km and distance to protected zones (i.e. national parks) greater or equal to 500 m, shown in [table 5B](#). With this benchmark, three run-of-river type sites (Lunzua, Victoria and Zengamina) failed on account of having a small area to accommodate an economically/commercially viable FPV project. The graphical distribution of this screening process is shown in [figures 5U and 5V](#).

Table 5B: showing the FPV stage 1 screening criteria

	Criteria 1 Area >=4000 (m2)	Criteria 2 CF >=14%	Criteria 3 Distance to grid (<=10km)	Criteria 4 Distance to protected zone (>=500)
Out of 6 Reservoir Type	6	6	6	6
Out of 2 Pondage Type	2	2	2	2
Out of 6 Run-of-River Type	3	6	6	6

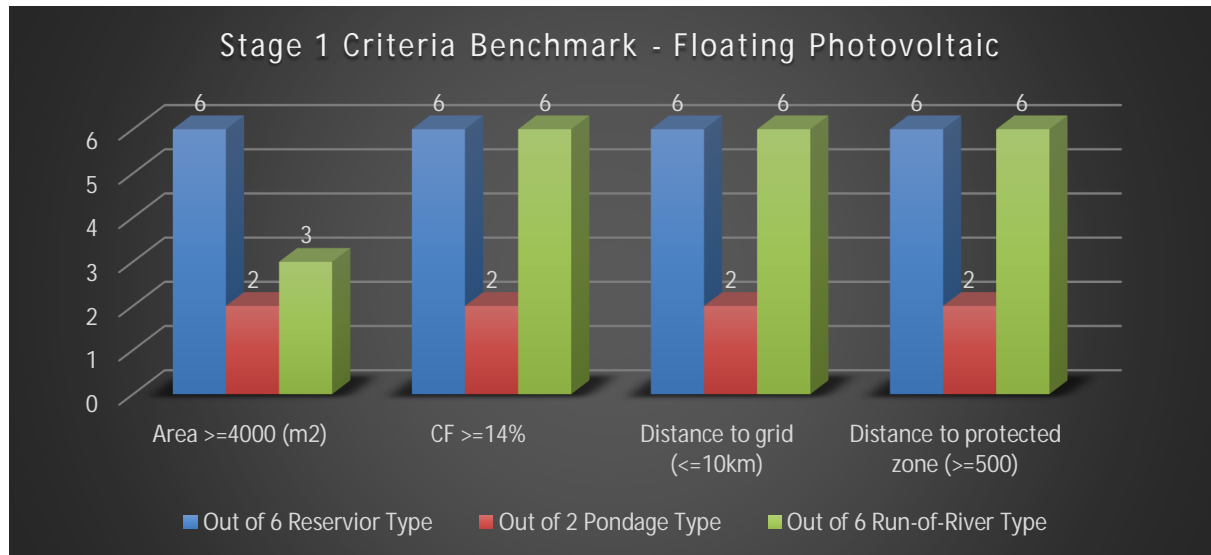


Figure 5U: showing FPV stage 1 criteria benchmark

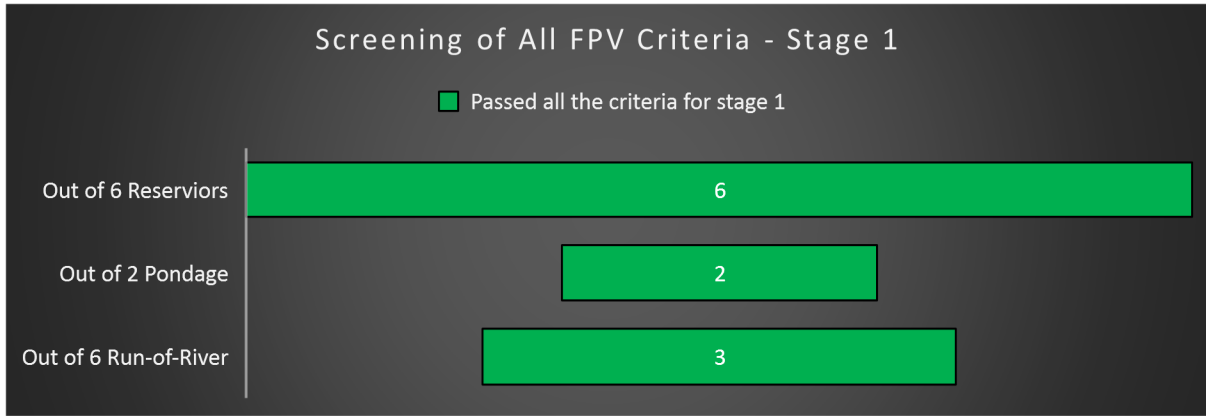


Figure 5V: showing the number of FPV sites that passed each defined criterion

Wind stage 2 screening

Six criteria were defined for onshore wind site filtering and these include capacity factor greater or equal to 26 percent, distance to grid less or equal to 60 km, flicker and noise allowance at five rotor diameter, wind speed value greater or equal to 6 m/s at 150 m above ground level, distance to protected zone greater or equal to 500 m and security risk of installation, table 5C. Only Zengamina wind site was filtered off due to proximity to security risk zone bordering the Democratic Republic of Congo, similar findings were obtained by the World Bank and DNV GL when selecting areas to install wind validation masts. Figure 5W shows the wind criteria benchmark distribution for all the sites.

Table 5C: showing defined screening and filtering for onshore wind

	Criteria 1	Criteria 2	Criteria 3	Criteria 4	Criteria 5	Criteria 6
	CF >= 26%	Distance to grid (<=60km)	Flicker and Noise (5D)	Windspeed >=6m/s @ 150m AGL	Distance to protected zone (>=500)	Security risk
Out of 6 Wind Sites Near Reservoir Type	6	6	6	6	6	6
Out of 2 Wind Sites Near Pondage Type	2	2	2	2	2	2
Out of 6 Wind Site Near Run-of-River	6	6	6	6	6	5

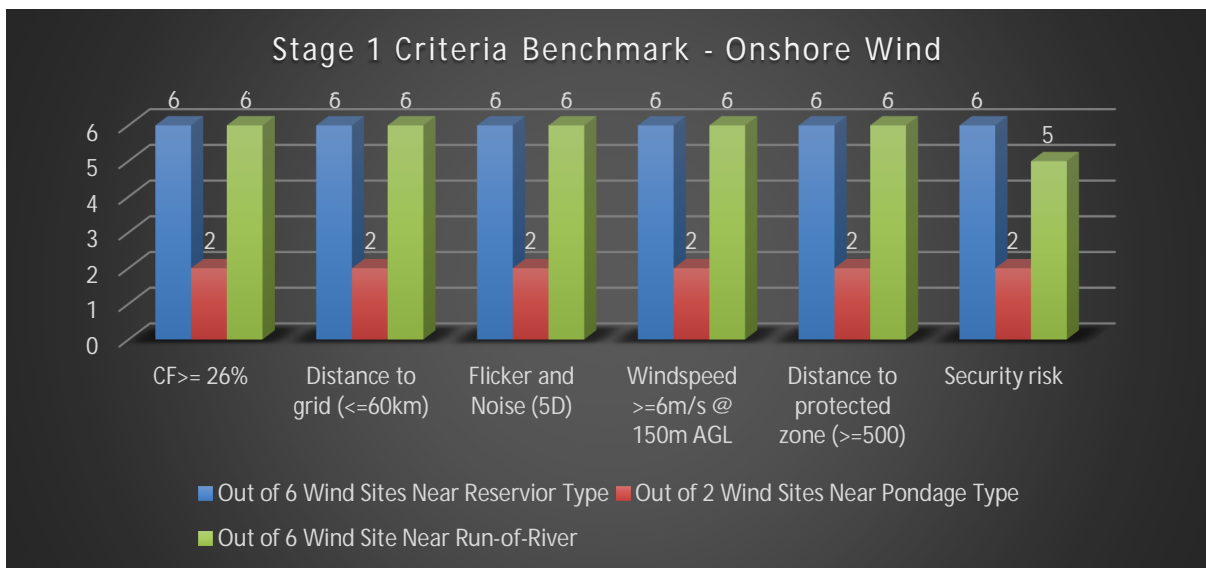


Figure 5W: showing onshore wind stage 1 criteria benchmark

Summary of Stage 1 Screening

The combined stage 1 screening outcome for both floating PV and onshore wind sites is given in [table 5D](#). The results of the screening process show that only 10 sites (i.e. Kafue gorge upper (KGU), Kariba north bank, Kafue gorge lower (KGL), Itezhi-tezhi, Lusiwasi, Musonda, Chishimba, Shiwangandu, Lunsemfwa, and Mulungushi) are viable to move to stage 2 scoring and ranking of potential floating PV and wind.

Table 5D: showing the combined stage 1 screening outcome for both FPV and onshore wind sites

Name of Site	Screening Criteria (Yes/No)						
	Capacity Factor	Area	Distance to protected zone	Distance to grid/substation	Flicker and Noise distance	Wind speed (m/s)	Security risk
KGU FPV / wind site	Yes	Yes	Yes	Yes	Yes	Yes	Yes
Kariba FPV / wind site	Yes	Yes	Yes	Yes	Yes	Yes	Yes
KGL FPV / wind site	Yes	Yes	Yes	Yes	Yes	Yes	Yes
Itezhi-tezhi FPV / wind site	Yes	Yes	Yes	Yes	Yes	Yes	Yes
Lusiwasi FPV/ wind site	Yes	Yes	Yes	Yes	Yes	Yes	Yes
Lunzua FPV / wind site	Yes	No	Yes	Yes	Yes	Yes	Yes
Musonda FPV / wind site	Yes	Yes	Yes	Yes	Yes	Yes	Yes
Chishimba FPV / wind site	Yes	Yes	Yes	Yes	Yes	Yes	Yes
Shiwangandu FPV/ wind site	Yes	Yes	Yes	Yes	Yes	Yes	Yes
Lunsemfwa FPV / wind site	Yes	Yes	Yes	Yes	Yes	Yes	Yes
Mulungushi FPV / wind site	Yes	Yes	Yes	Yes	Yes	Yes	Yes
Victoria FPV wind site	Yes	No	Yes	Yes	Yes	Yes	Yes
Zengamina FPV / wind site	Yes	No	Yes	Yes	Yes	Yes	No

5.3 Stage 2 Scoring & Ranking

This section presents the scoring and ranking process of the 10 sites that passed the screening stage. Three scoring and ranking options have been developed for the sites and these include the balanced ranking which balances the FPV and wind criteria for a possible hybrid system ([section 5.3.1](#)), the floating PV ranking which only looks at the prospects of developing FPV ([section 5.3.2](#)) and onshore wind ranking for locations with good wind resource but constrained with FPV development or deployment ([section 5.3.3](#)). However, it is worth noting that floating photovoltaics (35percent) is given a higher relative weight in the balanced ranking in comparison to wind (25percent) because Zambia has a more pronounced solar irradiation than wind speed for FPV and wind development respectively.

5.3.1 Hybrid Balanced Ranking

Table 5E illustrates the site balanced ranking for hybrid system prospects using the weighted sum method. The relative weight distribution is as follows; 25% for wind potential, 35% for FPV potential, 20% for energy export, 15% for ease of access and 5% for demand. Figure 5X shows the application of the weighted sum equation taking “FPV distance to grid” under the “Energy export” attribute layer. The results of this process places Itezhi-tezhi and Kafue gorge upper (KGU) at first and second rank with total attribute values of 90% and 86.9 % respectively, while Chishimba site is ranked the least with 70.6% total combined attribute value.

Table 5E: showing balanced scoring and ranking matrix table

Rank#	Name of Site	Wind potential (25% weight)				FPV Potential (35% weight)			
		score*weight (10%)	score*weight (10%)	score*weight (5%)	Σ	score*weight (17.5%)	score*weight (17.5%)	Σ	FPV Total
=1'	Itezhi-tezhi FPV / wind site	10.0%	7.5%	5.0%	22.5%	17.5%	17.5%	35.0%	
=2'	KGU FPV / wind site	10.0%	7.5%	3.8%	21.3%	13.1%	17.5%	30.6%	
=3'	KGL FPV / wind site	10.0%	10.0%	5.0%	25.0%	8.8%	17.5%	26.3%	
=4'	Kariba FPV / wind site	10.0%	5.0%	3.8%	18.8%	8.8%	17.5%	26.3%	
=5'	Lusiwasi FPV/ wind site	10.0%	5.0%	5.0%	20.0%	17.5%	17.5%	35.0%	
=6'	Musonda FPV / wind site	10.0%	7.5%	5.0%	22.5%	13.1%	17.5%	30.6%	
=6'	Mulungushi FPV / wind site	10.0%	7.5%	5.0%	22.5%	13.1%	17.5%	30.6%	
=8'	Shiwangangu FPV/ wind site	10.0%	7.5%	3.8%	21.3%	8.8%	17.5%	26.3%	
=9'	Lunsemfwa FPV / wind site	10.0%	10.0%	5.0%	25.0%	4.4%	17.5%	21.9%	
=10'	Chishimba FPV / wind site	10.0%	5.0%	5.0%	20.0%	4.4%	17.5%	21.9%	

Rank#	Name of Site	Energy Export (20% weight)				Ease of Access (15% weight)			Demand (5% weight)		Site Total (100% weight)	
		score*weight (5%)	score*weight (5%)	score*weight (5%)	Σ	score*weight (5%)	score*weight (5%)	score*weight (5%)	Σ	score*weight (5%)		Σ
=1'	Itezhi-tezhi FPV / wind site	5.0%	2.5%	5.0%	12.5%	5.0%	5.0%	5.0%	15.0%	5.0%	5.0%	90.0%
=2'	KGU FPV / wind site	5.0%	3.8%	10.0%	18.8%	5.0%	5.0%	1.3%	11.3%	5.0%	5.0%	86.9%
=3'	KGL FPV / wind site	2.5%	2.5%	10.0%	15.0%	5.0%	5.0%	3.8%	13.8%	5.0%	5.0%	85.0%
=4'	Kariba FPV / wind site	5.0%	5.0%	10.0%	20.0%	5.0%	5.0%	5.0%	15.0%	5.0%	5.0%	85.0%
=5'	Lusiwasi FPV/ wind site	5.0%	5.0%	2.5%	12.5%	5.0%	5.0%	5.0%	15.0%	2.5%	2.5%	85.0%
=6'	Musonda FPV / wind site	1.3%	5.0%	2.5%	8.8%	5.0%	5.0%	5.0%	15.0%	2.5%	2.5%	79.4%
=6'	Mulungushi FPV / wind site	2.5%	5.0%	2.5%	10.0%	5.0%	5.0%	3.8%	13.8%	2.5%	2.5%	79.4%
=8'	Shiwangangu FPV/ wind site	5.0%	5.0%	2.5%	12.5%	5.0%	5.0%	3.8%	13.8%	2.5%	2.5%	76.3%
=9'	Lunsemfwa FPV / wind site	5.0%	1.3%	2.5%	8.8%	5.0%	5.0%	5.0%	15.0%	2.5%	2.5%	73.1%
=10'	Chishimba FPV / wind site	5.0%	3.8%	2.5%	11.3%	5.0%	5.0%	5.0%	15.0%	2.5%	2.5%	70.6%

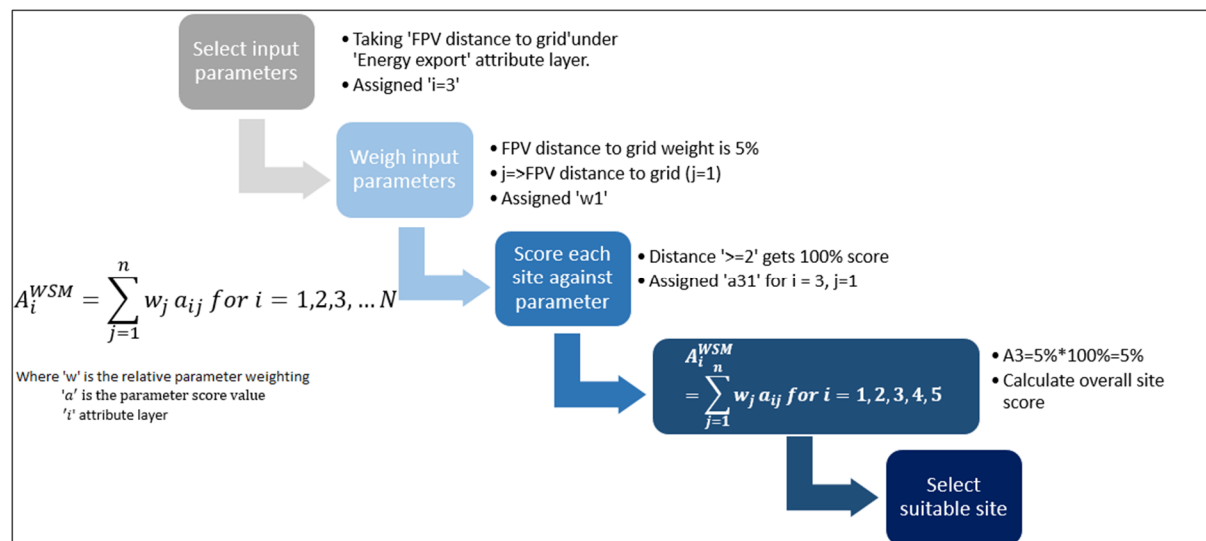


Figure 5X: showing application of the weighted sum equation under balanced scoring and ranking

5.3.2 Floating PV Ranking

Table 5F shows the site floating photovoltaics ranking prospects using the weighted sum method. The relative weight distribution is as follows; 60% for FPV potential, 20% for energy export, 15% for ease of access and 5% for demand. Figure 5Y shows the application of the weighted sum equation taking “FPV surface area” under the “FPV potential” attribute layer. The results of this process places Itezhi-tezhi and Kafue gorge upper (KGU) at first and second rank with total attribute values of 95% and 92.5 % respectively, while Chishimba site is ranked the least with 67.5% total combined attribute value.

Table 5F: showing floating PV scoring and ranking matrix table

Rank#	Name of Site	FPV Potential (60% weight)			Energy Export (20% weight)		
		score*weight (30%)	score*weight (30%)	Σ	score*weight (10%)	score*weight (10%)	Σ
=1'	Itezhi-tezhi FPV	30.0%	30.0%	60.0%	10.0%	5.0%	15.0%
=2'	KGU FPV	22.5%	30.0%	52.5%	10.0%	10.0%	20.0%
=3'	Lusiwasi FPV	30.0%	30.0%	60.0%	10.0%	2.5%	12.5%
=4'	Kariba FPV	15.0%	30.0%	45.0%	10.0%	10.0%	20.0%
=5'	KGL FPV	15.0%	30.0%	45.0%	5.0%	10.0%	15.0%
=6'	Shiwangangu FPV	15.0%	30.0%	45.0%	10.0%	2.5%	12.5%
=6'	Mulungushi FPV	22.5%	30.0%	52.5%	5.0%	2.5%	7.5%
=8'	Musonda FPV	22.5%	30.0%	52.5%	2.5%	2.5%	5.0%
=9'	Lunsemfwa FPV	7.5%	30.0%	37.5%	10.0%	2.5%	12.5%
=9'	Chishimba FPV	7.5%	30.0%	37.5%	10.0%	2.5%	12.5%

Rank#	Name of Site	Ease of Access (15% weight)				Demand (5% weight)		Site Total (100% weight)
		score*weight (5%)	score*weight (5%)	score*weight (5%)	Σ	score*weight (5%)	Σ	Σ
=1'	Itezhi-tezhi FPV	5.0%	5.0%	5.0%	15.0%	5.0%	5.0%	95.0%
=2'	KGU FPV	5.0%	5.0%	5.0%	15.0%	5.0%	5.0%	92.5%
=3'	Lusiwasi FPV	5.0%	5.0%	5.0%	15.0%	2.5%	2.5%	90.0%
=4'	Kariba FPV	5.0%	5.0%	5.0%	15.0%	5.0%	5.0%	85.0%
=5'	KGL FPV	5.0%	5.0%	2.5%	12.5%	5.0%	5.0%	77.5%
=6'	Shiwangangu FPV	5.0%	5.0%	5.0%	15.0%	2.5%	2.5%	75.0%
=6'	Mulungushi FPV	5.0%	5.0%	2.5%	12.5%	2.5%	2.5%	75.0%
=8'	Musonda FPV	5.0%	5.0%	1.3%	11.3%	2.5%	2.5%	71.3%
=9'	Lunsemfwa FPV	5.0%	5.0%	5.0%	15.0%	2.5%	2.5%	67.5%
=9'	Chishimba FPV	5.0%	5.0%	5.0%	15.0%	2.5%	2.5%	67.5%

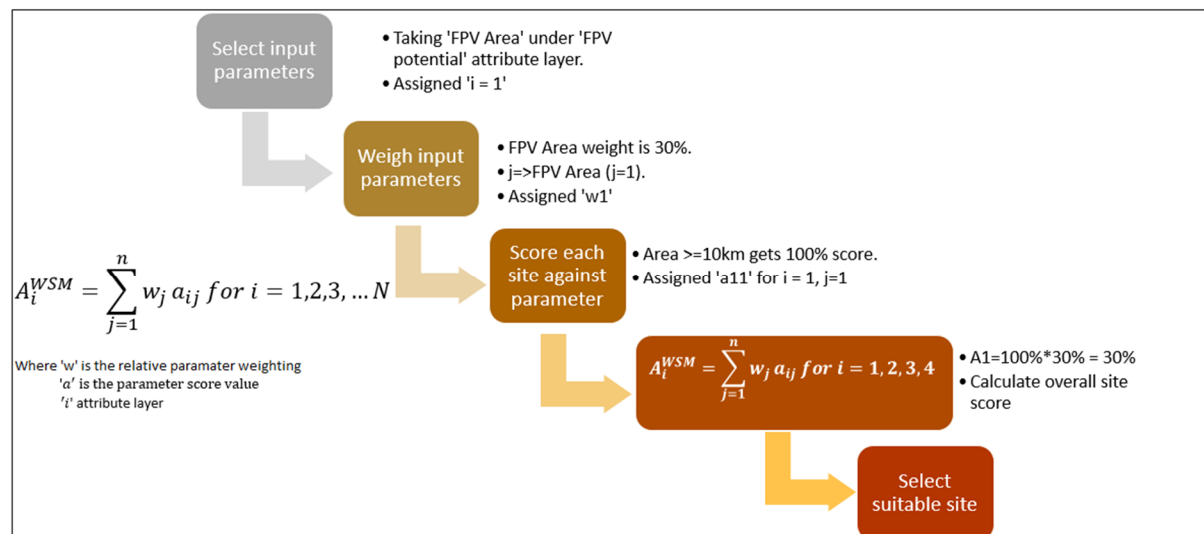


Figure 5Y: showing application of the weighted sum equation under FPV scoring & ranking

5.3.3 Onshore Wind Ranking

Table 5G shows the site floating photovoltaics ranking prospects using the weighted sum method. The relative weight distribution is as follows; 60% for wind potential, 20% for energy export, 15% for ease of access and 5% for demand. Figure 5Z shows the application of the weighted sum equation taking “capacity factor” under the “wind potential” attribute layer. The results of this process places Kafue gorge lower (KGL) and Kafue gorge upper (KGU) at first and second rank with total attribute values of 93.8% and 83.8 % respectively, while Chishimba site is ranked the least with 72.5% total combined attribute value.

Table 5G: showing onshore wind scoring and ranking matrix table

Rank#	Name of Site	Wind potential (60% weight)				Energy Export (20% weight)		
		score *weight (20%)	score *weight (30%)	score *weight (10%)	Σ	score *weight (10%)	score *weight (10%)	Σ
		Number of turbines	Capacity Factor	Slope	Wind Total	Wind distance to grid	Grid capacity	Total
=1'	KGL wind site	20.0%	30.0%	10.0%	60.0%	5.0%	10.0%	15.0%
=2'	KGU wind site	20.0%	22.5%	7.5%	50.0%	7.5%	10.0%	17.5%
=3'	Kariba wind site	20.0%	15.0%	7.5%	42.5%	10.0%	10.0%	20.0%
=3'	Itezhi-tezhi wind site	20.0%	22.5%	10.0%	52.5%	5.0%	5.0%	10.0%
=3'	Musonda wind site	20.0%	22.5%	10.0%	52.5%	10.0%	2.5%	12.5%
=3'	Lunsemfwa wind site	20.0%	30.0%	10.0%	60.0%	2.5%	2.5%	5.0%
=7'	Mulungushi wind site	20.0%	22.5%	10.0%	52.5%	10.0%	2.5%	12.5%
=8'	Shiwangangu wind site	20.0%	22.5%	7.5%	50.0%	10.0%	2.5%	12.5%
=9'	Lusiwasi wind site	20.0%	15.0%	10.0%	45.0%	10.0%	2.5%	12.5%
=10'	Chishimba wind site	20.0%	15.0%	10.0%	45.0%	7.5%	2.5%	10.0%

Rank#	Name of Site	Ease of Access (15% weight)				Demand (5% weight)		Site Total (100% weight)
		score *weight (5%)	score *weight (5%)	score *weight (5%)	Σ	score *weight (5%)	Σ	Σ
		Land use	Land ownership	Distance to road	Total	Distance to demar	Demand Total	score *weight
=1'	KGL wind site	5.0%	5.0%	3.8%	13.8%	5.0%	5.0%	93.8%
=2'	KGU wind site	5.0%	5.0%	1.3%	11.3%	5.0%	5.0%	83.8%
=3'	Kariba wind site	5.0%	5.0%	5.0%	15.0%	5.0%	5.0%	82.5%
=3'	Itezhi-tezhi wind site	5.0%	5.0%	5.0%	15.0%	5.0%	5.0%	82.5%
=3'	Musonda wind site	5.0%	5.0%	5.0%	15.0%	2.5%	2.5%	82.5%
=3'	Lunsemfwa wind site	5.0%	5.0%	5.0%	15.0%	2.5%	2.5%	82.5%
=7'	Mulungushi wind site	5.0%	5.0%	3.8%	13.8%	2.5%	2.5%	81.3%
=8'	Shiwangangu wind site	5.0%	5.0%	3.8%	13.8%	2.5%	2.5%	78.8%
=9'	Lusiwasi wind site	5.0%	5.0%	5.0%	15.0%	2.5%	2.5%	75.0%
=10'	Chishimba wind site	5.0%	5.0%	5.0%	15.0%	2.5%	2.5%	72.5%

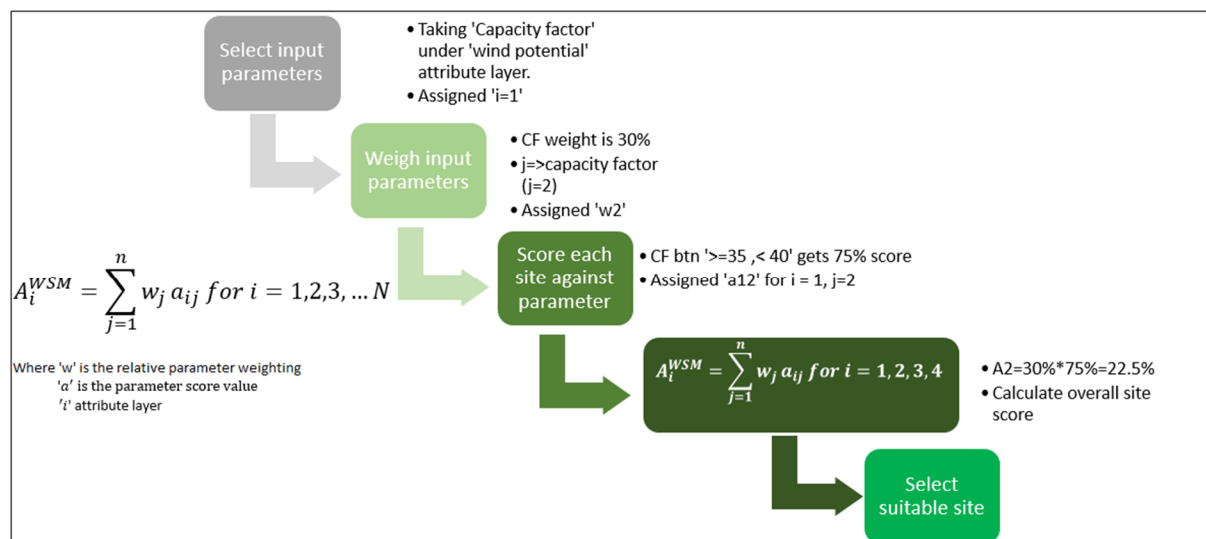


Figure 5Z: showing application of the weighted sum equation under wind scoring and ranking

5.4 Methodology Application Limitations

According to [Malczewski \(2004\)](#), the weighted sum method (WSM) is often applied without having insight about the layer combination procedures and the assigned relative weight to the attribute layers. The analytic hierarchy procedure (AHP) on the other hand is able to mitigate the concern raised with the WSM ([Watson and Hudson, 2015](#)), even though models remain quite sensitive to the used relative weightings as evidenced by refusal of planning permissions for high level of projects within the UK. To further address the parameter weighting concern, [Rensburg et al. \(2015\)](#) demonstrated the relationship between project receiving planning permissions and the key parameters influencing the decision by a quantitative assessment. This process was then integrated with geographic information system modelling to assess the influential geospatial parameters in the UK ([Harper et al., 2017](#)).

To reduce the concern raised about WSM, this study looked at broad array of parameters ranging from climate, topography, economic, social and environmental to attain a more acceptable and realistic screening and ranking process. This was done with the help of extensive literature review, stakeholder engagement and solicitation of local expert opinions in the decision-making process. Further, this contributed to a reduction in the uncertainties due to certain assumptions made in categorizing the score for the attribute suitability scale.

Since there is currently no commercial wind project or floating PV projects in the country, there is an element of expert and stakeholder bias in the contribution to the study based on the forecast agenda in line with seventh national development plan and vision 2030 which is a road map of attaining middle income status for the country. Additionally, the author acknowledges that this developed process is ongoing and thus is prone to adjustment as more stakeholders come on board with their specific viewpoints and interests.

5.5 Summary

The author has presented an application of the devised screening and ranking multicriteria based methodology for floating PV and onshore wind, near hydro sites. The extensive data collection for stage 1, filtered off 3 sites (Lunzua, Victoria and Zengamina), thereby presenting the remaining 10 sites to the stage 2 scoring and ranking process. This ranking process was developed for three scenarios which are the balanced hybrid, floating PV and onshore wind. The three-level scoring and ranking yielded the following results: the balanced ranking placed Itzhi-tezhi and Kafue gorge upper (KGU) at first and second rank with total attribute values

of 90% and 86.9 % respectively; FPV ranking placed Itezhi-tezhi and Kafue gorge upper (KGU) at first and second rank with total attribute values of 95% and 92.5 % respectively; while the wind ranking placed Kafue gorge lower (KGL) and Kafue gorge upper (KGU) at first and second rank with total attribute values of 93.8% and 83.8 % respectively. In all the three scoring and ranking levels, Chishimba site was ranked the least.

This study presents great insight for planners and prospectus investors in floating photovoltaics and onshore wind as the factors influencing the suitability of the respective sites can easily be understood.

The next chapter develops a scoping design study methodology in readiness for applicability at one of the highly ranked sites.

CHAPTER SIX: SCOPING DESIGN STUDY METHODOLOGY

Having determined the site suitability of the variable renewable energy sources (VRES) in the previous chapter, this chapter aims to develop a scoping design study methodology that will be applied to one of the highly ranked sites (i.e. either Itezhi-tezhi, Kafue Gorge Upper, Kariba or Kafue Gorge Lower) in chapter seven. [Section 6.1](#) presents the design methodology formulation by defining how various components of the system would interact. [Section 6.2](#) illustrates the details the hydro-FPV-wind daily dispatch model. [Section 6.3](#) describes a simplified flowchart for applying the developed methodology, while [section 6.4](#) summarizes the significant outcomes of the chapter.

6.1 Design Methodology Formulation

Motivated by previous work presented in the [literature review](#), this section will define a scoping of a design methodology to be applied to a case study which will provide answers to key questions with respect to technical and economic feasibility of the hybrid energy system (hydro + FPV + Wind). The developed method aims to:

- ✓ Assess the technical parameters of the local grid.
- ✓ Assess current generation situation considering hour by hour basis throughout the year.
- ✓ Assess floating photovoltaics and onshore wind potential and ascertain how much of the hydro generation profile matches with FPV and wind.
- ✓ Assess storage potential (implied by throttling down hydro in presence of wind and FPV).
- ✓ Maximise daily energy production within grid constraints using optimal dispatch strategy and ascertain the levelized cost of energy of the system.

This approach will optimize the daily-seasonal generation of the hybrid energy system while balancing the specified system load characteristics within the constraint of the local grid.

Consequently, the following pertinent questions will be answered:

- i. What complementary FPV and wind would fit without extra upgrades and additional energy storage devices?
- ii. By how much real power contribution from floating PV or/and wind would make the system cost optimal?

The schematic for the proposed system dispatch strategy consisting of the utility grid, hydro unit(s), floating photovoltaic and onshore wind is shown in figure 6A. The schematic shows the current dispatch strategy which employs automatic generation control (AGC) without VRES. It worth noting that details of the AGC of the existing setup is no shown for simplicity. The proposed dispatch strategy is called the “Hydro-FPV-Wind Daily Dispatch” (HFWDD). This model assumes that all generation sources under consideration are connected to the same generation bus. Further, the model gets inputs from the reservoir inflow ‘ $Q_{in}(t)$ ’, the penstock water flowrate ‘ $Q_p(t)$ ’, reservoir height variation ‘ $H_r(t)$ ’, hydro head variation ‘ $H_h(t)$ ’, water consumption/usage ‘ $Q_T(t)$ ’, hourly hydro generation schedule ‘ $P_{HYg}(t)$ ’, hourly variable wind output ‘ $P_{WDg}(t)$ ’, hourly variable floating photovoltaic output ‘ $P_{PVg}(t)$ ’, perceived virtual battery from saved water ‘ $Q_s(t)$ ’ and the hourly grid load $P_{LD}(t)$ in a given day of the season.

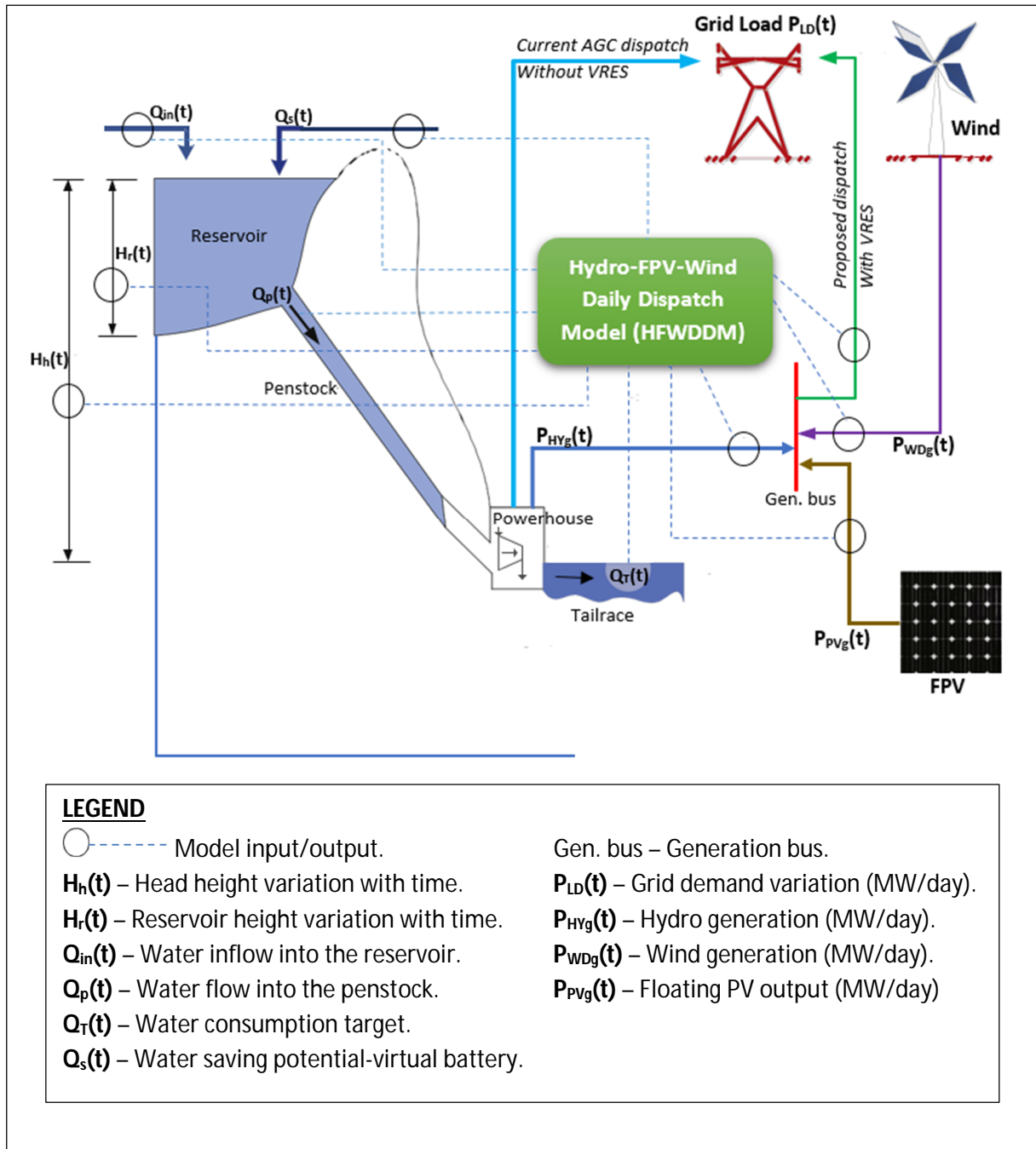


Figure 6A: showing the schematic for the hydro-FPV-Wind grid tied system

6.2 Details of the Hydro-FPV-Wind Daily Dispatch Model

The goal of the “Hydro-FPV-Wind Daily Dispatch” HFWDD model is to find the optimal daily generation dispatch for the various seasons (i.e. on a typical summer and winter day) to balance the load characteristic curve on the grid. For simplification in computation, the model excludes predictive analytics in the used variable renewable energy source (VRES) generation data, but instead incorporates daily time series data of RES production. The daily data used to determine an optimal generation mix is obtained from validated local and global satellite meteorological

datasets (and assumes perfect foresight). Additionally, the model uncertainties of VRES (FPV + wind) are evened out by the dispatchable hydro. [Wei and Liu \(2019\)](#) revealed that daily reservoir inflows (Q_{in}) have insignificant uncertainty to impact the output of large hydro power plants, thus, justifying the notions of the model. As such, only uncertainties from the VRES must be considered in the HFWDD scheduling.

The two-stage model firstly, assesses the electrical grid to ascertain the extent of FPV and onshore wind integration that would not negatively impact network parameters (i.e. voltage magnitude and power losses). Further, network assessment incorporates cost functions to cater for any curtailment in FPV or wind scenarios. These cost functions are embedded in the power system analysis using optimal power flow (OPF) by inclusion of supply and demand bids of all modelled generation sources. This is in line with other research that aims to minimize the operating cost of the energy system ([Alsammak, A.N.B., 2011](#); [Princy et al., 2018](#)).

The second stage of the model incorporates total generation scenarios (i.e. hydropower, FPV and wind), load characteristic for the grid, water consumption target and reservoir inflows on an hour by hour basis for any day of a season. Thereafter, the energy to be injected into the grid is determined through a dispatch strategy that aims to prioritize the integration of FPV and wind by throttling down on hydrogeneration to meet the electrical demand at any instant. The water storage potential is proportional to the reduction in hydrogeneration. However, for a very wet year which is 'rarely experienced' the storage can have limitations in terms of reservoir capacity and thus excess water is just wasted by opening the flood gates.

Therefore, the first phase in the modelling process is the technical assessment of the local grid to help ascertain the maximum energy that can be added to the grid while maintaining power losses, voltage profile, voltage stability within grid code limits. This agrees with other research ([Asaduz-Zaman et al., 2018](#)). Lastly, without considering the stochastic nature of the VRES (FPV and wind power), the seasonal dispatch strategy on a typical day is an optimization problem based on minimizing the operating cost of the 'AGC' dispatch system (existing dispatch which mainly comprises of conventional hydro).

$$\text{Min}_k \rightarrow \text{Conv}_{\text{operate}}(k) \quad (17)$$

Where $\text{Conv}_{\text{operate}}(\cdot)$ is the power system conventional-hydro daily operating cost. 'k' is the daily dispatch scenario including the status of the hydro plant (i.e. number of online units,). The model flow chart showing systematic flow of decision level is shown in [figure 6B](#) below;

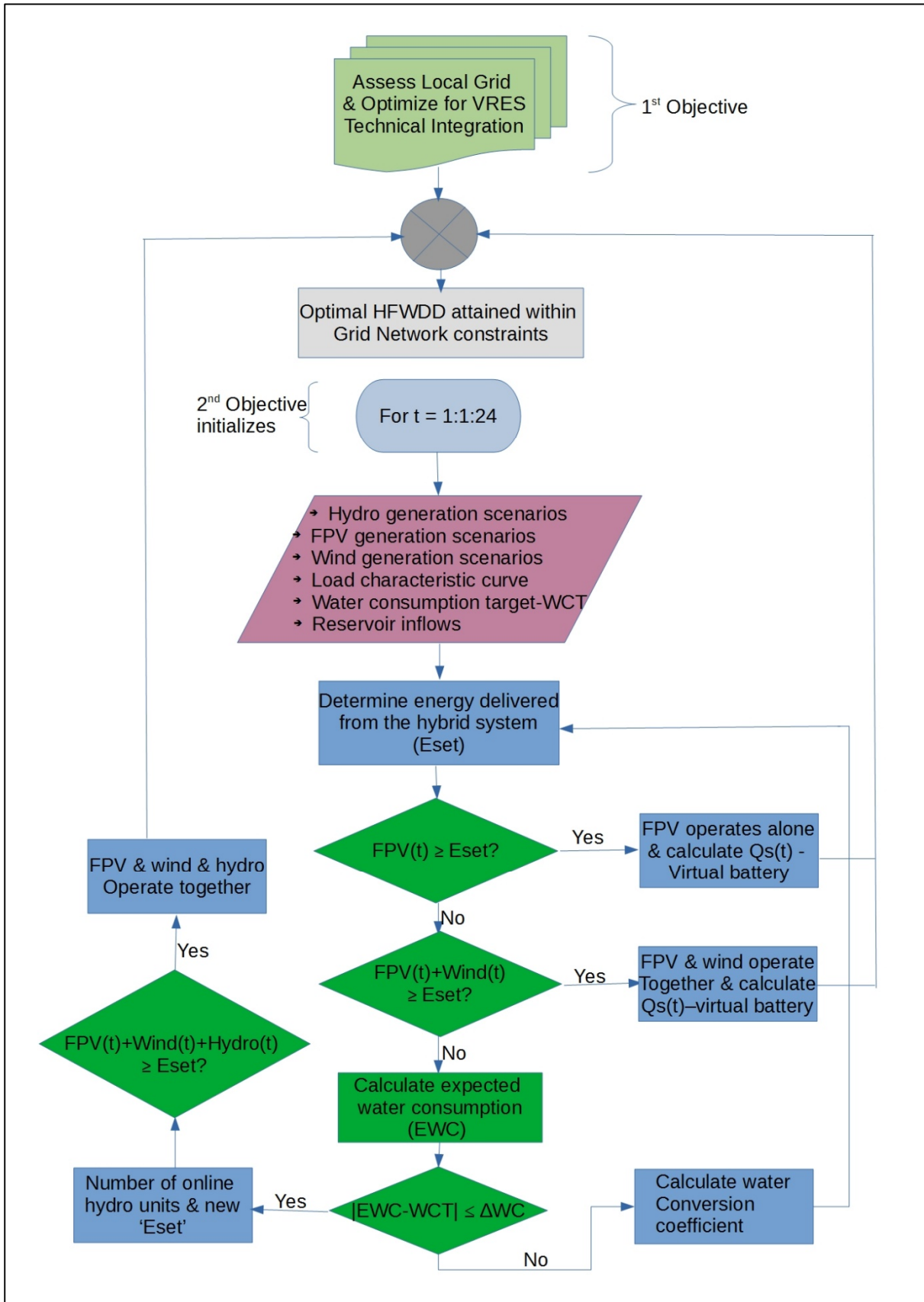


Figure 6B: showing systematic flow of decision level to attain optimal hydro-FPV-Wind daily dispatch(HFWDD)

6.2.1 VRES Parameter Uncertainty

Adopted from (Wei and Liu, 2019), the floating photovoltaic and onshore wind outputs can be represented as shown below;

$$\text{For FPV} \rightarrow P_{PVg,t} \in [P_{PVg,t(\text{pre})} - P_{PVg,t(\text{flu})}, P_{PVg,t(\text{pre})} + P_{PVg,t(\text{flu})}] \quad (18)$$

$$\text{For wind} \rightarrow P_{WDg,t} \in [P_{WDg,t(\text{pre})} - P_{WDg,t(\text{flu})}, P_{WDg,t(\text{pre})} + P_{WDg,t(\text{flu})}]$$

Where $P_{PVg/WDg,t}$ is the power output of the VRES at any given time of the day. $P_{PVg/WDg,t(\text{pre})}$ is the expected or predicted output of the VRES while $P_{PVg/WDg,t(\text{flu})}$ is the maximum fluctuation in the output.

6.2.2 Dispatch Model Objective Function

To attain the optimal economical dispatch scenario 'k', cost parameters for the different stages are considered. The first stage is the generation cost of hydro units C_{operate} (' C_{ope} = in short form' = C_{HYg}). The second stage costs (C_{ope}^+) mostly include adjustment costs of hydro units $C_{HYg\Delta}$, floating photovoltaic curtailment cost $C_{PVg(\text{curt})}$, onshore wind curtailment cost $C_{WDg(\text{curt})}$. Therefore, the objective function on cost minimization is given as;

$$C_{\text{ope}} = C_{HDg} = \sum_{t=1}^T (a * P_{HYg,t}^2 + b * P_{HYg,t} + c) \quad (19)$$

$$C_{\text{ope}}^+ = C_{HYg\Delta} + C_{PVg(\text{curt})} + C_{WDg(\text{curt})} = \sum_{t=1}^T [\lambda_{HYg} * \Delta P_{HYg,t} + \lambda_{PVg(\text{curt})} * (P_{PVg,t} - P_{PVg,t(\text{inject})}) + \lambda_{WDg(\text{curt})} * (P_{WDg,t} - P_{WDg,t(\text{inject})})]$$

Where a, b and c are cost coefficients of the hydro units. $P_{HYg,t}$ is the power output of hydro units at time t, $\Delta P_{HYg,t}$ is the hydro unit(s) power output adjustment, λ_{HYg} is the penalty price for the adjustment of hydro units. $\lambda_{PVg(\text{curt})}$ and $\lambda_{WDg(\text{curt})}$ are penalty prices for FPV and wind curtailment respectively. $P_{PVg,t(\text{inject})}$ and $P_{WDg,t(\text{inject})}$ is the FPV and wind injected power into the grid at time 't' respectively.

6.2.3 Dispatch Model Constraints

The daily dispatch constraints of the model consist of the following;

6.2.3.1 Hydro Constraints

$$P_{HYg(\text{min})} \leq P_{HYg,t} \leq P_{HYg(\text{max})} \quad (20)$$

$$Q_{HYg,t} = \Lambda^{a}_{HYg} * P_{HYg,t} + \Lambda^{b}_{HYg} \quad (21)$$

$$V_{flow(min)} \leq Q_{HYg,t} \leq V_{flow(max)} \quad (22)$$

$$Q_{t+1} = Q_{s,t} + Q_{in,t} - Q_{HYg,t} - Q_{HYg,t(curt)} \quad (23)$$

$$Q^{min} \leq Q_{s,t} \leq Q^{max} \quad (24)$$

$$Q_{s,1} = Q_{s,ini} \quad (25)$$

$$Q_{s,T} = Q_{s,term} \quad (26)$$

Where $Q_{HYg,t}$ is the hydrogenator water consumption at any time t ; $P_{HYg,t}$ hydro-generator power output at time t ; Λ^{a}_{HYg} and Λ^{b}_{HYg} are water conversion coefficients of hydro-generators; $V_{flow(min)}$ and $V_{flow(max)}$ are the lower and upper limit of water consumption in a given period; $Q_{HYg,t(curt)}$ is the reservoir water curtailment; $Q_{s,t}$ is the storage of the hydro reservoir at time t ; $Q_{in,t}$ is the reservoir inflow at time t ; Q^{min} and Q^{max} are the lower and upper reservoir storage limits. $Q_{s,ini}$ and $Q_{s,term}$ are the initial and final reservoir storage values.

6.2.3.2 Power Balance Constraint

$$P_{HYg,t} + P_{PVg,t(pre)} + P_{WDg,t(pre)} = P_{LD,t} \quad (27)$$

Where $P_{LD,t}$ is the power demand of the load in the system at any given time t .

6.2.3.3 Branch Power flow Constraints

$$\sum_{i=1}^{Ni} (f_{bi} * P_{i,t}) \leq S_{b(max)} \quad (28)$$

Where 'b' is the branch identifier for the power system; 'i' is the node identifier; N_i is the total number of nodes; $P_{i,t}$ is the net real power injected into the 'i' node at any given time t ; $S_{b(max)}$ is the maximum branch capacity at unity power factor.

6.2.3.4 Floating Photovoltaic Power Constraint

$$0 \leq P_{PVg,t(inject)} \leq P_{PVg,t} \quad (29)$$

Where $P_{PVg,t}$ is the variable power output of the floating photovoltaic at time t .

6.2.3.5 Onshore Wind Power Constraint

$$0 \leq P_{WDg,t(inject)} \leq P_{WDg,t} \quad (30)$$

Where $P_{WDg,t}$ is the variable power output of the onshore wind generator at time t .

6.3 Methodology Application Flowchart

The simplified application of the devised design methodology to a specific case study is as shown in figure 6C below;

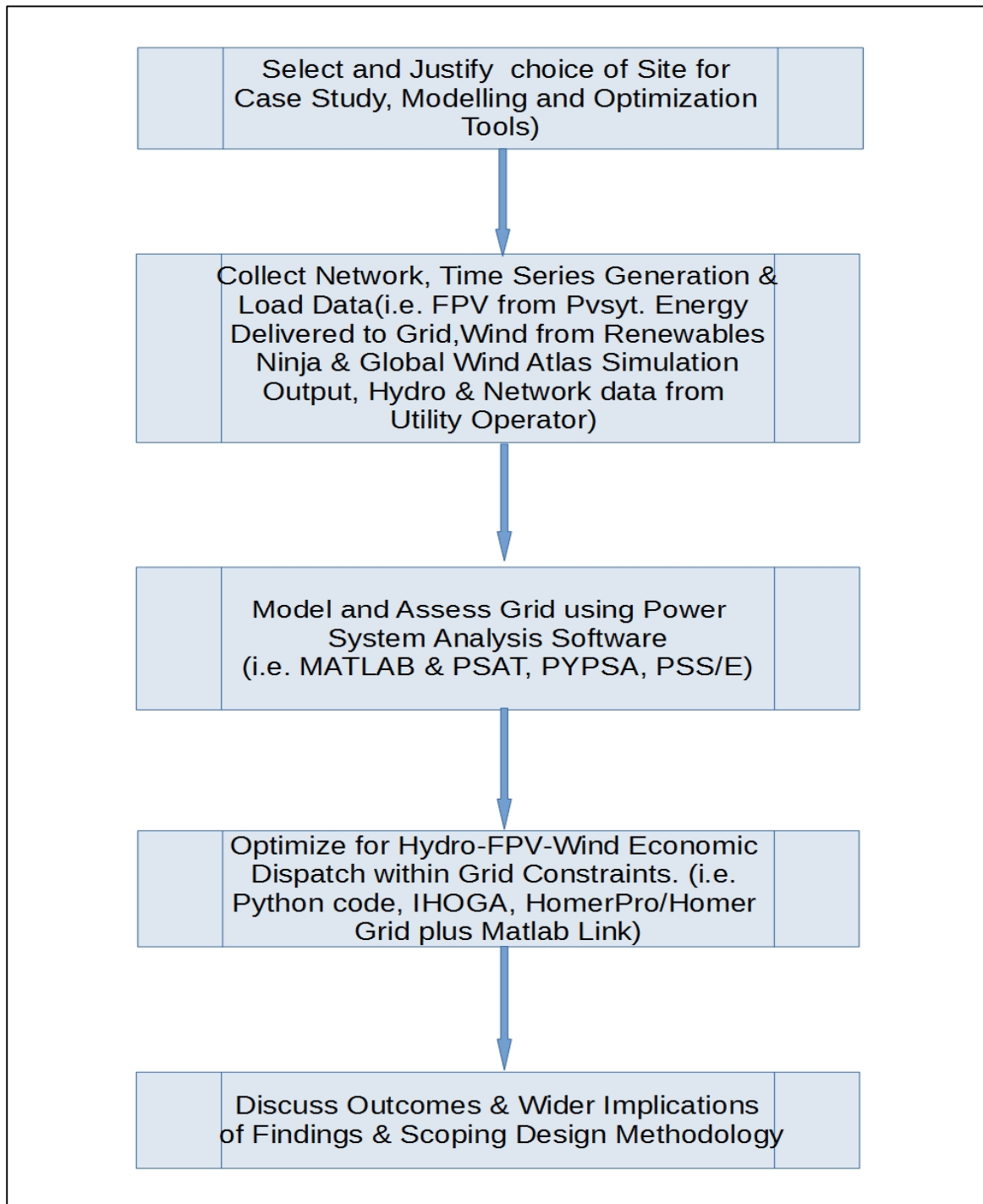


Figure 6C - showing methodology application process

6.4 Summary

The author developed a scoping design methodology to be applied at any one of the 10 potential sites. The summarized methodology for the case study application includes assessing technical parameters of the local electrical grid, for integration of variable renewable energy sources (VRES), assessing current seasonal hydro generation and grid electrical demand in a year on a hour by hour basis, detailed assessment and design of the VRES (floating

photovoltaics and onshore wind) for the chosen case study, assessing the storage potential (implied by throttling down hydro in presence of VRES for the reservoir type), optimize daily energy production of the system within grid constraints and ascertain the levelized cost of energy of system.

The next chapter applies the scoping design methodology to a case study proposed by the stakeholder (i.e. national power utility).

CHAPTER SEVEN: APPLICATION OF SCOPING DESIGN STUDY METHODOLOGY

This chapter applies the scoping design methodology to a case study proposed by the stakeholder (ZESCO Ltd). ZESCO was presented with three ranking matrices of 10 potential sites to choose from and opted to adopt the hybrid balanced ranking with Kafue Gorge Upper (KGU) as the candidate site for detailed design. Moreover, KGU was chosen over Itezhi-tezhi due to the presence of dead trees in the reservoir of the latter which could impact FPV installation, presence of wind mast at KGU for wind data validation, distance to load centre (100 km for KGU compared to 300 km at Itezhi-tezhi), stability and reliability of the grid at KGU, with three 330 kV lines emanating from KGU compared to one 220 kV from Itezhi-tezhi to the grid. The chapter is structured as follows: [Section 7.1](#) presents a detailed grid assessment for the integration of FPV and wind. [Section 7.2](#) assesses the seasonal hydro generation and grid demand while [sections 7.3, 7.4, 7.5 and 7.6](#) tackle detailed design and assessment of FPV and wind, hydro storage potential assessment, hybrid energy system optimization and optimum dispatch strategies versus the baseline case without VRES integration respectively.

7.1 Grid Assessment for VRES Integration at KGU

This section investigates the VRES integration impact on the overall operating costs (and thus embedded losses) for the national grid. The national electrical network under study has the following modelled generation operating capacity based on data received from the utility: 127 MW Maamba Collieries Limited (MCL) coal plant, 76 MW solar farm at LSMFEZ, and a total hydro generation of 2001 MW at Kafue Gorge, Kariba North Bank, Itezhi-tezhi, Lunzua, Victoria Falls power plants. In view of the future integration of more renewables to reduce emissions and increase generation capacity, it is envisaged in this study that the operational cost of running the network will drastically reduce due to ramping down of the coal plant. Further, for the hybrid dispatch of hydro-FPV-wind, cost reductions are possible due to the optimal throttling down of hydro to prioritise utilization of VRES (introducing virtual storage in the mix). The perceived future reduction in investment costs of PV and Wind at economies of scale will also be another added advantage in cost saving ([IRENA, 2019](#)).

In line with research ([Princy et al., 2018](#)), this study will not look at fixed cost of generating units but will tackle proportional (hydro, wind, PV) and quadratic costs (i.e. coal). Against this background, the rest of the sections are structured as follows: [section 7.1.1](#) examines the

existing 330 kV grid that has been modelled in PSAT software by looking at the power flow solution (i.e. voltage magnitude profile and network power losses). [Section 7.1.2](#) presents the impacts of VRES integration of voltage magnitude profile and losses. Further, the section also emphasizes on utilizing optimal power flow (OPF) in minimizing operating costs, active power losses and optimization of the overall energy resource after grid integration in line with other scholarly analyses ([Princy et al.,2018](#)). [Section 7.1.3](#) presents an analysis of the simulation results.

7.1.1 Existing Grid Analysis

This was done using simple power flow (SPF) to ascertain the network parameters (i.e. voltage magnitude profile, power losses) as they exist before integrating the variable renewable energy sources. This was done in order to track the change in parameters in-line with grid code constraints after additional generation was modelled (VRES).

7.1.1.1 Network Modelling Using Power System Analysis Toolbox (PSAT)

The ZESCO grid 330 kV – 27 bus system market model has been modelled with existing generation (kafue gorge upper, Kariba north bank, LSMFEZ, MCL, Victoria falls, Lunzua, Itezhi-tezhi) and load. The modelled existing 330 kV network has the following network statistics as shown in the [figure 7.1A](#) below;

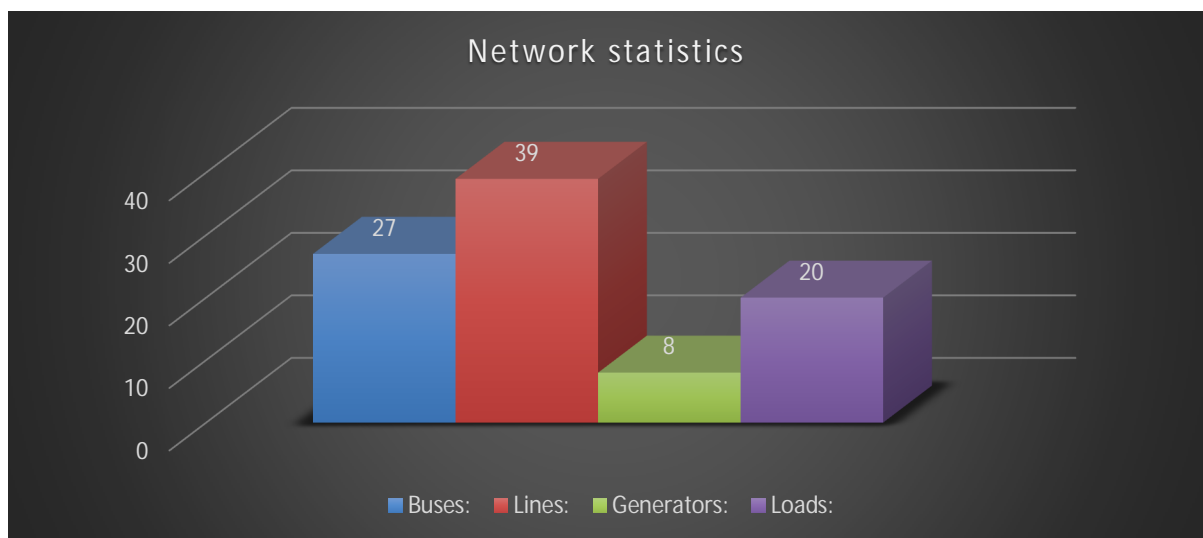


Figure 7.1A: showing network statistics of main power components

The actual PSAT model for the existing network is shown in [Appendix B](#) together with the ZESCO grid single line diagram; To improve the voltage profile and power factor of then network, compensation equipment was added to the model at strategic buses, as illustrated in [Table 7.1A](#).

Table 7.1A: showing network compensation equipment

#	SUBSTATION	SHUNT CAPACITOR (MVar)		SHUNT REACTOR (MVar)	
		Unit Capacity	Total	Unit Capacity	Total
1	Luano	3 X 30 MVar	90		
2	Luano	2 x 20 MVar	40		
3	Kitwe	1 X 33 MVar	33	1 x 20MVar	20
4	Kitwe	1 X 16.8MVar	16.8		
5	Kitwe	1 X 29MVar	29		
6	Chambishi	4 X 30MVar	30		
7	Kafue Town	1 x 20 MVar	20		
8	Victoria Falls	1 x 20 MVar	20		
9	Pensulo			2 x 36.5 MVar	73
10	Pensulo			1 x 15 MVar	15
11	Pensulo			3 x 30 MVar	90
12	Kasama			2 x 30 MVar	60
13	Kasama			1 x 30MVar	30
14	Msoro			1 x 30MVar	30
15	Kansanshi	1 x 10MVar	10	1 x 20MVar	20
16	Kansanshi	1 x 15MVar	15		
17	Kansanshi	3 x 25MVar	75		
18	Lumwana	3 x 25.2MVar	75.6	1 x10MVar	10
19	Kalumbila	3 x 25MVar	75	2 x 30 MVar	60

7.1.1.2 Simulation Results of Existing Grid

This section presents simulations results before and after the addition of network compensating equipment to the model.

Before Addition of Compensating Equipment

The power flow results for the existing network before the addition of shunt compensation and step voltage compensation equipment is given in [table 7.1B](#) and [7.1C](#) below;

Table Table 7.1B - showing power flow results before addition of network compensating equipment. 9 buses exhibit voltage violations with 8 for minimum and Kalumbila showing maximum violation.

Bus	V	phase	P gen	Q gen	P load	Q load
	[kV]	[rad]	[MW]	[MVar]	[MW]	[MVar]
Chambeshi 330kV	267.2	-0.8	0.0	0.0	72.6	14.5
Chipata West 330kV	241.9	-1.2	0.0	0.0	47.6	35.7
Itezhi-Tezhi via Nambala 330kV	330.0	-0.4	107.0	-283.3	0.0	0.0
Kabwe 330kV	297.1	-0.6	0.0	0.0	102.4	33.7
Kafue Gorge 330kV	330.0	-0.3	929.0	238.5	0.0	0.0
Kafue Town 330kV	328.6	-0.4	0.0	0.0	225.0	109.0
Kafue West 330kV	328.9	-0.4	0.0	0.0	0.0	0.0

Kalumbila 330kV	347.3	-0.4	0.0	0.0	80.4	60.3
Kansanshi 330kV	251.8	-0.9	0.0	0.0	51.6	38.7
Kariba North 330kV	330.0	-0.3	846.0	41.1	0.0	0.0
Kitwe 330kV	267.4	-0.8	0.0	0.0	287.5	174.7
LSMFEZ 330kV	330.0	-0.4	76.0	647.0	0.0	0.0
Leopards Hill 330kV	323.4	-0.4	0.0	0.0	332.0	109.0
Luano 330kV	267.5	-0.8	0.0	0.0	491.5	72.8
Lumwana 330kV	248.2	-0.9	0.0	0.0	50.1	37.6
Lunzua via Kasama 330kV	330.0	-1.5	15.0	173.7	123.5	20.0
Lusaka West 330kV	329.1	-0.4	0.0	0.0	80.0	60.0
MCL 330kV	330.0	-0.3	126.9	-9.4	0.0	0.0
Mpika SD 330kV	294.6	-1.4	0.0	0.0	70.7	53.0
Msoro 330kV	245.5	-1.2	0.0	0.0	49.1	36.8
Muzuma 330kV	329.9	-0.3	0.0	0.0	80.0	60.0
Pensulo 330kV	261.1	-1.1	0.0	0.0	79.1	26.0
Swing	330.0	0.0	327.7	21.6	0.0	0.0
To Siavonga	329.3	-0.3	0.0	0.0	80.0	60.0
To ZESA	330.0	-0.3	0.0	0.0	0.0	0.0
To ZESA1	330.0	-0.3	0.0	0.0	0.0	0.0
Vicotiria Falls via Mukuni 330kV	330.0	-0.3	103.0	28.1	80.0	60.0

Table 7.1C: showing line flows before addition of network compensating equipment. ZESA 1 and 2 were disconnected at the time of running simulations.

From Bus	To Bus	Line	P Flow [MW]	Q Flow [MVar]	P Loss [MW]	Q Loss [MVar]
Swing	Kafue Gorge 330kV	1	327.7	21.6	10.8	107.7
Kafue Gorge 330kV	Leopards Hill 330kV	2	495.6	81.6	4.8	20.5
Pensulo 330kV	Kabwe 330kV	3	-367.0	18.4	26.2	126.9
Pensulo 330kV	Msoro 330kV	4	98.4	27.0	1.6	-31.9
Leopards Hill 330kV	Kabwe 330kV	5	507.4	213.4	12.5	67.0
Leopards Hill 330kV	Kabwe 330kV	6	507.4	213.4	12.5	67.0
Leopards Hill 330kV	Kabwe 330kV	7	507.4	213.4	12.5	67.0
Leopards Hill 330kV	LSMFEZ 330kV	8	-297.6	-587.4	1.8	10.5
Vicotiria Falls via Mukuni 330kV	Muzuma 330kV	9	23.0	-31.9	0.0	-58.7
MCL 330kV	Muzuma 330kV	10	63.4	-4.7	0.0	-3.6
MCL 330kV	Muzuma 330kV	11	63.4	-4.7	0.0	-3.6
Muzuma 330kV	Kafue Town 330kV	12	69.8	-35.5	0.4	-66.9
Kafue Gorge 330kV	Leopards Hill 330kV	13	495.6	81.6	4.8	20.5
Kafue Town 330kV	Kafue West 330kV	14	-155.5	-77.6	0.0	-0.8
Kafue West 330kV	Lusaka West 330kV	15	54.6	-20.3	0.1	-18.3
Itezhi-Tezhi via Nambala 330kV	Lusaka West 330kV	16	12.7	-22.5	0.0	-53.5
Itezhi-Tezhi via Nambala 330kV	Lusaka West 330kV	17	12.7	-22.5	0.0	-53.5

Kalumbila 330kV	Itezhi-Tezhi via Nambala 330kV	18	-40.2	-30.1	0.6	-149.2
Kalumbila 330kV	Itezhi-Tezhi via Nambala 330kV	19	-40.2	-30.1	0.6	-149.2
Pensulo 330kV	Mpika SD 330kV	20	189.5	-71.4	6.6	65.5
Mpika SD 330kV	Lunzua via Kasama 330kV	21	112.3	-189.9	3.8	-36.2
Kitwe 330kV	Chambeshi 330kV	22	196.5	-16.4	0.5	-1.2
Kansanshi 330kV	Lumwana 330kV	23	50.3	23.6	0.2	-14.0
Kariba North 330kV	Leopards Hill 330kV	24	291.7	8.4	4.2	-11.4
Luano 330kV	Kansanshi 330kV	25	103.5	30.1	1.6	-32.2
Luano 330kV	Chambeshi 330kV	26	-123.1	26.1	0.2	-3.6
Kabwe 330kV	Luano 330kV	27	244.5	64.6	8.5	0.1
Kabwe 330kV	Luano 330kV	28	244.5	64.6	8.5	0.1
Kitwe 330kV	Kabwe 330kV	29	-242.0	-79.1	7.9	4.7
Kitwe 330kV	Kabwe 330kV	30	-242.0	-79.1	7.9	4.7
Lumwana 330kV	Kalumbila 330kV	31	0.0	0.0	0.0	0.0
Chipata West 330kV	Msoro 330kV	32	-47.6	-35.7	0.2	-13.6
Kafue West 330kV	LSMFEZ 330kV	33	224.3	-57.8	0.9	-8.7
Kariba North 330kV	Leopards Hill 330kV	34	291.7	8.4	4.2	-11.4
Kafue Gorge 330kV	Kafue West 330kV	35	254.8	-10.8	1.1	-7.1
Kariba North 330kV	To ZESA	36	0.0	-0.1	0.0	-0.1
Kariba North 330kV	To ZESA1	37	0.0	-0.1	0.0	-0.1
Kariba North 330kV	Kafue West 330kV	38	182.6	-32.0	1.7	-34.4
Kariba North 330kV	To Siavonga	39	80.0	56.6	0.0	-3.4

The voltage network profile showing 9 voltage violations (i.e. 8 minimum voltage violations and 1 maximum voltage violation) is shown in figure 7.1B.

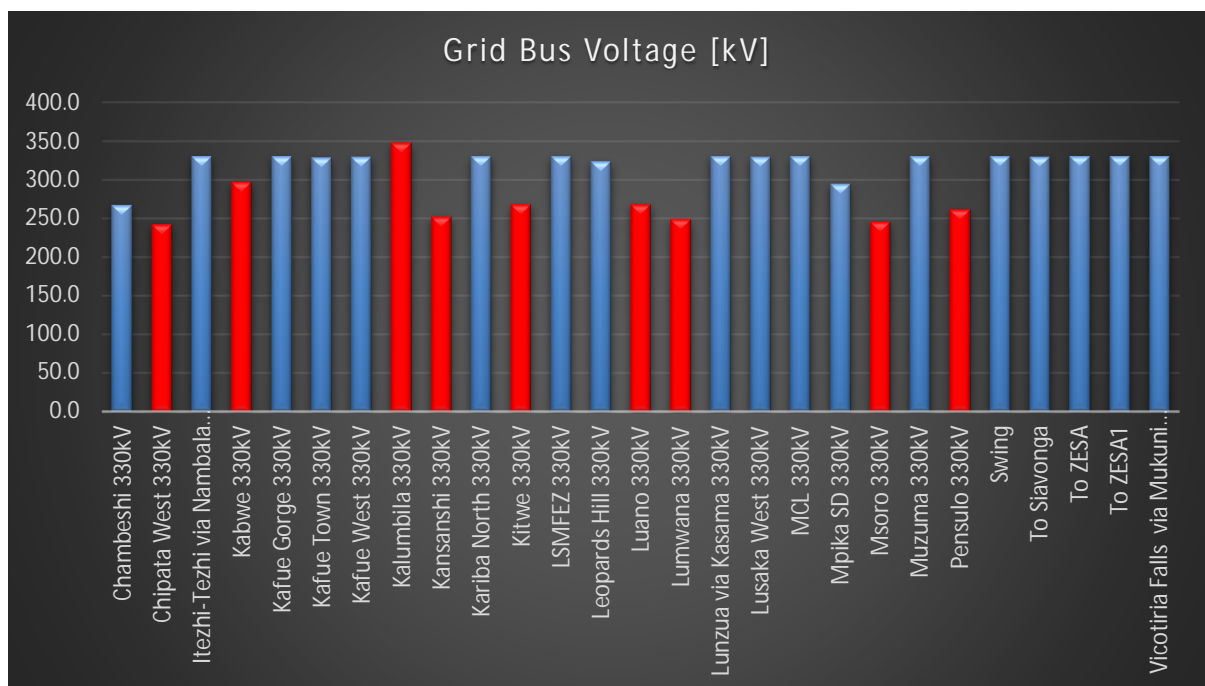


Figure 7.1B: showing voltage magnitude profile before addition of compensation equipment.

Blue bars are within grid code range [313.5 346.5]. (voltage violation buses outside the range shown in red).

After Addition of Compensating Equipment

Figures 7.1C and 7.1D show the voltage magnitude profile and global power summary with compensation equipment added at the respective buses.

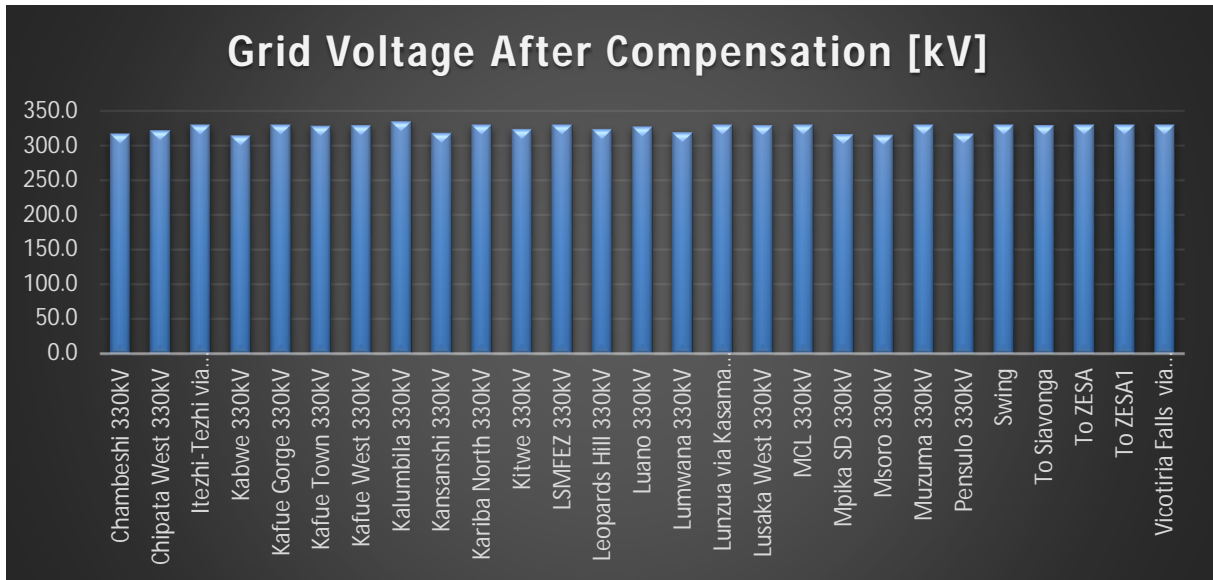


Figure 7.1C: showing voltage magnitude after grid compensation

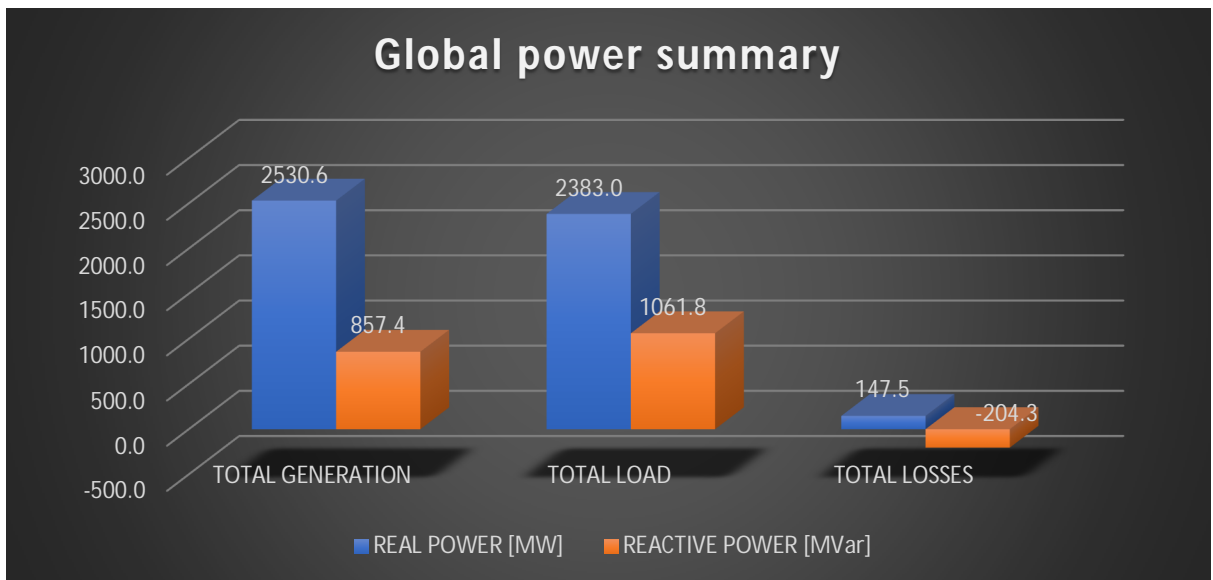


Figure 7.1D: showing the global power summary of the network

7.1.2 VRES Integration

7.1.2.1 VRES Modelling

This involved modelling of floating PV and Onshore wind both connected at the Kafue Gorge Upper Generation bus. The PSAT model of the network with VRES integration is shown in [Appendix B](#).

PSAT Modelling of Wind Farm

The Wind farm model consists of a variable speed wind turbine with doubly fed induction generator (DFIG) coupled with a wind speed model as shown in [figure 7.1E](#);

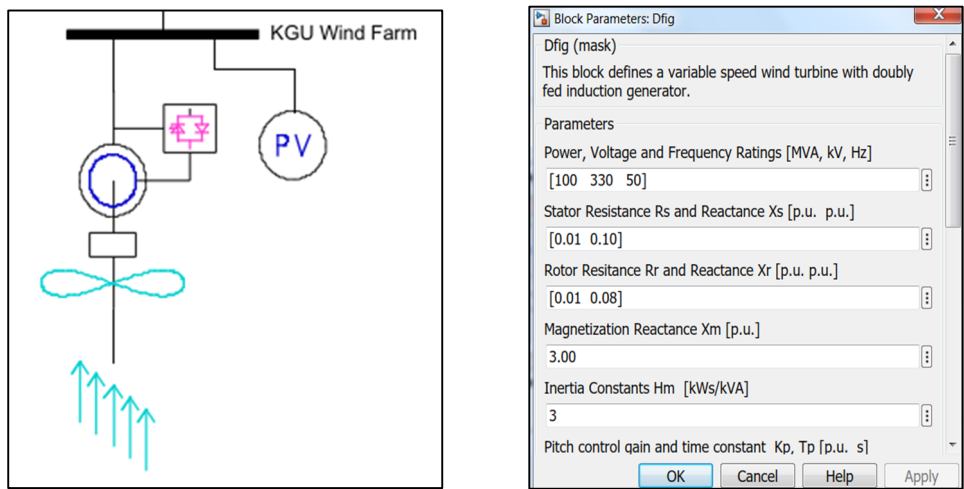


Figure 7.1E: wind farm modelling with DFIG generator

PSAT Modelling of Floating Photovoltaics

The floating photovoltaics is modelled as shown below using the PSAT solar photovoltaic generator as shown in the figure [7.1F](#) below;

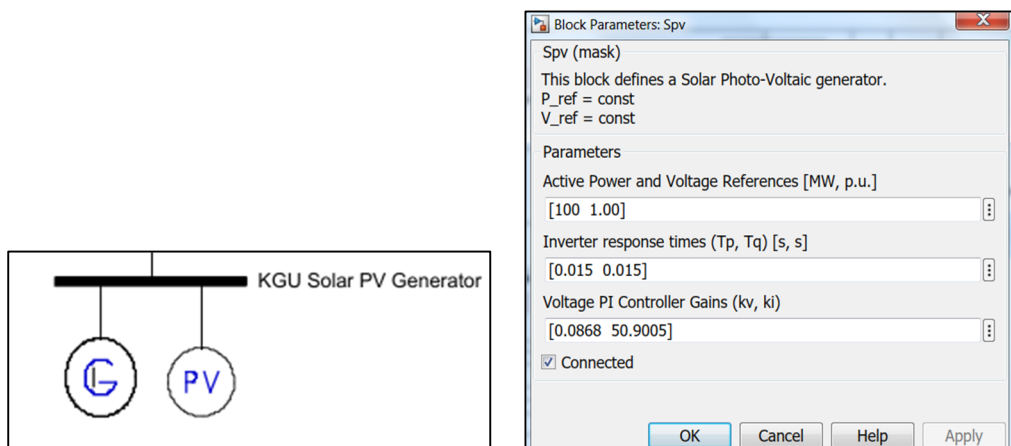


Figure 7.1F: showing the PSAT solar PV generator model

7.1.2.2 Optimal Power Flow Market Model Formulation of National Grid

The impact of VRES integration on operating cost and loss is analysed for the case study considering Kafue Gorge 330 kV generation bus. This is achieved using optimal power flow in PSAT software. The system has been modelled to investigate and optimize energy management in the six different cases shown in [table 7.1D](#).

Table 7.1D: showing the different energy optimization cases using OPF

Economic Dispatch Scenario	Unit Commitment
Scenario 1 (existing setup)	Hydro (2001MW) + coal (127MW) + PV(76MW)
Scenario 2 (existing without coal)	Hydro (2001MW) + PV (76MW)
Scenario 3 (without coal with floating PV)	Hydro (2001MW) + PV (76MW) + FPV (100MW)
Scenario 4 (without coal with onshore wind)	Hydro(2001MW) + PV(76MW) + Wind (100MW)
Scenario 5 (existing without coal plus VRES)	Hydro(2001MW) + PV(76) + FPV(100) + Wind(100)
Scenario 6 (existing with coal & VRES)	Hydro + Coal + PV + FPV + Wind

Note: Unit commitment problem is out of available units, which unit will be on or off and how much each unit should be loaded depending on need or depending on some objective function such as the economy, reliability, voltage control and security.

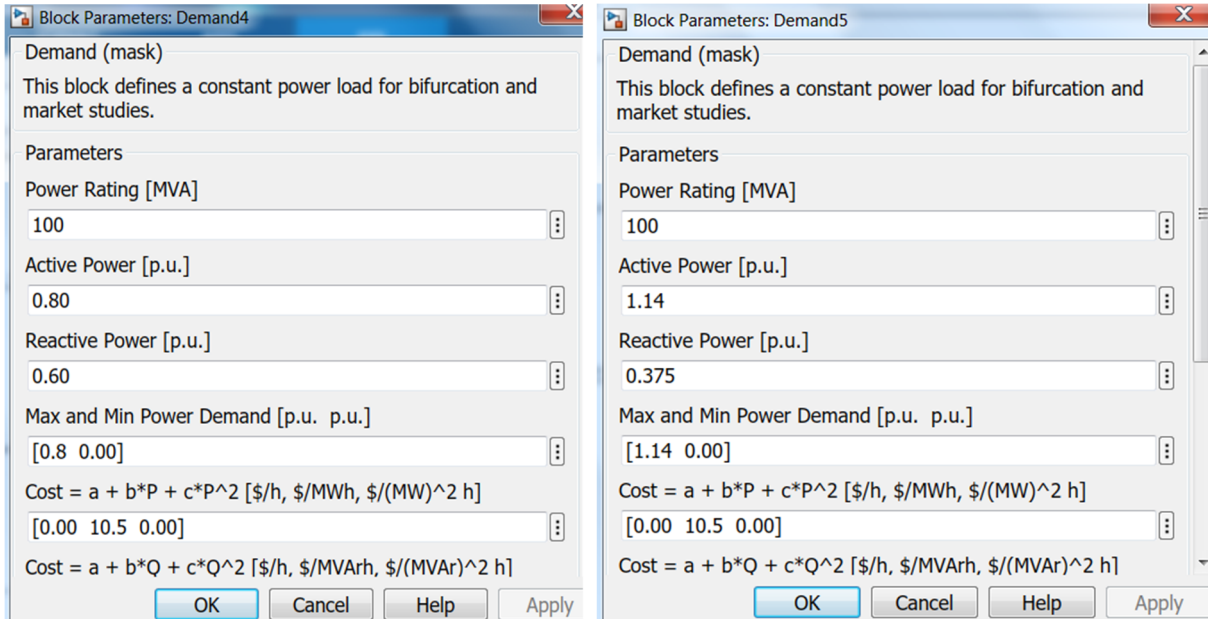
Appendix B shows the market models for the Zambian electrical grid with and without VRES integration. The cost functions coefficients ([table 7.1E](#)) used for this study are adopted from research ([Princy et al., 2018](#); [Molina et al., 2017](#)).

Table 7.1E: showing cost function coefficient for the different generators. Fixed costs are omitted and only proportional costs and quadratic costs for coal thermal are considered in this study.

#	Generator Type	PSAT Cost Coefficients			Generation Limit (MW)	
		a_i (\$/h)	b_i (\$/MWh)	c_i \$/(MW) ² h		
1	Coal (Princy et. al., 2018)	0	79.2	0.001562	50	150
2	Hydro (Princy et al., 2018)	0	3.0	0		
3	Wind (Princy et al., 2018)	0	4.1	0		
4	Photovoltaics	0	2.6	0		

Note: MCL has 2x150MW units installed. The 127MW value was the average for 2019-2020 because of a fault on one unit. Generation output for both units was not available. The cost coefficient for coal, hydro and wind are based on research (Princy et al., 2018) as this data was not readily available for Zambia. The cost coefficients for land PV and floating PV are assumed the same and are assumed less than hydro at 2.6\$/MWh due to absence of moving parts for a fixed mounted installation.

The details for the load showing the cost function for the demand is given below; The cost coefficients for the demand are the same for the entire network (only the actual load differs).



Showing two demand blocks for market studies

7.1.2.3 Optimal Power Flow Model Validation

The IEEE06 bus test system model is used for optimal power flow analysis validation of the ZESCO market model. Figure 7.1G shows the IEEE-06 bus system model for OPF validation.

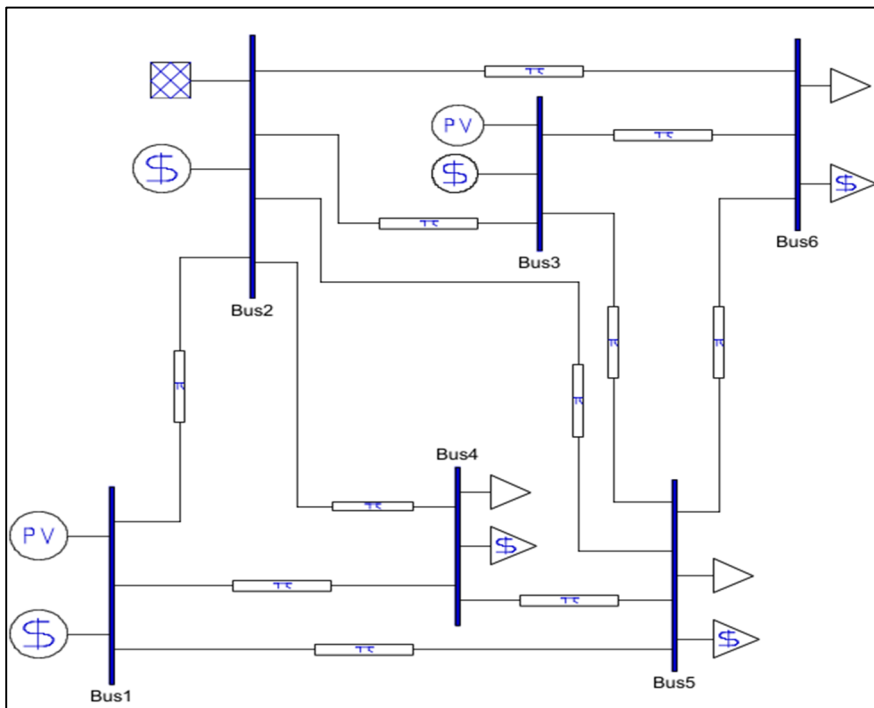
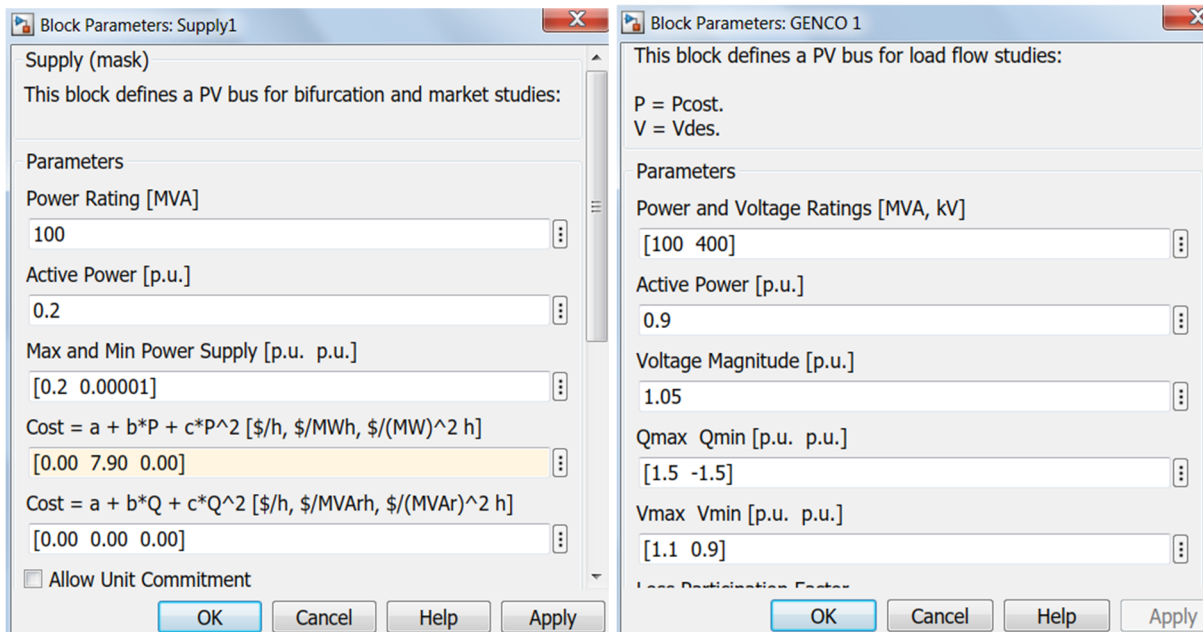


Figure 7.1G: showing the PSAT IEEE-06 test system for OPF

The model consists of 3 loads and 3 generators connected to 6 bus system. Here VRES comprising of floating photovoltaics and wind are connected to bus -1, bus-2 is the swing bus, bus1&3 are PV buses and bus-4, 5 and 6 are load buses. Loads were modelled as constant PQ load.

The details of the PV bus for market and power flow studies at bus 1 in the IEEE test system is shown below;



Showing PV bus for market and powerflow studies

Solution statistics of the IEEE PSAT test system market model with and without VRES integration is shown in table 7.1F and 7.1G. The simulation results show that the operating cost is reduced by renewable integration (Princy et al., 2018; Toma, R. and Gavrilas, M., 2014).

Table 7.1F: showing IEEE 6 bus results statistics without VRES

TOTAL LOSSES [MW]:	12.6
BID LOSSES [MW]	2.7
TOTAL DEMAND [MW]:	55
TOTAL TRANSACTION LEVEL [MW]:	335
IMO PAY [\$ /h]:	66

Table 7.1G: showing IEEE 6 bus results statistics with VRES

TOTAL LOSSES [MW]:	12.2
BID LOSSES [MW]	2.4
TOTAL DEMAND [MW]:	55
TOTAL TRANSACTION LEVEL [MW]:	335
IMO PAY [\$ /h]:	50

Note: Simulation results of the IEEE test system for OPF validation

7.1.2.4 Simulations Results

Simple Power Flow (SPF)

The line flows after integration of the variable renewable energy sources (VRES) are given in [table 7.1H](#);

Table 7.1H: showing lines flows after VRES integration

From Bus	To Bus	Line	P Flow	Q Flow	P Loss	Q Loss
			[MW]	[MVar]	[MW]	[MVar]
Swing	Kafue Gorge 330kV	1	120.3	-4.8	1.5	14.4
Kafue Gorge 330kV	Leopards Hill 330kV	2	495.6	81.6	4.8	20.5
Pensulo 330kV	Kabwe 330kV	3	-367.0	18.4	26.2	126.9
Pensulo 330kV	Msoro 330kV	4	98.4	27.0	1.6	-31.9
Leopards Hill 330kV	Kabwe 330kV	5	507.4	213.4	12.5	67.0
Leopards Hill 330kV	Kabwe 330kV	6	507.4	213.4	12.5	67.0
Leopards Hill 330kV	Kabwe 330kV	7	507.4	213.4	12.5	67.0
Leopards Hill 330kV	LSMFEZ 330kV	8	-297.6	-587.4	1.8	10.5
Vicotiria Falls via Mukuni 330kV	Muzuma 330kV	9	23.0	-31.9	0.0	-58.7
MCL 330kV	Muzuma 330kV	10	63.4	-4.7	0.0	-3.6
MCL 330kV	Muzuma 330kV	11	63.4	-4.7	0.0	-3.6
Muzuma 330kV	Kafue Town 330kV	12	69.8	-35.5	0.4	-66.9
Kafue Gorge 330kV	Leopards Hill 330kV	13	495.6	81.6	4.8	20.5
Kafue Town 330kV	Kafue West 330kV	14	-155.5	-77.6	0.0	-0.8
Kafue West 330kV	Lusaka West 330kV	15	54.6	-20.3	0.1	-18.3
Itezhi-Tezhi via Nambala 330kV	Lusaka West 330kV	16	12.7	-22.5	0.0	-53.5
Itezhi-Tezhi via Nambala 330kV	Lusaka West 330kV	17	12.7	-22.5	0.0	-53.5
Kalumbila 330kV	Itezhi-Tezhi via Nambala 330kV	18	-40.2	-30.1	0.6	-149.2
Kalumbila 330kV	Itezhi-Tezhi via Nambala 330kV	19	-40.2	-30.1	0.6	-149.2
Pensulo 330kV	Mpika SD 330kV	20	189.5	-71.4	6.6	65.5
Mpika SD 330kV	Lunzua via Kasama 330kV	21	112.3	-189.9	3.8	-36.2
Kitwe 330kV	Chambeshi 330kV	22	196.5	-16.4	0.5	-1.2
Kansanshi 330kV	Lumwana 330kV	23	50.3	23.6	0.2	-14.0
Kariba North 330kV	Leopards Hill 330kV	24	291.7	8.4	4.2	-11.4
Luano 330kV	Kansanshi 330kV	25	103.5	30.1	1.6	-32.2
Luano 330kV	Chambeshi 330kV	26	-123.1	26.1	0.2	-3.6
Kabwe 330kV	Luano 330kV	27	244.5	64.6	8.5	0.1
Kabwe 330kV	Luano 330kV	28	244.5	64.6	8.5	0.1
Kitwe 330kV	Kabwe 330kV	29	-242.0	-79.1	7.9	4.7
Kitwe 330kV	Kabwe 330kV	30	-242.0	-79.1	7.9	4.7
Lumwana 330kV	Kalumbila 330kV	31	0.0	0.0	0.0	0.0

Chipata West 330kV	Msoro 330kV	32	-47.6	-35.7	0.2	-13.6
Kafue West 330kV	LSMFEZ 330kV	33	224.3	-57.8	0.9	-8.7
KGU Wind Farm	Kafue Gorge 330kV	34	100.0	-5.0	1.0	9.9
Kariba North 330kV	Leopards Hill 330kV	35	291.7	8.4	4.2	-11.4
KGU Solar PV Generator	Kafue Gorge 330kV	36	100.0	-5.0	1.0	9.9
Kafue Gorge 330kV	Kafue West 330kV	37	254.8	-10.8	1.1	-7.1
Kariba North 330kV	To ZESA	38	0.0	-0.1	0.0	-0.1
Kariba North 330kV	To ZESA1	39	0.0	-0.1	0.0	-0.1
Kariba North 330kV	Kafue West 330kV	40	182.6	-32.0	1.7	-34.4
Kariba North 330kV	To Siavonga	41	80.0	56.6	0.0	-3.4

The global power summary with the integration of VRES is given in figure 7.1H below.

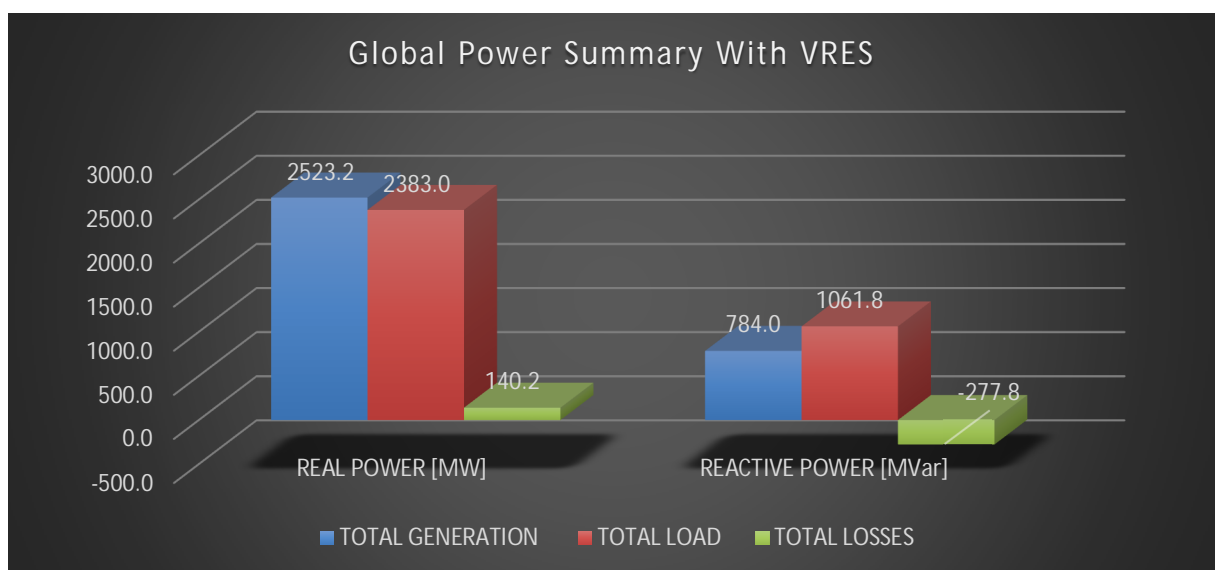


Figure 7.1H: showing global power summary with VRES integration at constant load

The active and reactive components of all the network generators before and after integration of VRES is shown in figure 7.1I and 7.1J respectively;

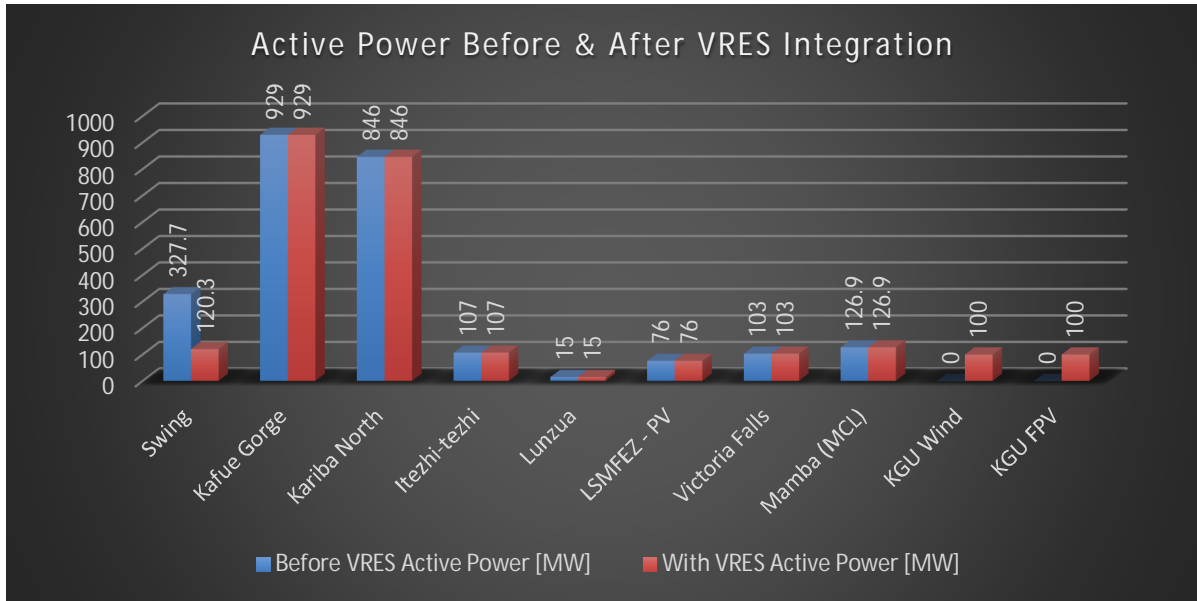


Figure 7.1I: showing active generation power before and after VRES integration

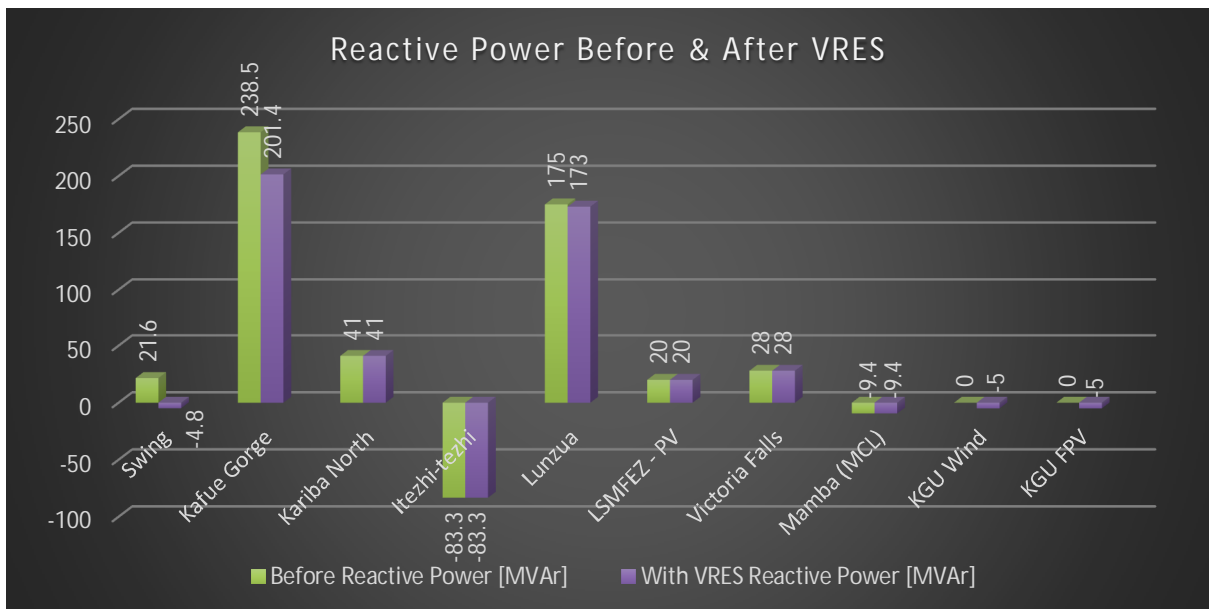


Figure 7.1J: showing active generation power before and after VRES integration

Optimal Power Flow

The table 7.1I below shows the results for the six different dispatch scenarios used for optimal power flow analysis with unit commitment.

Table 7.1I: showing optimal power flow results for six different dispatch scenarios

Dispatch Scenario	Total Transaction Level (MW)	Total Loss(MW)	Bid Loss(MW)	Cost(\$/h) x10 ⁶
Scenario 1	3248	55	-88.7	0.578
Scenario 2	3231.4	62	-91.2	2.578
Scenario 3	3227.9	62	-85.3	3.677
Scenario 4	3230.5	55	-92.5	0.471
Scenario 5	3151	58.5	-85.2	11167.5
Scenario 6	3120	57	-82.8	28302.6

Figures 7.1K, 7.1L and 7.1M shows the total transaction, total losses and operating costs for 6 scenarios.

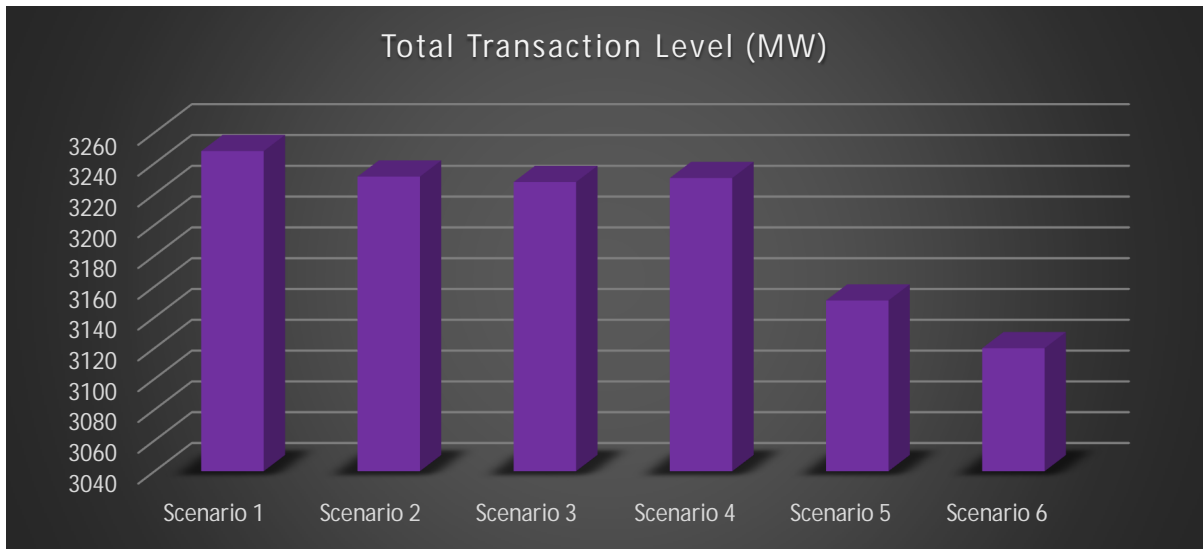


Figure 7.1K: showing transaction level for the different dispatch scenarios



Figure 7.1L: showing losses for the different dispatch scenarios



Figure 7.1M: showing cost (\$/h) for the different dispatch scenarios

7.1.3 Results Analysis

Existing Network

- ✓ From the results obtained in section 7.1.1.2, the voltage magnitude profile and losses improved after the addition of network compensating equipment at different buses. All the 9 voltage violations were corrected by this action.
- ✓ The results also showed all the line power flows to be within range (i.e. less than the maximum line capacity of 700 MVA at unit power factor).

VRES Integration

- ✓ The integration of the floating photovoltaic (100 MW) and onshore wind (100 MW) improved the network voltage profile even further especially for buses near the Kafue Gorge generating bus.
- ✓ The VRES integration also reduced the reactive power generated by the Kafue Gorge hydro plant from 239 to 201 MVar. This reduction is due to reduced voltage support requirement of the network with additional generation.
- ✓ The active power loss of the network reduced from 147 MW to 140 MW with integration of VRES.
- ✓ The total reactive power loss also changed from -204 MVar to -278 MVar with the addition of VRES.

Optimal Power Flow

- ✓ Scenario 4 dispatch (hydro + existing PV + onshore Wind) was found to be the most economical with a reduction in operation cost of 471 k\$/h. This scenario also had the least total loss of 55 MW.
- ✓ Scenario 6 dispatch (hydro + existing PV + coal + onshore wind + FPV) was found to be least economical with cost of 28 B\$/h and loss of 57 MW.
- ✓ Even though scenario 1 (existing network scenario) has reasonable operating cost margin, this is not preferred due to the emissions produced by operating the coal plant. Therefore, scenario 2 (hydro + existing PV) and 3 (hydro + existing PV + floating PV) are the preferred scenarios after scenario 4.

7.2 Assessment of Seasonal Hydro Generation & Grid Demand

To understand the seasonal daily dispatch potential between hydro and VRES, it was imperative to collect time series hourly data for Kafue Gorge Upper hydro generation and national electrical grid demand. ZESCO Ltd availed the hydro generation and grid load hourly data for the 2018-2019 period. Further, a sensitivity analysis was done for the grid load at intervals of 25%, 50%, 75% and 100% of the actual demand. Against this background, the other sections are structured as follows: [section 7.2.1](#) assesses the hydro generation at Kafue Gorge Upper with emphasis on the HVA table, reservoir operation rule curves, generation modelling and defines three generation scenarios, while [section 7.2.2](#) looks at the national electrical grid load.

7.2.1 Kafue Gorge Generation Assessment

Based on the scope methodology and the recent study conducted by CESI (2020), different hydrological conditions are defined to analyse the impact of climate change on the variable renewable energy source (VRES) integration. Firstly, the prevailing scenario is considered as the current water availability with reference to the Kafue Gorge upper (KGU) hydropower plant. Thereafter, two more scenarios are considered, the condition with normal water availability which depicts the reference/plant design scenario based on the average 30-year record of water inflows; and the low water availability condition below the average 30-year water inflows (i.e. assumed -33 percent of existing scenario in this study). Against this background, the KGU generation assessment is structured as follows; [section 7.2.1.1](#) illustrates the HVA table that shows the relationship between reservoir level and corresponding surface

area (and volume), [section 7.2.1.2](#) presents the KGU operation rule curves, while [sections 7.2.1.3](#) and [7.2.14](#) models and presents the hydro generation and generation scenarios respectively.

7.2.1.1 Kafue Gorge HVA Table

To fully understand the extent of seasonal generation and operating limits with reference to reservoir level and volume, the Kafue Gorge Upper HVA [table 7.2A](#) was used. The table defines a reservoir minimum and maximum operating range of 974 m and 977 m above sea level respectively.

Table 7.2A: showing the HVA table for Kafue Gorge Upper

Kafue Gorge Upper (existing)				
Table 3.22. Kafue Gorge Upper Reservoir – storage, area, outlet and elevation				
Storage (million m ³)	Area (km ²)	Outlet capacity (m ³ /s)	Elevation (m)	Note
19.5	35	233	973.0	
39.8	47	291	973.5	
68.9	70	350	974.0	
110.6	98	408	974.5	
170.4	142	466	975.0	
262.5	235	525	975.5	
423.1	430	1,166	976.0	
709.0	725	2,333	976.5	
785.0	805	3,500	976.6	FSL
1177.5	1,175	4,900	977.0	

*Source: ZRA 2007.
Note: FSL: full supply level.*

7.2.1.2 Kafue Gorge Upper Reservoir Operation Rule Curves

Reservoir operation rule curves are lines designed to guide the operation regime of the reservoirs. There are essentially two types of rule curves;

- i. Lower rule curves: Reservoir level trajectory that should be followed in reservoir operation during stressed hydrological conditions.
- ii. Upper rule curves: Reservoir level trajectory that normally has to do with the safety of the reservoir. This operating guideline is usually adopted in exceptional hydrological years characterized by water spillage from the reservoir.

In ZESCO, only the three major reservoirs have operating rule curves; Itezhi-tezhi Reservoir - both curves were developed, Kafue Gorge - only the Upper rule curve was developed, Kariba

- only the upper rule curve was developed. Table 7.2B shows the end of month reservoir levels for Kafue Gorge. These are a set of End of Month (EOM) Reservoir levels which serve as a guide for operating a reservoir between two contrasting Hydrological years. Figure 7.2A shows the upper rule curve for Kafue Gorge.

Table 7.2B: showing E.O.M Upper reservoir rule levels for KGU

Month	E.O.L (m A.S.L)	Volume (MCM)	Reservoir Area (km ²)
January	976.50	709	Interpolate from the HVA table 7.2a
February	977.00	1,178	
March	977.00	1,178	
April	977.00	1,178	
May	976.52	724	
June	975.93	268	
July	975.42	397	
August	975.40	242	
September	975.40	242	
October	974.40	242	
November	975.40	242	
December	975.89	383	

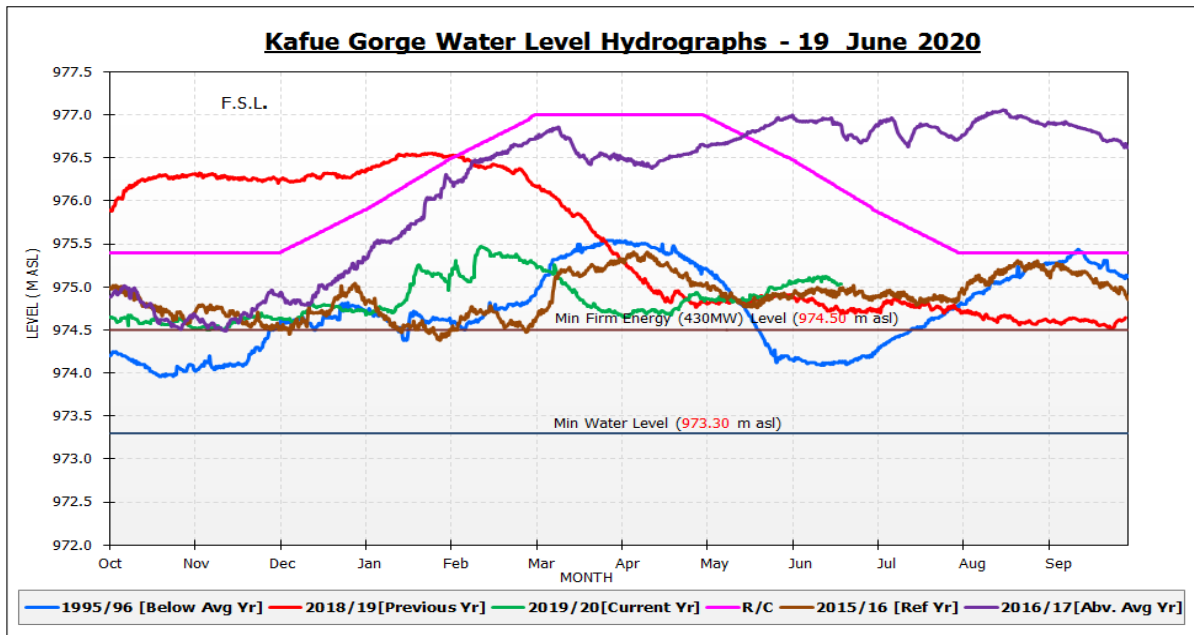


Figure 7.2A: showing the upper rule curve for KGU

7.2.1.3 Hydro Generation Modelling

The Kafue Gorge Upper hydro generation was modelled in iHoga using the power plant ratings provided by the national power utility (ZESCO Ltd) in table 7.2C. The iHoga model for one

turbine is given in figure 7.2B with 4% losses in penstock, 0% daily/hourly variability and 85% total turbine efficiency.

Table 7.2C: showing rating parameters of Kafue Gorge Upper generation plant

Parameter	Unit 1 - 6		Generation Vs. Turbine - One Unit	
			Gen (MW)	Tub (m ³ /s)
Installed capacity (MW)	990			
Number of units	6		75	22.00
Max Turbine Q (m ³ /s)	278.1		80	23.00
Head (m)	382		85	25.00
Minimum operating level (m ASL)	972.3		90	26.00
Constraints/Requirements			95	27.00
Minimum release req (m ³ /s)	29		100	29.00
Minimum generation (MW)	100		105	30.00
Efficiency table			110	31.00
Height (m)	Percent (%)		115	33.00
0	0		120	34.00
360	89		125	35.00
387	92		130	37.00
396	91		135	38.00
Tailwater table			140	40.00
Discharge (m³/s)	Level (m ASL)		145	41.00
0	579.0		150	42.00
115	579.6		155	43.45
212	580.8		160	44.90
400	582.1		165	46.35
615	583.2			
820	584.0			
1590	586.4			

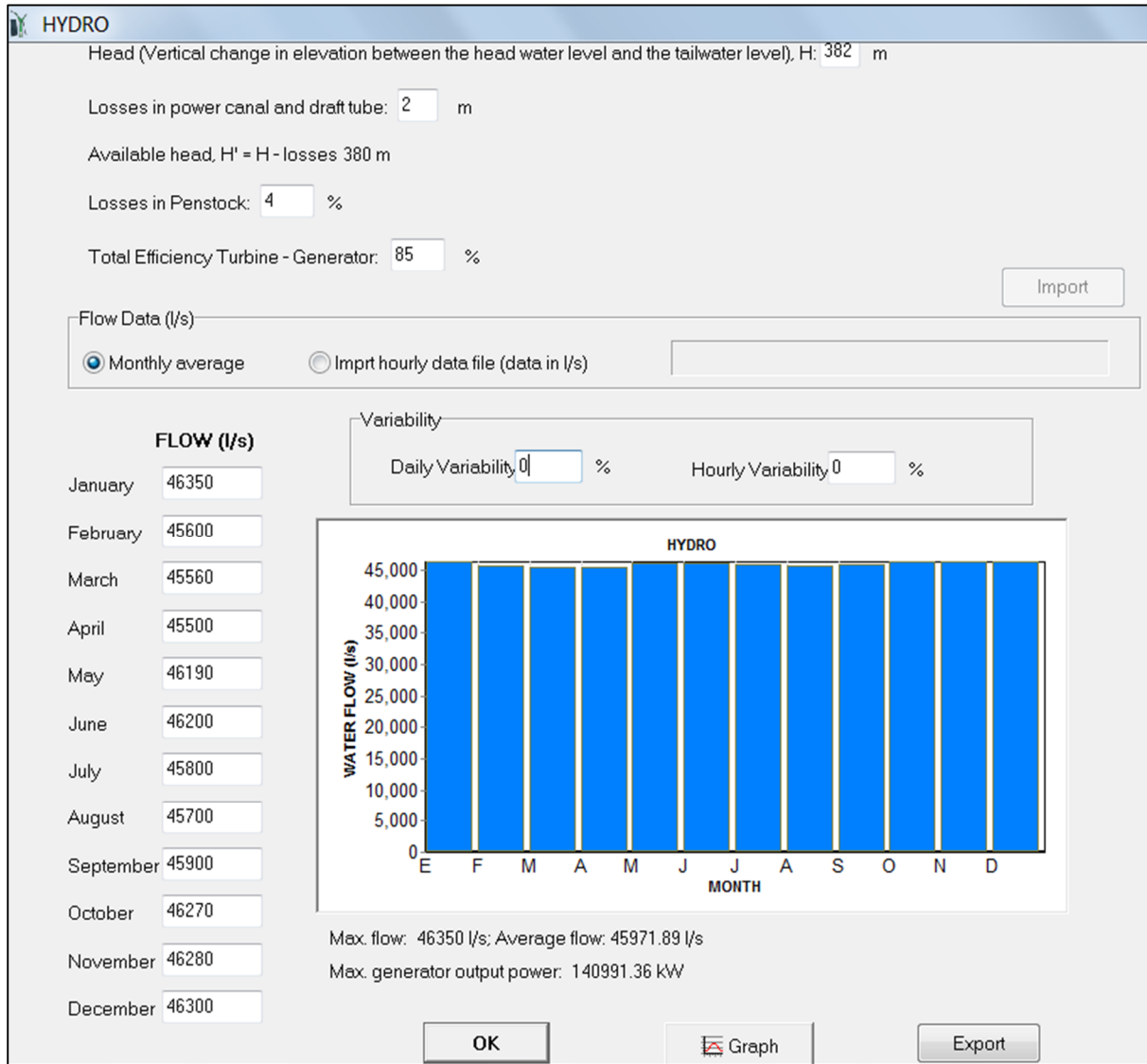


Figure 7.2B: showing the modelled KGU hydrogeneration for one turbine in iHoga software

7.2.1.4 Kafue Gorge Generation Scenarios

Three generation scenarios are considered for Kafue Gorge Upper and these include current water availability (CWA), low water availability (LWA) and normal water availability (NWA). The CWA is the generation scenario of 2019 to July 2020 at Kafue Gorge powerplant, while the other two scenarios are defined in the introductory part of section 7.2.1. Figures 7.2C, 7.2D, 7.2E depict the timeseries hourly profile for the first day of each month for CWA, LWA and NWA respectively. July and August are months with the highest generation output at Kafue Gorge, while May is the month with the least generation.

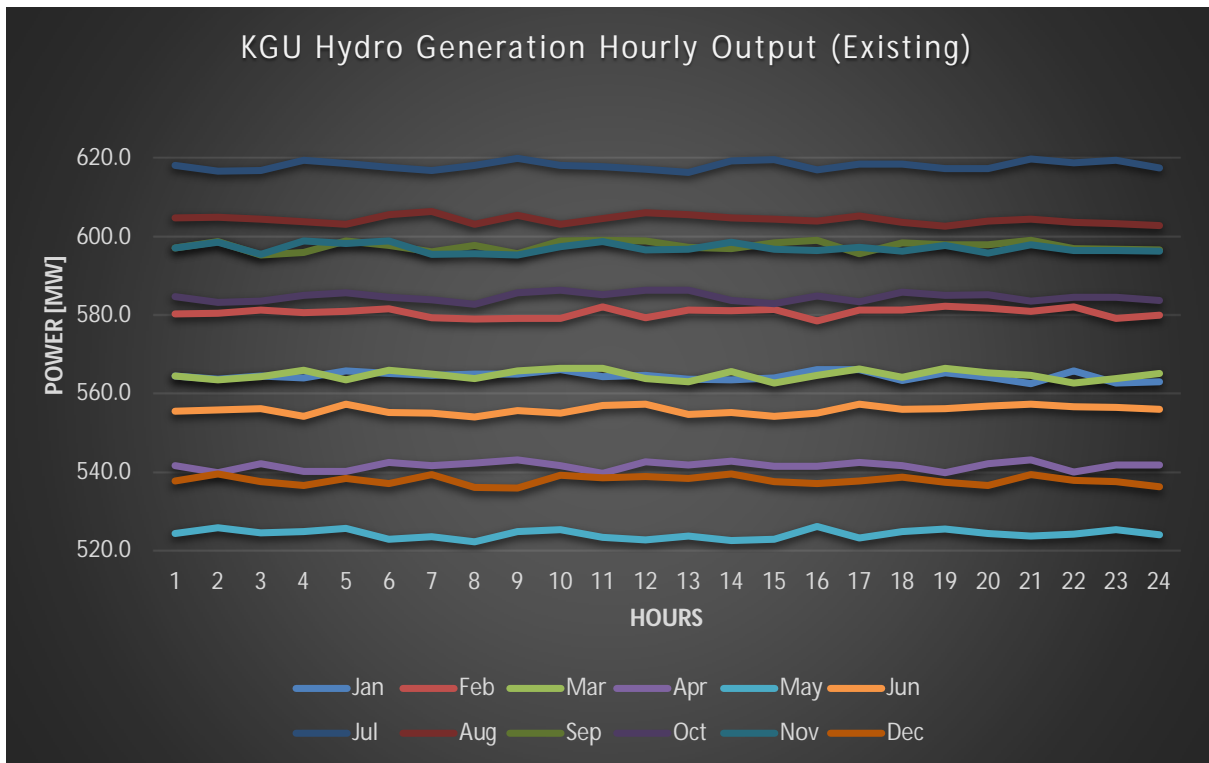


Figure 7.2C: showing current water availability generation first day of each month With July having an average output of about 620MW while May has approximately 525MW.

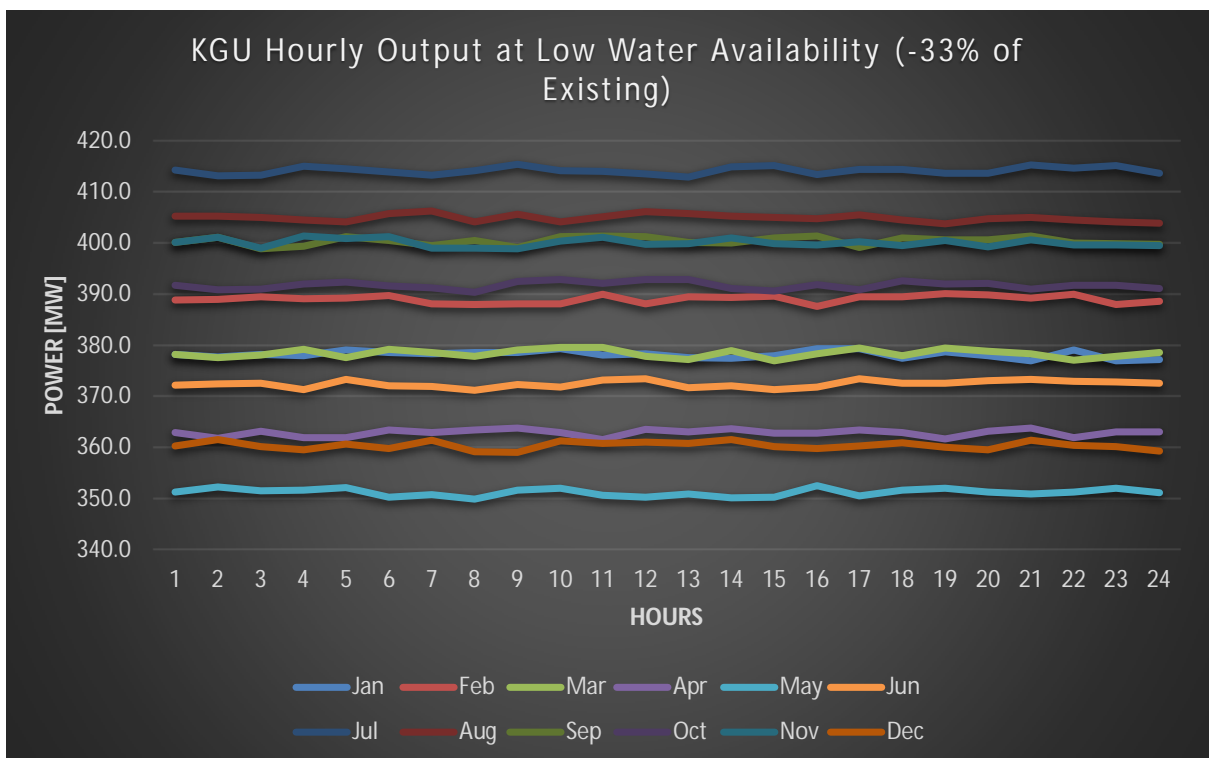


Figure 7.2D: showing low water availability generation for first day of each month. With July having average output of 414MW while May has 350MW.

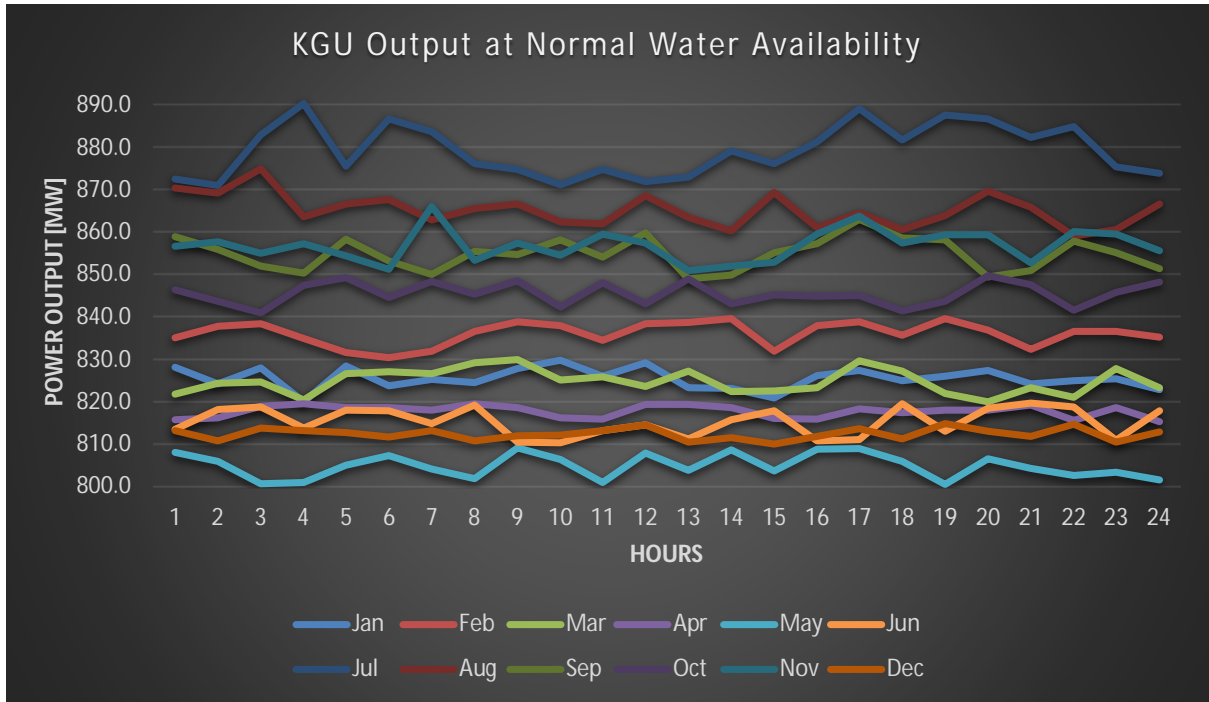


Figure 7.2E: showing normal water availability generation for first day of each month

7.2.2 National Electrical Grid Load Assessment

The maximum national electricity consumption has remained the same from 2018 to 2020. However, the challenge has been the reduction in generation capacity due to reduced water levels at all reservoir type hydro plants (including run-of-river type). Based on data collected from the national utility and CESI, electrical demand varies distinctively in five months of the year and these have been plotted as shown in figure 7.2F. November has the highest electrical grid peak demand of approximately 2200 MW while March has the least with 1800 MW.

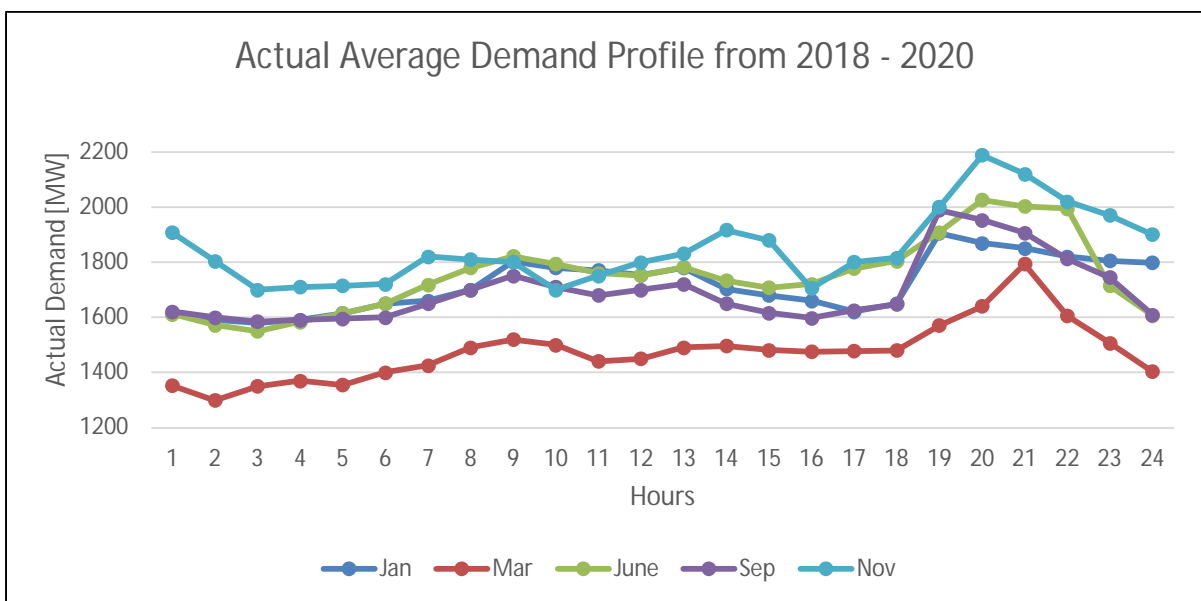


Figure 7.2F: showing seasonal variation of demand.

7.3 Detailed VRES (FPV & Wind) Assessment and Design at KGU

This section presents a detailed assessment and design for floating photovoltaics and onshore wind at Kafue Gorge Upper powerplant. The actual FPV potential at KGU with maintenance access, shading, equipment placement, mooring and anchoring put into consideration is about 116 MWp direct current, which gave an inverter output design equivalent of 100 MWac. With this capacity, a wind farm of similar rating (100 MWac) was designed approximately 14 km from the FPV site.

[Section 7.3.1](#) covers the detailed design analysis of the photovoltaic system using PVSYST software, covering interrow spacing, system layout, composition and characteristic of system design components, comparing the yield of three known FPV configurations (free standing, small footprint and large footprint) to that of a ground mounted system. Further, detailed analysis was done for the large footprint FPV configuration which emulates the system capacity at KGU, this includes shading scene analysis, system main results (normalized production in kWh/kWp, performance ratio and time series hourly power output for the first day of the month in MW), loss diagram assessment and an economic evaluation of the PV system in PVSYST.

[Section 7.3.2](#) covers the detailed design analysis using renewables ninja / homerpro and presents an optimal turbine placement based on the site wind rose diagram and wind speed variability as obtained using global wind atlas software. Further, yield analysis of the wind farm is done for optimistic and conservative scenarios.

7.3.1 KGU Floating Photovoltaics Assessment & Design

7.3.1.1 Interrow Spacing of FPV System

To get a high-performance ratio from the FPV system, the appropriate spacing between rows was calculated based on [figure 7.3A](#) to avoid inter-panel shading. The PV modules to be used in this project are the 285 Wp with a size of (W x L) 0.992 m x 1.640 m. The modules will be north facing tilted at an optimal angle of 20°.

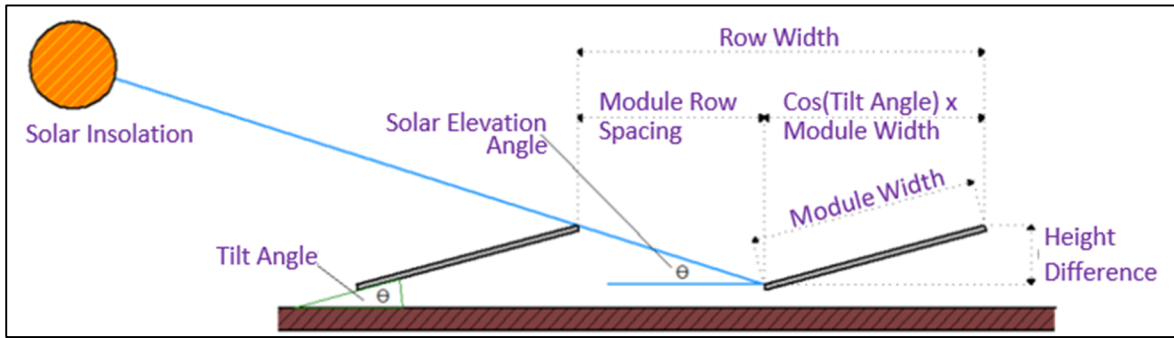


Figure 7.3A: showing the principle used to calculate interrow spacing (Adopted from CED GREENTECH)

$$\begin{aligned} \text{The height difference} &= \sin 20^\circ \times 1.984 \text{ m} \\ &= 0.6786 \text{ m} \end{aligned} \tag{31}$$

Where 20° is the tilt angle while 1.984 is the length/width of the two modules (module width = 0.992×2). Using the solar chart of the Kafue Gorge site (figure 7.3B) and using the worst-case scenario of no shading and factoring in the terrain horizon between 9AM and 3PM during the winter solstice (21st June), the solar elevation angle was estimated to be 30° . The winter solstice is when the sun is the lowest in the sky and thus creates pronounced shadows.

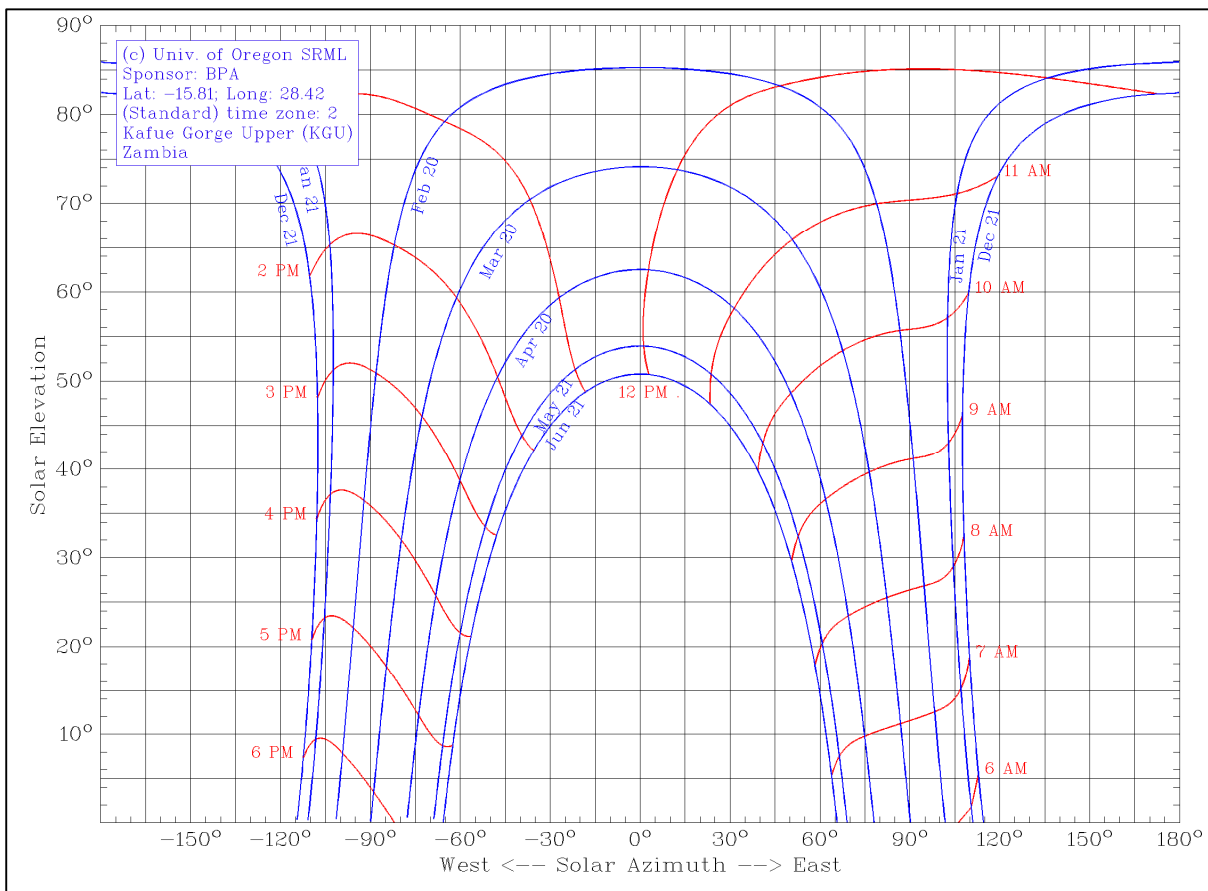


Figure 7.3B: showing the solar chart for KGU site (Source: Sun Path Chart Program, University of Oregon)

$$\text{Module row space} = \text{height difference} / \tan (30) \tag{32}$$

$$= 0.6785/\tan (30)$$

$$\approx 1.18 \text{ m}$$

The module row space can be reduced further if one takes account of the solar azimuth. Using the solar chart given below, the azimuth angle correction was found to be approximately 50° between that time (09AM to 3PM).

$$\begin{aligned} \text{Minimum module row space} &= \text{module row space} \times \cos 50 & (33) \\ &= 1.18 \times \cos (50) \\ &= 0.755 \text{ m} \end{aligned}$$

Therefore, **the pitch** (from the edge of one row to the next row will be):

$$\begin{aligned} &= \text{minimum row space} + \cos (\text{tilt angle}) \times \text{module length} & (34) \\ &= 0.755 + \cos 20 \times 1.984 \\ &\approx 2.62 \text{ m (3m used in PVSYST)} \end{aligned}$$

7.3.1.2 System Layout, Design Components & Characteristics

System Layout & Design

The site effective area, the form factor (ratio of array “nominal power dc”/“Inverter nominal power ac”) and shading analysis was used to develop the overall system capacity of the photovoltaic system. Adopted from PVSYST design manual and industry practice, the recommended form factor when sizing arrays is between 1 to 1.3 (1-1.1 for many inverter providers and 1.25 – 1.3 for well oriented systems). The KGU project proposes a form factor of 1.16. The proposed system design layout is as shown in [figure 7.3C](#) which comprises of 8 sub-arrays connected in parallel. Each sub-array consists of a 120 series string of 17 PV solar modules (unit PV module rating of 285 Wp with 72 polycrystalline cells) connected to a 500kWac inverter, with 25 inverters in parallel linking into the ac combiner box for 1 sub-array. The maximum power point voltage (U_{mpp}) and current (I_{mpp}) for each sub-array is 549 V and 23.7 kA respectively.

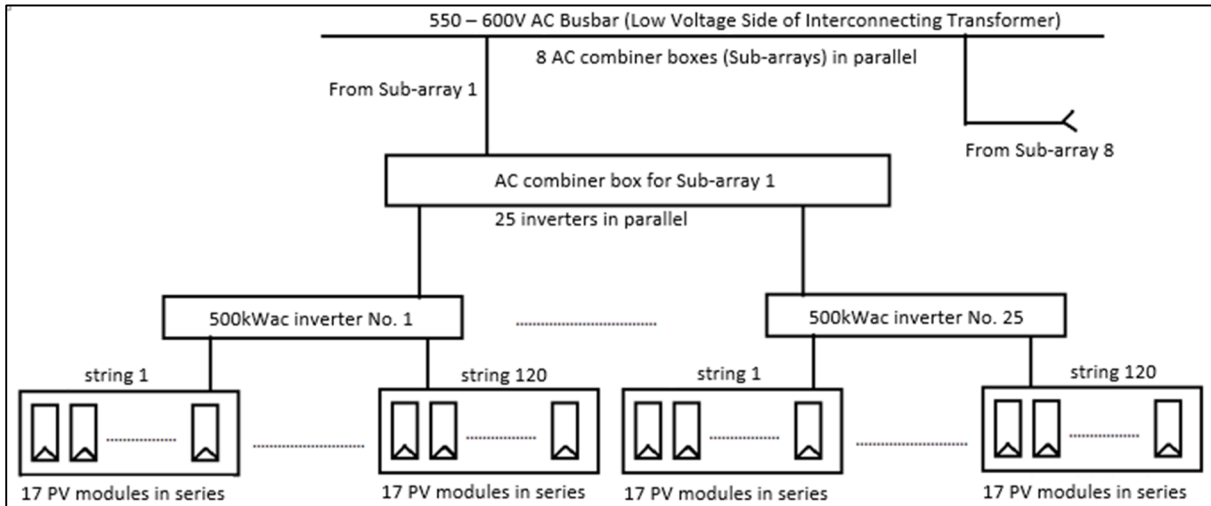
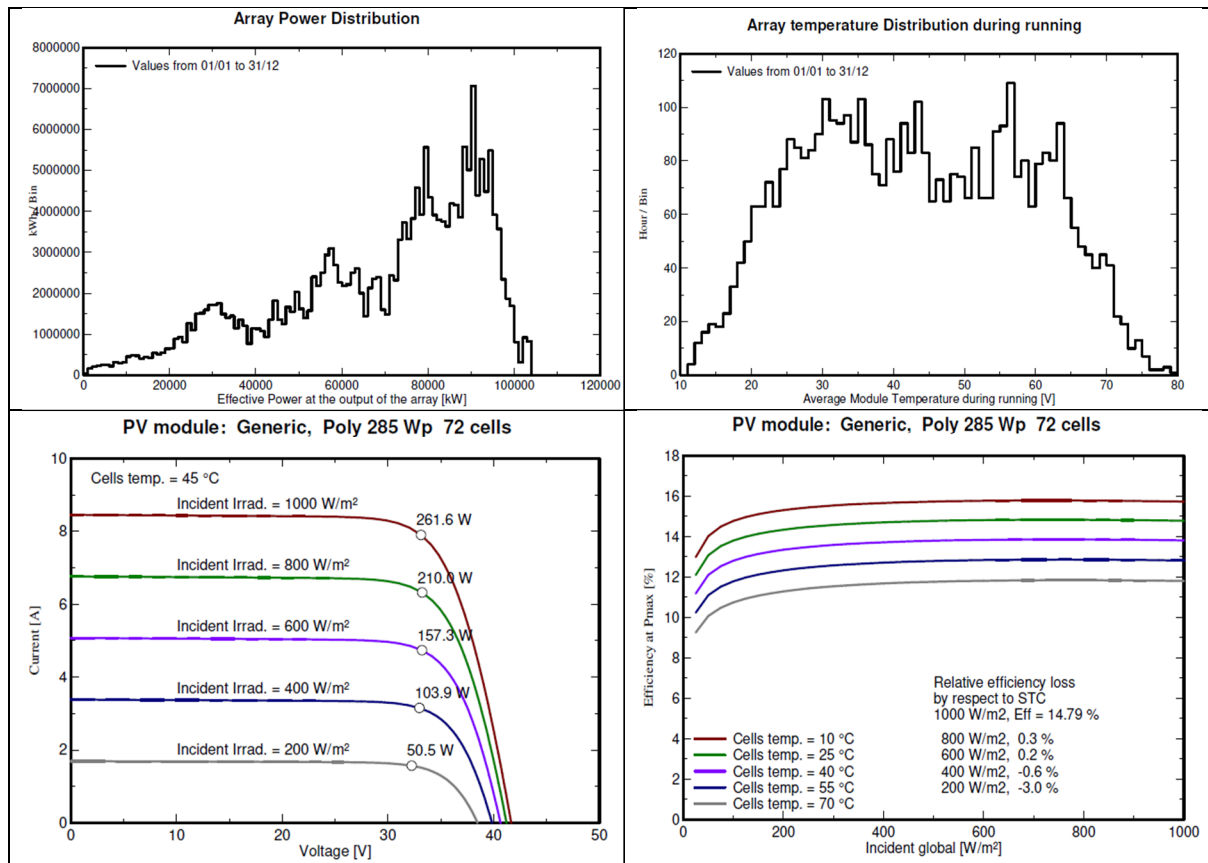


Figure 7.3C: showing component layout of photovoltaic system design

PV Module and Array Design Characteristics

The photovoltaic and array characteristics for the designed system are summarized in figure 7.3D showing array power and temperature distribution, voltage vs current (VI) at constant temperature and variable irradiance, global irradiation vs efficiency at variable temperature, power vs voltage at constant temperature and variable irradiation, P vs V at constant irradiation and variable temperature.



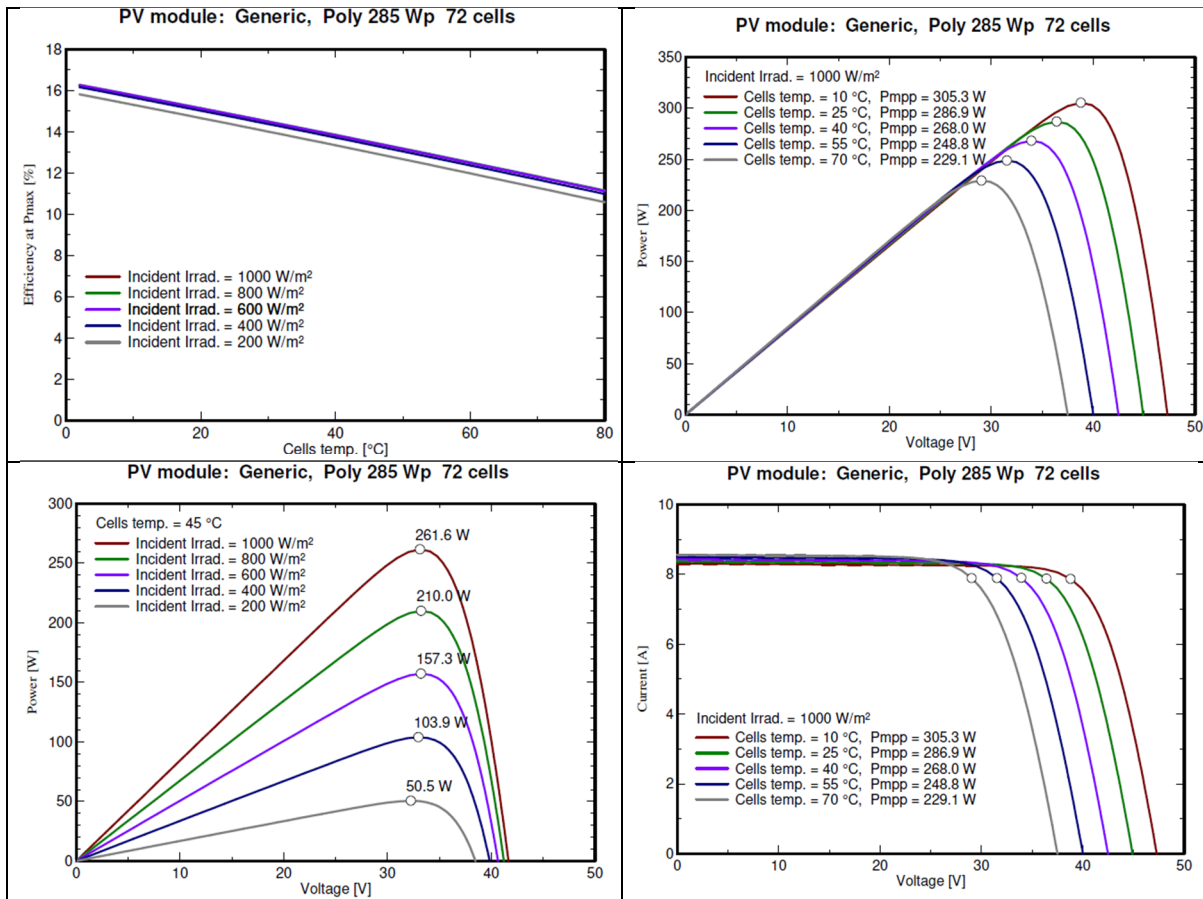


Figure 7.3D: showing PV module and array characteristics of designed system

7.3.1.3 Yield Comparison Between FPV Configurations and Ground Mounted System

This section compares the energy yield and performance ratio between three different floating photovoltaic configurations and a ground-mounted system at the same location (KGU) and with all other design parameters the same, except the albedo and heat loss factor (U-value in W/m^2K) that correspond to the cooling effect of each system. Table 7.3A illustrates the albedo and U-value for the four different system configurations.

Table 7.3A: showing the albedo and U-value of the four different configurations

#	System Configuration Type	Albedo Value	U-Value (W/m^2K)
1	Free standing FPV	0.1	46
2	Small footprint FPV	0.1	35
3	Large footprint FPV	0.1	31
4	Ground-mounted PV	0.2	20

Each system was designed separately with simulations run independently in PVSYST to ascertain the yield in GWh/year and performance ratio as shown in figures 7.3E and 7.3F respectively.

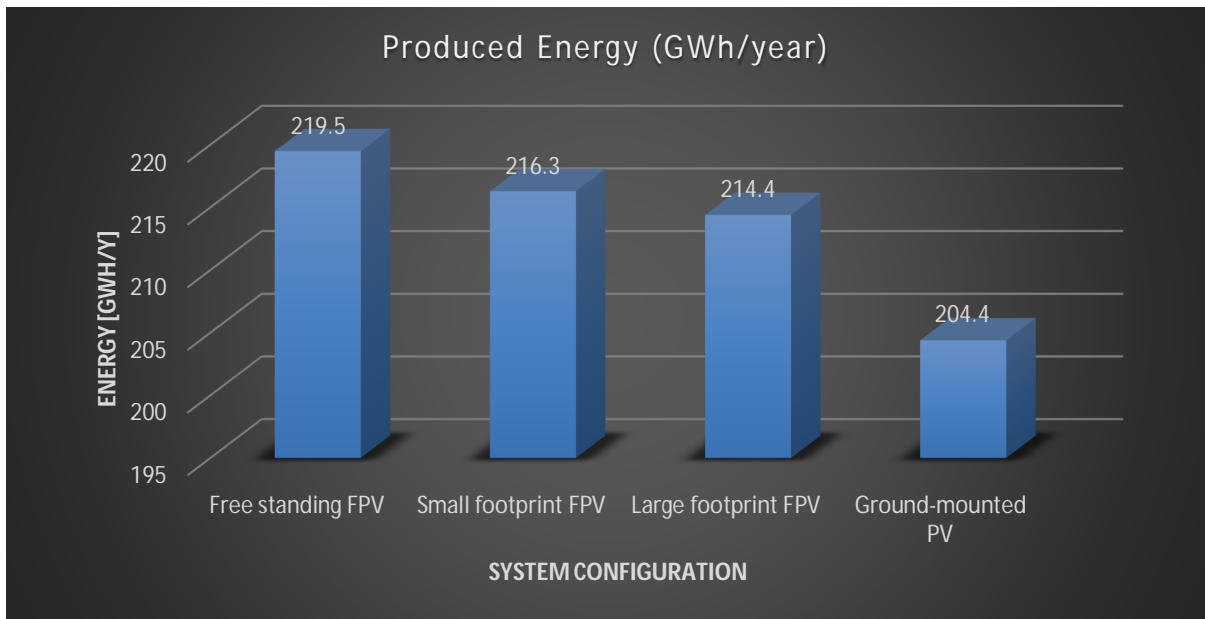


Figure 7.3E: showing energy production in GWh/year for each system configuration

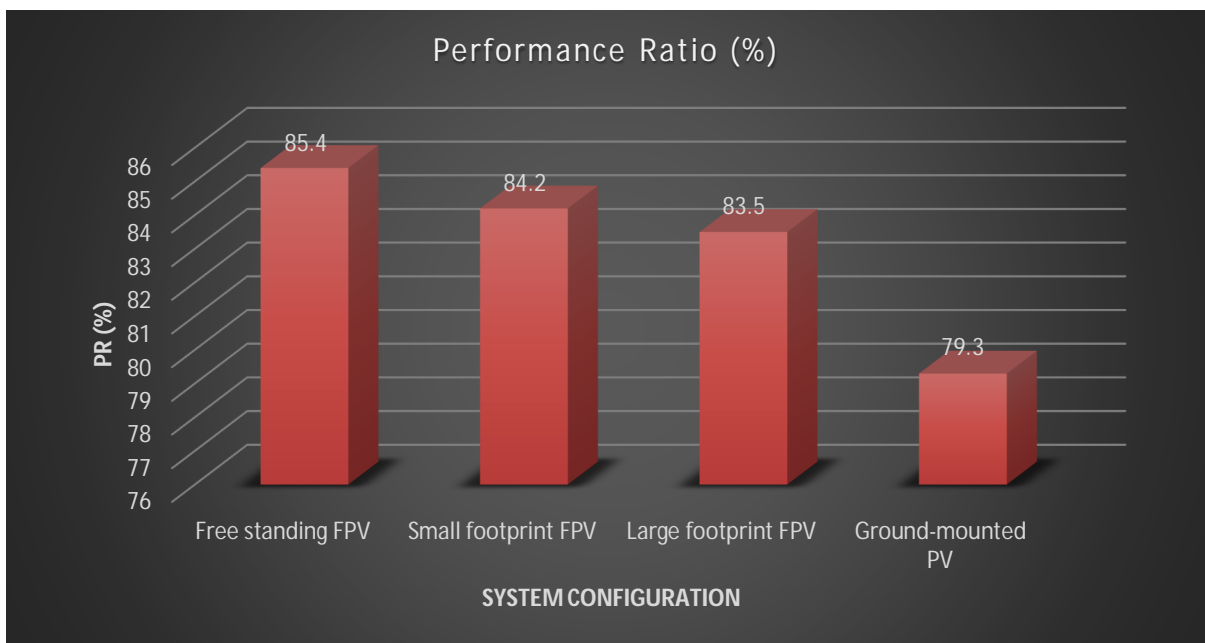


Figure 7.3F: showing performance ratio for each system configuration

This analysis shows that free standing floating PV has better performance (energy yield of 219.5 GWh/y and PR of 85.4%) of the four systems while ground mounted PV has the least performance (energy yield of 204.4 GWh/y and PR of 79.3%).

The large footprint configuration is assumed to emulate the capacity at KGU in the proceeding analysis from [sections 7.3.1.4 to 7.3.1.8](#).

7.3.1.4 FPV Shading Scene (large footprint)

The shading scene and layout for the large footprint FPV is illustrated in figure 7.3G.

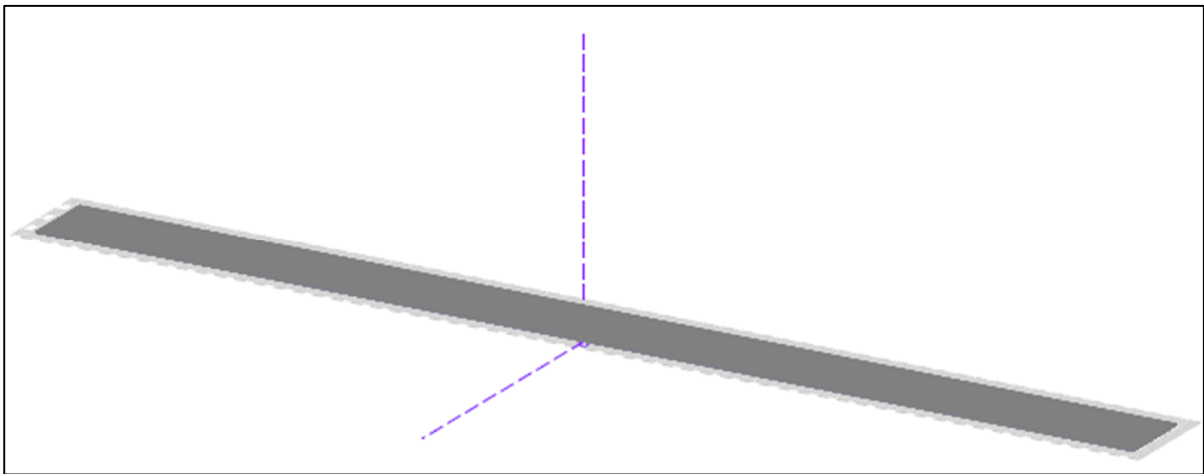


Figure 7.3G: showing perspective of the PV-field and surrounding shading scene

From the iso-shading diagram in figure 7.3H, the sun is at the lowest point on June 22, while December 22 is the highest point of the sun in the sky. The main source of shading is the inter row spacing between modules and the shading due to the reservoir bank. There is no shading analysis due to vegetation or buildings since the Kafue gorge reservoir is far from tall trees and buildings with the surrounding area having a roughness length value of about 0.1.

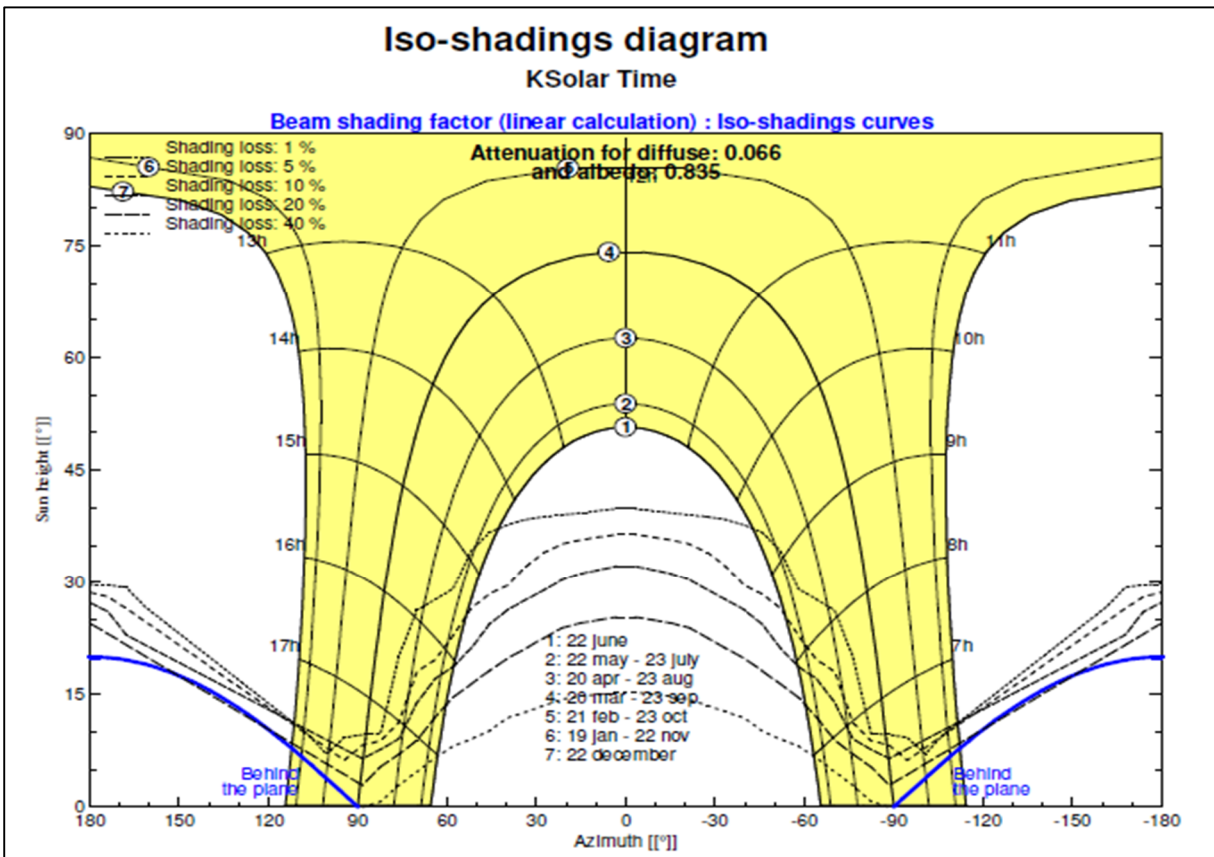


Figure 7.3H: showing the shading loss diagram for the design with pitch 3m

The PV system layout (i.e. interrow spacing) was designed for the worst-case scenario on 22 June between 09am and 3pm which is the solar window for the location. There is a shading loss of 1% between 3pm - 2:30pm and between 9am- 9:30am on the winter solstice. On May 22 (and July 23), there is 1% shading between 3pm – 2:50pm and between 9am-9:10am. There is zero percent shading between 9am-3pm on April 20, August 23, March 20, September 23, February 21, October 23, January 19, November 22 and December 22. Further, the solar window was extended to 10hrs(7am-5pm) from the initial design of 6hrs (9am-3pm) without any shading on March 22, September 23, February 21, October 23, January 19, November 22 and December 22.

7.3.1.5 System Main Results (large footprint)

Figure 7.3I illustrates the performance ratio and normalized productions per installed kWp. August and May yielded the most useful normalized energy from the floating PV system of about 6 kWh/kWp/day, while January and December yielded the least with about 3.7 kWh/kWp/day. Further, June and July are the two months with the highest performance ratio of the FPV system with October being the least.

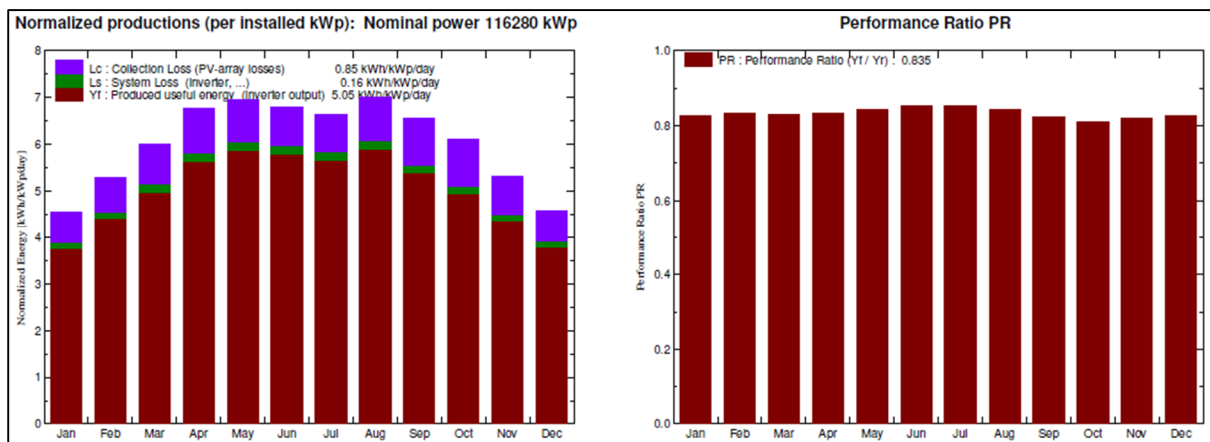


Figure 7.3I: showing normalized productions and performance ratio for the large footprint FPV

Table 7.3B presents a summary of FPV system average results for a year and these include global horizontal irradiation, ambient temperature, global incident in collector plane, effective energy output of the array, energy injected into the grid, array efficiency and system efficiency over a rough area. The months from April to September have high average values of effective array energy output and energy injected into the grid which also corresponds to low ambient temperatures and high effective global irradiation corrected for incident angle modifiers (IAM) and shadings. January and December are the months with least energy injection into the grid, 13.6 GWh and 13.7 GWh respectively.

Table 7.3B: showing summary of system performance on average from January to December

	GlobHor kWh/m ²	T Amb °C	GlobInc kWh/m ²	GlobEff kWh/m ²	EArray MWh	E_Grid MWh	EffArrR %	EffSysR %
January	155.3	21.43	141.3	131.0	14032	13591	12.54	12.15
February	155.2	21.46	148.3	138.5	14816	14365	12.62	12.23
March	182.4	21.57	186.1	177.0	18554	17984	12.59	12.21
April	183.1	20.36	203.0	194.2	20313	19700	12.64	12.26
May	178.5	18.76	215.6	206.1	21825	21183	12.79	12.41
June	161.9	16.80	204.3	193.9	20854	20255	12.89	12.52
July	166.6	16.78	206.2	196.2	21079	20458	12.91	12.53
August	187.6	20.06	217.0	208.6	21936	21288	12.77	12.39
September	186.2	23.23	196.6	187.3	19420	18842	12.48	12.11
October	193.4	25.61	189.1	178.5	18397	17852	12.29	11.92
November	174.7	23.56	159.8	148.8	15712	15244	12.42	12.05
December	158.7	21.47	142.3	131.6	14099	13670	12.51	12.13
Year	2083.6	20.92	2209.7	2091.8	221036	214432	12.64	12.26

Legends:	GlobHor	Horizontal global irradiation	EArray	Effective energy at the output of the array
	T Amb	Ambient Temperature	E_Grid	Energy injected into grid
	GlobInc	Global incident in coll. plane	EffArrR	Effic. Eout array / rough area
	GlobEff	Effective Global, corr. for IAM and shadings	EffSysR	Effic. Eout system / rough area

Figure 7.3J shows the power output of the 8 arrays of the system for the first day of each month. 1st September has the highest peak output of about 97 MW at midday.

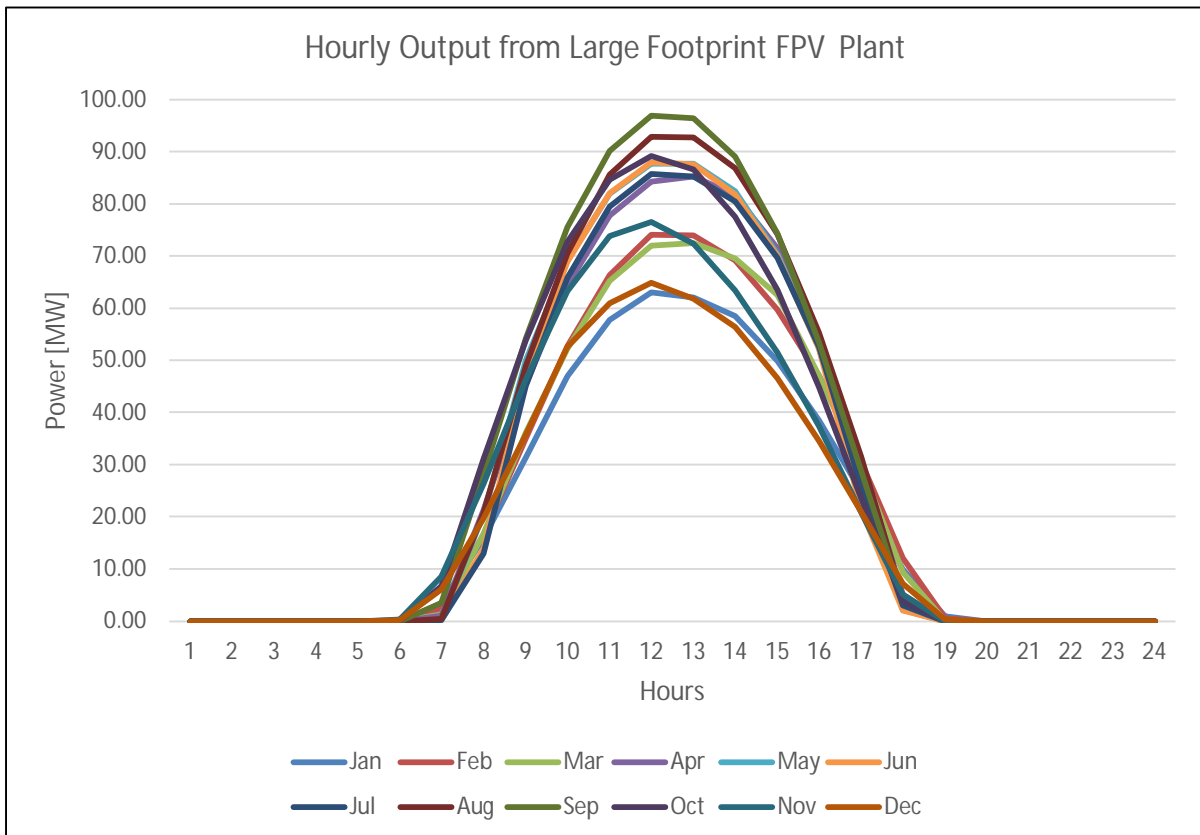


Figure 7.3J: showing array power output for the first day of each month

7.3.1.6 Loss Diagram Assessment (large footprint)

Figure 7.3K shows the distribution of significant system losses from the onset of horizontal global irradiation on the collector plane to the injection of energy into the grid. With array nominal energy of 244.8 GWh and at standard test condition efficiency of 14.78%, the system exhibits a series of array and inverter losses before the energy is injected into the grid. The total array losses (~-9.7%), with temperature being the highest contributor with -7.9%, reduce the nominal array energy to a virtual array energy of 221.6 GWh at maximum power point tracking. This energy is then reduced further by the total inverter losses (~-3.2%) to 214.4 GWh for injection into the grid.

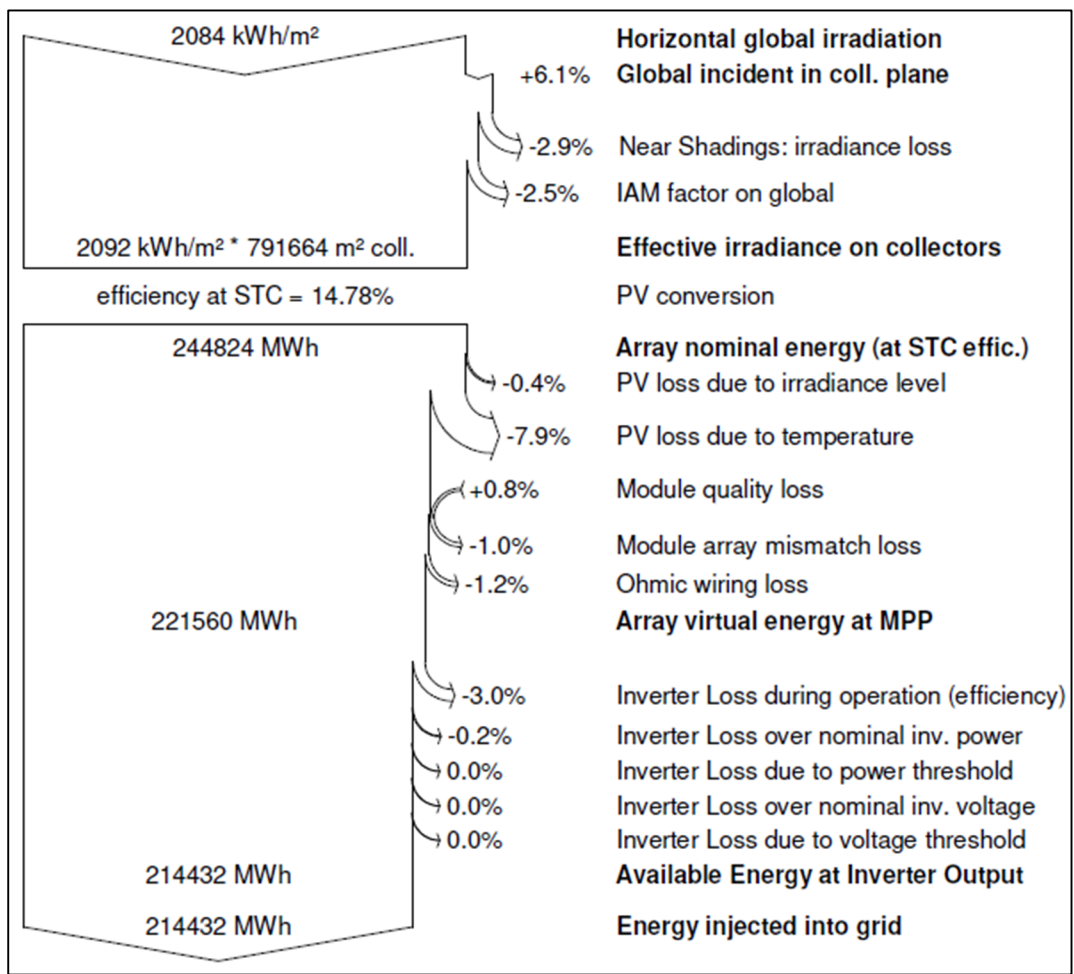


Figure 7.3K: showing the loss diagram of the large footprint FPV at KGU

7.3.1.7 Economic Evaluation (large footprint)

The economic evaluation (in PVSYST) of the large footprint floating photovoltaic system at Kafue Gorge Upper is illustrated in figure 7.3L. With an investment cost of 0.68 £/Wp and zero running costs, the cost of producing 214.4 GWh energy per annum is approximately 4 pence/kWh. This value, even though acceptable, assumes no maintenance costs on the energy system which is not pragmatic and therefore a more conservative value is given in section 7.5 (i.e. 6.7 pence/kWh).

Investment			
PV modules (Pnom = 285 Wp)	408000 units	56 £ / unit	22901040 £
Supports / Integration		34 £ / module	13700640 £
Inverters (Pnom = 500 kW ac)	200 units	23700 £ / unit	4740000 £
Settings, wiring, ...			11900000 £
Design & Construction			1280000 £
Misc			3237552 £
Engineering			9000000 £
Substitution underworth			0 £
Gross investment (without taxes)			66759232 £
Financing			
Gross investment (without taxes)			66759232 £
Taxes on investment (VAT)	Rate 19.0 %		12684254 £
Gross investment (including VAT)			79443486 £
Subsidies			0 £
Net investment (all taxes included)			79443486 £
Annuities	(Loan 10.0 % over 20 years)		9331402 £/year
Annual running costs: maintenance, insurances ...			0 £/year
Total yearly cost			9331402 £/year
Energy cost			
Produced Energy			214432 MWh / year
Cost of produced energy			0.04 £ / kWh

Figure 7.3L: showing the economic evaluation of the large footprint FPV (from PVSYST)

7.3.1.8 System Optimization (large footprint)

This section presents the optimization of the large footprint FPV system to increase the energy yield injected into the grid. Four parameters were used in PVSYST for system optimization and these include ground cover ratio (GCR), tilt angle, pitch and azimuth angle. Figure 7.3M shows that a GCR of 5 would yield the maximum injected energy of 220 GWh (2.6% increase), while a ratio between 80 and 100 decreases the yield steeply. Figure 7.3N reveals that a tilt angle between 10 and 20 degrees produces about 214 to 215 GWh grid injected energy. Figure 7.3O shows that the higher the pitch (i.e. 15 m compared to nominal design of 3 m) the more the energy injected into the grid. However, this scenario is not recommended because the

energy increase is only 2.5% for a 400% increase in pitch (3 m to 15 m). Furthermore, the design azimuth angle of 0° is already the optimized angle since a negative or positive sensitivity analysis to this value yields a reduction in grid injected energy as shown in figure 7.3P.

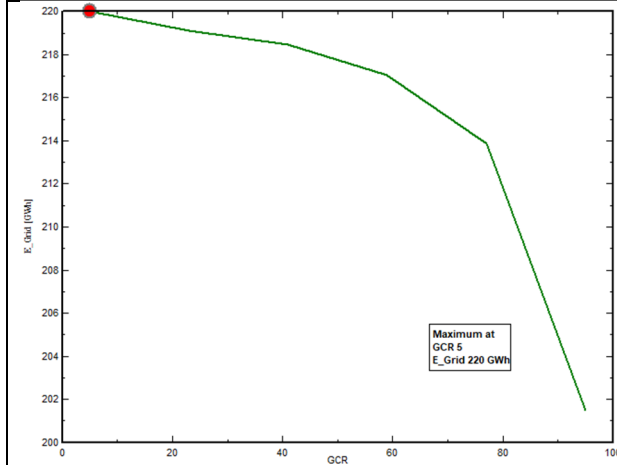


Figure 7.3M: showing ground cover ratio optimization of the large footprint FPV

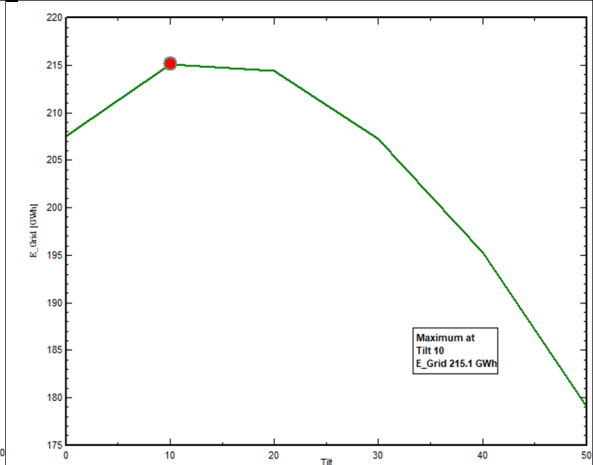


Figure 7.3N: showing tilt angle optimization of the large footprint FPV

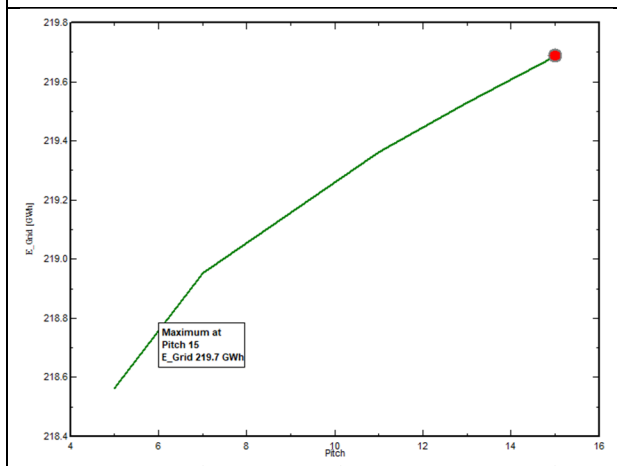


Figure 7.3O: showing pitch optimization of the large footprint FPV

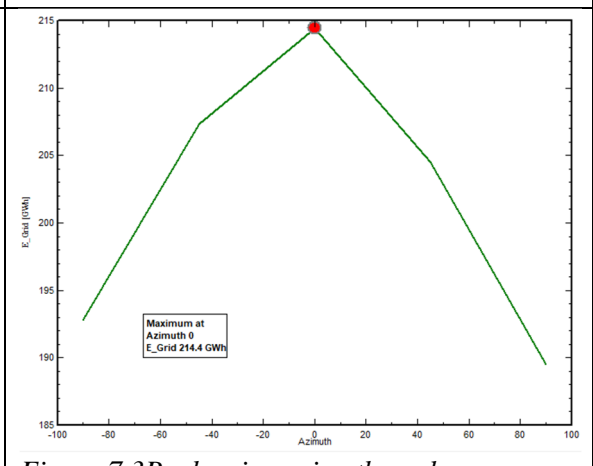


Figure 7.3P: showing azimuth angle optimization of the large footprint FPV

7.3.2 KGU Onshore Wind Assessment and Optimal Placement

7.3.2.1 Wind Farm Layout & Capacity Density

The layout of the windfarm at Kafue Gorge Upper wind site (-15.67064°, 28.32604°) is illustrated in figure 7.3Q. The wind frequency, speed and power rose diagrams show the predominant easterly winds. The wind farm has 25 turbines each with 4 MW rating, 129 m hub height, 142 m rotor diameter. For optimal placement (i.e. minimizing turbulence and wake effects), a row to row spacing (turbine distance in prevailing wind direction) of 8 rotor diameter (D) and an intra row spacing (Turbine distance perpendicular to prevailing wind direction) of 4D is proposed at KGU.

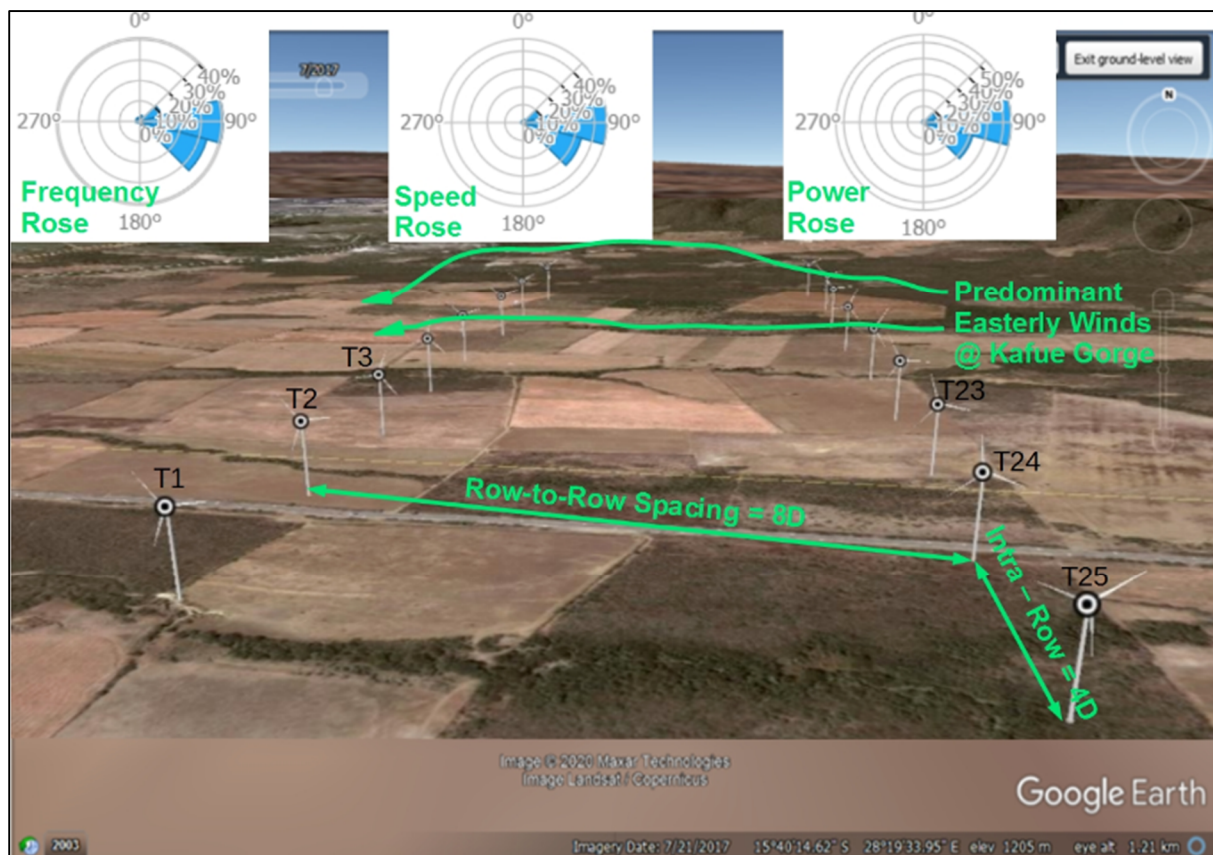


Figure 7.3Q: showing Kafue Gorge (-15.67064°, 28.32604°) Wind Farm layout for 25 turbines (T1 to T25).

Each turbine with 4MW power rating, 129m hub height and 142m rotor diameter. Turbine spacing of 8 rotor diameter Row-to-Row spacing and 4 rotor diameter intra-row spacing.

The capacity density (or power density) of the wind farm is given in equation 35 below:

$$\text{Power Density [MW/km}^2\text{]} = \frac{(\text{Turbine Power Rating[MW]})}{\frac{8D}{D} * \frac{4D}{D} * D^2} \quad (35)$$

$$\Rightarrow \text{Power Density [MW/km}^2\text{]} = \frac{(4.0\text{MW})}{32 \cdot (0.142)^2} = 6.2\text{MW/km}^2$$

Where D is the rotor diameter, 8D/D is the relative distance in the prevailing wind direction, 4D/D is the relative distance parallel to the easterly prevailing winds.

7.3.2.2 Wind Turbine Characteristics

The turbine model used for design is the generic 4 MW power rating, 129 m hub height and 142 m rotor diameter. The turbine that emulates these specifications in renewable's ninja is the Siemens "SWT-DD-142". Thereafter, the windspeed output of this model was exported to homerpro software to create a customized power curve as shown in figure 7.3R.

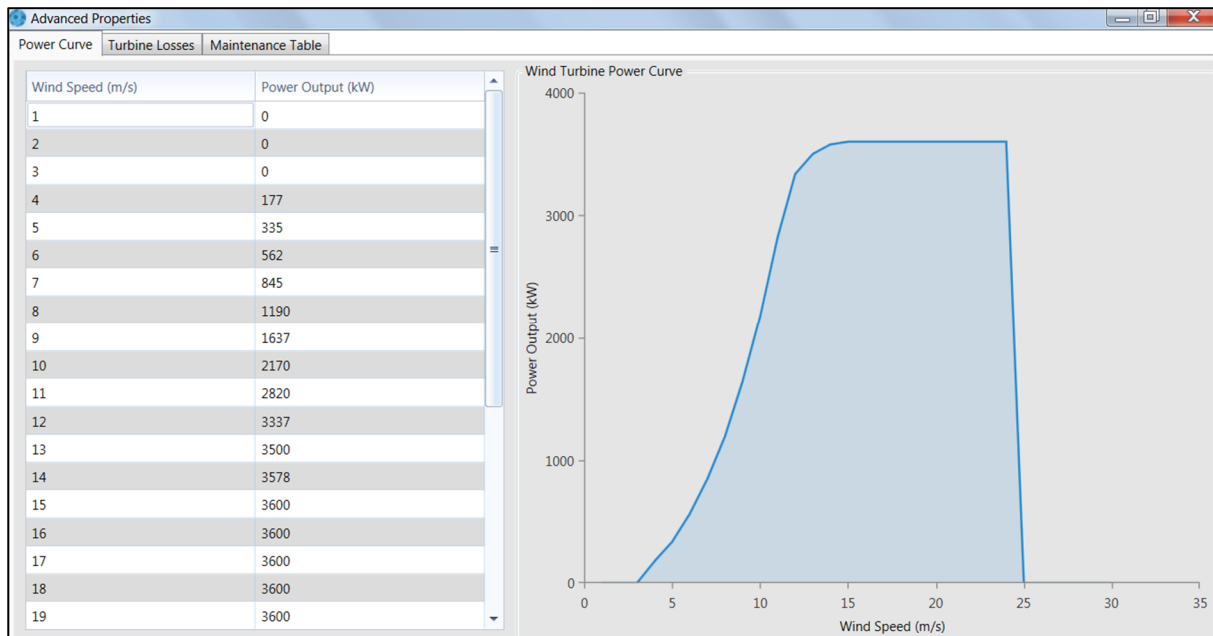


Figure 7.3R: showing turbine power curve

The distribution of losses for this turbine design is shown in figure 7.3S.



Figure 7.3S: showing the turbine losses for the design

7.3.2.3 Site Wind Variability

The wind speed variability at Kafue Gorge is illustrated in figure 7.3T. The wind speed at KGU has been consistent between 2013 and 2017 with a wind speed index ranging between 1.0 and 1.03. The wind speed resource is high between June and October (with less variability) and thus these are the months with expected high energy production. Further, the hourly vs monthly cross table shows a high wind speed index between June and October and between 12am/0am to 11am. Wind speed variability is important for prospectus investors to ascertain the expected yield from the actual resource based on trend data of between 5 to 20years.

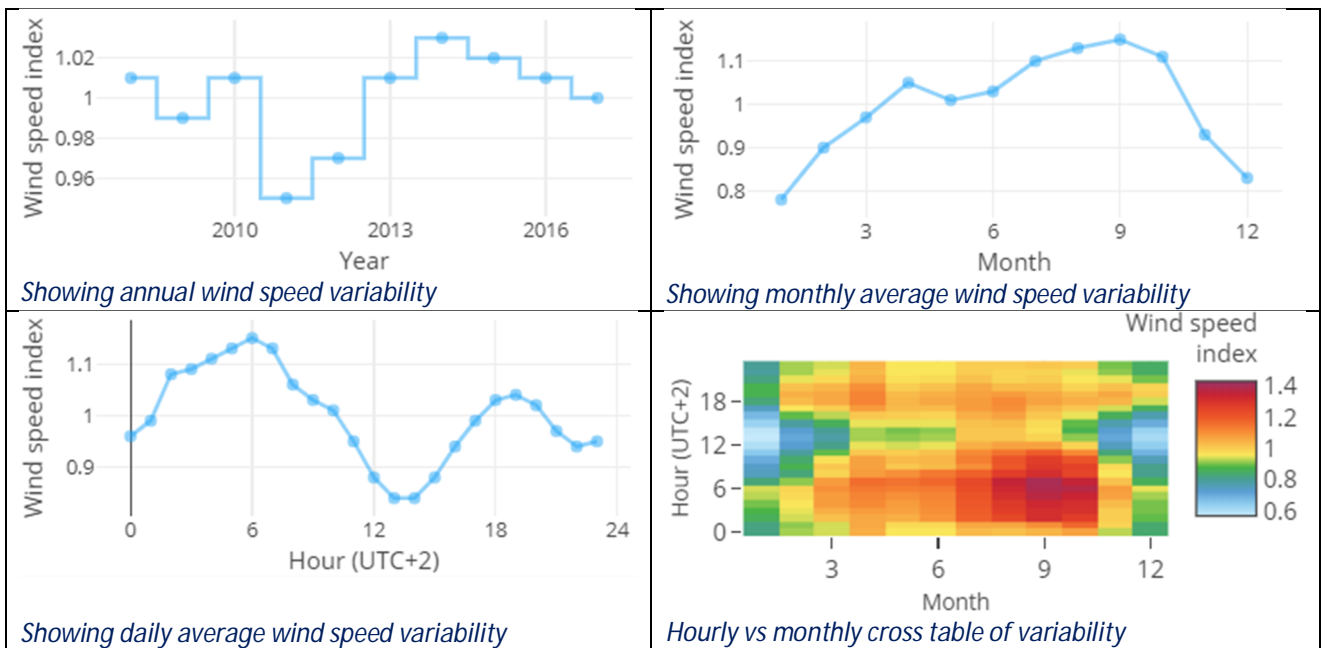


Figure 7.3T: showing GWA wind variability at Kafue Gorge wind site (-15.67064°, 28.32604°).

7.3.2.4 Wind Farm Energy Yield Assessment

Renewables ninja gives a more optimistic energy yield as evidenced from the daily mean values, average capacity factor of 39.6% and hourly power output in figures 7.3U and 7.3V. The optimistic gross energy for the wind farm can be estimated as shown in equation 37.

$$\text{Gross Energy} = \text{Power Rating} \times \text{Capacity Factor} \times \text{Hours of Operation} \quad (37)$$

Where power rating is 25 x 4 MW, average capacity factor is 39.6%, hours of operation is 8760hours (365 x 24).

$$\text{Gross Energy} = 4 \times 25 \times 0.396 \times 8760 = \sim 347 \text{ GWh per year}$$

Therefore, the optimistic net energy is given in equation 38.

$$\text{Net Energy} = \text{Gross Energy} \times \text{Loss Factors} \quad (38)$$

$$\text{Net Energy} = 347 \times 0.85 = 294 \text{ GWh per year.}$$

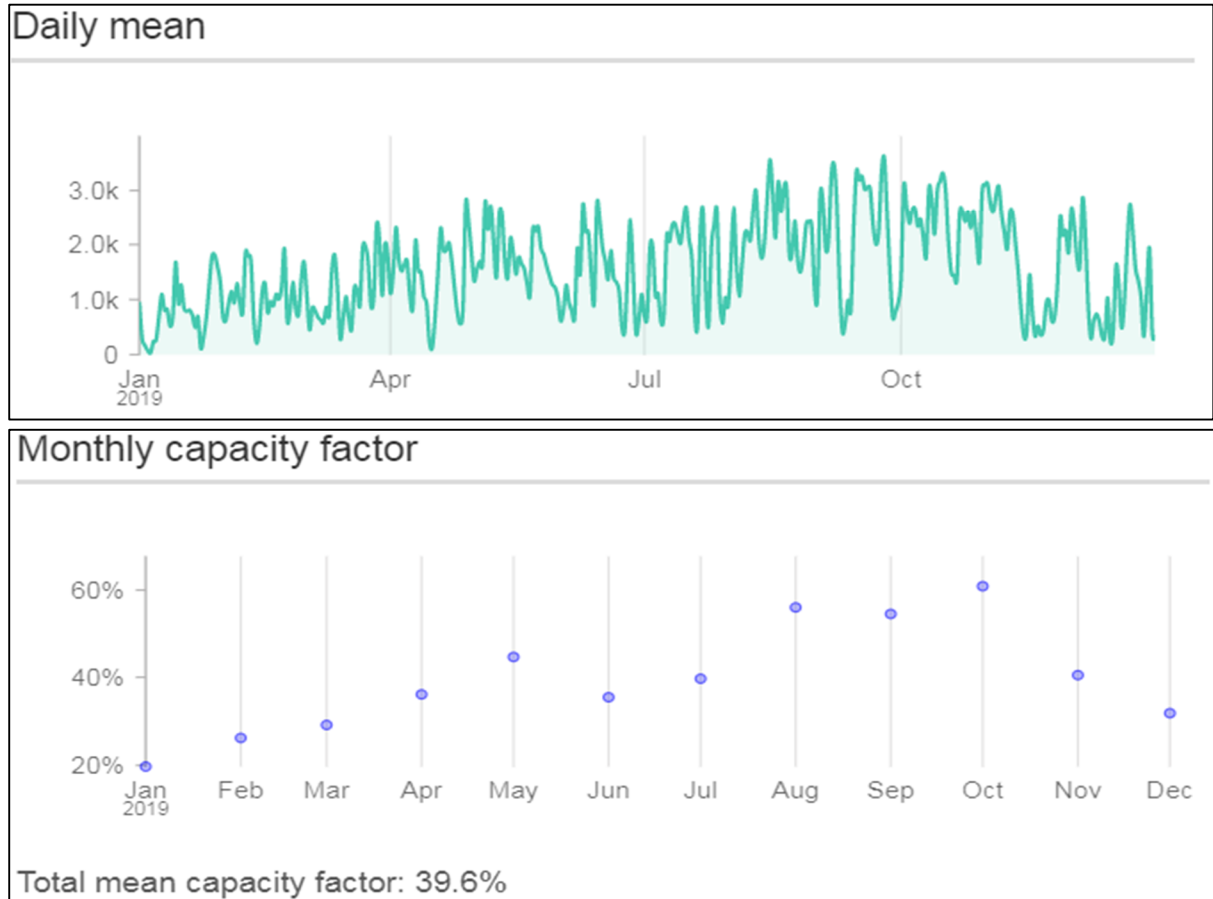


Figure 7.3U: showing the optimistic daily mean power output and monthly capacity factors for 1 wind turbine at (simulations from renewables ninja)

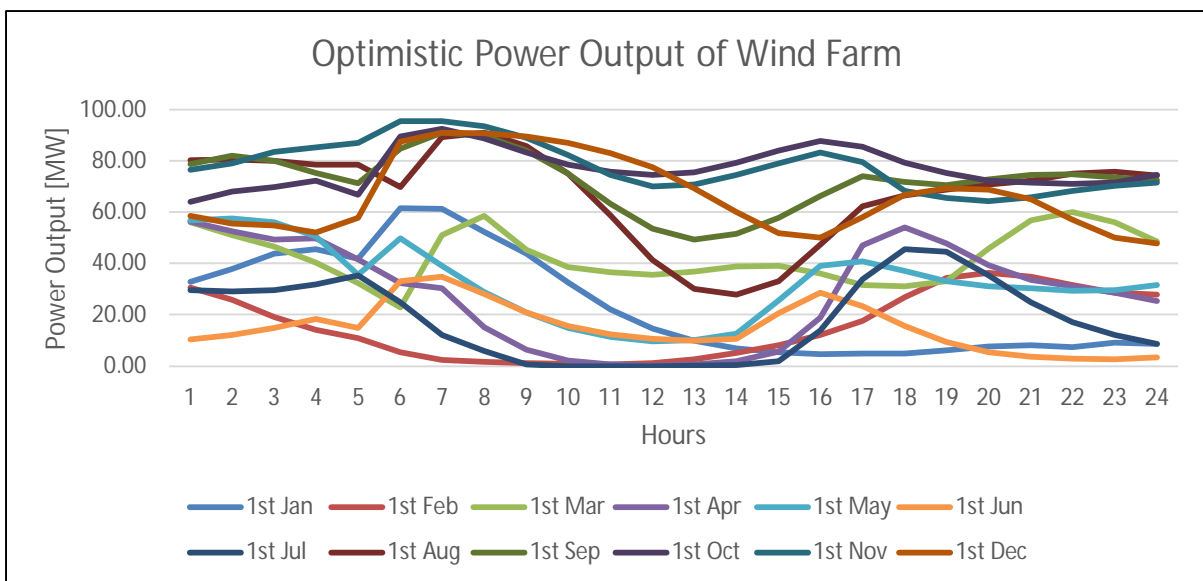


Figure 7.3V: showing hourly power output for the first day of each month (from renewables ninja)

Renewables ninja and homerpro were used in a complimentary fashion. Firstly, the Merra-2 global validated dataset in renewables ninja which has a wide coverage compared to Homerpro was used to simulate the KGU wind site potential by defining the actual turbine characteristics which are comparable to a wind resource study conducted by the world bank (4 MW rating, 142 m rotor diameter, 129 m hub height). Thereafter, the wind speed output in renewables ninja was exported to homer pro to facilitate detailed design by incorporation of a customized wind turbine power curve with loss factors (i.e. curtailment loss, wake effects etc) which reflect a more pragmatic design for an actual wind farm with 25 turbines.

Homer Pro gave a more conservative energy yield with reduced number of operation hours owing to inclusion of curtailment losses and eventually reduction in capacity factor. Figure 7.3W shows the wind power output distribution with 8174 hours of operation in a year. This scenario produced about 167 GWh of energy per year with a levelized cost of energy of about 7 pence/kWh.

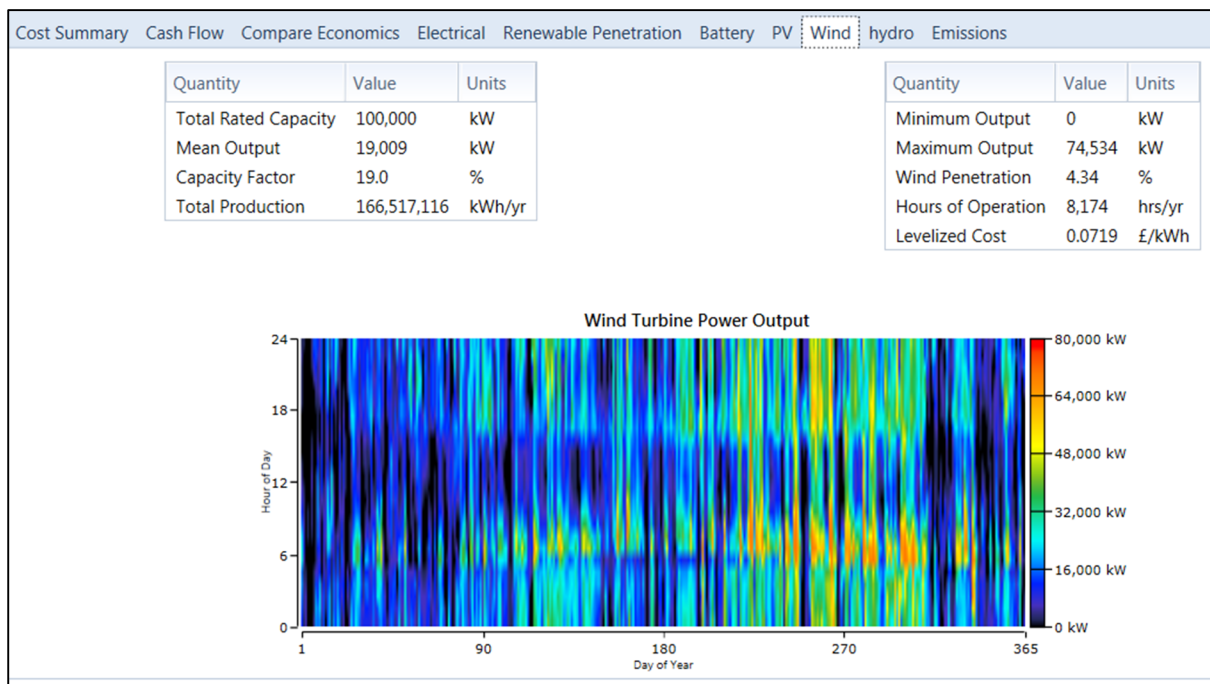


Figure 7.3W: showing more conservative output simulations in Homerpro

7.4 Assessing the Hydro Storage Potential at KGU

Reference was made to the KGU HVA table in section 7.2.1.1 to ascertain a practical storage value. The Custom Virtual Hydro Battery at Kafue Gorge has a reservoir that can store an assumed maximum capacity of 20million meter cube of water (0.5 m rise assuming its operating at minimum elevation of 974m above sea level), which can discharge over a 173 hour

($20000000\text{m}^3 / (32\text{ m}^3/\text{s} \times 60 \times 60)$) period at a rate of 32 meter cube per second. The effective head is $\sim 382\text{ m}$, and the generator efficiency is $\sim (85-90)\%$, the power and energy of the Virtual Hydro Battery system during discharging can be calculated as follows:

Discharging

$$\text{Power Generated} = (\rho) \times (g) \times (v) \times (h) \times (\text{eff}) \quad (39)$$

Where (ρ) is the density of water with a value 1000 kg/m^3 , (g) is the gravitational constant of 9.81 m/s^2 , (v) is the flow rate in m^3/s , (h) is the head of 382 m , (eff) is the generator efficiency value of 90% .

$$\rightarrow \text{Power Generated} = 1000 \times 9.81 \times 32 \times 382 \times 0.9 \sim 108\text{ MW.}$$

For 20million meter cube of water at a flow rate of $32\text{ m}^3/\text{s}$, the water utilization duration is approximately 173 hours for one turbine based on the plant rating table in [section 7.2.1.3](#). However, if more turbines operate to consume the stored water the duration would be proportional to the number of units in operation. The electrical energy generated over the 173 hours is given in equation 40.

$$\text{Energy generated} = \text{Power generated} \times \text{hours of usage} \quad (40)$$


$$\rightarrow \text{Energy generated} = 108000\text{kW} \times 173\text{ hours} = 18684000\text{kWh} (\sim 18.7\text{GWh})$$

Charging

The initial charging assumes of having a wet season and thus abundant water supply while other charging periods of virtual battery system involve throttling down on the hydro when there is availability of floating photovoltaics and onshore wind. The Round-trip efficiency of the virtual battery is just the efficiency of the turbo-generator unit including friction losses in the penstock (Assumed to be 90% total efficiency). The maximum capacity is the maximum electrical output divided by the nominal voltage; $= 18684000 \times 1000 / 17500 = \sim 1067657\text{ Amp Hours}$, this assumes the utilization of generation voltage of 17.5 kV for storage calculations at KGU.

With the above calculations and assumptions, the virtual storage was modelled (emulating pumped hydro) using the advanced custom storage feature in Homer Pro as shown in [figure 7.4A](#).

Add/Remove Hydro Storage

STORAGE  Name: Abbreviation: Remove
Copy To Library

Properties
 Idealized Battery Model
 Nominal Voltage (V): 1.75E+04
 Maximum Charge Current (A): 6.17E+03
 Maximum Discharge Current (A): 6.17E+03
www.homerenergy.com
 [Adopted from pumped hydro]
 The Custom Virtual Hydro Battery at Kafue Gorge has a reservoir that can store a assumed maximum capacity of 20million meter cube of water (0.5m rise assuming its operating at minimum elevation of 974m A.S.L) , which can be discharge over a 173 hour period at a rate of 32meter cube per second. The effective head is ~382m, and the generator efficiency is ~90%, the power


Cost

Quantity	Capital (£)	Replacement (£)	O&M (£/year)
<input type="text" value="1"/>	<input type="text" value="5,000,000.00"/>	<input type="text" value="500.00"/>	<input type="text" value="2,000.00"/>

Lifetime
 time (years): (-) More...

Sizing
 HOMER Optimizer™
 Search Space

Site Specific Input
 Electrical Bus AC DC
 Model Dedicated Converter Dedicated Converter...
 Initial State of Charge (%): (-)
 Minimum State of Charge (%): (-)

Generic
homerenergy.com 

General **Lifetime** **Defaults**

Name: Last Modified: 11/18/2016 10:56:07 PM
 Abbreviation:
 Manufacturer:
 Notes:
 [Costs for Pumped Hydro]
 The Electricity Storage Association gives a range of costs for Pumped - Hydro of US \$500 / kW to US\$1500 / kW.
 Accordingly the costs of this generic pumped hydro system can vary between 11,000\$ to

Electrical Bus: AC DC Requires one minute timestep

Energy Model: Idealized Model; Storage type: Chemistry:

Nominal Voltage (V): Max. Charge Rate (A/Ah):
 Round Trip Efficiency (%): Max. Charge Current (A):
 Minimum State of Charge (%): Max. Discharge Current (A):
 Nominal Capacity (Ah)

Figure 7.4A: showing the customized virtual storage model in homerpro

7.5 System Optimization (Maximizing Energy & Reducing Cost)

This section presents a way of optimizing the energy system by maximising energy production at a reduced cost at Kafue Gorge Upper. This was achieved by finding the most economical dispatch scenario for the hydro-FPV-Wind hybrid system. Therefore, the remainder of the section is structured as follows; [Section 7.5.1](#) looks at the times series dispatch of generation and load data (i.e. hydro current water availability, hydro low water availability, hydro normal water availability versus VRES and grid demand). [Section 7.5.2](#) presents the actual cost of floating photovoltaics and wind energy at Kafue Gorge Upper without any consideration for economic dispatch. Thereafter, [section 7.5.3](#) tries to optimize the hybrid energy system using Homerpro's advanced dispatch controllers (i.e. load following, cycle charging, combined dispatch, generation order, homer predictive and matlab link).

7.5.1 Timeseries Dispatch

This section presents a timeseries dispatch of generation and grid load without any optimization consideration. The hydro scenarios considered in this section are as presented in [section 7.2.1.4](#) which includes current water availability (CWA), low water availability and normal water availability. Time series hourly dispatch was done considering the different seasons of the year to cater for a broader spectrum of water level variations, grid load variations and VRES output variations. As such, five months were considered to give a clear picture of the study (i.e. January, March, June, September and November). The first day of each month was considered for hourly distribution of generation and grid load time series data.

Dispatch with Current Water Availability (CWA) Hydro

The timeseries dispatch between hydro at CWA, VRES and grid load (at 25, 50, 75 and 100% sensitivity analysis of actual demand) is illustrated in figures 7.5.1A to 7.5.1K.

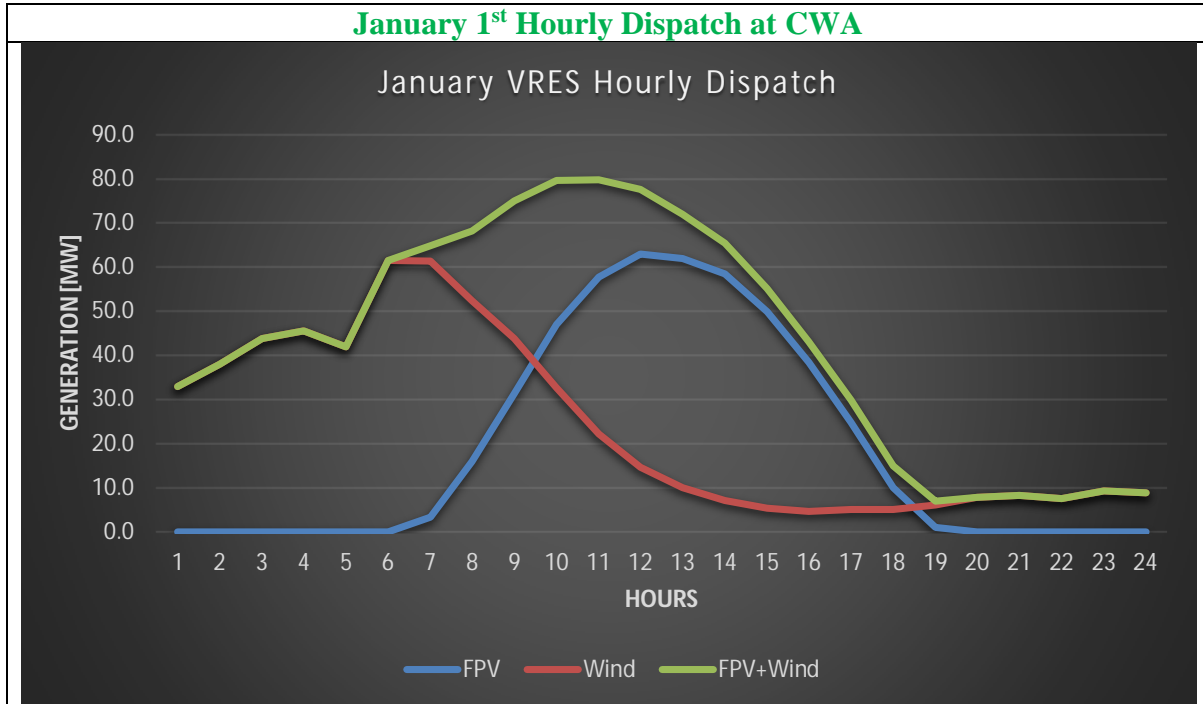


Figure 7.5.1A: showing floating PV and wind dispatch on 1st January

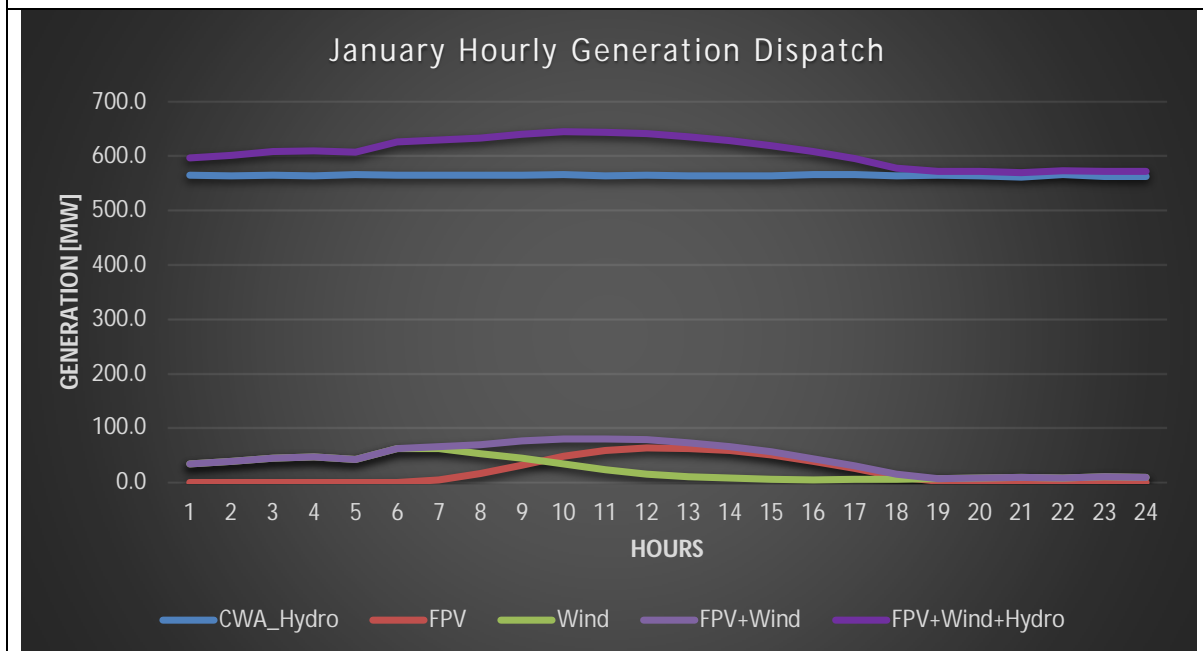


Figure 7.5.1B: showing total generation dispatch on 1st January

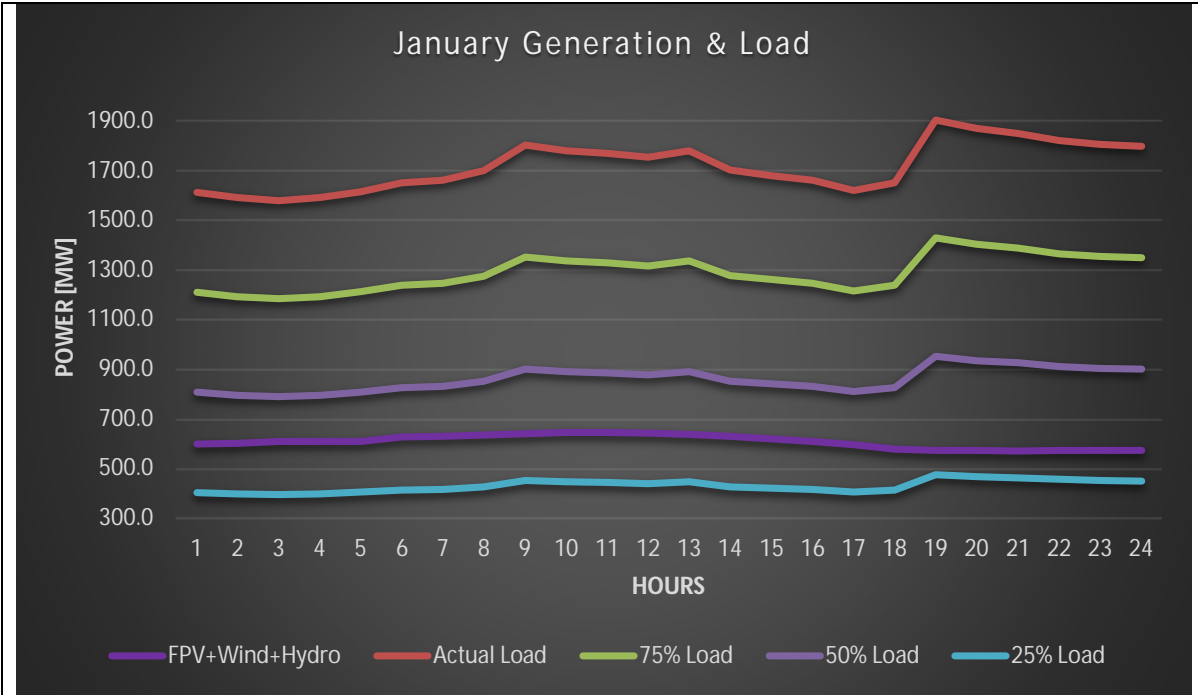


Figure 7.5.1C: showing generation dispatch and load on 1st January

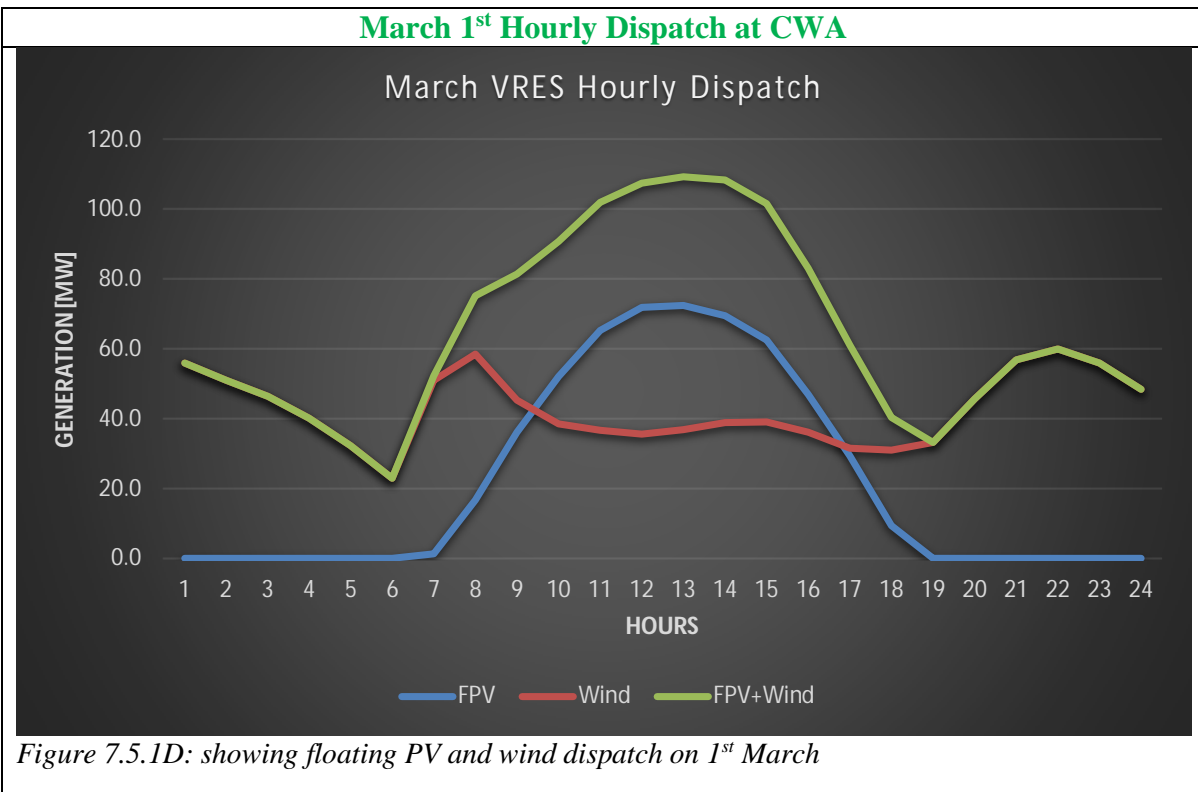


Figure 7.5.1D: showing floating PV and wind dispatch on 1st March

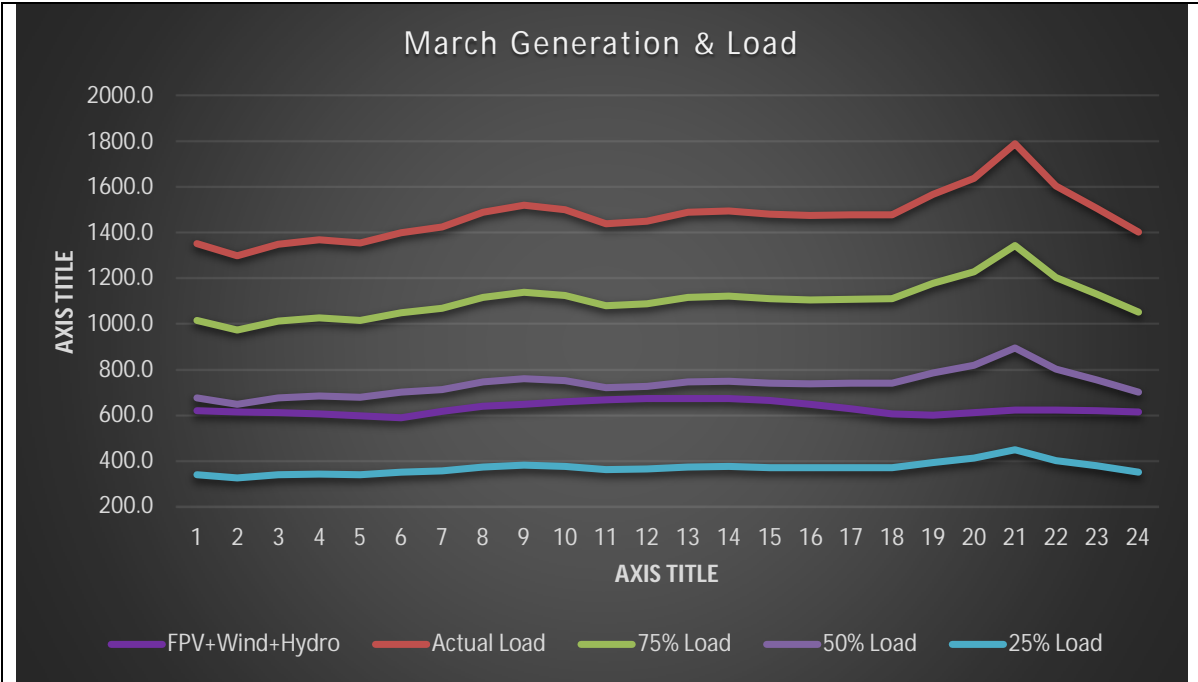


Figure 7.5.1E: showing generation dispatch and load on 1st March

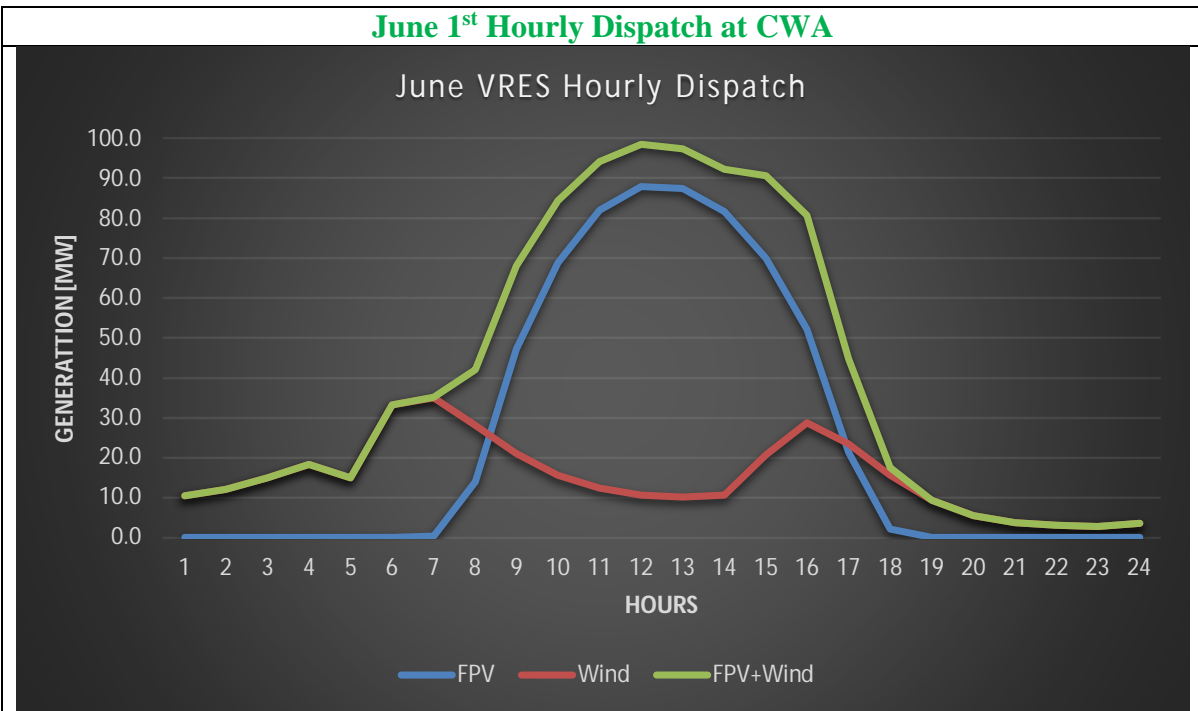


Figure 7.5.1F: showing floating PV and wind dispatch on 1st June

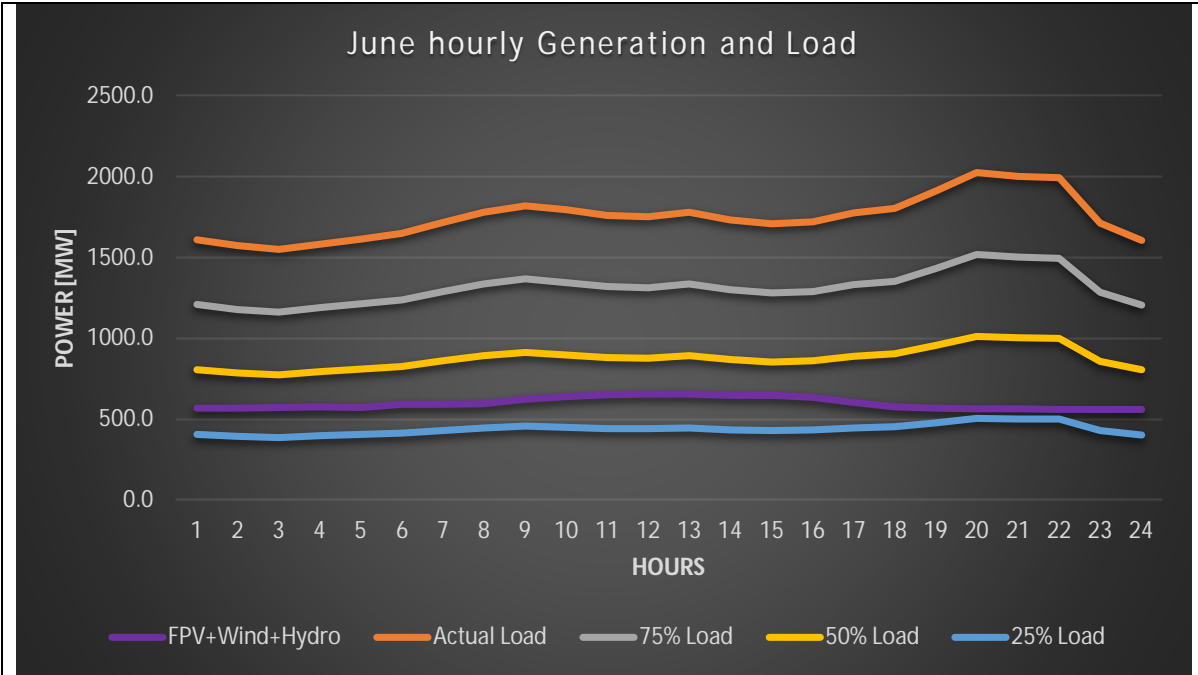


Figure 7.5.1G: showing generation dispatch and load on 1st June

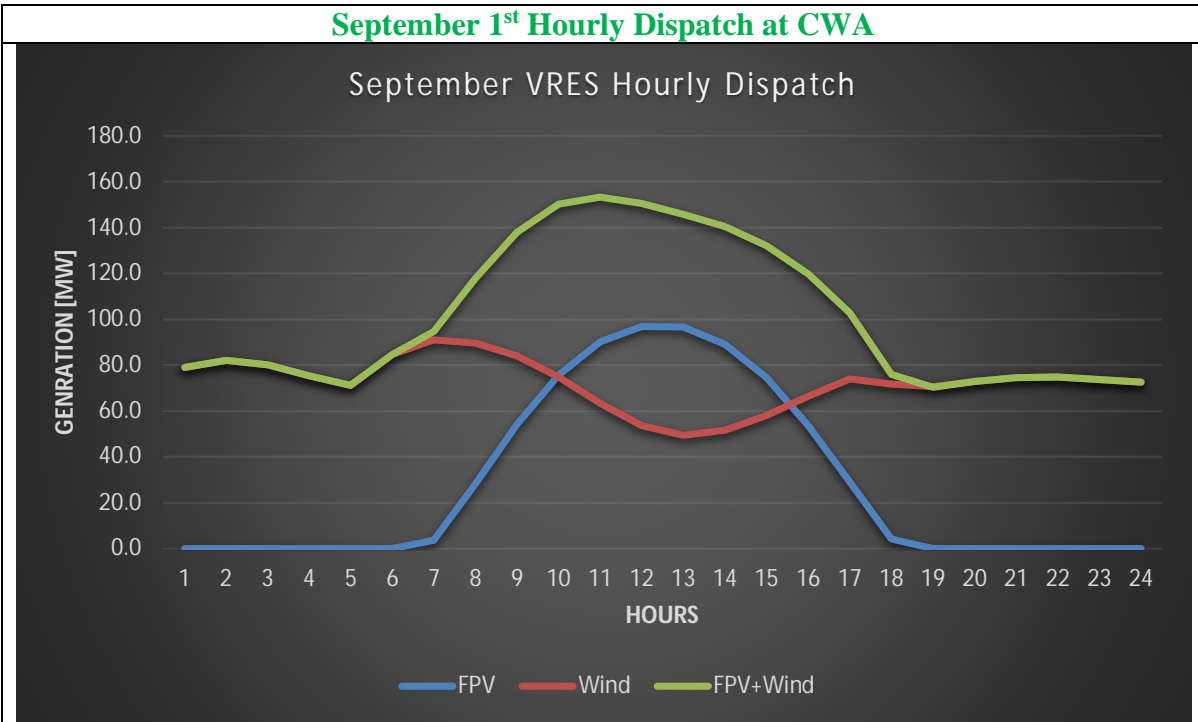


Figure 7.5.1H: showing floating PV and wind dispatch on 1st September GG

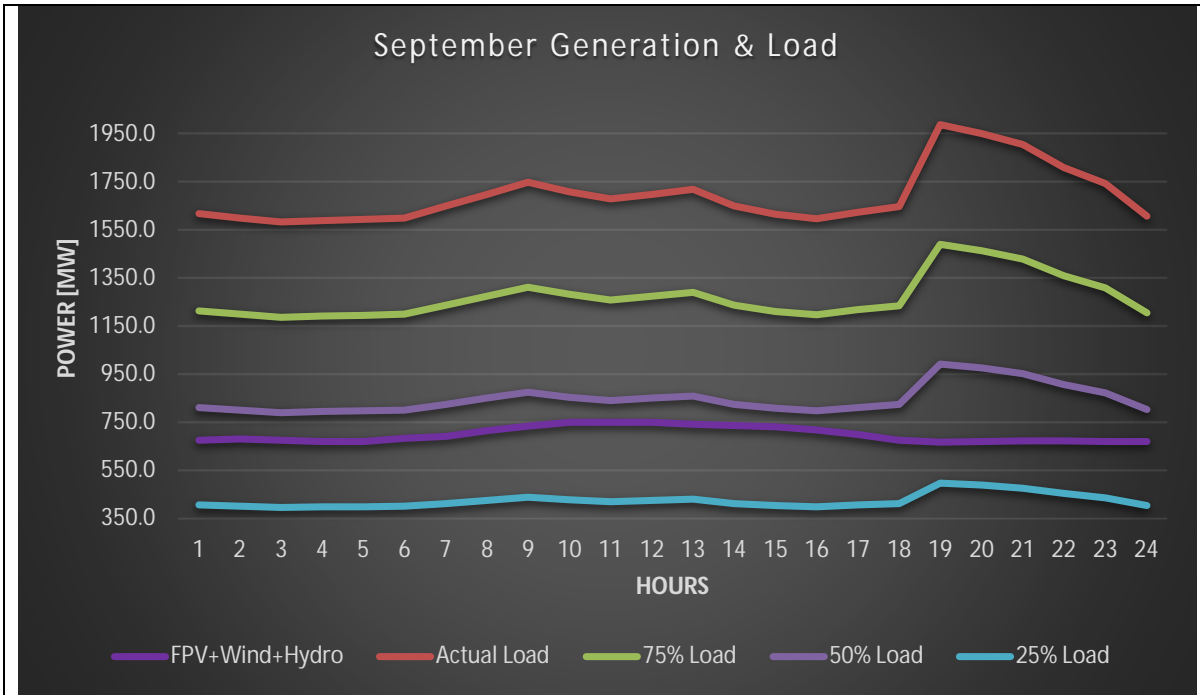


Figure 7.5.1I: showing generation dispatch and electrical grid load on 1st September

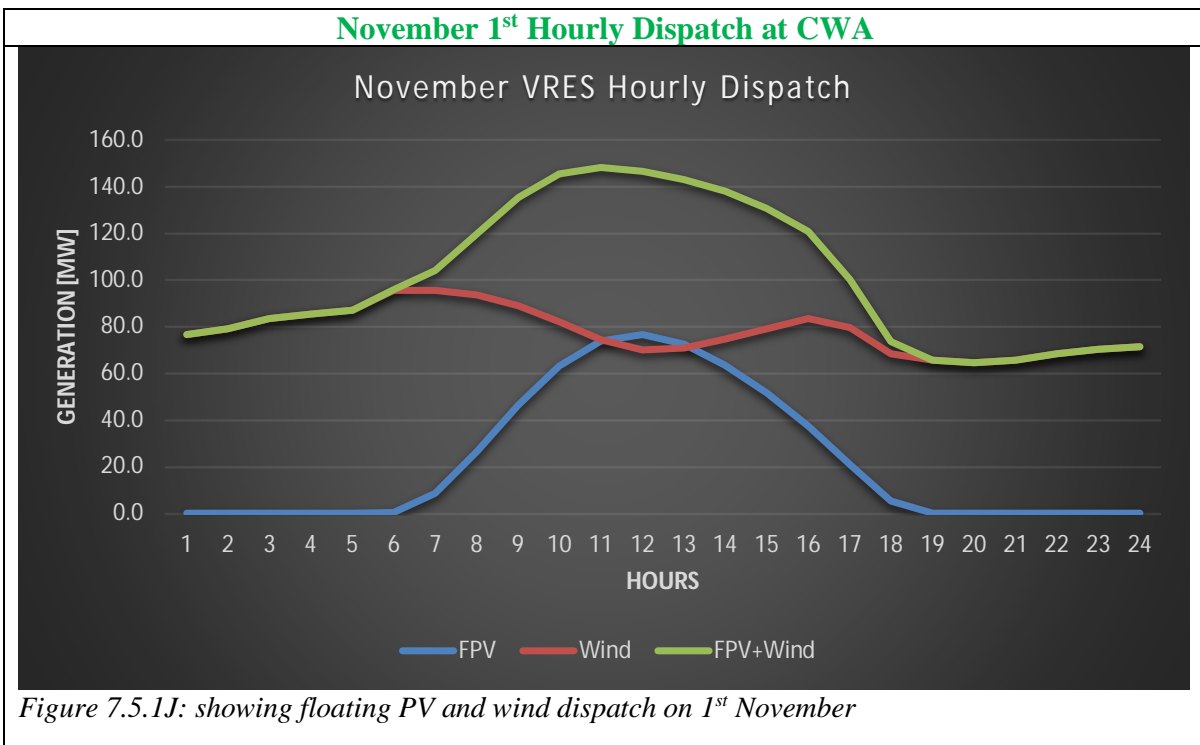


Figure 7.5.1J: showing floating PV and wind dispatch on 1st November

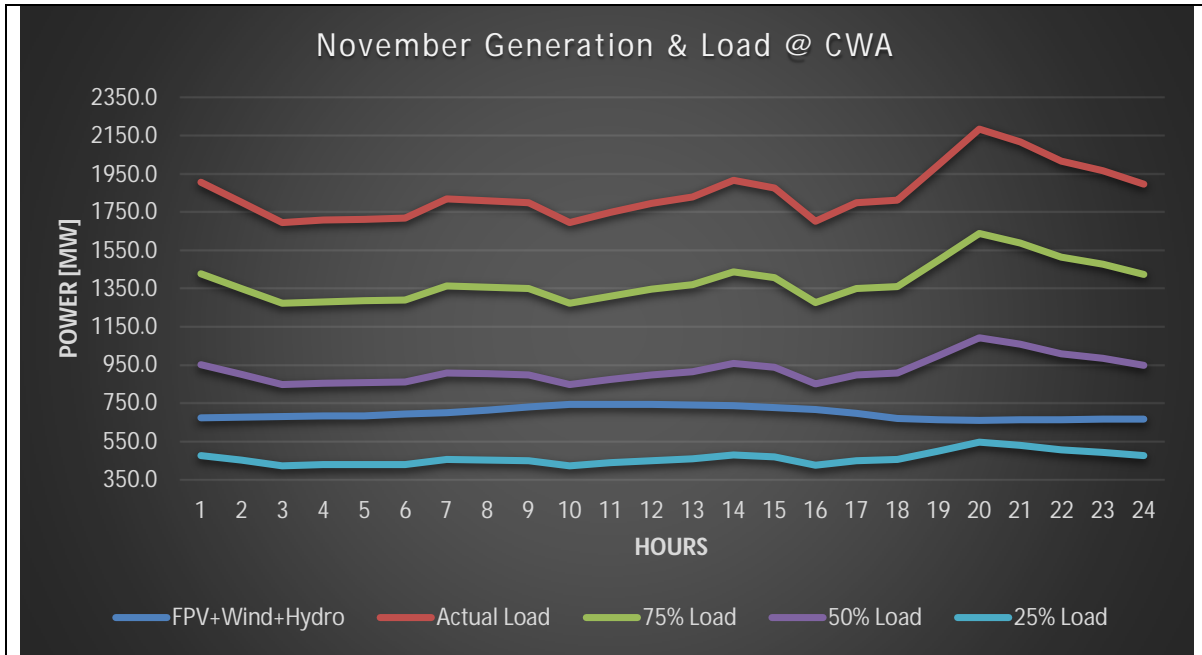


Figure 7.5.1K: showing generation dispatch and electrical grid load on 1st November

Dispatch with Low Water Availability (LWA) Hydro

The timeseries dispatch between hydro at LWA, VRES and grid load (at 25, 50, 75 and 100% sensitivity analysis of actual demand) is illustrated in figures 7.5.1L to 7.5.1P.

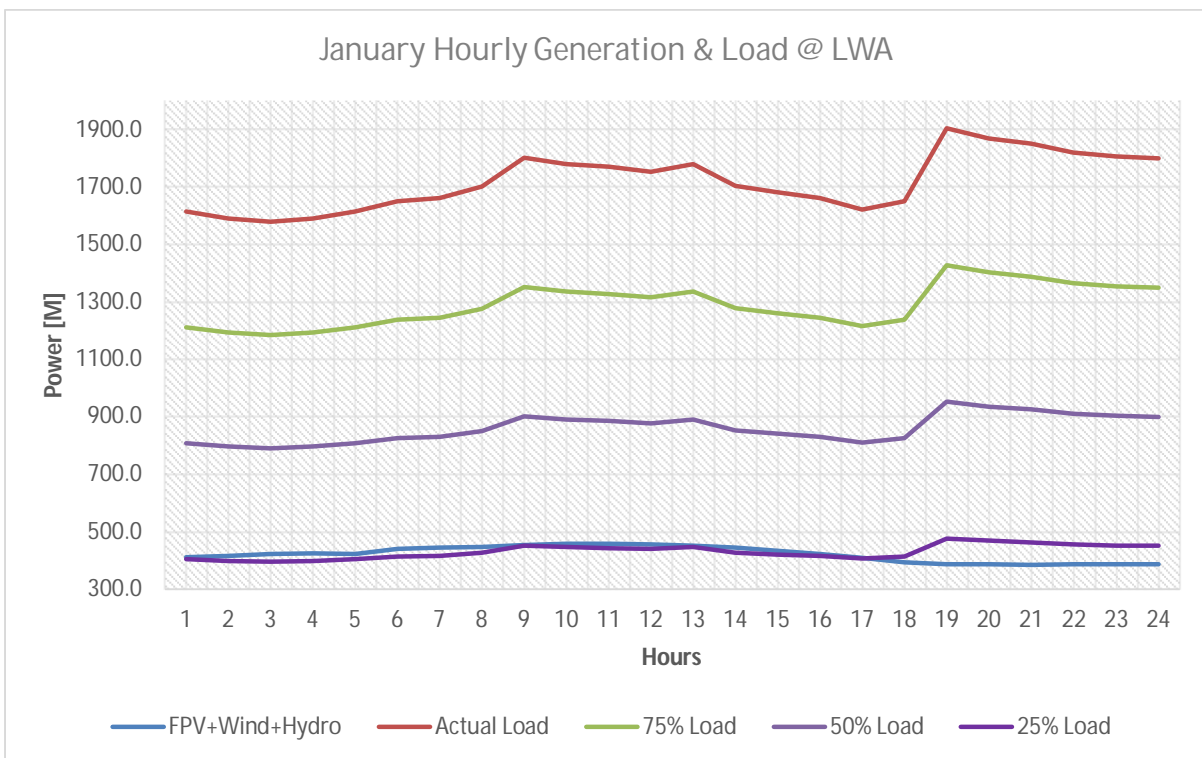


Figure 7.5.1L: showing generation dispatch and electrical grid load on 1st January

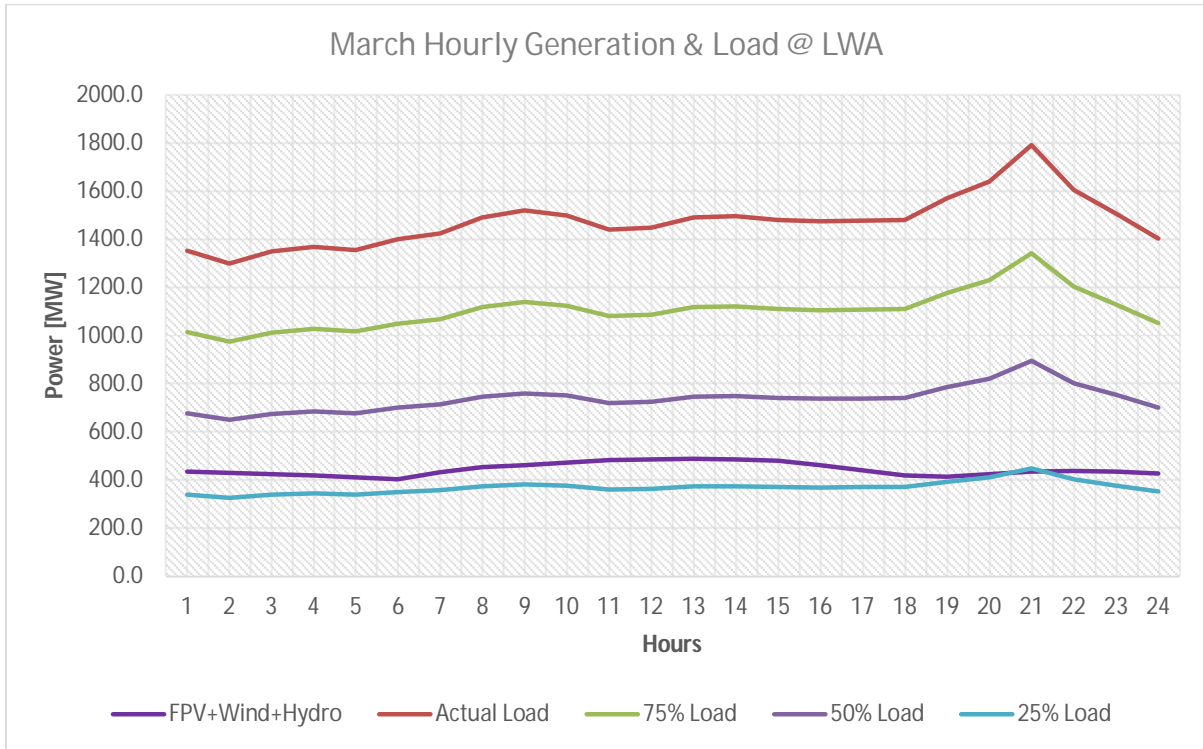


Figure 7.5.1M: showing generation dispatch and electrical grid load on 1st March

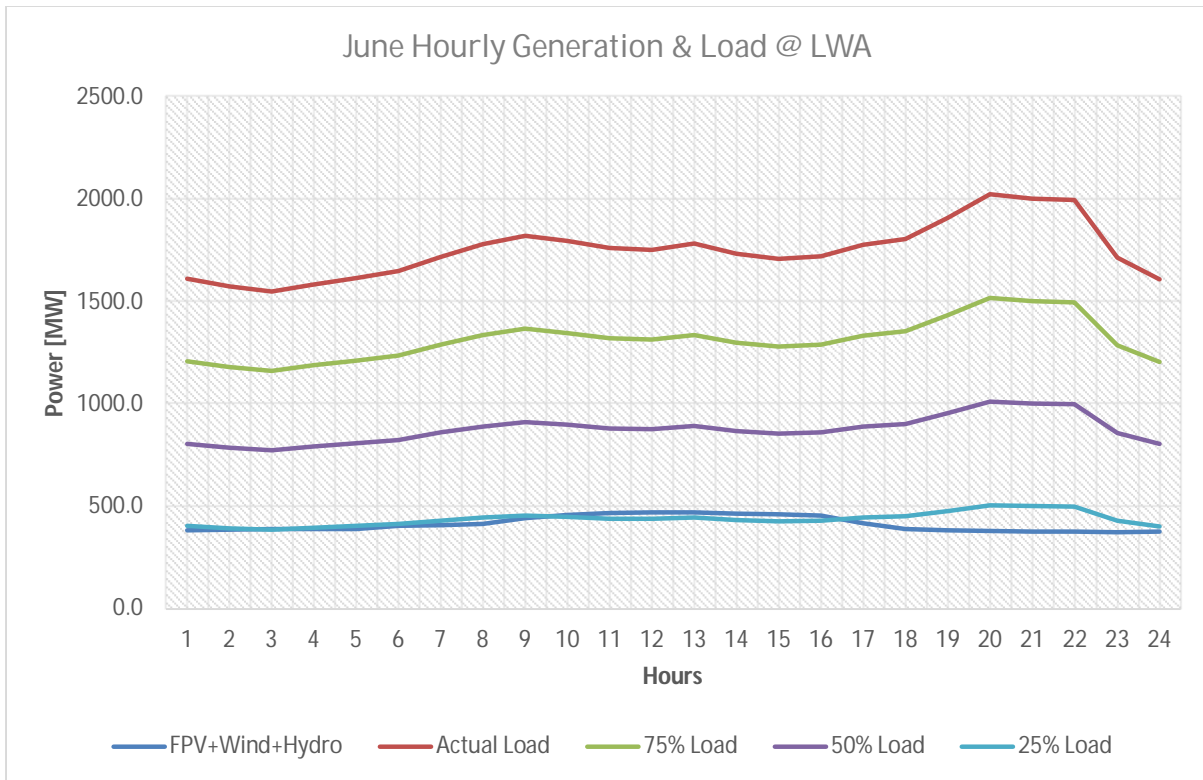


Figure 7.5.1N: showing generation dispatch and electrical grid load on 1st June

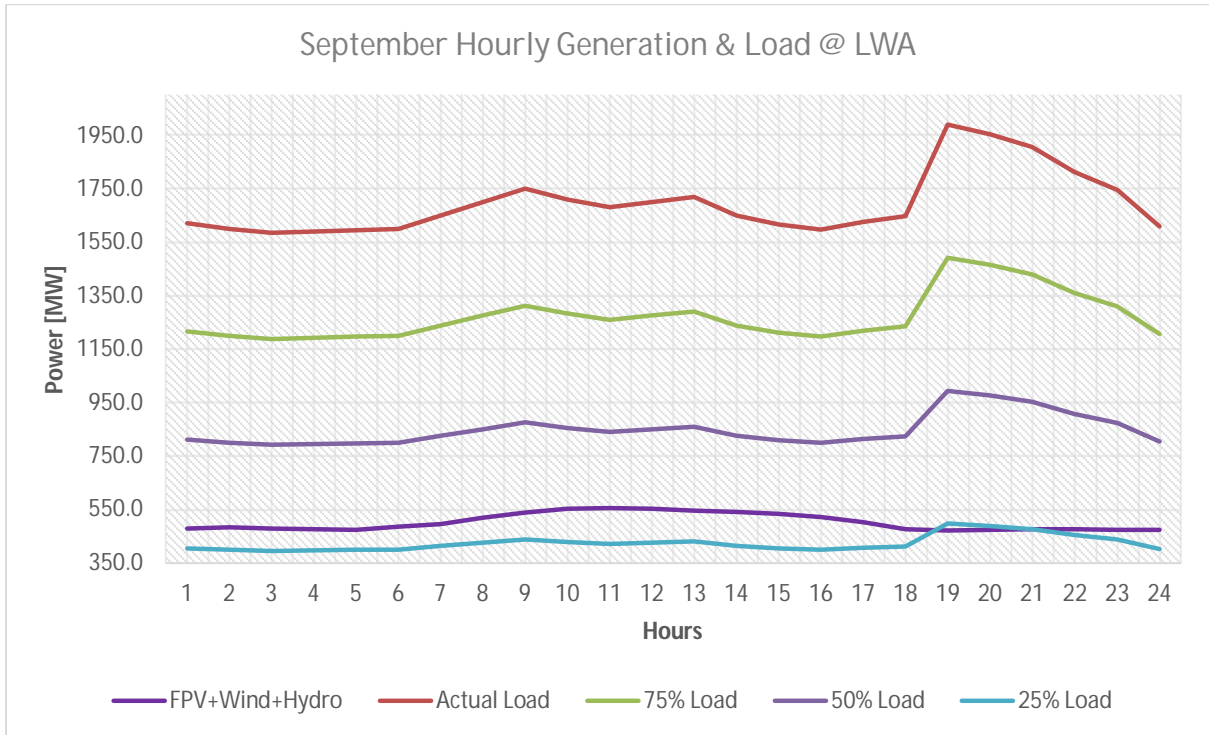


Figure 7.5.10: showing generation dispatch and electrical grid load on 1st September

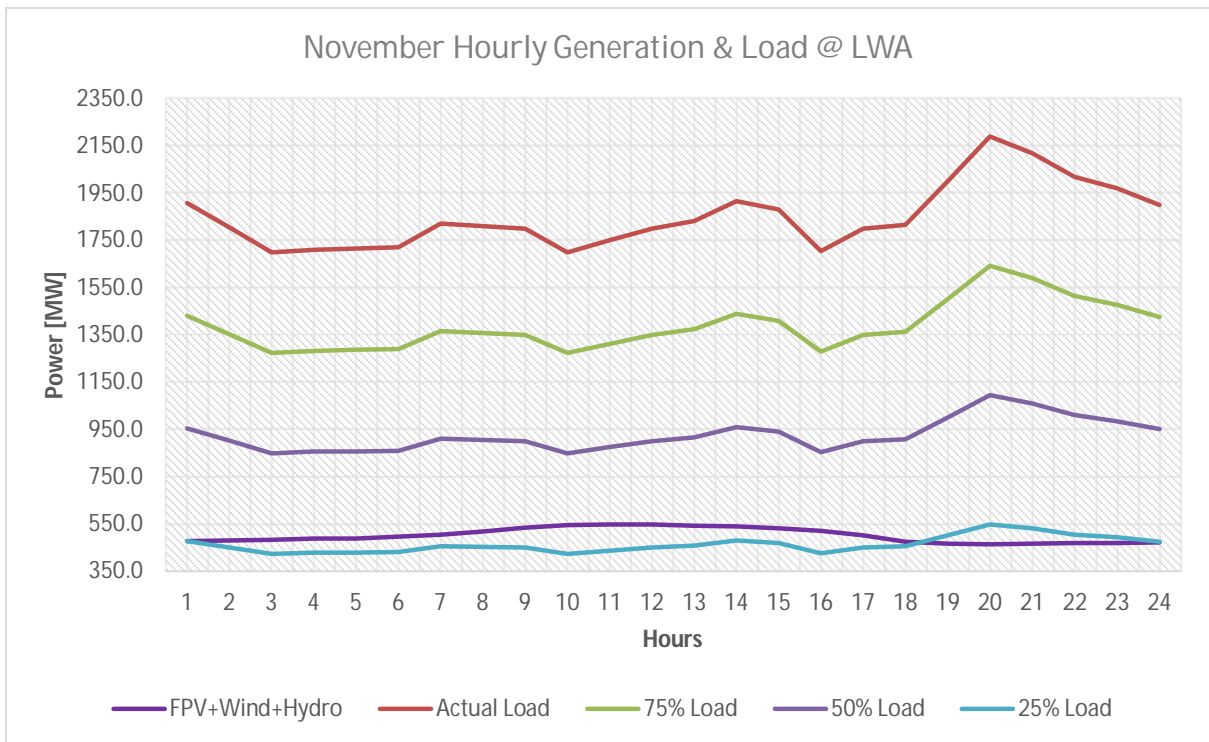


Figure 7.5.1P: showing generation dispatch and electrical grid load on 1st November

Dispatch with Normal Water Availability (NWA) Hydro

The timeseries dispatch between hydro at NWA, VRES and grid load (at 25, 50, 75 and 100% sensitivity analysis of actual demand) is illustrated in figures 7.5.1Q to 7.5.1U

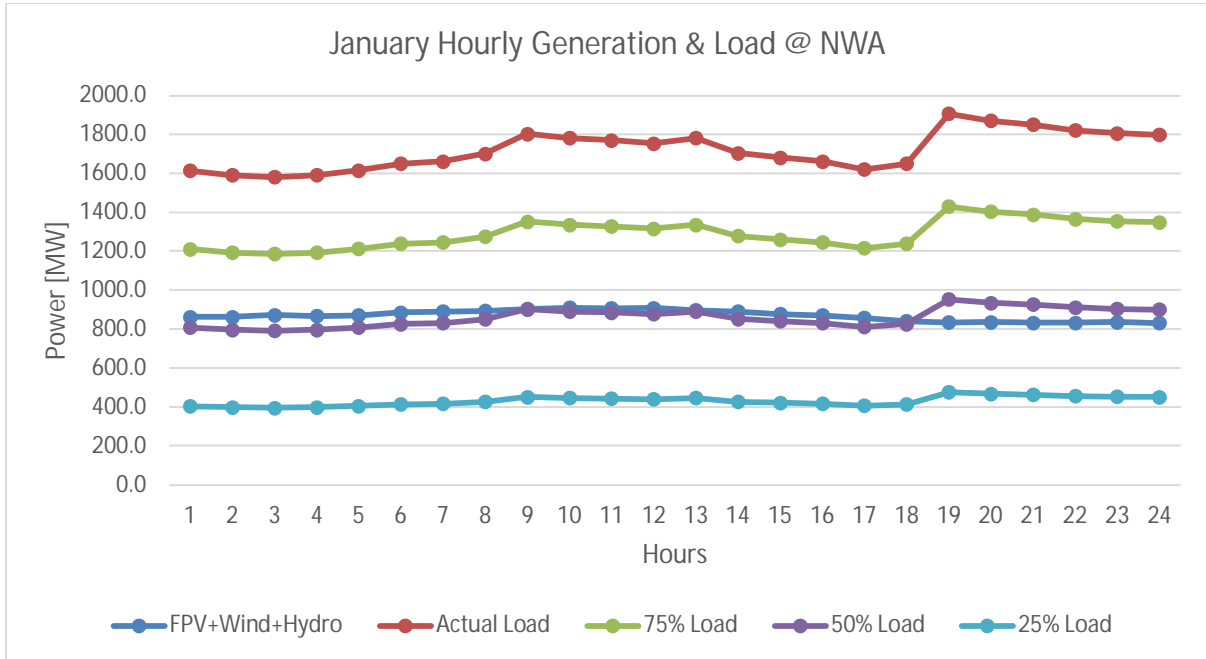


Figure 7.5.1Q: showing generation dispatch and electrical grid load on 1st January

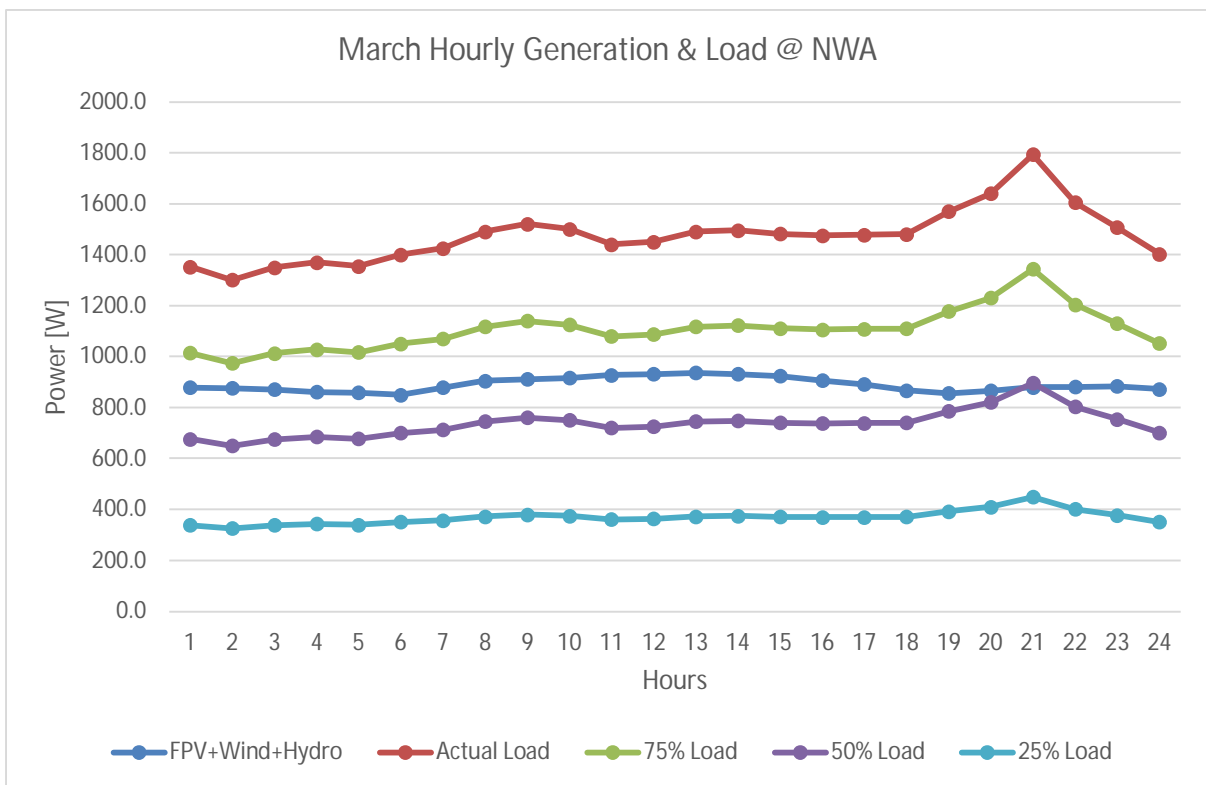


Figure 7.5.1R: showing generation dispatch and electrical grid load on 1st March

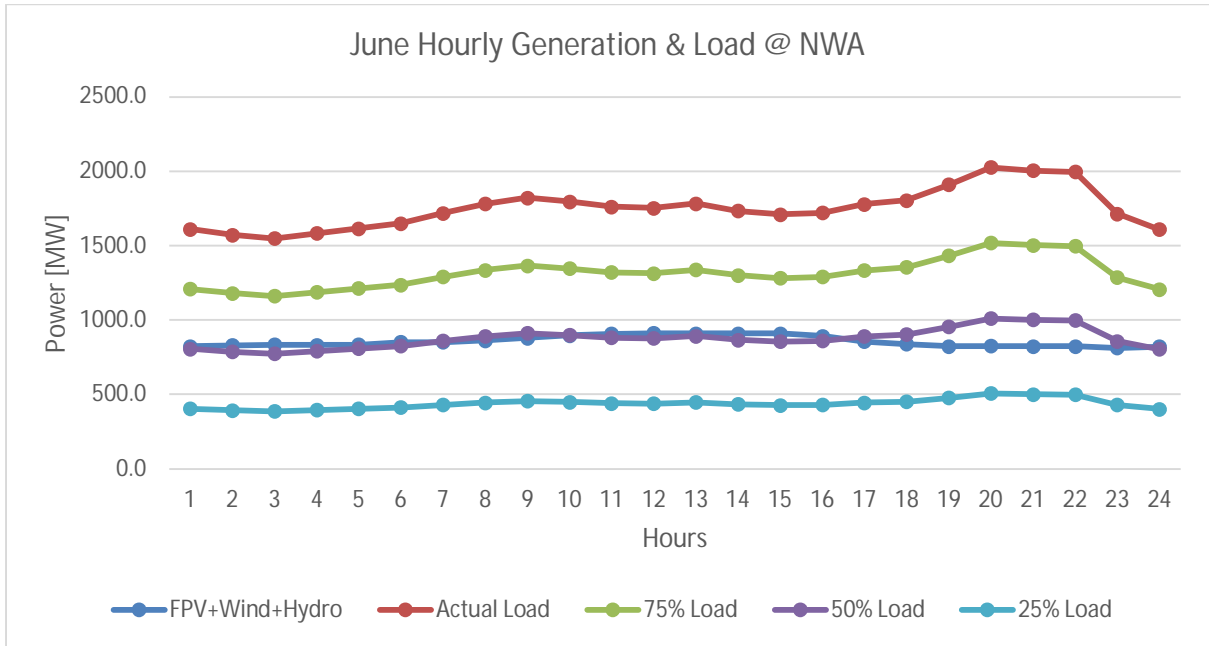


Figure 7.5.1S: showing generation dispatch and electrical grid load on 1st June

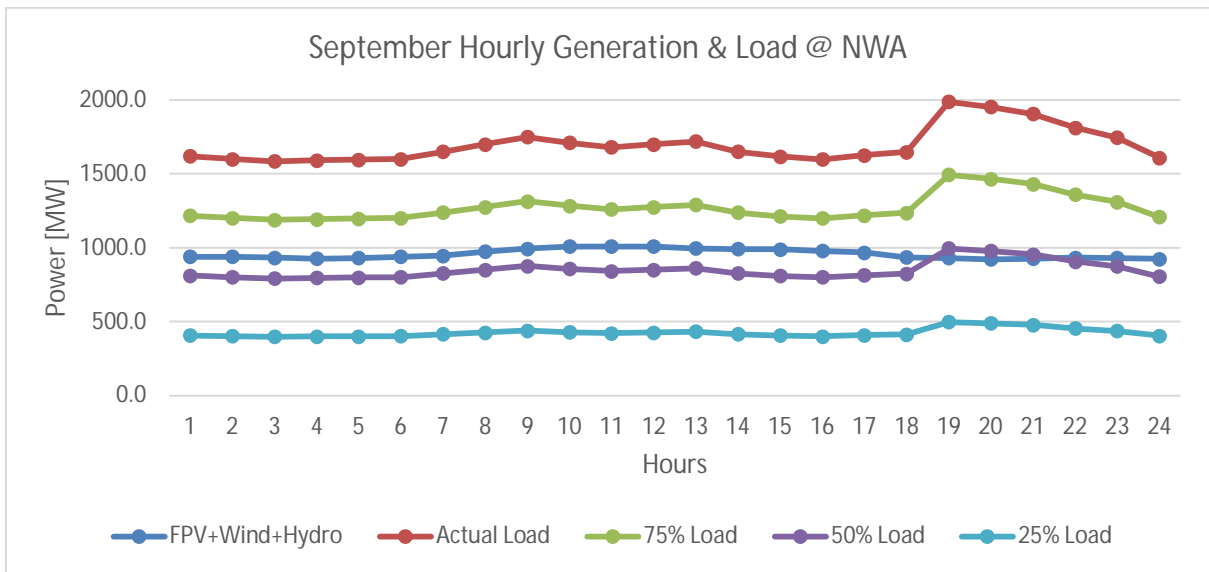


Figure 7.5.1T: showing generation dispatch and electrical grid load on 1st September

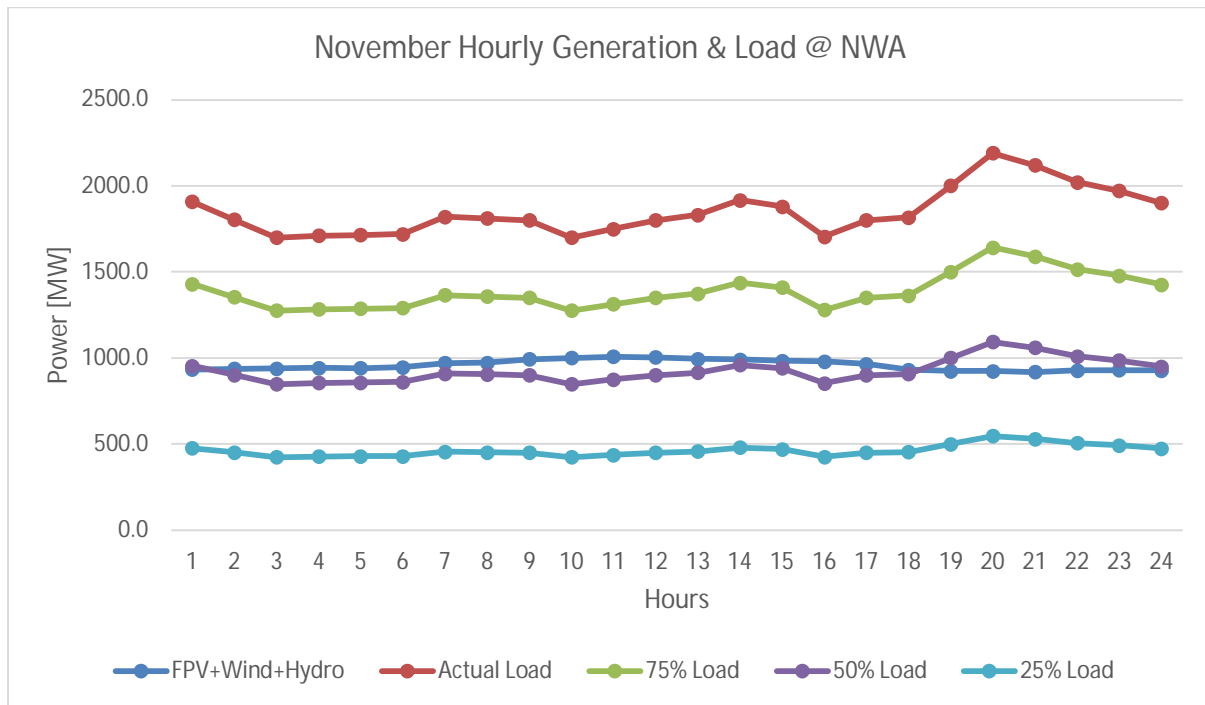


Figure 7.5.1U: showing generation dispatch and electrical grid load on 1st November

7.5.2 Cost of VRES (Wind & FPV)

The levelized cost of energy for wind and photovoltaics was based on the homerpro model whose schematic is shown in figure 7.5.3A. The capital expenditure (CAPEX) and operating expenditure (OPEX) for the wind and FPV is based on IRENA(2019), World Bank (2019) and CESI (2020) data, as shown in table 7.5.2A and section 3.7 of the literature review.

Table 7.5.2A: showing cost and energy production distribution.

	FPV (116MWpdc/100MWac)	Wind (100MWac)	FPV+Wind
CAPEX	£80,233,200.00	£109,393,980.00	£189,627,180.00
	£0.69/kWp	£1.09/kWp	£0.88/kWp
OPEX	£1,679,083.20	£2,00,000.00	£3,264,503.20
	£0.017/kWp	£0.02kWp	£0.017/kWp
GWh/year	214.4 (in PVSyst)@ 100MWac output. 175(Homerpro)@96MWpac output.	295(in Renewables ninja) @ 100MW, 166(in Homerpro) @75MW output	513 (PVSyst +Renewables Ninja). 341 (in Homerpro)

Note: The hydro model in homerpro had a capital cost of 2.8€/Wp with operation and maintenance cost of 1.7pence/Wp

The LCOE for the base architecture (in Homerpro) of the FPV and wind system with the CAPEX and OPEX as given in table 7.5.2A, is illustrated in figure 7.5.2A. Therefore, it would

cost 6.7pence/kWh to produce 175GWh/y of floating PV and 7.2pence/kWh to produce 166GWh/y of onshore wind at KGU.

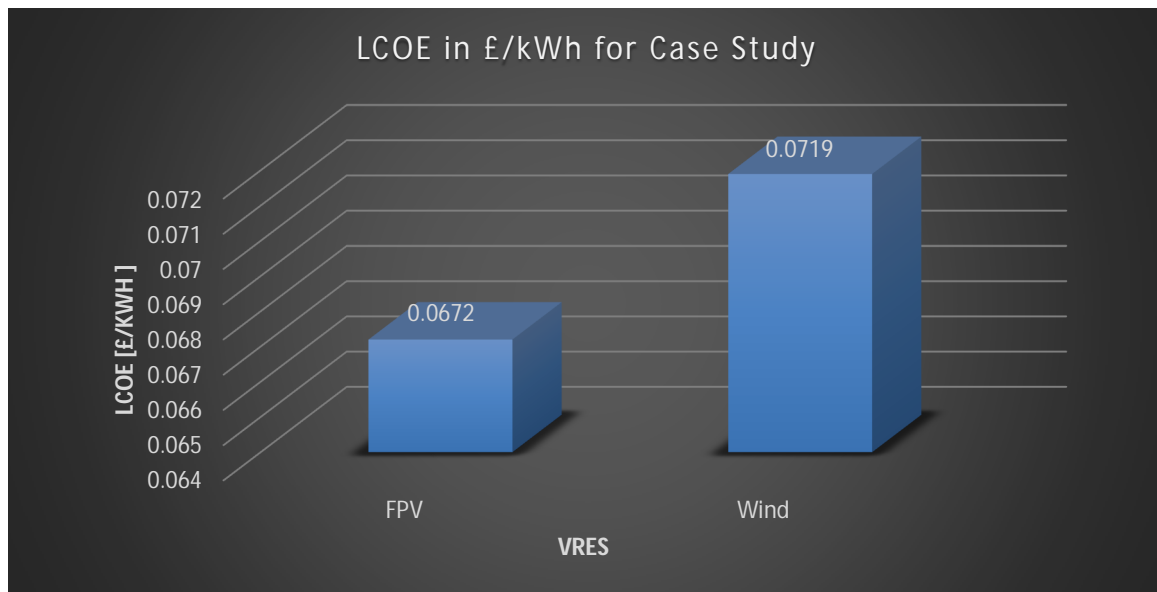


Figure 7.5.2A: showing the LCOE of the large footprint floating PV and Wind at KGU

7.5.3 Hybrid System Optimization Using HomerPro Advanced Dispatch

This section is structured as follows: [Section 7.5.3.1](#) defines the energy system as modelled in Homerpro. [Section 7.5.3.2](#) describes the six different dispatch strategies available in homerpro, while [section 7.5.3.3](#) presents a detailed optimization of the energy system using the six homerpro dispatch strategies and compares their net present cost (NPC), operating costs, virtual storage utilization, renewable fraction, maximum renewable penetration and levelized cost of energy.

7.5.3.1 Energy System Model

The energy system has the following components: wind farm, grid load, floating PV, KGU hydro plant, virtual battery (and converter) and embedded dispatch controllers. The system schematic is shown in [figure 7.5.3A](#).

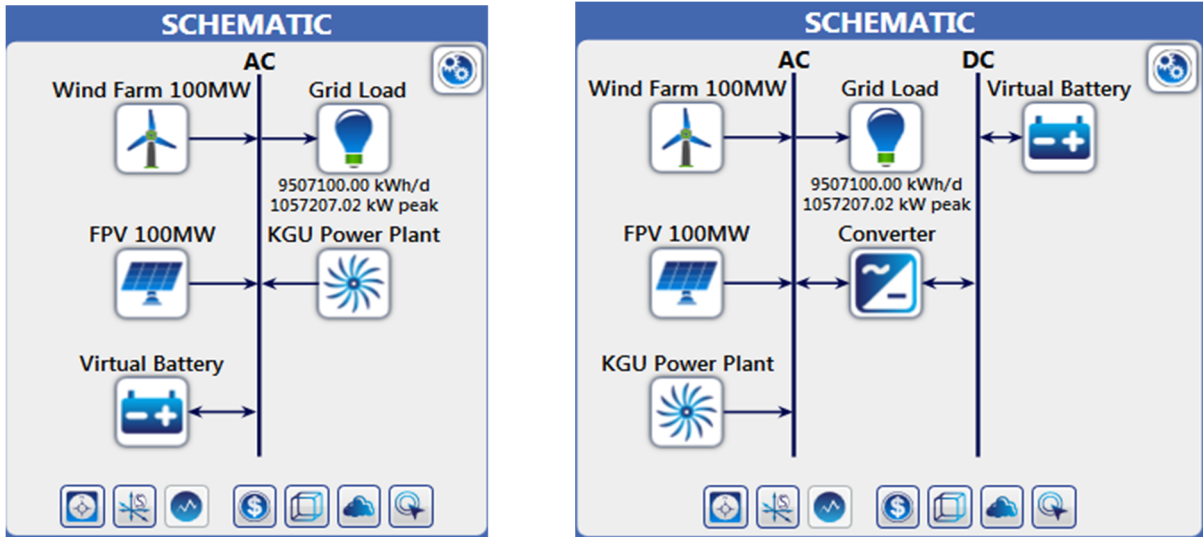


Figure 7.5.3A: showing energy system schematic in Homerpro

Sensitivity and Optimization Parameters

The sensitivity and optimization parameters are given in figure 7.5.3B and 7.5.3C respectively.

Sensitivity Inputs

This table displays the values of each sensitivity variable (variable for which you have specified multiple values). You can add sensitivity values by clicking this button (⋮) when it appears next to input fields.

KGU Power Plant time (years)	Grid Load Scaled Average (kWh/d)	Nominal Discou (%)	Project Lifetime (years)
50	9507100.00	8	20.00
60	10507100	10	25
70	11507100	12	
80	12507100	14	
	13507100		

Figure 7.5.3B: showing sensitivity inputs

Search Space

You can also edit these inputs for each component individually in each component page. The lower table summarizes the results of the optimization if they have been calculated.

KGU Power Plant Capacity (Quantity)	FPV 100MW Size (kW)	conv Dedicated Conv (kW)	Virtual Battery Strings	Wind Farm 100 Quantity (#)
<input type="checkbox"/> Optimizer	<input type="checkbox"/> Optimizer	<input type="checkbox"/> Optimizer	<input type="checkbox"/> Optimizer	<input type="checkbox"/> Optimizer
0	0	1	0	0
1	25000		1	5
2	50000		2	10
3	75000		3	15
4	100000		4	20
5				25
6				

Overall Winner Category Winner Calculate OK

Figure 7.5.3C: showing sensitivity inputs

Electrical Grid Load

The electrical grid load is modelled in Homerpro as provided per the national utility and ERB data (2018). However, the modelled load is only fraction of the total national electrical load shown in figure 7.5.3D.

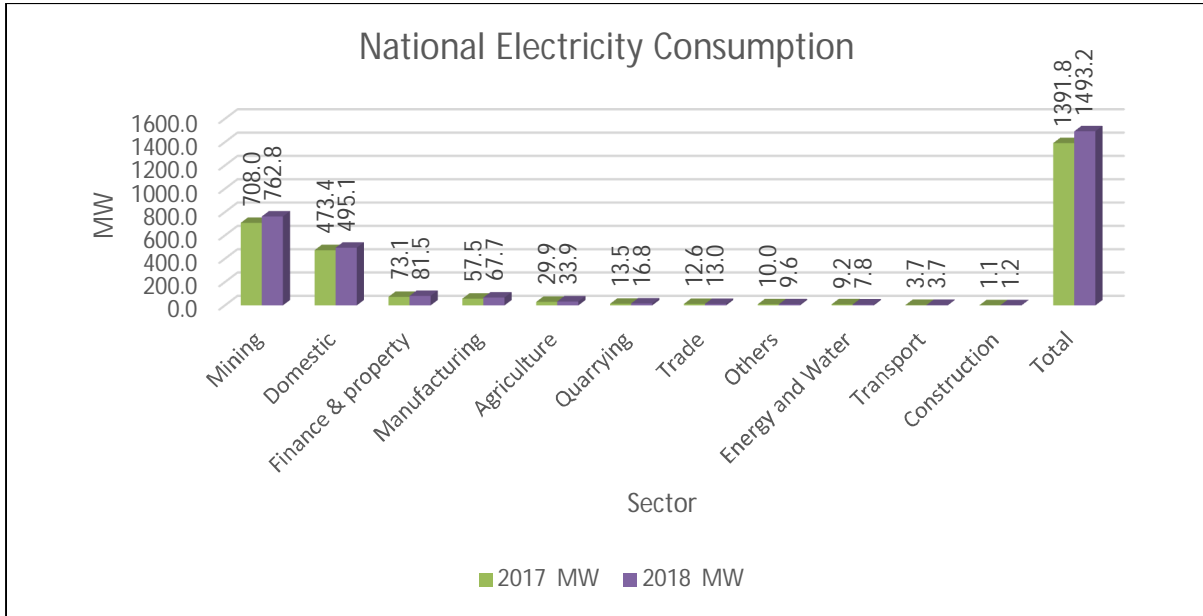
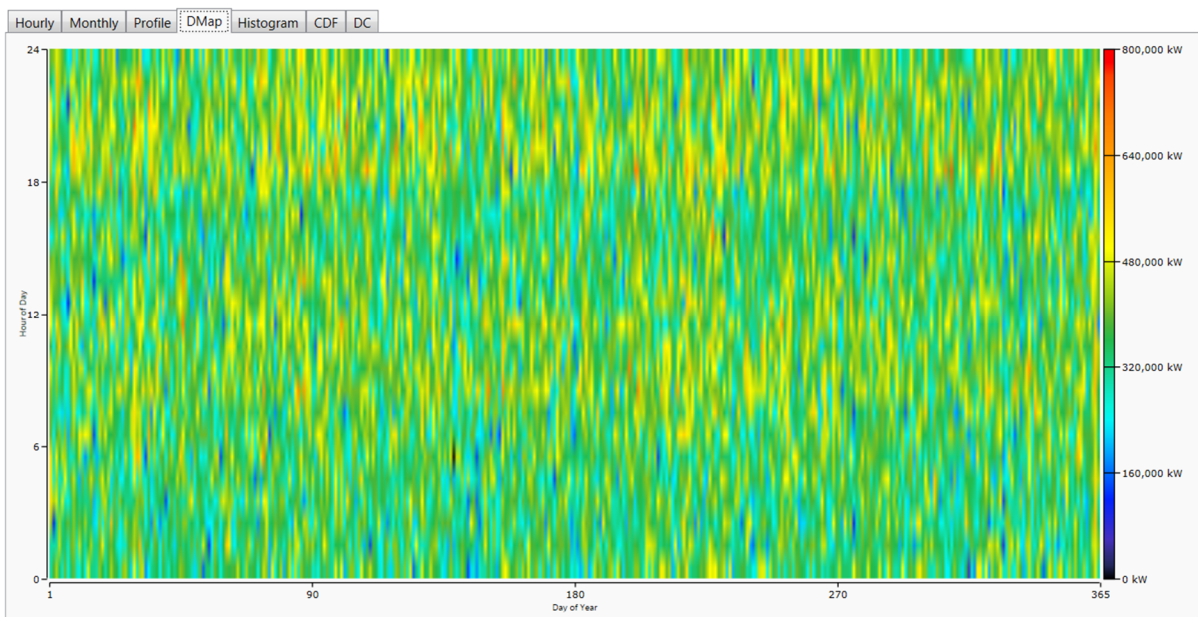


Figure 7.5.3D: showing national electricity consumption by economic sector

Based on national electricity grid consumption profile, a load pattern was created, which was then scaled to the daily energy consumption with 5 sensitivity parameters (9.5GWh/d, 10.5GWh/d, 11.5GWh/d, 12.5GWh/d, 13.5GWh/d) with an average and peak demand of 396MW and 744MW respectively. The modelled load is shown in figure 7.5.3E below.



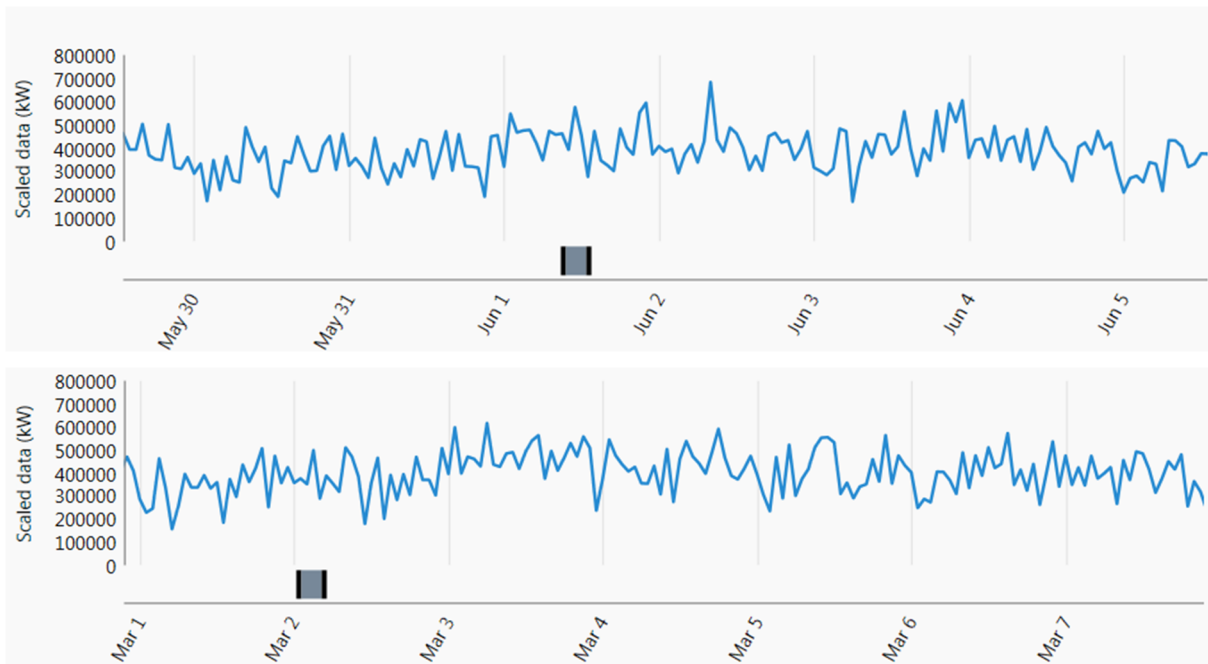


Figure 7.5.3E: showing fraction of national load modelled in homerpro

Floating PV

The floating photovoltaic system was designed in PVSyst ([section 7.3.1](#)) and later exported to Homerpro with all the relevant design parameters embedded (i.e. arrays, inverter, shading analysis, water compensation of the PV modules).

KGU Hydro

The KGU hydro generation was first modelled in iHoga using the power plant ratings provided by the national power utility (ZESCO Ltd) as illustrated in [section 7.2.1.3](#). Thereafter, a model was made in Homerpro.

Onshore Wind

The onshore wind was modelled in renewables ninja ([section 7.3.2](#)) and later exported to homerpro with actual wind speed values for the location.

Virtual Battery

Using the advanced storage features of Homerpro, a custom storage module was designed emulating pumped hydro ([section 7.4](#)).

7.5.3.2 Homperpro Dispatch Strategy Capabilities

Before the existence of controller components in homerpro, only cycle charging and load following strategies existed. Currently, four additional controllers exist in Homerpro (i.e. Homer Combined Dispatch, Homer Predictive, Homer Pro Matlab Link and Homer Generator Order). However, the Matlab Link is only available in the advanced licence package.

Homer Load Following (HLF):

Under the HLF strategy, a generator produces only enough power to meet the load when it is needed. When the renewable power exceeds the demand, HLF seems to be optimal in such systems with a lot of renewable energy.

Homer Cycle Charging (HCC):

Under the HCC strategy, when a generator operates, it does so at full capacity with the surplus energy charging the battery bank. This strategy is optimal in systems with minimal or no renewable energy.

Homer Combined Dispatch (HCD):

This dispatch strategy improves the performance of load following and cycle charging by utilizing the generator in an efficient manner.

Homer Generator Order (HGO):

Under the HGO strategy, Homer follows the generator combinations that are defined, with the first combination taking priority to meet the operating capacity. However, this strategy only supports systems with PVs, generators, wind turbines, storage components and converters.

Homer Predictive (HP):

Under the HP dispatch strategy, the Homer dispatch algorithm can predict the upcoming thermal and electric load, as well as the availability of the upcoming wind and solar resource. Homer predictive usually produces results which have a system with lower operating costs when compared to other strategies in Homer Pro.

Homer Matlab Link (HML):

Under this strategy, a user can customize a dispatch algorithm for Homer Pro using written code in Matlab. Homer Pro communicates with Matlab software during calculations and function calls to run all lines of code during the simulation.

7.5.3.3 Energy System Optimization

Determining the best Controller (and dispatch strategy) depends on many factors, including the sizes of the generators and battery bank, the price of fuel, the O&M cost of the generators, the amount of renewable power in the system, and the character of the renewable resources. This section compares the performance of the various control strategies by benchmarking system costs and renewable fraction (table 7.5.3A), generator operational results (table 7.5.3B) and storage system operation results (table 7.5.3C). The model has also included costs for hydro (IRENA, 2019) and virtual storage (ESA, 2020) for homer to give more coherent results.

Homer Load Following, Cycle Charging and Combined Dispatch

Homer load following, cycle charging and combined dispatch displayed similar dispatch characteristics of 0 percent renewable fraction, 0 percent maximum renewable penetration and a levelized cost of energy for the hybrid system of approximately 7.7pence/kWh.

Homer Generator Order

The system cost summary, electrical summary and hydro storage under the generator order dispatch strategy are given in figures 7.5.3F, 7.5.3G and 7.5.3H respectively.

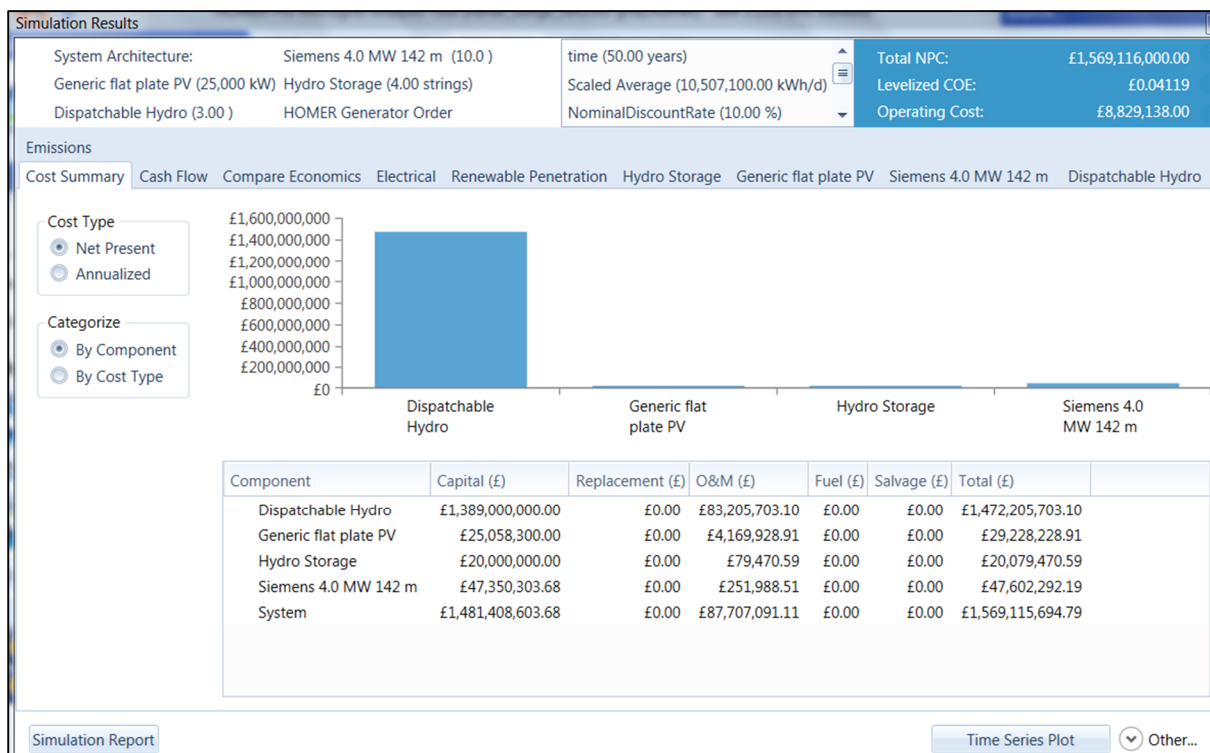


Figure 7.5.3F: showing system cost summary of the energy system under HGO strategy

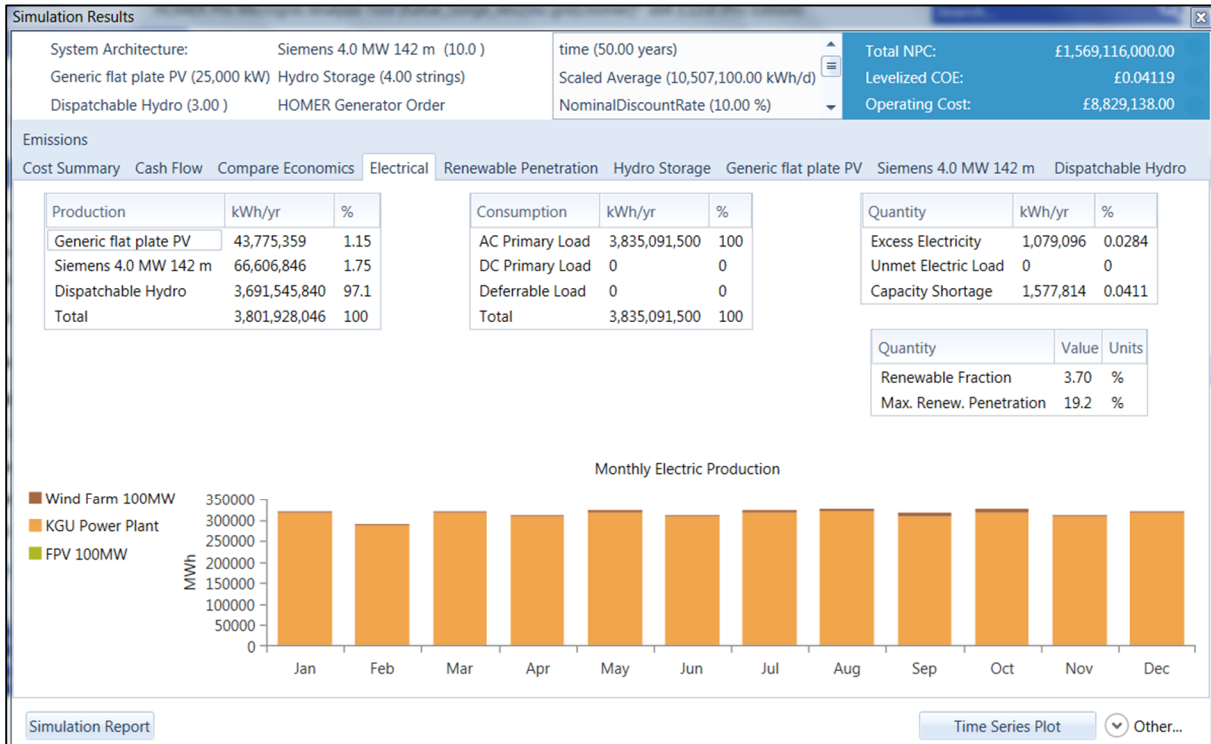


Figure 7.5.3G: showing electrical summary of the energy system under HGO strategy.

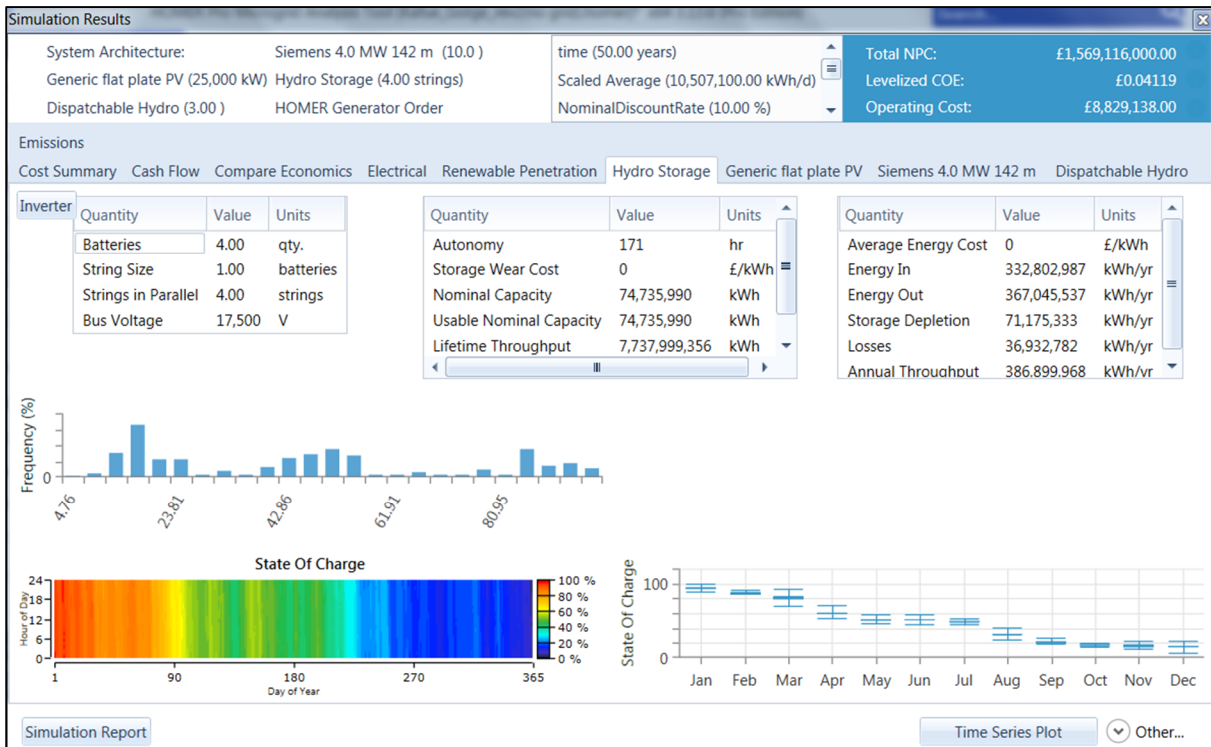


Figure 7.5.3H: showing hydro storage of the energy system under HGO strategy.

Homer Predictive

The system cost summary, electrical summary and hydro storage under the homer predictive dispatch strategy are given in figures 7.5.3I, 7.5.3J and 7.5.3K respectively.

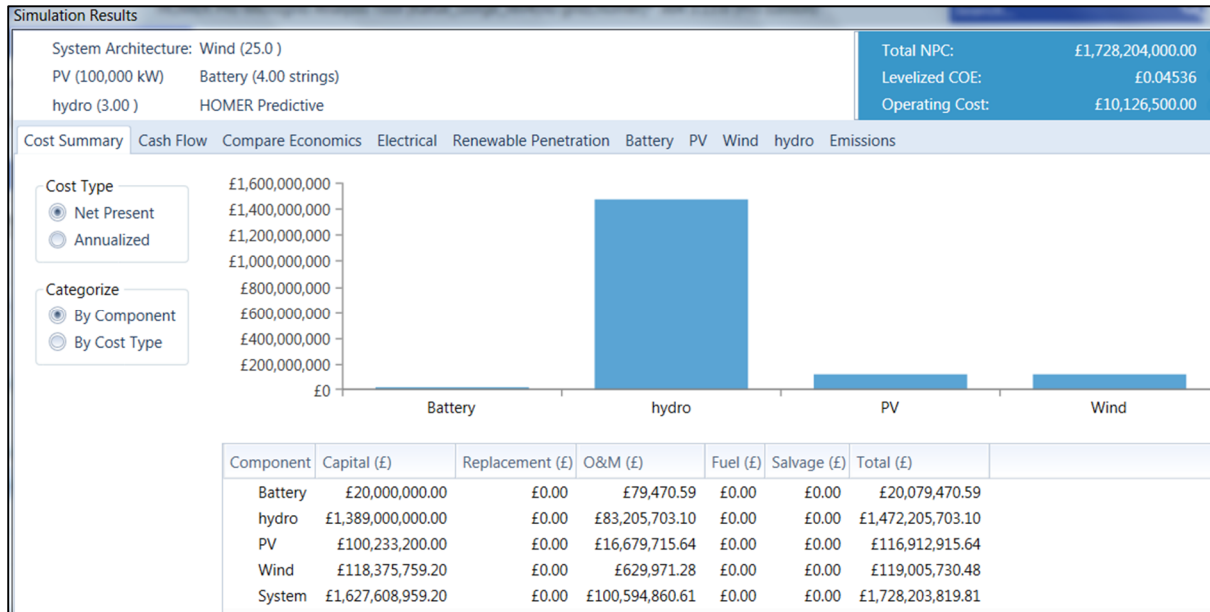


Figure 7.5.3I: showing system cost summary of the energy system under HP strategy



Figure 7.5.3J: showing electrical summary of the energy system under HP strategy

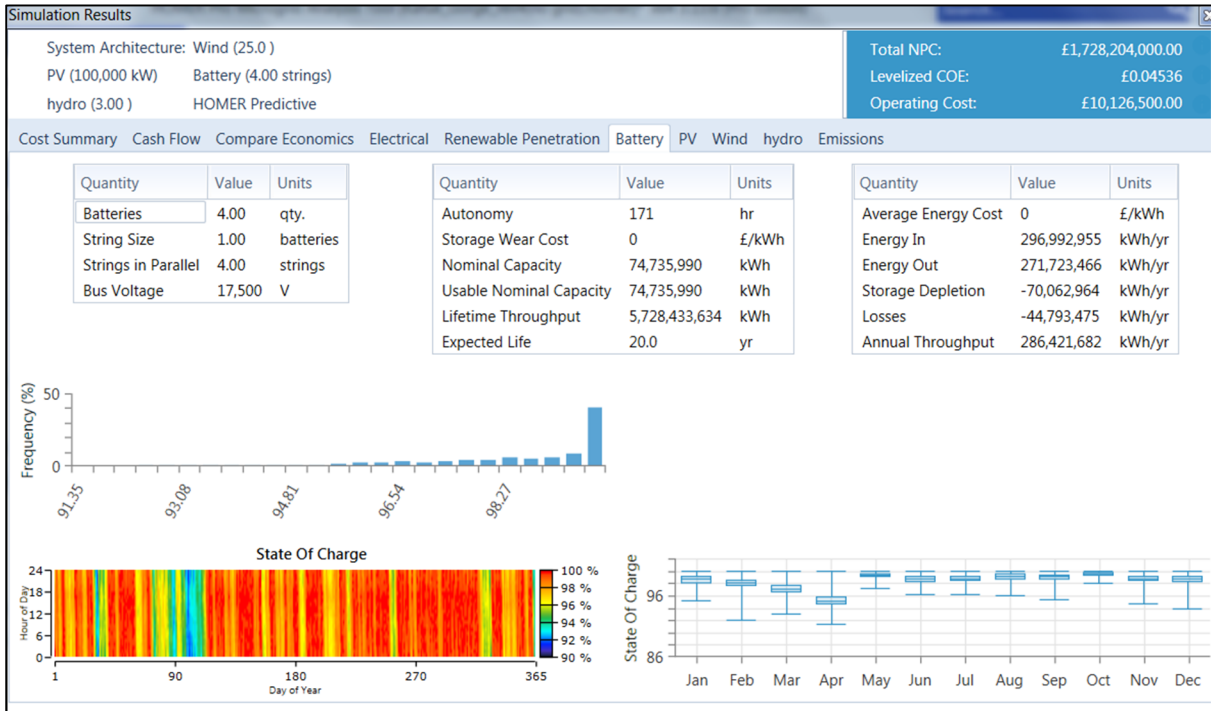


Figure 7.5.3K: showing hydro storage of the energy system under HP strategy.

Homer Matlab Link

The dispatch algorithm is designed to handle systems with components on the AC bus only, with no DC components or converter. Thus, the model was simplified by removing the DC bus and converter (making the code simpler and easy to understand). Figure 7.5.3l shows the Matlab link inputs.

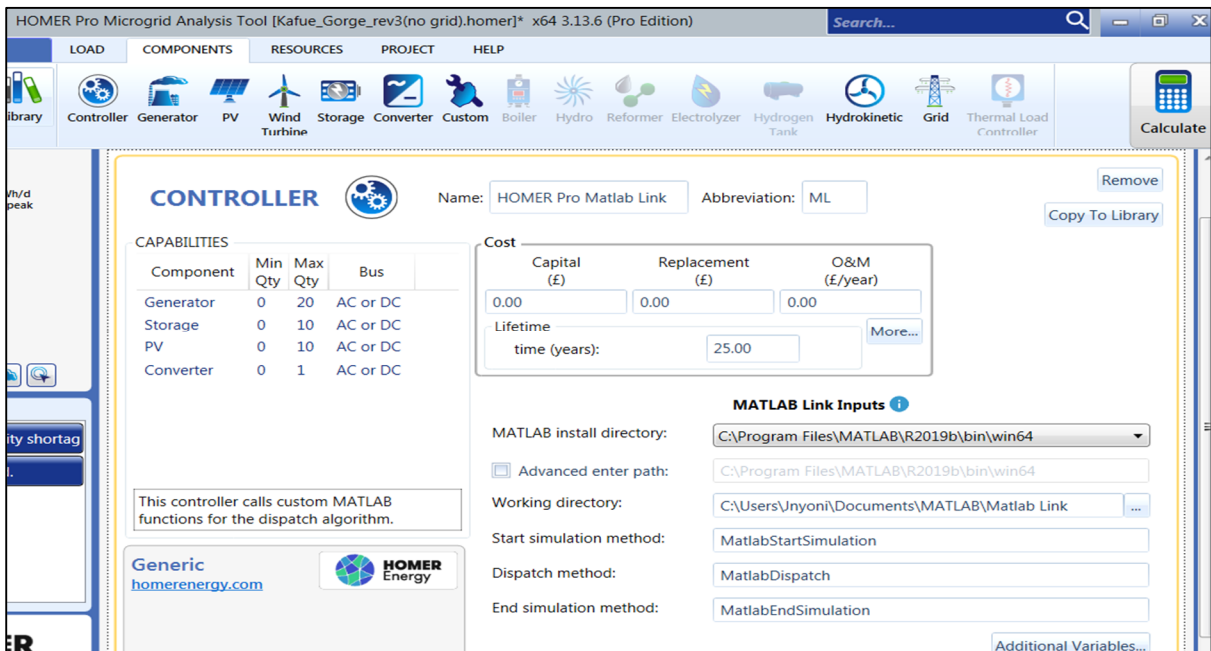


Figure 7.5.3L: showing the Matlab link inputs

The Matlab code was used to ascertain a customized dispatch with high VRES penetration. HOMER calls MatlabDispatch at the beginning of each time step in the simulation. Matlab dispatch has three input variables:

- ✓ **Simulation_state:** In simulation state structure, in order to control the operation of the system using the Matlab Dispatch function, one must set up values for every time step. These variables can vary in each simulation time step.
- ✓ **Simulation_parameters:** The Homer Model defines the variables contained in this structure. These do not change during the simulation process and are read only.
- ✓ **Custom_variables:** The user defined variables are used by Matlab and not Homer Pro. These are used to keep track of values required for the custom algorithm over the simulation process. The variable can be a scalar, a structure, array, depending how the user defines it.

The calculations and function call between Homerpro and Matlab are given in the figure 7.5.3M.

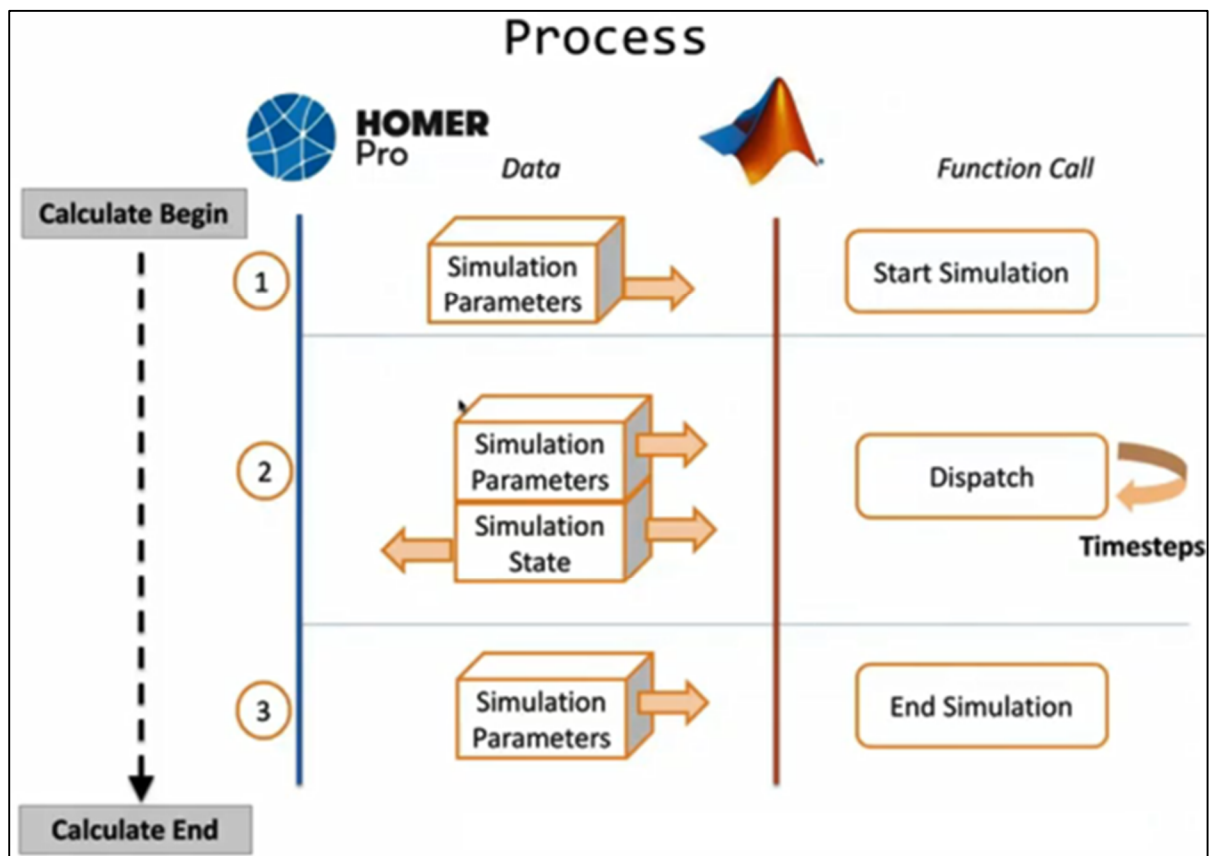


Figure 7.5.3M: showing the process of calculations and function calls between homerpro and matlab

Appendix C shows the Matlab code for the HML dispatch strategy.

The 3 tables (7.5.3A, 7.5.3B, 7.5.3C) below summarize the performance on the 6 dispatch strategies in Homerpro as applied to the Kafue Gorge Upper case study. These tables are analysed in section 8.1 on system optimization.

Table 7.5.3A: showing renewable fraction and system costs

	Dispatch Strategy	Renewable Fraction (%)	Generator Cost (£million)	Operational Cost (£million)	NPC (£million)	System LCOE (£/kWh)
1	HLF	0	2778	16.8	2944.4	0.07729
2	HCC	0	2778	16.8	2944.4	0.07729
3	HCD	0	2778	16.8	2944.4	0.07729
4	HGO	4	1481.4	8.8	1569.1	0.04119
5	HP	100	1627.6	10	1728.2	0.04536
6	HML	100	2534	14.9	2710	0.05511

Note: Generation/operational cost is high due to the additional system components (i.e. hydro, storage). NPC – Net Present Cost, LCOE – Levelized Cost of Energy.

Table 7.5.3B: showing system operation results

	Dispatch Strategy	Excess Electricity (%)	Max Renew. Penetration (%)	Production (TWh/year)	Consumption (TWh/year)	Capacity shortage (%)
1	HLF	48.1	0	7.38	3.84	0.09
2	HCC	48.1	0	7.38	3.84	0.09
3	HCD	48.1	0	7.38	3.84	0.09
4	HGO	0.03	19.2	3.80	3.84	0.04
5	HP	50.6	59.5	4.00	3.84	0.00710
6	HML	0	59.5	4.93	4.93	0.02

HML (13507100kWh/day) serves more load compared to (10507100kWh/day) for the other five dispatch strategies.

Table 7.5.3C: showing storage system operation results

	Dispatch Strategy	Expected Life(years)	Energy input (GWh/year)	Energy output (GWh/year)	Losses (GWh/year)	Throughput (GWh/year)	Life T/P (GWh)
1	HLF	-	-	-	-	-	-
2	HCC	-	-	-	-	-	-
3	HCD	-	-	-	-	-	-
4	HGO	20	333	367	37	387	7738
5	HP	20	297	271	-45	286	5728
6	HML	-	-	-	-	-	-


Note: T/P – Throughput.


7.6 Optimal Dispatch versus Baseline Case

To make these dispatch strategies compatible with the energy system under study, the load is treated as a grid connected load and thus the actual grid is omitted in the configuration. The custom dispatch changes how the simulation sequence occurs in homerpro to suit the specific needs of the system. The three most techno-economic dispatch strategies are the homer generator order (HGO), homer predictive (HP) and homer Matlab link (HML) as can be seen by the lower operating costs and low levelized cost of energy in [table 7.5.3A](#). The HGO, HP and HML dispatch strategies are illustrated in [figures 7.6A, 7.6B and 7.6C](#) respectively, these are also compared with the baseline case which does not utilize any renewable energy to serve part of the load as shown in [figure 7.6D](#). These figures are a snapshot of the generation and load distribution on the 15th of August. This date is chosen because of the maximum availability of PV and wind with peak power ranging between 90 to 100 MW.


HGO Dispatch Summary: The homer generator order dispatch was implemented with 420 MW of hydro, 68 MW of wind, 44 MW of floating PV and a virtual storage equivalent of 4 units. [Figure 7.6A](#) shows the time series distribution of generation to serve the load on August 15 for 24hrs. This figure shows a near constant hydrogeneration from 00:00hrs to 23:00hrs with a battery state of charge of about 88.2%. The morning peak demand of approximately 620 MW between 08:00hrs and 10:00hrs is served by 420 MW hydro, ~ 20 MW of FPV and ~ 40 MW of wind with the unmet load of ~ 140MW served by virtual battery storage (i.e. virtual storage discharge power graph). The afternoon peak at noon is served by 420 MW hydro, ~ 40 MW FPV and ~ 40 MW wind with the unmet load served by battery storage, while the evening peak is served by 420 MW hydro, ~ 35 MW wind and battery storage (i.e. virtual storage discharge power graph).

Winning System Architecture


 HOMER Generator Order


 Virtual Storage - 4.00


 Wind - KGU - 17.0


 KGU Hydro - 3.00


Base Case Architecture

 HOMER Generator Order

 FPV - KGU - 44,000 kW

 Virtual Storage - 4.00

 Wind - KGU - 17.0

 KGU Hydro - 3.00

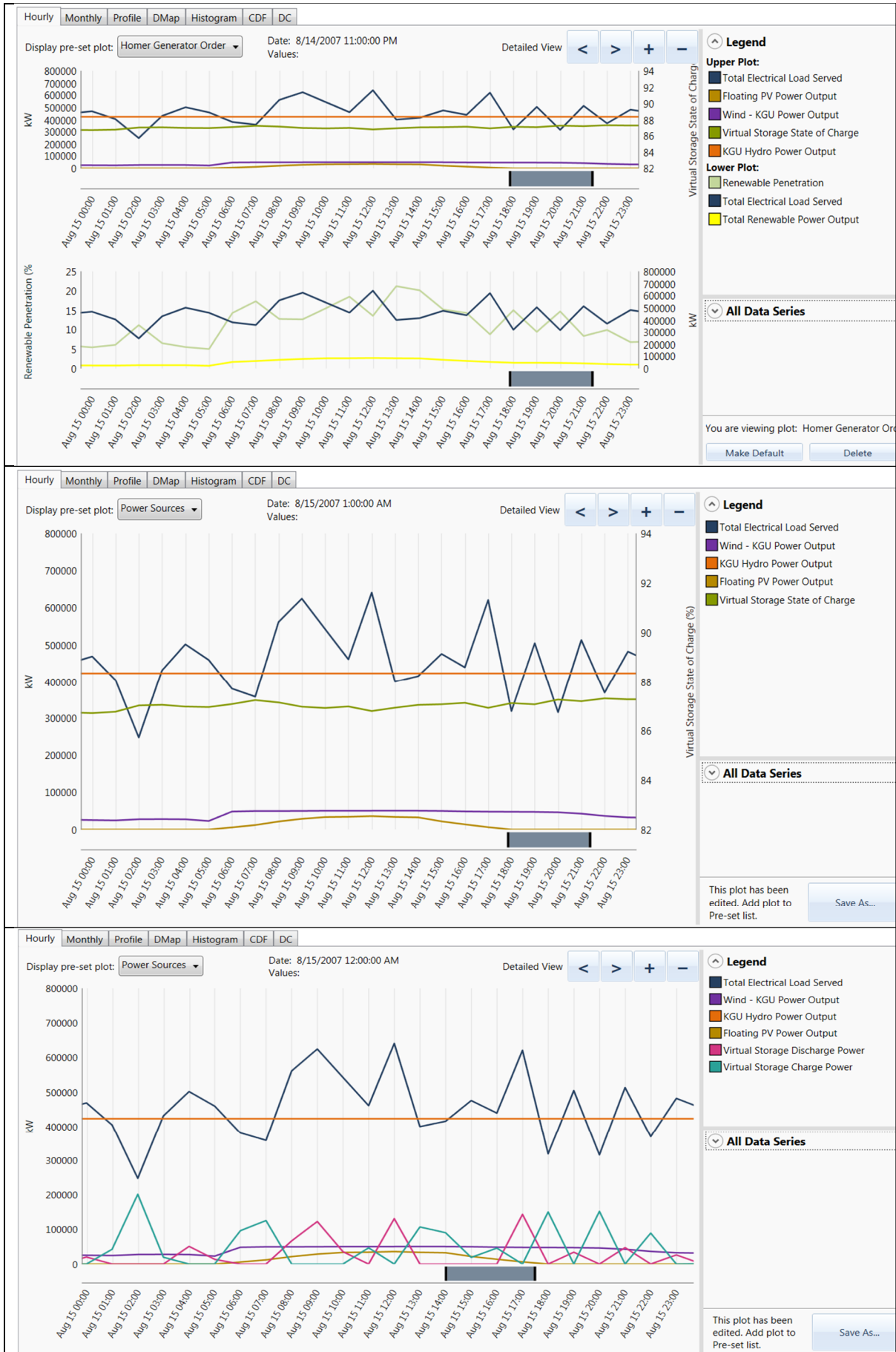











Figure 7.6A: showing the generator order dispatch strategy

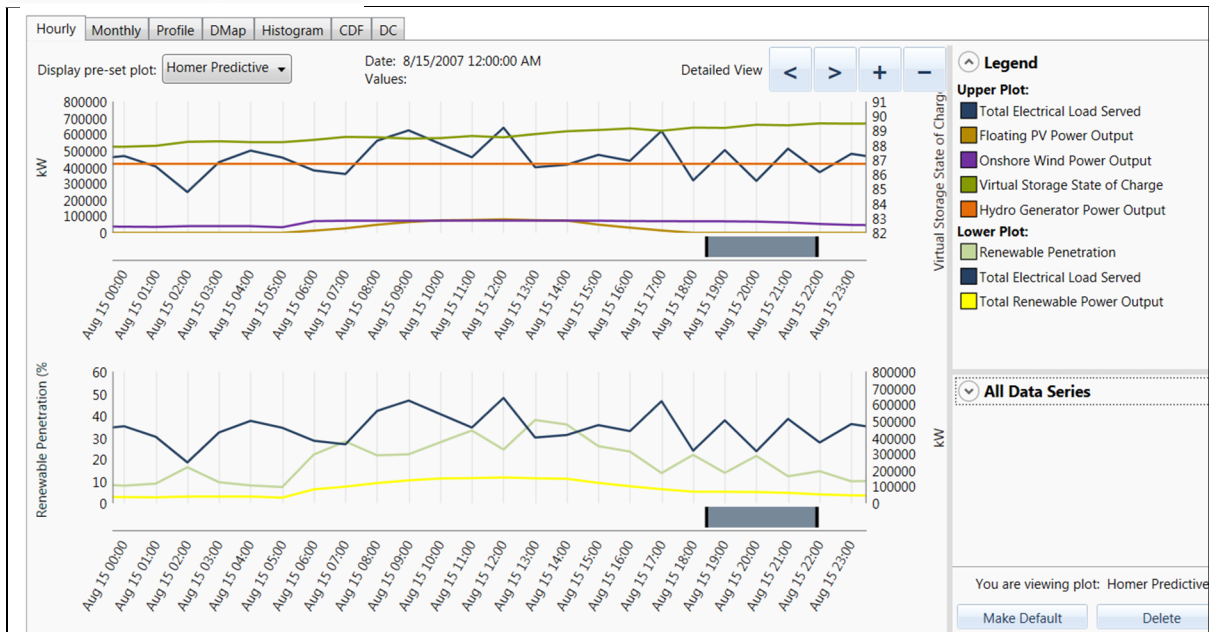
HP Dispatch Summary: The homer predictive dispatch utilizes 420 MW of hydrogeneration, 100 MWac-peak of FPV, 25 wind turbines each rated at 4 MW (100 MWp) with 4 units of virtual storage. However, on August 15, this strategy utilizes more of the FPV and wind as can be seen in figure 7.6B with a 620 MW noon peak demand served by approximately 90 MW of FPV, 90 MW of wind, 420 MW of hydro and the remainder met by battery storage (as seen by the virtual storage discharge power graph). Further, the evening peak between 17:00hrs and 21:00hrs was served by 420 MW of hydro, 70 MW of wind and virtual storage as seen by the virtual storage charge power graph in figure 7.6B.

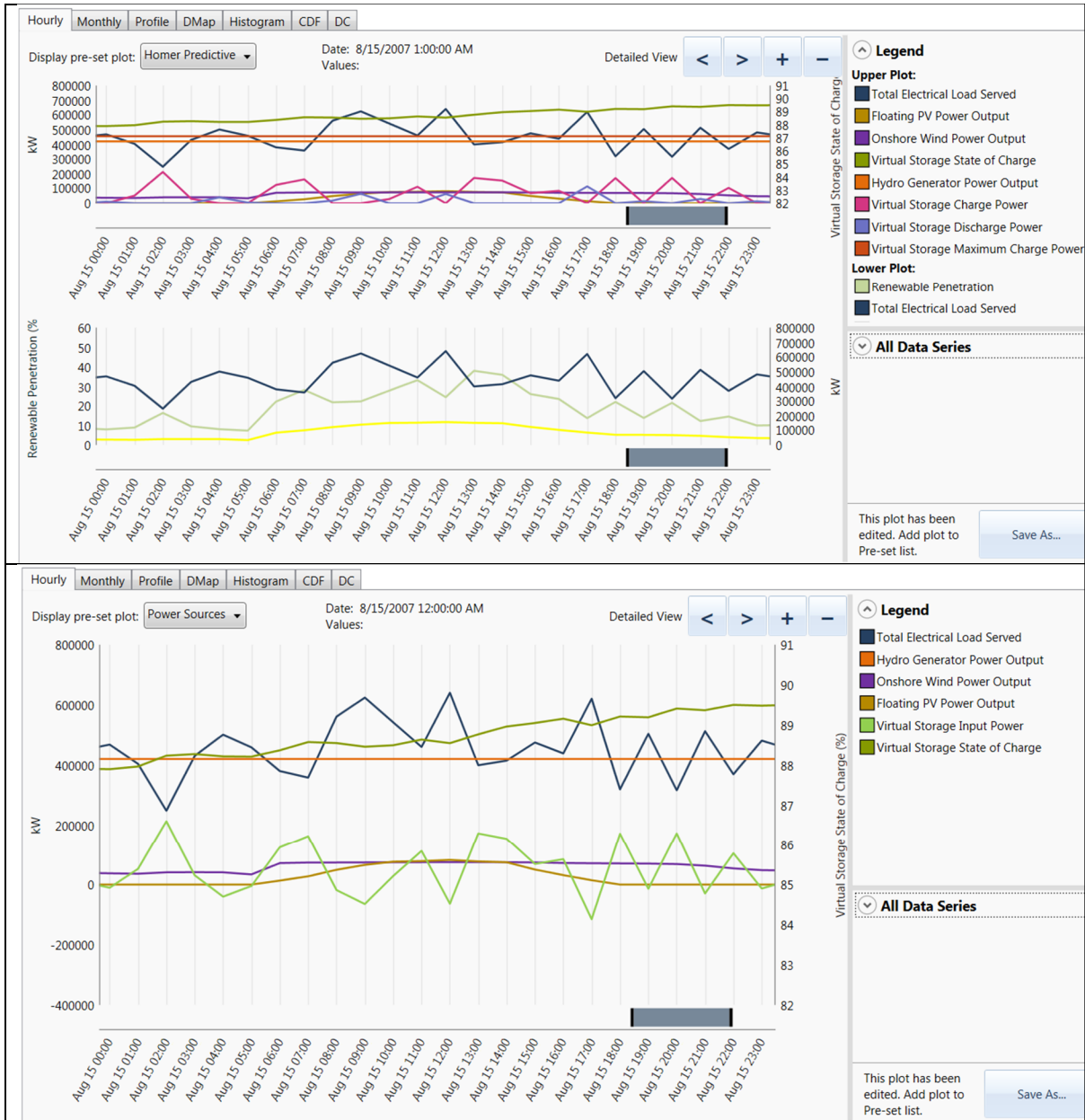
Winning System Architecture

-  **HOMER Predictive**
-  **KGU Hydro - 420,000 kW**
-  **FPV - KGU - 100,000 kW**
-  **Virtual Storage - 4.00**
-  **Wind - KGU - 25.0**

Base Case Architecture

-  **HOMER Predictive**
-  **KGU Hydro - 420,000 kW**
-  **FPV - KGU - 100,000 kW**
-  **Virtual Storage - 4.00**





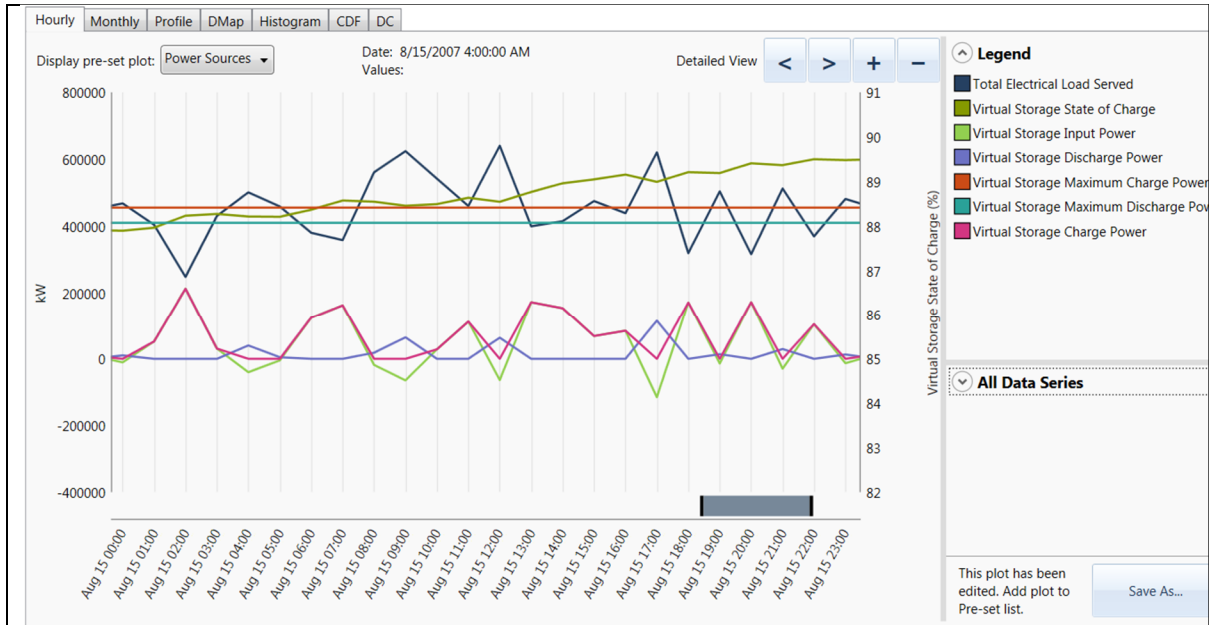










Figure 7.6B: showing the homer predictive dispatch strategy

HML Dispatch Summary: The homer matlab dispatch was implemented using a customized dispatch algorithm and utilized 5 hydro units which is equivalent to 700 MW, 100 MWp of FPV, 100 MWp of wind. This is the only dispatch strategy that throttled down hydro generation in the presence of floating PV and wind. The reduced generation is the storage saving potential of 1 virtual storage unit equivalent (~ 108 MW). Figure 7.6C shows the hydro generation throttled down at each time step in the presence of FPV and wind on August 15. All the load was met with no excess electricity production on the day in question as can be seen in figure 7.6. The throttling down of hydro is more pronounced between 06:00 and 07:00hrs, at 11:00hrs and between 13:00 and 14:00hrs with reduction in peak demand.

-  **HOMER Pro Matlab**
-  **KGU Hydro - 700,000 kW**
-  **FPV - KGU - 100,000 kW**
-  **Virtual Storage - 1.00**
-  **Wind - KGU - 25.0**
- Base Case Architecture**
-  **HOMER Predictive**
-  **KGU Hydro - 700,000 kW**
-  **Virtual Storage - 1.00**



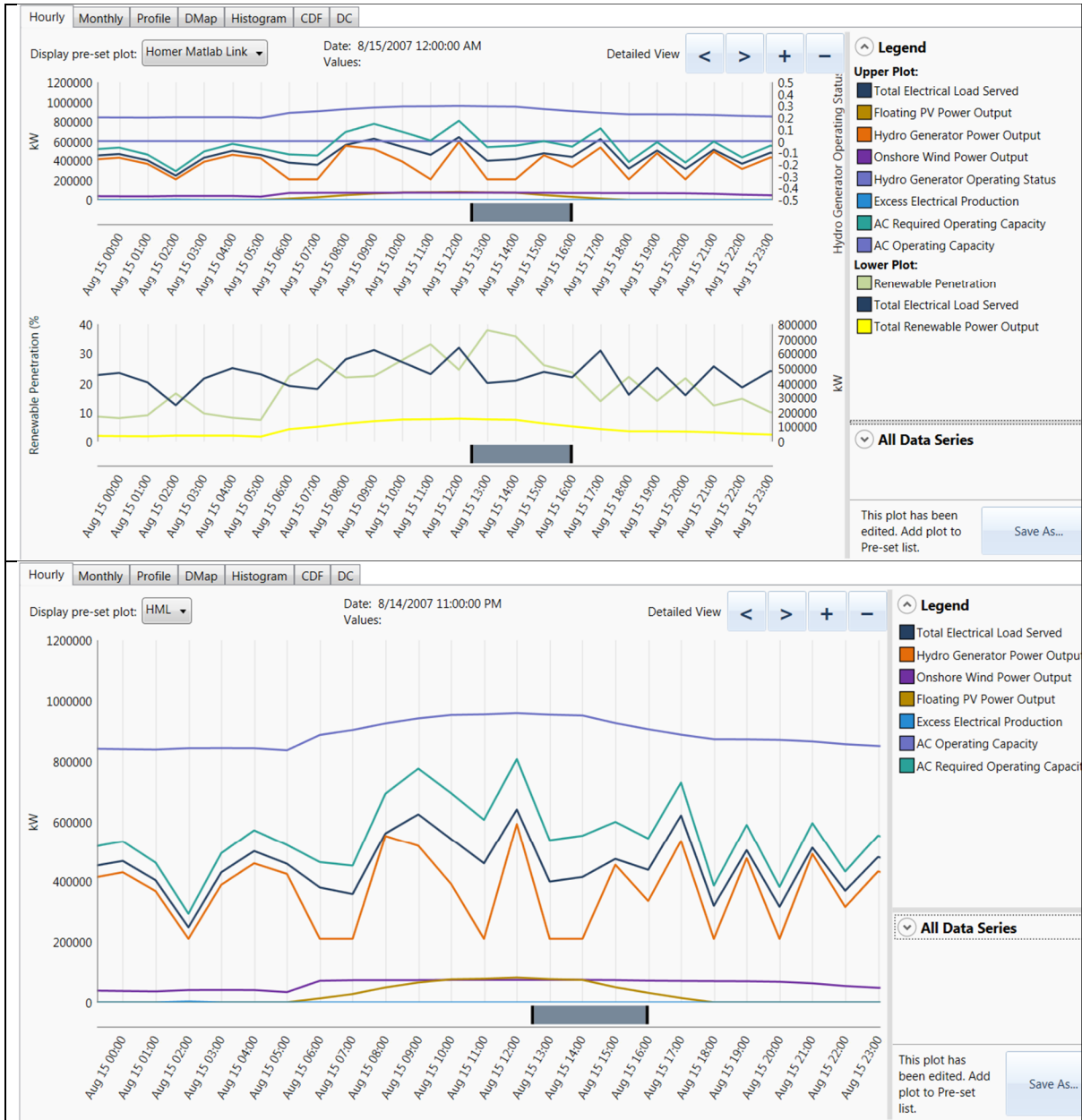


Figure 7.6C: showing timeseries dispatch using Matlab link (FPV, wind and 5 hydro turbines are dispatched to serve the load).

Baseline Case Without VRES: The baseline case is the existing setup at Kafue Gorge Upper without any variable renewable energy source (FPV and Wind) integration. This case utilizes only hydrogeneration as evidenced by the operation of all the 6 165 MW hydro units (operating at a conservative generating efficiency of 85%) to meet the load. The baseline case for the customized hydro unit dispatches 6 hydro units to meet an annual peak demand of 744 MW.

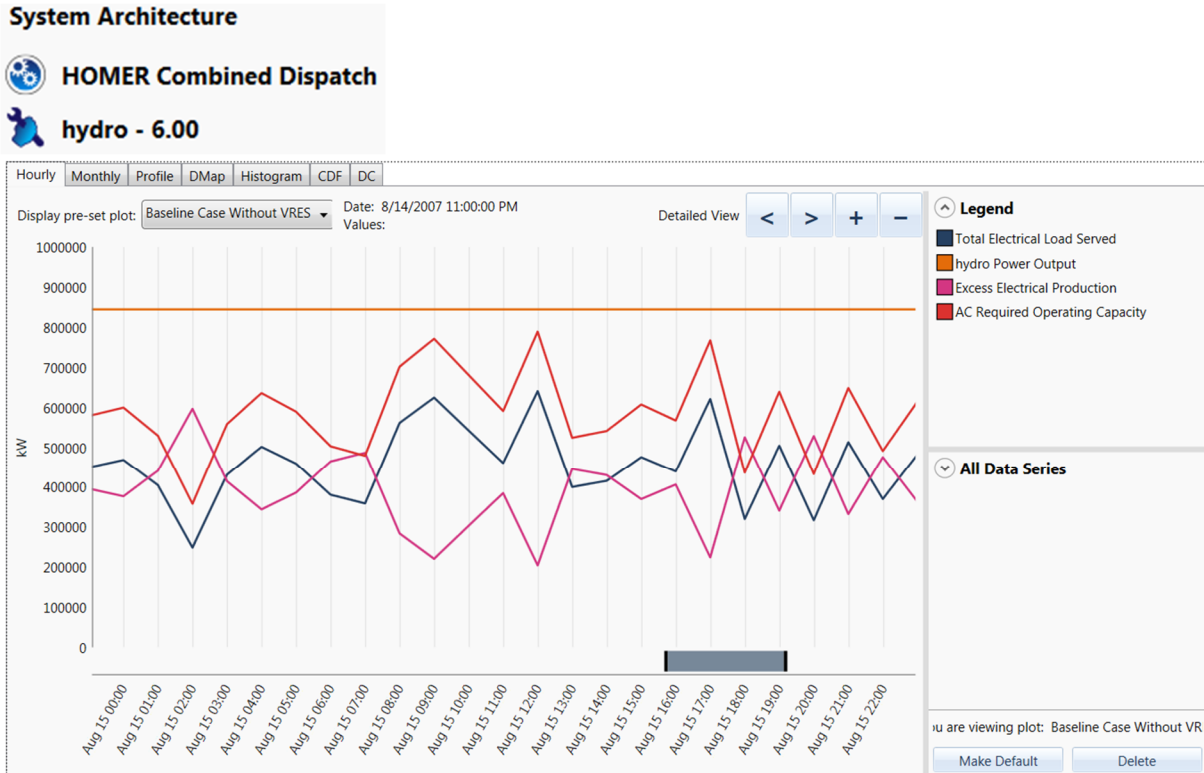


Figure 7.6D: showing baseline case without floating PV and onshore wind. Load is served by 6 hydro units

The custom hydro unit in homerpro is given in figure 7.6E below with search space optimization of up to six hydro units (0, 1, 2, 3, 4, 5, 6) with operating reserve margin of 10%.

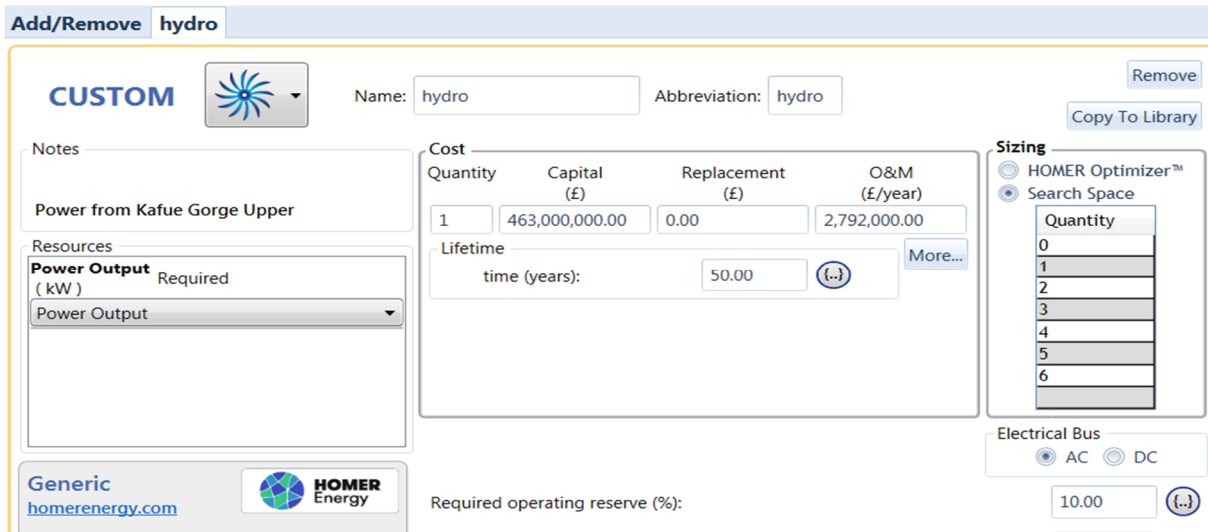


Figure 7.6E: showing the customized hydro unit in homerpro

7.7 Summary

A grid assessment was done to ascertain the extent of FPV and onshore wind integration at Kafue Gorge Upper (KGU) that would not negatively impact network parameters (i.e. voltage profile and power losses). Thereafter, an optimal power flow market model was developed to find the most optimal high-level scenario in reducing operating cost and losses considering the total network generation comprising of hydro (2001 MW), coal(126 MW), PV(76 MW) and how the addition of extra generation at KGU would impact the network market model as a whole.

The next step was to zero in at KGU by performing detailed design and dispatch analysis of the hybrid system comprising of 840 MW hydro (six 165 MW turbines modelled at 85% conservative efficiency), 100 MWac floating PV and 100 MWac onshore wind. The dispatch was developed by first understanding the relationship between time series generation (hydro and VRES) and demand data for the 2018/2019 timeline by looking at average hourly data for the first day of the month (i.e. January, March, June, September and November) capturing wide range seasonal variations. Therefore, three different scenarios were defined surrounding the hydro plant (i.e. dispatch with current water availability, low water availability and normal water availability). Further, a sensitivity analysis was done as a percentage of actual demand (i.e. 25%, 50% and 75%). Having understood the temporal complementarity between hydro, floating photovoltaics and onshore wind from the time series, the energy system was then modelled in an optimization software (Homerpro). Optimization and sensitivities parameters were defined for the generation and demand so that the most optimal dispatch strategy that maximises on integration of renewables at the least possible cost could be found. Determining the most optimal dispatch strategy in this context was about comparing the techno-economic capabilities of the system. This was done by looking at the strategy which utilizes and prioritizes variable renewables sources - VRES (floating photovoltaics and onshore wind) when they are readily available in homerpro. Therefore, the hydro output is throttled down, and this acts as virtual storage of the system.

The next chapter examines and discusses the results of the detailed case study design in line with literature and similar project studies. It also summarizes the project research outcomes, study limitation and proposes further work to be done.

CHAPTER EIGHT: DISCUSSION, OUTCOMES, LIMITATIONS, FURTHER WORK & CONCLUSIONS

The results and findings of the case study design application are discussed in [section 8.1](#). while [sections 8.2](#), [8.3](#) and [8.4](#) address the project research outcomes, limitations and the potential for further work respectively. Finally, [section 8.5](#) draws a conclusion to the project research.

8.1 Discussion

Grid assessment:

The detailed analysis of the national network grid was based on results obtained from PSAT and Matlab and is presented in [section 7.1.3](#). The notable points are the improvement in voltage magnitude profile and reduction in network power losses owing to the addition of compensating equipment and the integration of FPV and wind as shown in [figures 7.1C](#) and [7.1H](#) respectively. To put this into perspective, the nine voltage violations presented in [figure 7.1B](#) were eliminated while the active power losses reduced by 5 percent (i.e. from 147 MW to 140 MW). Further, based on the optimal power flow market model simulation results shown in [table 7.1I](#), the fourth unit commitment scenario involving the integration of onshore wind but excluding coal was found to be the most economical with 55 MW total losses and 28 percent reduction in operating cost while the sixth scenario (including coal, hydro, existing PV, FPV and onshore wind) was the least economical with total losses increasing by 4 percent (i.e. from 55 to 57 MW).

Floating PV design analysis:

This analysis is based on the results obtained from PVSYST and is presented in [section 7.3.1](#). Firstly, the PV array and module characteristics are analysed based on the results in [figure 7.3D](#). The PV module average running temperature with at least 60 hours of operation between January and December is between 10 and 65°C. With a design temperature operating range of between 10 and 70°C, and standard irradiation of 1 kW/m², the module efficiency was ranging between 15.8 to 11 percent respectively. However, the efficiency increase with decrease in temperature was observed at all irradiation levels. Moreover, at the same standard irradiation, the module power output at maximum power point was found to be 305.3 W (7% increase) and 229.1 W (20% decrease) at the lowest and highest operating temperature respectively.

Secondly, the energy yield and performance ratio of three different FPV configurations were compared with a ground-mounted PV system as shown in [section 7.3.1.3](#). Taking the ground

mounted system as reference, figure 7.3E shows an increase in the produced energy for the freestanding, small footprint and large footprint FPV configurations by 7.4%, 5.8% and 4.9% respectively. Figure 7.3F also shows an improvement in performance ratio by 7.7%, 6.2% and 5.3% in the same order. This was due to the different levels of cooling effect offered by the four system configurations as shown in table 7.3A.

Thirdly, detailed shading and loss analysis was done for the large footprint configuration to emulate the system at KGU owing to the system capacity. Figure 7.3H shows that the inter-row spacing design which led to an input pitch value of approximately 3m in PVSYST extended the solar window to 10hours (7am to 5pm) on March 20, February 21, January 19 and December 22 when compared to the worst case scenario consideration of 6 hours (9am to 5pm) on winter solstice. Figure 7.3K shows that the PV array and inverter losses reduce the array nominal energy by 12.4 percent (from 244.8 GWh to 214.4 GWh).

Fourthly, the economic evaluation of the large footprint FPV system excluding the operation and maintenance cost is illustrated in figure 7.3L. The analysis revealed that the cost of producing 214.4 GWh/year of energy at an investment cost of 68 pence/Wp was 4 pence/kWh.

Lastly, the large footprint FPV configuration was optimized for ground cover ratio (GCR), tilt angle, pitch and azimuth angle as shown in figures 7.3M, 7.3N, 7.3O and 7.3P respectively. The optimization revealed that the system was already at an optimized azimuth angle of 0°, while the GCR of 5%, tilt angle of 10° and pitch of 15m increased the energy yield by 2.6%, 0.3% and 2.5% respectively. Therefore, the optimal tilt angle for the location is between 10 and 20° while a pitch of 15m is not economical on space since it only contributes about 2.5% increase in energy yield for the 400% increase in pitch.

Onshore wind assessment:

The wind resource analysis is based on results obtained from renewables ninja and homerpro as presented in section 7.3.2. Figure 7.3Q shows the wind farm layout optimized to minimize wake effects. The capacity density for this configuration is approximately 6.2MW/km². Figure 7.3T shows a stable distribution of the wind resource at KGU between 2012 and 2017 with the highest average speed index between July and October, and between 12am and 11am as shown in the hourly monthly cross table. Figure 7.3U shows an optimistic daily mean power output and monthly capacity factor for each turbine, and consequently a wind farm peak power output of between 50 and 90 MW for the months (i.e. July – November) with the highest resource.

This translates into a net optimistic energy yield of approximately 294 GWh per year, excluding curtailment and wake effects. However, [figure 7.3W](#) shows a more conservative energy yield of 167 GWh per year at reduced hours of operation and capacity factor as simulated in homerpro based on the customized power curve and wind speed values imported from renewables ninja.

Timeseries dispatch:

The time series dispatch analysis of total generation at KGU (hydro + FPV + wind) and how it relates to total electrical grid load is based on results presented in [section 7.5.1](#) before system optimization. The demand for all the days under review seems to have an evening peak between 6pm and 11pm when compared to the morning or afternoon periods and relative to the three hydro generation scenarios (i.e. current water availability, low water availability and normal water availability). At the current water availability hydro dispatch with FPV and wind, only 30%, 35%, 28%, 34% and 30% of total demand was met on the first day of January, March, June, September and November, and is illustrated in [figures 7.5.1C, 7.5.1E, 7.5.1G, 7.5.1I and 7.5.1K](#) respectively. The percentage of met demand was seen to reduce under low water availability hydro dispatch with VRES as illustrated in [figures 7.5.1L, 7.5.1M, 7.5.1N, 7.5.1O and 7.5.1P](#). The results show that for the same sequence of months and day under consideration approximately 20%, 24%, 18%, 24% and 20% demand was met respectively. However, the results show an improvement in met demand during the normal water availability also referred to as a wet year, with a met demand percentage of 44, 50, 41, 46 and 42 as depicted in [figures 7.5.1Q, 7.5.1R, 7.5.1S, 7.5.1U and 7.5.1V](#) respectively.

Cost of FPV and Wind:

According to [figure 7.5.2A](#), the levelized cost of energy (LCOE) for producing 175 GWh/year of FPV energy at approximately 4 percent penetration and 4409hours/year hours of operation is 6.7 pence/kWh while the LCOE for producing 167 GWh/year of wind at ~3 percent penetration and 8174 hours/year hours of operation is 7 pence/kWh. When compared to the 2020 perceived costs of VRES in Zambia, illustrated in [tables 3Q and 3R](#), it is found that the cost of producing standalone FPV at KGU is approximately 30 percent higher while the cost of producing onshore wind is 34 percent higher. Further, when benchmarked with [IRENA](#) generation costs for 2020, FPV and wind at KGU are costlier by 20 and 40 percent respectively. This shows that the cost of producing an energy system as stand-alone is higher than when you

have a hybrid of three energy systems with time complementarity operation as will be seen in the system optimization section on cost analysis below.

System Optimization:

System optimization of the hybrid energy system is tackled in [section 7.5.3](#). With a homerpro model comprising of a customized virtual storage, customized hydro initially modelled in iHoga, PVSYST based FPV system, onshore wind based on renewables ninja wind speed data, the following analysis can be made: Of the six homerpro dispatch strategies used, three (i.e. load following, cycle charging and combined dispatch) were the least optimal/economical, with 48 percent excess electricity produced, without any renewable energy penetration and with a LCOE of the system of 7.7 pence/kWh.

The most economical dispatch was homer generator order (HGO) with a LCOE of 4.1 pence/kWh, net present cost reduction by 47%, 4% renewable fraction as illustrated in [tables 7.5.3A](#) and [7.5.3B](#). [Table 7.5.3C](#) and [figure 7.5.3H](#) shows the battery state of charge ranging between 60 to 100% from January to April, 50 to 30% from May to August and 10 to 20% from September to December with 333 GWh/year and 367 GWh/year of the total amount of energy charged and discharged to the storage respectively. This shows that the months with more peak demand (notably November as seen in [figure 7.2F](#)) used more of storage to serve the load. [Figure 7.6A](#) shows the HGO optimized time series dispatch of total generation with served load, battery input power, and battery state of charge on August 15.

The second most economical dispatch was homer predictive (HP) with a LCOE of 4.5 pence/kWh, 100% renewable fraction, 40% reduction in operating cost, 59.5% maximum renewable penetration, 5% excess generation excluding storage as illustrated in [figures 7.5.3I](#), [7.5.3J](#) and [tables 7.5.3A](#), [7.5.3B](#). The HP strategy had approximately 297 GWh/year and 271 GWh/year of total energy charged and discharged to the storage, with a throughput of 286 GWh/year which was 35 % lower than in the HGO strategy.

Homer Matlab link (HML) was the third economical dispatch based on the Matlab dispatch program in [Appendix C](#). No battery storage was utilized in the dispatch however, the algorithm/program utilized all the available floating PV and wind with five out of the six hydro generating units. Further, this strategy had 59.5% maximum renewable penetration, 100% renewable fraction, LCOE of 5.5 pence/kWh and served 28% more load than the other five

strategies (i.e. annual consumption of 4.93 TWh/year compared to 3.84 TWh/year as shown in [table 7.5.3B](#)).

Optimal Dispatch versus Baseline

The detailed time series dispatch graphical results comparing the three optimal strategies (HGO, HP and HML) to the baseline case which does not have any VRES integration is presented in [section 7.6](#). Firstly, the modelled grid load is not the total national electrical grid but only a fraction of the total since other generators of the grid are not part of the case study. Secondly, the orange line graph showing hydro generation in figure 7.6C for Homer Matlab link is lower than the load served due to the customized nature of the matlab code. Thirdly, homer generator order and homer predictive have a seemingly constant hydro of about 420 MW which serves the load together with the FPV and wind while the virtual storage power discharge is what serves the unmet load (to cater for the peak demand). The peak load for the day (August 15) is about 620 MW, the 420 MW hydro acts as generation to meet base load whose search space optimization started at 3 units which is equivalent to 420 MW (generation less than 3 hydro units was giving insufficient capacity in homerpro). The average annual generation of the modelled load is 396 MW as can be seen in figure 7.5.3E. Fourthly, the baseline case is a scenario which was dispatched with optimization search space of 6 hydro units utilizing the homer combined dispatch to meet 744 MW of annual peak demand. There is excess electricity because there is more load to be served on the actual grid and the algorithm in HOMERPRO gives insufficient generation capacity if less than 6 units are dispatched (5 units at 700 MW are not able to meet annual peak demand of 744 MW). Homer matlab link is able to meet the load without excess electricity production for the same custom hydro component followed by homer generator order which has about 0.03% excess electricity production. Homer predictive has about 5% excess generation from the actual production. However, this appears more due to presence of excess virtual storage as shown in [table 7.5.3B](#).

Therefore, this analysis makes the homer matlab link stand out in that it is able to serve 28% more load compared with the other 5 strategies with zero percent excess generation as shown in [table 7.5.3](#) and [figure 7.6C](#).

8.2 Research Outcomes

The following are the project research outcomes:

- ✓ A methodology was developed for the selection of all software tools used in the modelling and analysis of the power system, renewable energy resources and hybrid optimization.
- ✓ A site appraisal methodology was developed for the potential of linking existing and future hydro sites with floating PV and onshore wind. Thereafter, the methodology was applied to all the 13 existing hydro sites in Zambia of which 3 were filtered off and the remaining 10 ranked according to attribute suitability.
- ✓ A scoping design methodology was developed and later applied to Kafue Gorge Upper as the case study which yielded the following:
 - Improvement in voltage magnitude profile by the addition of compensating equipment, and further noticeable improvement by the integration of 100 MWac of FPV and 100 MWac of wind.
 - Reduction in active power losses by 5 percent due to integration of FPV and wind.
 - Reduction in optimal power flow based operating costs due to integration of wind by 28 percent.
 - The floating photovoltaic has a better energy yield compared to ground mounted system as evidenced by 7.4%, 5.8% and 4.9% increase in power production for the freestanding, small footprint and large footprint FPV configurations respectively.
 - The grid connected large footprint floating photovoltaic has an optimistic potential of injecting 214.4 GWh into the grid annually at a competitive LCOE of 4 pence/kWh (excluding operation and maintenance costs).
 - Excluding curtailment, wake and environmental losses, the wind farm has an optimistic potential of producing 294 GWh of energy per year.
 - Through the creation of the national electrical demand profile with five sensitivity inputs in homerpro, it was illustrated using homer predictive dispatch that the system could meet an all year-round demand of 3.84 TWh by prioritizing the deployment of FPV (175 WWh/year) and wind (166 GWh/year), with hydro generation of 3.2 TWh in the presence of 286 GWh/year of virtual storage at a competitive LCOE of 4.5 pence/kWh.
 - Using homer generator order, the system can meet an annual demand of 3.84 TWh with 44 GWh/year of FPV and 67 GWh/year of wind, in the presence of 3.7 TWh/year of hydro and 386 GWh/year of storage at a competitive LCOE of 4.1 pence/kWh.

- The customized Matlab dispatch was able to serve 4.93 TWh/year of consumption which translates into 28% more load served when compared to other strategies. This demand was met by 175 GWh/year of FPV, 166 GWh/year of wind in the presence of five out of six 140 MW hydro generator units operating at 10% reserve margin and at a competitive LCOE of 5.5 pence/kWh. The one unit not used in dispatch presents the virtual storage potential (~108 MW) by throttling down 17 percent of hydrogeneration.

8.3 Project Limitation

The following are prominent project limitations;

- Covid 19 imposed travel restrictions to physically visit the appraised sites and confirm certain parameters (i.e. topography, land development prospects) on the ground. As such, the data collection was heavily reliant on stakeholder engagement, literature review, referencing of reports (i.e. utility, ministerial, regulating bodies) and site mapping using google earth pro.
- Lack of project funding to conduct detailed prefeasibility analysis on the case study (i.e. bathymetry and topography study, soil study, environmental impact analysis and geotechnical analysis).
- Project duration not enough to facilitate detailed mechanical design of FPV system and wind turbine analysis using computation fluid dynamics.
- The optimal power flow-based market model used in the research is based on cost inputs from other projects and literature and thus does not give a true picture of the energy market in Zambia. Therefore, there is need to for stakeholder engagement to harmonize and eventually validate the model.

8.4 Further Work

There is potential for future work which includes:

- Opportunity to conduct similar grid assessment studies at the other remaining nine ranked sites and ascertain overall impact on network losses, voltage magnitude profile and operating cost by different scenarios of unit commitment. Additionally, there is potential to conduct detailed power network analysis to capture;
 - Transient stability performance.

- Effects of spinning reserve.
 - Voltage regulation during transient.
 - Long and short-term frequency response.
 - Short circuit analysis and protection coordination.
 - N-1 static security assessment.
 - Demand forecast model.
- Potential to extend study to all viable water bodies in the country not just limited to hydro sites.
 - Conducting prefeasibility studies (i.e. environmental impact assessment) not only at the case study but for all the other potential sites.

8.5 Conclusions

A comprehensive assessment of integrating floating photovoltaics and onshore wind near the existing and future hydro sites in Zambia has been presented in this study. All the project outcomes were achieved successfully, and these include creation of a site appraisal methodology to rank possible hydro sites for potential retrofitting of FPV and addition of wind, development of a methodology for scoping of case study design and its application. The results for the Kafue Gorge case study were promising with annual maximum potential VRES integration within grid limits of 508 GWh and 341 GWh, for the optimistic and conservative case respectively. Consequently, all the three research questions posed in [section 1.3](#) have been successfully answered in the affirmative.

REFERENCES

- ABB GROUP, Technical Application Papers No. 10. Photovoltaic plants. *Zurique*: ABB.
- A Dispatch and Investment Evaluation Tool with Endogenous Renewables , “DIETER”. [Online]. Available from (https://www.diw.de/de/diw_01.c.599753.de/modelle.html#ab_599749), [Accessed 29 June 2020].
- Ajgaonkar, Y., Bhirud, M. and Rao, P., 2019, January. Top-Down Approach in Design and Simulation of Grid Integrated Solar Rooftop PV System. In *2019 International Conference on Nascent Technologies in Engineering (ICNTE)* (pp. 1-5). IEEE.
- Al Garni, H.Z. and Awasthi, A., 2017. Solar PV power plant site selection using a GIS-AHP based approach with application in Saudi Arabia. *Applied energy*, *206*, pp.1225-1240.
- Ali, S., Taweekun, J., Techato, K., Waewsak, J. and Gyawali, S., 2019. GIS based site suitability assessment for wind and solar farms in Songkhla, Thailand. *Renewable Energy*, *132*, pp.1360-1372.
- Alsammak, A.N.B., 2011. *Optimal Power Flow Solution with Maximum Voltage Stability*. *AL-Rafdain Engineering Journal (AREJ)*, *19*(6), pp.40-53.
- Anwarzai, M.A. and Nagasaka, K., 2017. Utility-scale implementable potential of wind and solar energies for Afghanistan using GIS multi-criteria decision analysis. *Renewable and Sustainable Energy Reviews*, *71*, pp.150-160.
- Asaduz-Zaman, M., Rahaman, M.H., Reza, M.S. and Islam, M.M., 2018. A Method for Distributed Generator Dispatch Strategy in Distribution Network. *Journal of Electrical Engineering*, *6*, pp.261-270.
- Baban, S.M. and Parry, T., 2001. Developing and applying a GIS-assisted approach to locating wind farms in the UK. *Renewable energy*, *24*(1), pp.59-71.
- Babatunde, A.A., Abbasoglu, S. and Senol, M., 2018. Analysis of the impact of dust, tilt angle and orientation on performance of PV Plants. *Renewable and Sustainable Energy Reviews*, *90*, pp.1017-1026.
- Bava, F. and Furbo, S., 2017. Development and validation of a detailed TRNSYS-Matlab model for large solar collector fields for district heating applications. *Energy*, *135*, pp.698-708.
- Bayón, L., Grau, J.M., Ruiz, M.M. and Suárez, P.M., 2016. A comparative economic study of two configurations of hydro-wind power plants. *Energy*, *112*, pp.8-16.
- Beluco, A., de Souza, P.K. and Krenzinger, A., 2012. A method to evaluate the effect of complementarity in time between hydro and solar energy on the performance of hybrid hydro PV generating plants. *Renewable Energy*, *45*, pp.24-30.
- Bica, D., Moldovan, C. and Muji, M., 2008, September. Power engineering education using NEPLAN software. In *2008 43rd International Universities Power Engineering Conference* (pp. 1-3). IEEE.
- Blair, N., Dobos, A.P., Freeman, J., Neises, T., Wagner, M., Ferguson, T., Gilman, P. and Janzou, S., 2014. *System advisor model, sam 2014.1. 14: General description* (No. NREL/TP-6A20-61019). National Renewable Energy Lab.(NREL), Golden, CO (United States).

- Blair, N.J., Dobos, A.P. and Gilman, P., 2013. *Comparison of photovoltaic models in the system advisor model* (No. NREL/CP-6A20-58057). National Renewable Energy Lab.(NREL), Golden, CO (United States).
- Bollen, M.H. and Hassan, F., 2011. *Integration of distributed generation in the power system* (Vol. 80). John Wiley & Sons.
- Bousseau, P., Belhomme, R., Monnot, E., Laverdure, N., Boëda, D., Roye, D. and Bacha, S., 2006. Contribution of wind farms to ancillary services. *Cigre, 21*, pp.1-11.
- Boveri, A.A.B., 2016. Technical Application Papers No. 10: Photovoltaic Plants. 2014.
- Brown, T., Hörsch, J. and Schlachtberger, D., 2017. PyPSA: Python for power system analysis. *arXiv preprint arXiv:1707.09913*.
- Campana, P.E., Li, H. and Yan, J., 2013. Dynamic modelling of a PV pumping system with special consideration on water demand. *Applied energy, 112*, pp.635-645.
- Carrara, S. and Marangoni, G., 2017. Including system integration of variable renewable energies in a constant elasticity of substitution framework: the case of the WITCH model. *Energy Economics, 64*, pp.612-626.
- Cazzaniga, R., Cicu, M., Rosa-Clot, M., Rosa-Clot, P., Tina, G.M. and Ventura, C., 2018. Floating photovoltaic plants: Performance analysis and design solutions. *Renewable and Sustainable Energy Reviews, 81*, pp.1730-1741.
- CED GREENTECH, “Determining Module Inter-Row Spacing”, [Online] Available: <https://www.civicsolar.com/article/determining-module-inter-row-spacing> [Accessed 30 July 2020].
- Conceição, R., Silva, H.G., Fialho, L., Lopes, F.M. and Collares-Pereira, M., 2019. PV system design with the effect of soiling on the optimum tilt angle. *Renewable energy, 133*, pp.787-796.
- Chauhan, S.S. and Khamparia, P., A Survey of Software Packages in Power System Analysis.
- Chen, J.J., Zhuang, Y.B., Li, Y.Z., Wang, P., Zhao, Y.L. and Zhang, C.S., 2017. Risk-aware short term hydro-wind-thermal scheduling using a probability interval optimization model. *Applied energy, 189*, pp.534-554.
- Chen, L. and Liu, Y., 2012. Scheduling strategy of hybrid wind-photovoltaic-hydro power generation system.
- Chen, Y., Wei, W., Liu, F. and Mei, S., 2016. Distributionally robust hydro-thermal-wind economic dispatch. *Applied Energy, 173*, pp.511-519.
- Chimres, N. and Wongwises, S., 2016. Critical review of the current status of solar energy in Thailand. *Renewable and Sustainable Energy Reviews, 58*, pp.198-207.
- Choi, Y.K., Choi, W.S. and Lee, J.H., 2016. Empirical Research on the Efficiency of Floating PV Systems. *Science of Advanced Materials, 8*(3), pp.681-685.
- Cornaro, C., Renzi, L., Pierro, M., Di Carlo, A. and Guglielmotti, A., 2018. Thermal and electrical characterization of a semi-transparent dye-sensitized photovoltaic module under real operating conditions. *Energies, 11*(1), p.155.

- Cornuejols, G. and Tütüncü, R., 2006. *Optimization methods in finance* (Vol. 5). Cambridge University Press.
- Correia, N., Gomes, C., Pinto, R., Luis, P.I.N.A., Moita, N. and Da Silva, J.T., Solarisfloat Lda, 2019. *Floating module for modular solar panel platforms*. U.S. Patent 10,480,828.
- CSO, (2019), “Central Statistical Office”, Republic of Zambia
- Dahlioui, D., Laarabi, B. and Barhdadi, A., 2019. Investigation of soiling impact on PV modules performance in semi-arid and hyper-arid climates in Morocco. *Energy for Sustainable Development*, 51, pp.32-39.
- DeCarolis, J., Hunter, K. and Sreepathi, S., 2010. The TEMOA project: tools for energy model optimization and analysis. *Stockholm, Sweden*.
- Deshmukh, M.K. and Deshmukh, S.S., 2008. Modeling of hybrid renewable energy systems. *Renewable and sustainable energy reviews*, 12(1), pp.235-249.
- DIGSILENT GmbH, “PowerFactory”. [online]. Available from <https://www.digsilent.de/en/> [Accessed 26 June 2020].
- Ding, M., Xu, Z., Wang, W., Wang, X., Song, Y. and Chen, D., 2016. A review on China's large-scale PV integration: Progress, challenges and recommendations. *Renewable and Sustainable Energy Reviews*, 53, pp.639-652.
- Dong, W., Wang, Q. and Yang, L., 2015. A coordinated dispatching model for a distribution utility and virtual power plants with wind/photovoltaic/hydro generators. *Autom. Electr. Power Syst*, 39, pp.75-81.
- Dorfner, J., Dorfner, M., Candas, S., Müller, S., Ozsahin, Y., Zipperle, T. and Herzog, S., Icedkk, and WYAUDI, “urbs: v0. 6,” Aug. 2016. DOI: <https://doi.org/10.5281/zenodo.60484>.
- Dufo-Lopez R. iHOGA – user manual version 2.5. 2020. [Online]. Available from <https://www.dropbox.com/s/kvrphljzvdbg622/iHOGA%202.5%20User%20manual.pdf?dl=0> [Accessed 30 June 2020].
- Đurović, M.Ž., Milačić, A. and Kršulja, M., 2012, January. A simplified model of quadratic cost function for thermal generators. In *23rd International DAAAM Symposium Intelligent Manufacturing & Automation: Focus on Sustainability*.
- Durvasulu, V. and Hansen, T.M., 2018. Market-based generator cost functions for power system test cases. *IET Cyber-Physical Systems: Theory & Applications*, 3(4), pp.194-205.
- Dvoracek, M.J. and Hannabas, B., 1990. Prediction of albedo for use in evapotranspiration and irrigation scheduling.
- Emmerling, J., Drouet, L., Reis, L., Bevione, M., Berger, L., Bosetti, V., Carrara, S., De Cian, E., De Maere D'Aertrycke, G., Longden, T. and Malpede, M., 2016. The WITCH 2016 model- documentation and implementation of the shared socioeconomic pathways.
- Energy - Economy - Environment Modelling Laboratory Research and Policy Analysis, “the PRIMES model”. [online]. Available from http://www.e3mlab.eu/e3mlab/index.php?searchword=The+primes+model&ordering=&searchphrase=all&Itemid=1&option=com_search&lang=en [Accessed 26 June 2020].

Energy Exemplar, “PLEXOS”. [online]. Available from <https://energyexemplar.com/solutions/plexos/> [Accessed 26 June 2020].

Enel Foundation, 2020. <https://www.enelfoundation.org/news/a/2019/02/new-research-on-grid-integration-of-renewables-starting-in-zambi>

Engin, M., 2013. Sizing and simulation of PV-wind hybrid power system. *International Journal of Photoenergy*, 2013.

ERB, 2018. Energy Regulation Board. Energy Sector Report. [Online]. Available from <http://www.erb.org.zm/reports/esr2018.pdf> . [Accessed on 10 July 2020]

ESA, 2020, “Energy Storage Association”. [Online]. Available from <https://energystorage.org/> . [Accessed 25 July 2020]

ESMAP (World Bank), “Solar Resource and PV Potential of Zambia Solar Resource Atlas”, April 2019.

ESMAP (World Bank), “Wind Resource Mapping in Zambia - Mesoscale Wind Modelling Report”, July 2015.

ESMAP (World Bank), “Wind Resource Mapping in Zambia - 12 Month Site Resource Report”, May 2018.

Fadaeenejad, M., Radzi, M.A.M., AbKadir, M.Z.A. and Hizam, H., 2014. Assessment of hybrid renewable power sources for rural electrification in Malaysia. *Renewable and Sustainable Energy Reviews*, 30, pp.299-305.

Fang, W., Huang, Q., Huang, S., Yang, J., Meng, E. and Li, Y., 2017. Optimal sizing of utility-scale photovoltaic power generation complementarily operating with hydropower: A case study of the world’s largest hydro-photovoltaic plant. *Energy Conversion and Management*, 136, pp.161-172.

Farfan, J. and Breyer, C., 2018. Combining floating solar photovoltaic power plants and hydropower reservoirs: a virtual battery of great global potential. *Energy Procedia*, 155, pp.403-411.

Fazlollahi, S., Becker, G., Ashouri, A. and Maréchal, F., 2015. Multi-objective, multi-period optimization of district energy systems: IV–A case study. *Energy*, 84, pp.365-381.

Fnaiech, N., Jendoubi, A., Taha Hussein, B.P. and Bacha, F., 2015. Voltage Stability Analysis In Power System Using Continuation Method and PSAT Software. *power*, 3, p.8.

Feng, Y., Lin, H., Ho, S.L., Yan, J., Dong, J., Fang, S. and Huang, Y., 2015. Overview of wind power generation in China: Status and development. *Renewable and Sustainable Energy Reviews*, 50, pp.847-858.

Ferrer-Gisbert, C., Ferrán-Gozálvez, J.J., Redón-Santafé, M., Ferrer-Gisbert, P., Sánchez-Romero, F.J. and Torregrosa-Soler, J.B., 2013. A new photovoltaic floating cover system for water reservoirs. *Renewable energy*, 60, pp.63-70.

Francesco Begnis, Luciano Masotti, Giulia Molino, Andrea Prudenzi, Andrea Venturini, 2020. “Integration of Variable Renewable Energy Sources in the National Electric System of Zambia”.

Francois, B., Borga, M., Creutin, J.D., Hingray, B., Raynaud, D. and Sauterleute, J.F., 2016. Complementarity between solar and hydro power: Sensitivity study to climate characteristics in Northern-Italy. *Renewable energy*, 86, pp.543-553.

Gevorgian, V. and O'Neill, B., 2016. *Advanced grid-friendly controls demonstration project for utility-scale PV power plants* (No. NREL/TP-5D00-65368). National Renewable Energy Lab.(NREL), Golden, CO (United States).

Gils, H.C., Scholz, Y., Pregger, T., de Tena, D.L. and Heide, D., 2017. Integrated modelling of variable renewable energy-based power supply in Europe. *Energy*, 123, pp.173-188.

Gigović, L., Pamučar, D., Božanić, D. and Ljubojević, S., 2017. Application of the GIS-DANP-MABAC multi-criteria model for selecting the location of wind farms: A case study of Vojvodina, Serbia. *Renewable Energy*, 103, pp.501-521.

Glasnovic, Z. and Margeta, J., 2009. Optimal sizing of photovoltaic-hydro power plant. *Progress in Photovoltaics: Research and Applications*, 17(8), pp.542-553.

Gonzalez-Longatt, F.M. and Rueda, J.L. eds., 2014. *PowerFactory applications for power system analysis*. Springer.

Greenhall, A., Christie, R. and Watson, J.P., 2012, July. Minpower: A power systems optimization toolkit. In *2012 IEEE Power and Energy Society General Meeting* (pp. 1-6). IEEE.

Grilli, G., Balest, J., De Meo, I., Garegnani, G. and Paletto, A., 2016. Experts' opinions on the effects of renewable energy development on ecosystem services in the Alpine region. *Journal of Renewable and Sustainable Energy*, 8(1), p.013115.

GSA, 2020, "Global Solar Atlas 2.0, a free, web-based application is developed and operated by the company Solargis s.r.o. on behalf of the World Bank Group, utilizing Solargis data, with funding provided by the Energy Sector Management Assistance Program (ESMAP). For additional information: <https://globalsolaratlas.info>". [Accessed 30 June 2020].

GSA World Bank, "QGIS Project Zambia" <https://globalsolaratlas.info/download/zambia>

GWA, 2020, "Global Wind Atlas 3.0, a free, web-based application developed, owned and operated by the Technical University of Denmark (DTU). The Global Wind Atlas 3.0 is released in partnership with the World Bank Group, utilizing data provided by Vortex, using funding provided by the Energy Sector Management Assistance Program (ESMAP). For additional information: <https://globalwindatlas.info>". [Accessed 30 June 2020].

Harper, M., Anderson, B., James, P. and Bahaj, A., 2017. Identifying suitable locations for onshore wind turbines using a GIS-MCDA approach.

Hilpert, S., Günther, S., Kaldemeyer, C., Krien, U., Plessmann, G., Wiese, F. and Wingebach, C., 2017. Addressing energy system modelling challenges: The contribution of the Open Energy Modelling Framework (oemof).

Ho, C.K., Sims, C.A. and Christian, J.M., 2015. Evaluation of glare at the Ivanpah solar electric generating system. *Energy Procedia*, 69, pp.1296-1305.

HOMER – Hybrid Renewable and Distributed Generation System; 2020. [Online] Available from <https://www.homerenergy.com/>. [Accessed 29 June 2020].

Höfer, T., Sunak, Y., Siddique, H. and Madlener, R., 2016. Wind farm siting using a spatial Analytic Hierarchy Process approach: A case study of the Städteregion Aachen. *Applied energy*, 163, pp.222-243.

Hörsch, J., Ronellenfitsch, H., Witthaut, D. and Brown, T., 2018. Linear optimal power flow using cycle flows. *Electric Power Systems Research*, 158, pp.126-135.

Howells, M., Rogner, H., Strachan, N., Heaps, C., Huntington, H., Kypreos, S., Hughes, A., Silveira, S., DeCarolis, J., Bazillian, M. and Roehrl, A., 2011. OSeMOSYS: the open source energy modeling system: an introduction to its ethos, structure and development. *Energy Policy*, 39(10), pp.5850-5870.

Huang, Z., Yu, H., Peng, Z. and Zhao, M., 2015. Methods and tools for community energy planning: A review. *Renewable and sustainable energy reviews*, 42, pp.1335-1348.

Hughes, F.M., Anaya-Lara, O., Ramtharan, G., Jenkins, N. and Strbac, G., 2008. Influence of tower shadow and wind turbulence on the performance of power system stabilizers for DFIG-based wind farms. *IEEE Transactions on Energy Conversion*, 23(2), pp.519-528.

Hunter, K., Sreepathi, S. and DeCarolis, J.F., 2013. Modeling for insight using tools for energy model optimization and analysis (Temoa). *Energy Economics*, 40, pp.339-349.

International Renewable Energy Agency (IRENA), "Renewables Readiness Assessment (RRA): Zambia", 2013.

IRENA (2019), "Renewable Power Generation Costs in 2018", International Renewable Energy Agency, Abu Dhabi.

Irigoyen Tineo, A., 2017. *Energy management system benchmarking for a remote microgrid* (Bachelor's thesis).

Jangid, J., Bera, A.K., Joseph, M., Singh, V., Singh, T.P., Pradhan, B.K. and Das, S., 2016. Potential zones identification for harvesting wind energy resources in desert region of India—A multi criteria evaluation approach using remote sensing and GIS. *Renewable and Sustainable Energy Reviews*, 65, pp.1-10.

Janke, J.R., 2010. Multicriteria GIS modeling of wind and solar farms in Colorado. *Renewable Energy*, 35(10), pp.2228-2234.

Jiang, L., Chi, Y., Qin, H., Pei, Z., Li, Q., Liu, M., Bai, J., Wang, W., Feng, S., Kong, W. and Wang, Q., 2011. Wind energy in China. *IEEE Power and Energy Magazine*, 9(6), pp.36-46.

Jin, X., Rong, Y. and Zhong, X., 2014. Wind turbine manufacturing industry in China: Current situation and problems. *Renewable and Sustainable Energy Reviews*, 33, pp.729-735.

Jurasz, J. and Ciapała, B., 2017. Integrating photovoltaics into energy systems by using a run-off-river power plant with pondage to smooth energy exchange with the power grid. *Applied energy*, 198, pp.21-35.

Katiraei, F. and Agüero, J.R., 2011. Solar PV integration challenges. *IEEE Power and Energy Magazine*, 9(3), pp.62-71.

Khan, B. and Singh, P., 2017. Optimal power flow techniques under characterization of conventional and renewable energy sources: A comprehensive analysis. *Journal of Engineering*, 2017.

Kost, C., Mayer, J.N., Thomsen, J., Hartmann, N., Senkpiel, C., Philipps, S., Nold, S., Lude, S., Saad, N. and Schlegl, T., 2013. Levelized cost of electricity renewable energy technologies. Fraunhofer Institute for Solar Energy Systems ISE, 144.

Kougias, I., Szabo, S., Monforti-Ferrario, F., Huld, T. and Bodis, K., 2016. A methodology for optimization of the complementarity between small-hydropower plants and solar PV systems. *Renewable Energy*, 87, pp.1023-1030.

Krewitt, W. and Nitsch, J., 2003. The potential for electricity generation from on-shore wind energy under the constraints of nature conservation: a case study for two regions in Germany. *Renewable energy*, 28(10), pp.1645-1655.

Lambert, T., Gilman, P. and Lilienthal, P., 2006. Micropower system modeling with HOMER. *Integration of alternative sources of energy*, 1(1), pp.379-385.

Lappalainen, K. and Valkealahti, S., 2017. Photovoltaic mismatch losses caused by moving clouds. *Solar Energy*, 158, pp.455-461.

Latinopoulos, D. and Kechagia, K., 2015. A GIS-based multi-criteria evaluation for wind farm site selection. A regional scale application in Greece. *Renewable Energy*, 78, pp.550-560.

Lazard. 2018. "Lazard's levelized cost of energy analysis—version 12.0", November 2018.

Liu, C., Xu, D., Zhu, N., Blaabjerg, F. and Chen, M., 2012. DC-voltage fluctuation elimination through a DC-capacitor current control for DFIG converters under unbalanced grid voltage conditions. *IEEE Transactions on Power Electronics*, 28(7), pp.3206-3218.

Lee, K.H., Lee, D.W., Baek, N.C., Kwon, H.M. and Lee, C.J., 2012. Preliminary determination of optimal size for renewable energy resources in buildings using RETScreen. *Energy*, 47(1), pp.83-96.

Liu, H., Daoxin, P. and Xin, H., 2016. Joint scheduling optimization model of multi-type generator with uncertainty. *Water Resources and Power*, 34(02), pp.153-158.

Liu, H., Krishna, V., Lun Leung, J., Reindl, T. and Zhao, L., 2018. Field experience and performance analysis of floating PV technologies in the tropics. *Progress in Photovoltaics: Research and Applications*, 26(12), pp.957-967.

Liu, Y., Tan, S. and Jiang, C., 2016. Interval optimal scheduling of hydro-PV-wind hybrid system considering firm generation coordination. *IET Renewable Power Generation*, 11(1), pp.63-72.

Lumby, B., 2015. *Utility-scale solar photovoltaic power plants: a project developer's guide* (No. 99396, pp. 1-216). The World Bank.

Lyden, A., Pepper, R. and Tuohy, P.G., 2018. A modelling tool selection process for planning of community scale energy systems including storage and demand side management. *Sustainable cities and society*, 39, pp.674-688.

Malczewski, J., 2004. GIS-based land-use suitability analysis: a critical overview. *Progress in planning*, 62(1), pp.3-65.

McLarty, D., Panossian, N., Jabbari, F. and Traverso, A., 2019. Dynamic economic dispatch using complementary quadratic programming. *Energy*, 166, pp.755-764.

- Mesbahi, M., & Minamino, S. (2018, January 3). Top 70 Floating Solar PV Plants. Retrieved June 20, 2020, from <https://www.solarplaza.com/channels/top-10s/11761/top-70-floating-solar-pv-plants/>
- Ming, B., Liu, P., Cheng, L., Zhou, Y. and Wang, X., 2018. Optimal daily generation scheduling of large hydro–photovoltaic hybrid power plants. *Energy Conversion and Management*, 171, pp.528-540.
- Mokoka, O.K. and Awodele, K.O., 2013, September. Reliability Evaluation of distribution networks using NEPLAN & DIgSILENT power factory. In *2013 Africon* (pp. 1-5). IEEE.
- Molina, F., Pérez, S. and Rivera, S., 2017. Uncertainty Cost Function Formulation in Small Hydropower Plants Inside a Microgrid. *Ingenierías USBMed*, 8(1), p.126.
- Moraitis, P., Kausika, B.B., Nortier, N. and Van Sark, W., 2018. Urban environment and solar PV performance: the case of the Netherlands. *Energies*, 11(6), p.1333.
- Murillo-Sánchez, C.E., Zimmerman, R.D., Anderson, C.L. and Thomas, R.J., 2013. Secure planning and operations of systems with stochastic sources, energy storage, and active demand. *IEEE Transactions on Smart Grid*, 4(4), pp.2220-2229.
- Natural Resources Canada, 2020, “RETSscreen”. [Online]. Available from <https://www.nrcan.gc.ca/maps-tools-publications/tools/data-analysis-software-modelling/retscreen/7465> [Accessed 30 June 2020]
- Nejdawi, I.M., Clements, K.A., Kimball, L.M. and Davis, P.W., 2000. Nonlinear optimal power flow with intertemporal constraints. *IEEE Power Engineering Review*, 20(5), pp.74-75.
- Nelson, J., Johnston, J., Mileva, A., Fripp, M., Hoffman, I., Petros-Good, A., Blanco, C. and Kammen, D.M., 2012. High-resolution modeling of the western North American power system demonstrates low-cost and low-carbon futures. *Energy Policy*, 43, pp.436-447.
- NEPLAN AG, “PowerFactory”. [online]. Available from <https://www.neplan.ch/> [Accessed 26 June 2020].
- Nguyen, D.A.T., 2017. *The global evolution of floating solar PV*. Working paper, IFC.
- NREL. 2017. “U.S. Solar Photovoltaic System Cost Benchmark: Q1 2017”, September 2017. Authors: Ran Fu, David Feldman, Robert Margolis, Mike Woodhouse, and Kristen Ardani.
- Olivares, D., Ferrada, P., de Matos, C., Marzo, A., Cabrera, E., Portillo, C. and Llanos, J., 2017. Characterization of soiling on PV modules in the Atacama Desert. *Energy Procedia*, 124, pp.547-553.
- Oliveira-Pinto, S. and Stokkermans, J., 2020. Assessment of the potential of different floating solar technologies—Overview and analysis of different case studies. *Energy Conversion and Management*, 211, p.112747.
- Orlando, N.A., Liserre, M., Monopoli, V.G., Mastromauro, R.A. and Dell'Aquila, A., 2008, June. Comparison of power converter topologies for permanent magnet small wind turbine system. In *2008 IEEE International Symposium on Industrial Electronics* (pp. 2359-2364). IEEE.
- Paska, J., Biczal, P. and Kłos, M., 2009. Hybrid power systems—An effective way of utilising primary energy sources. *Renewable energy*, 34(11), pp.2414-2421.

Pfenninger, S., 2017. Dealing with multiple decades of hourly wind and PV time series in energy models: A comparison of methods to reduce time resolution and the planning implications of inter-annual variability. *Applied energy*, 197, pp.1-13.

Pfenninger, S. and Staffell, I., 2016. Renewables. ninja. URL <https://www.renewables.ninja>. [Accessed 30 June 2020].

Photovoltaic System, “PVSYST”. [Online]. Available: <https://www.pvsyst.com/> [Accessed:20 July 2020]

Portero, U., Velázquez, S. and Carta, J.A., 2015. Sizing of a wind-hydro system using a reversible hydraulic facility with seawater. A case study in the Canary Islands. *Energy Conversion and Management*, 106, pp.1251-1263.

PowerWorld Corporation, “PowerWorld”. [online]. Available from <https://www.powerworld.com/> [Accessed 26 June 2020].

Princy, U., Sreedharan, S. and Jaseena, S., Optimum Power Flow Analysis For Integration Of Renewable Energy Sources Into Kerala Grid.

PSS@SINCAL. [online] Available from <https://new.siemens.com/global/en/products/energy/services/transmission-distribution-smart-grid/consulting-and-planning/pss-software/pss-sincal.html> [Accessed 26 June 2020].

Reddy, S.S. and Bijwe, P.R., 2015. Real time economic dispatch considering renewable energy resources. *Renewable Energy*, 83, pp.1215-1226.

Reddy, S.S., 2017. Optimal scheduling of wind-thermal power system using clustered adaptive teaching learning based optimization. *Electrical Engineering*, 99(2), pp.535-550.

REFIT, “Zambia Renewable Feed-in Tariff Program”, 2016. [Online], Available from http://www.erb.org.zm/downloads/eregulation/refit/finalReports/FINAL_Zambia%20REFIT%20Rules.pdf . [Accessed 19 July 2020].

Reich, N.H., Mueller, B., Armbruster, A., Van Sark, W.G., Kiefer, K. and Reise, C., 2012. Performance ratio revisited: is PR > 90% realistic?. *Progress in Photovoltaics: Research and Applications*, 20(6), pp.717-726.

Republic of Zambia, Ministry Of Energy And Water Development “Power System Development Master Plan For Zambia, 2010-2030”, June 2011.

RETScreen, 2020. “Clean Energy Management Software System”. [Online], Available from: https://openei.org/wiki/RETScreen_Clean_Energy_Project_Analysis_Software [Accessed 20 July 2020].

Richard Lincoln (2017), Power System Engineering Research Center, “PYPOWER”. [online] Available from <https://github.com/rwl/PYPOWER> [Accessed 26 June 2020].

Richard Loulou (2016), Energy Technology Systems Analysis Programme, “Documentation for the TIMES Model”. [online]. Available from https://iea-etsap.org/docs/Documentation_for_the_TIMES_Model-Part-I_July-2016.pdf [Accessed 26 June 2020].

Ringkjøb, H.K., Haugan, P.M. and Solbrekke, I.M., 2018. A review of modelling tools for energy and electricity systems with large shares of variable renewables. *Renewable and Sustainable Energy Reviews*, 96, pp.440-459.

Rosa-Clot, M. and Tina, G.M., 2017. *Submerged and Floating Photovoltaic Systems: Modelling, Design and Case Studies*. Academic Press.

Rosa-Clot, M., Tina, G.M. and Nizetic, S., 2017. Floating photovoltaic plants and wastewater basins: an Australian project. *Energy Procedia*, 134, pp.664-674.

Sabley, M. and Adhau, S., 2014. RELIABILITY AND CONTROL STRATEGY FOR INTEGRATION OF SOLAR WIND HYBRID POWER SYSTEM FOR REMOTE LOCATIONS. *Journal of Sustainable Manufacturing and Renewable Energy*, 3(1/2), p.85.

Salameh, Z.M., 2011, July. Modeling and simulation of a wind turbine-generator system. In *2011 IEEE Power and Energy Society General Meeting* (pp. 1-7). IEEE.

SAM, (2020), "System Advisor Model". [Online], Available from: <https://sam.nrel.gov/> [Accessed 20 July 2020].

SAPP, "SAPP Pool Plan 2017 – Main volume", December 2017.

SAPP, "Annual Report 2017".

Sahu, A., Yadav, N. and Sudhakar, K., 2016. Floating photovoltaic power plant: A review. *Renewable and sustainable energy reviews*, 66, pp.815-824.

Schill, W.P., Zerrahn, A. and Kunz, F., 2017. Prosumage of solar electricity: pros, cons, and the system perspective.

Schoene, J., Zheglov, V., Houseman, D., Smith, J.C. and Ellis, A., 2013, July. Photovoltaics in distribution systems—Integration issues and simulation challenges. In *2013 IEEE Power & Energy Society General Meeting* (pp. 1-5). IEEE.

Scholz, Y., Gils, H.C. and Pietzcker, R.C., 2017. Application of a high-detail energy system model to derive power sector characteristics at high wind and solar shares. *Energy Economics*, 64, pp.568-582.

Sen, R. and Bhattacharyya, S.C., 2014. Off-grid electricity generation with renewable energy technologies in India: An application of HOMER. *Renewable Energy*, 62, pp.388-398.

Serrano-González, J. and Lacal-Aránzategui, R., 2016. Technological evolution of onshore wind turbines—a market-based analysis. *Wind Energy*, 19(12), pp.2171-2187.

Shabani, M. and Mahmoudimehr, J., 2018. Techno-economic role of PV tracking technology in a hybrid PV-hydroelectric standalone power system. *Applied energy*, 212, pp.84-108.

Shah, R., Mithulananthan, N., Bansal, R.C. and Ramachandramurthy, V.K., 2015. A review of key power system stability challenges for large-scale PV integration. *Renewable and Sustainable Energy Reviews*, 41, pp.1423-1436.

Siemens AG, "PSS/E". [online] Available from <https://new.siemens.com/global/en/products/energy/services/transmission-distribution-smart-grid/consulting-and-planning/pss-software/pss-e.html> [Accessed 26 June 2020]

Shah, R., Mithulananthan, N., Bansal, R.C. and Ramachandaramurthy, V.K., 2015. A review of key power system stability challenges for large-scale PV integration. *Renewable and Sustainable Energy Reviews*, 41, pp.1423-1436.

Shalwala, R.A., 2012. *PV integration into distribution networks in Saudi Arabia* (Doctoral dissertation, University of Leicester).

Skoplaki, E.P.J.A. and Palyvos, J.A., 2009. Operating temperature of photovoltaic modules: A survey of pertinent correlations. *Renewable energy*, 34(1), pp.23-29.

Sola, A., Corchero, C., Salom, J. and Sanmarti, M., 2018. Simulation tools to build urban-scale energy models: A review. *Energies*, 11(12), p.3269.

Solanki, S.K., Ramachandran, V. and Solanki, J., 2012, May. Steady state analysis of high penetration PV on utility distribution feeder. In *PES T&D 2012* (pp. 1-6). IEEE.

Spencer, R.S., Macknick, J., Aznar, A., Warren, A. and Reese, M.O., 2018. Floating photovoltaic systems: assessing the technical potential of photovoltaic systems on man-made water bodies in the continental United States. *Environmental science & technology*, 53(3), pp.1680-1689.

Stallman, R., 2002. *Free software, free society: Selected essays of Richard M. Stallman*. Lulu. com.

Sultan, M., Reeve, J. and Adapa, R., 1998. Combined transient and dynamic analysis of HVDC and FACTS systems. *IEEE Transactions on Power Delivery*, 13(4), pp.1271-1277.

Sunak, Y., Höfer, T., Siddique, H., Madlener, R. and De Doncker, R.W., 2015. *A GIS-based decision support system for the optimal siting of wind farm projects*. E. ON ERC.

Sun Path Chart Program, University of Oregon, Solar Radiation Monitoring Laboratory.

Svendsen, H.G. and Spro, O.C., 2016. PowerGAMA: A new simplified modelling approach for analyses of large interconnected power systems, applied to a 2030 Western Mediterranean case study. *Journal of Renewable and Sustainable Energy*, 8(5), p.055501.

Swarna, K.S.V., Vinayagam, A., yang Khoo, S. and Stojcevski, A., 2015, October. Impacts of Integration of Wind and Solar PV in a Typical Power Network. In *2015 International Conference on Sustainable Energy and Environmental Engineering*. Atlantis Press.

Switch Power System Planning Model, 2020, "SWITCH". [Online]. Available from <http://switch-model.org/> [Accessed 30 June 2020].

Tanavud, C., Yongchalerchai, C., Bennui, A. and Densreeserekul, O., 2004. Assessment of flood risk in Hat Yai municipality, Southern Thailand, using GIS. *Journal of Natural Disaster Science*, 26(1), pp.1-14.

The System Advisor Model, 2020. "SAM". [Online]. Available from <https://sam.nrel.gov/> [Accessed 30 June 2020].

Thi, N.D.A., 2017. *The Evolution of Floating Solar Photovoltaics*. Research Gate: Berlin, Germany.

Turner, L., Scheidler, A., Schäfer, F., Menke, J.H., Dollichon, J., Meier, F., Meinecke, S. and Braun, M., 2018. pandapower—an open-source python tool for convenient modeling, analysis, and optimization of electric power systems. *IEEE Transactions on Power Systems*, 33(6), pp.6510-6521.

Toma, R. and Gavrilas, M., 2014, October. The impact on voltage stability of the integration of renewable energy sources into the electricity grids. In *2014 International Conference and Exposition on Electrical and Power Engineering (EPE)* (pp. 1051-1054). IEEE.

Tools for Energy Model Optimization and Analysis, 2020. "TEMOA". [Online]. Available from <https://temoacloud.com/>. [Accessed 30 June 2020].

Trapani, K., 2014. *Flexible floating thin film photovoltaic (PV) array concept for marine and lacustrine environments* (Doctoral dissertation, Laurentian University of Sudbury).

Trapani, K. and Millar, D.L., 2013. Proposing offshore photovoltaic (PV) technology to the energy mix of the Maltese islands. *Energy Conversion and Management*, 67, pp.18-26.

Trapani, K. and Redón Santafé, M., 2015. A review of floating photovoltaic installations: 2007–2013. *Progress in Photovoltaics: Research and Applications*, 23(4), pp.524-532.

Tsanova, T. (2018, May 21). Floating solar installs to top 1.5 GW in 2019.

Umar, N., Bora, B., Banerjee, C. and Panwar, B.S., 2018. Comparison of different PV power simulation softwares: case study on performance analysis of 1 MW grid-connected PV solar power plant. *Int J Eng Sci Invent*, 7, pp.11-24.

USAID Southern Africa Energy Program, "Zambia Power Sector Assessment", 2018.

Uyan, M., 2013. GIS-based solar farms site selection using analytic hierarchy process (AHP) in Karapinar region, Konya/Turkey. *Renewable and Sustainable Energy Reviews*, 28, pp.11-17.

Vanfretti, L. and Milano, F., 2007, June. Application of the PSAT, an open source software, for educational and research purposes. In *2007 IEEE Power Engineering Society General Meeting* (pp. 1-7). IEEE.

Van Haaren, R. and Fthenakis, V., 2011. GIS-based wind farm site selection using spatial multi-criteria analysis (SMCA): Evaluating the case for New York State. *Renewable and sustainable energy reviews*, 15(7), pp.3332-3340.

Van Hulle, F., Holttinen, H., Kiviluoma, J., Faiella, M., Kreutzkamp, P., Cutululis, N., Reking, M., Gubina, A., Chapalain, F., Ernst, B. and Wachtel, S., 2014. Grid support services by wind and solar PV: a review of system needs, technology options, economic benefits and suitable market mechanisms: Synthesis report of the REserviceS project.

Van Rensburg, T.M., Kelley, H. and Jeserich, N., 2015. What influences the probability of wind farm planning approval: Evidence from Ireland. *Ecological Economics*, 111, pp.12-22.

Vittal, E., O'Malley, M. and Keane, A., 2011. Rotor angle stability with high penetrations of wind generation. *IEEE Transactions on Power Systems*, 27(1), pp.353-362.

Voivontas, D., Assimacopoulos, D., Mourelatos, A. and Corominas, J., 1998. Evaluation of renewable energy potential using a GIS decision support system. *Renewable energy*, 13(3), pp.333-344.

WANG Siming, NIU Yugang, FANG Lei, JIA Tinggang. Dual stage scheduling strategy for microgrid community considering uncertainty of renewable energy[J].*Power System Protection and Control*, 2018, V46(17):89-98

Walla, T., Widén, J., Johansson, J. and Bergerland, C., 2012. Determining and increasing the hosting capacity for photovoltaics in Swedish distribution grids. In *27th European Photovoltaic Energy Conference (EU-PVSEC), Frankfurt, Germany, September 24-28, 2012*.

Wang, X., Mei, Y., Kong, Y., Lin, Y. and Wang, H., 2017. Improved multi-objective model and analysis of the coordinated operation of a hydro-wind-photovoltaic system. *Energy*, 134, pp.813-839.

Watson, J.J. and Hudson, M.D., 2015. Regional Scale wind farm and solar farm suitability assessment using GIS-assisted multi-criteria evaluation. *Landscape and Urban Planning*, 138, pp.20-31.

Wei, G., Xiaomeng, A.I. and Jiakun, F.A.N.G., 2017. Coordinated optimal operation of the wind coal hydro gas units with energy storage [J]. *Transactions of China Electrotechnical Society*, 32(S1), pp.11-20.

Wei, P. and Liu, Y., 2019. The integration of wind-solar-hydropower generation in enabling economic robust dispatch. *Mathematical Problems in Engineering*, 2019.

Widén, J., Wäckelgård, E., Paatero, J. and Lund, P., 2010. Impacts of distributed photovoltaics on network voltages: Stochastic simulations of three Swedish low-voltage distribution grids. *Electric power systems research*, 80(12), pp.1562-1571.

Wiese, F., 2015. repass Renewable Energy Pathways Simulation System-Open Source as an approach to meet challenges in energy modeling.

Wiese, F., Bökenkamp, G., Wingenbach, C. and Hohmeyer, O., 2014. An open source energy system simulation model as an instrument for public participation in the development of strategies for a sustainable future. *Wiley Interdisciplinary Reviews: Energy and Environment*, 3(5), pp.490-504.

Willis, H.L., 2004. *Power distribution planning reference book*. CRC press.

World Bank, (2018), “Zambian Statistical Data”.

World Bank Group, ESMAP, and SERIS. (2019). *Where Sun Meets Water: Floating Solar Handbook for Practitioners*. Washington, DC: World Bank. Available from https://www.esmap.org/where_sun_meets_water_handbook [Accessed 19 July 2020]

World Induced Technical Change Hybrid model, 2020. “WITCH”. [Online]. Available from (<https://www.witchmodel.org/>), [Accessed 30 June 2020].

Wurster, T.S. and Schubert, M.B., 2014. Mismatch loss in photovoltaic systems. *Solar energy*, 105, pp.505-511.

Yadav, A.K. and Chandel, S.S., 2013. Tilt angle optimization to maximize incident solar radiation: A review. *Renewable and Sustainable Energy Reviews*, 23, pp.503-513.

Yang, X., Chen, Q., Wang, M. and Zhang, L., 2017. Cooperating control for wind farm and hydro power plant based on the fruit fly optimization. *Proceedings of the Chinese Society of Electrical Engineering*, 37(18), pp.5286-5293.

Yang, X., Wang, W., Xue, B. and Huang, Q., 2013. On short-term united optimal operation of wind power, thermal power and waterpower. *J. Hydroelectr. Eng*, 4, pp.199-203.

Yixin, L.I.U., Li, G.U.O. and Chengshan, W.A.N.G., 2018. Economic dispatch of microgrid based on two stage robust optimization. *Proceedings of the CSEE*, 38(14), pp.1-11.

Yue, C.D. and Wang, S.S., 2006. GIS-based evaluation of multifarious local renewable energy sources: a case study of the Chigu area of southwestern Taiwan. *Energy Policy*, 34(6), pp.730-742.

Zahurul Islam (June 2019), "Power System Analysis Software", Engineers Advice. [online]. Available from <https://www.engineersadvice.com/power-systems-analysis-software/> [Accessed 27 June 2020].

ZESCO, (2020), "Zambia Electricity Supply Corporation".

Zimmerman, R.D., Murillo-Sánchez, C.E. and Thomas, R.J., 2010. MATPOWER: Steady-state operations, planning, and analysis tools for power systems research and education. *IEEE Transactions on power systems*, 26(1), pp.12-19.

Zuo, C., Wang, B., Zhang, M., Khanwala, M.A. and Dang, S., 2015, August. Power flow analysis using PowerWorld: A comprehensive testing report. In *2015 International Conference on Fluid Power and Mechatronics (FPM)* (pp. 997-1002). IEEE.

Zou, Y. and Yang, L., 2015. Synergetic dispatch models of a wind/PV/hydro virtual power plant based on representative scenario set. *Power System Technology*, 39(7), pp.1855-1859.

APPENDICES

Appendix A – Site Appraisal Data Collection Tables Floating Photovoltaics Assessment

No.	WATER SITE	COORDINATES	TYPE	FLOW	MIN OP. LEVEL (m)	MAX OP. LEVEL (m)	ELEVATION (m)	RESERVOIR AREA (km ²)	POTENTIAL FPI (km ²)	PEAK POWER FPI (MWp)	OPTIMAL TILT ANGLE (deg.)	AZMUTH ANGLE (deg.)	CAPACITY FACTOR (%)	FPV (RNS) (GWh per annum)	FPV (GSAS) (GWh per annum)	FPV REVENUE @ 3p/kWh (£m)
1	Katie Gorge Upper	15°48'25.0"S 28°25'16.0"E	Reservoir	Calm	974	974	974	70	2.88	173	20 North facing (°)	17%	258	270	£8.09	
2	Kariza North Bank	16°3'20.0"S 28°45'42.0"E	Reservoir	Calm	475	488	475	4.354	0.5	30	20 North facing (°)	17%	45	46	£1.39	
3	Katie Gorge Lower	15°52'04.4"S 28°31'31.0"E	Reservoir	Calm	530	610	530	0.55	0.3	18	20 North facing (°)	17%	27	28	£0.83	
4	Itezhi Tezhi	15°45'55.0"S 26°01'05.0"E	Reservoir	Calm	1005	1031	1009	113	55.4	3324	20 North facing (°)	17%	5041	5323	£159.7	
5A	Lusiwasi Main Dam	12°59'18.2"S 30°51'53.6"E	Pondage				1596	35	12	720	18 North facing (°)	17%	1082	1106	£33.2	
5B	Lusiwasi Lower Head Pond	13°20'47.3"S 31°18'18"E	Pondage				769									
5C	Lusiwasi Diversion Weir	13°19'12.04"S 31°18'32"E	Weir				1292									
6A	Musonda Main Dam	10°41'51.09"S 28°53'46.47"E	Reservoir	Calm			1167	11.4	7.99	481	17 North facing (°)	17%	704	745	£22.4	
6B	Musonda Head Pond	10°42'36.55"S 28°48'26.64"E	Pondage	Calm			1134	0.00033	0.00023							
6C	Musonda Diversion Weir	10°42'54.48"S 28°48'50.11"E	Weir	Calm			1136	0.043	0.021							
7A	Chishimba Falls Dam	10°18'33.5"S 30°54'54.22"E	Reservoir	Calm			1332	0.051	0.030	2	16 North facing (°)	18%	4	3	£0.09	
7B	Chishimba Diversion Weir	10°18'30.03"S 30°54'59.07"E	Weir	Calm			1347	0.019	0.011							
8	Shiwangandi Diversion Weir	11°19'18.67"S 31°33'36.80"E	Weir	Calm			1413	0.38	0.26	16	17 North facing (°)	18%	24	25	£0.74	
9	Lunseriwa	14°23'34.79"S 28°18'57.68"E	Reservoir	Calm			1012	0.034	0.013	0.8	19 North facing (°)	17%	1	1	£0.04	
10A	Mlungushi Dam	14°41'51.14"S 28°49'15.67"E	Reservoir	Calm			1066	9.540	1.49	90	19 North facing (°)	17%	135	142	£4.26	
10B	Mlungushi Diversion Weir	14°43'47.65"S 28°50'39.04"E	Reservoir	Calm			1031	0.0060	0.0034							
11	Victoria Falls Station C-H	17°55'57.16"S 25°51'42.38"E	Pondage	Calm			874	0.00098	0.00065	Unviable	22 North facing (°)	N/A	N/A	N/A	N/A	N/A
12	Zengoma	11°17'30.82"S 24°11'47.11"E	Turbulent				1231	0.026	0.0009	Unviable	17 North facing (°)	N/A	N/A	N/A	N/A	N/A

RNS: Renewables Nirja Simulation. This does not have temperature compensation feature for floating photovoltaics.

GSAS Global Solar Atlas Simulation. This has temperature compensation feature for floating photovoltaics

Note1: MWp = the area of the floating island - 1.7 hectares of water area after taking into account anchoring. (Source: http://www.seriis.nus.edu.sg/doc/publications/ESMAP_FloatingSolar_Ge_A4%20WEB_REV2.pdf)

Note2: FPI PV electricity potential is calculated based on a set of assumptions and rules of thumb shown in the table. These assumptions are indicative, as they will differ in actual detailed design and real projects. This will be seen in cases study design.

Note3: The sites generally have still (calm) conditions in the diversion ponds and dams except probably on the intake gate

Note4: Lunzu has no reservoir or diversion weir for FPI potential and is omitted on the list.

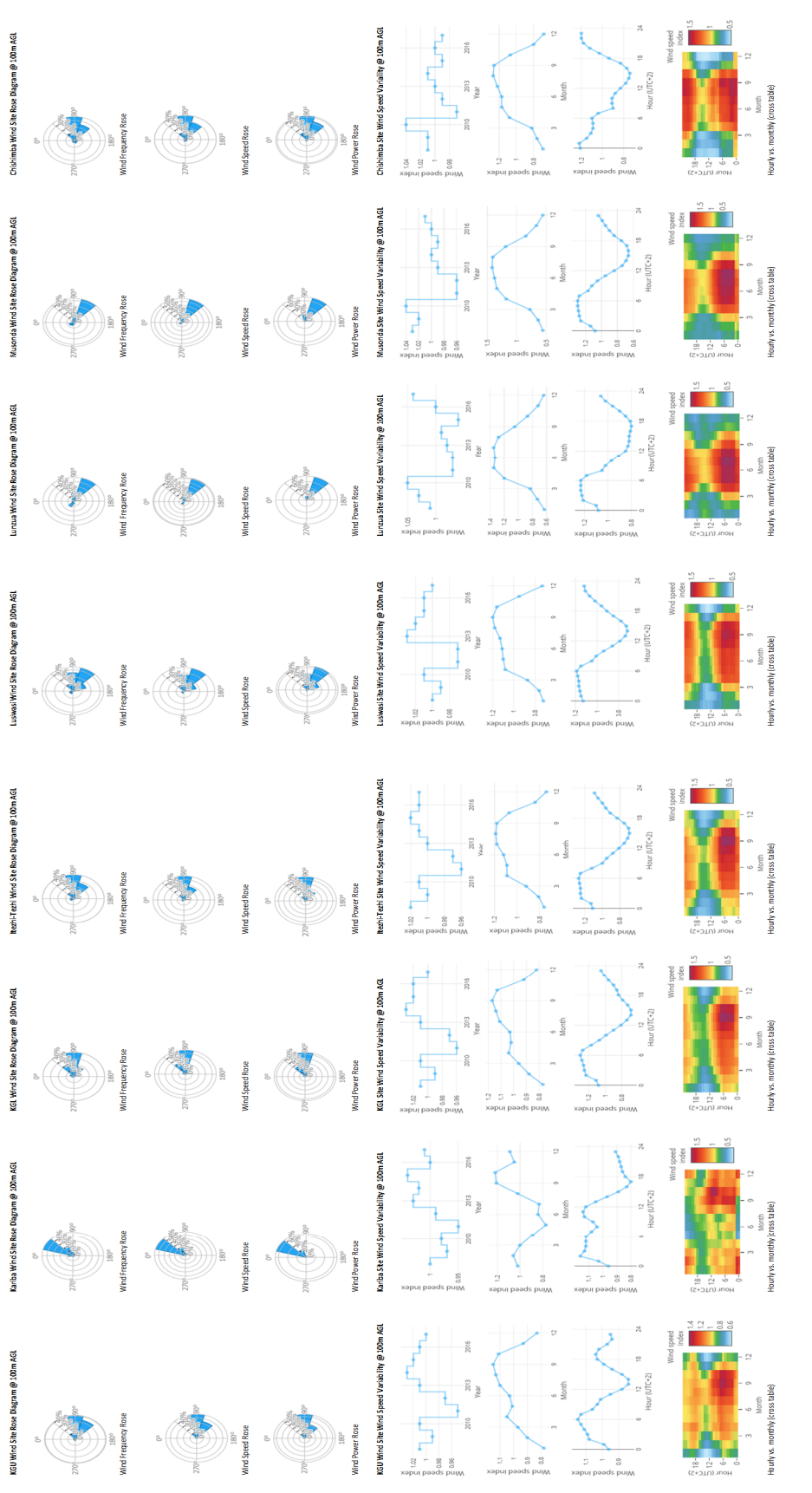
Note5: In PVsyst the azimuth orientation conventions are (contrary to Architect's conventions): In Renewables Nirja Compass direction the panel is facing (clockwise). An azimuth angle of 180 degrees means poleward facing, so for latitudes >= 0 is interpreted as southwards facing, else northwards facing.

Note6: Assumed selling price of 3p/kWh. The commercial tariff by ZESCO limited is 0.045euro/kWh which is approximately 1pence/kWh (euro = 0.9pound as of 28/05/2020)

Onshore Wind Assessment

No.	POWER STATION ASSOCIATED WITH WIND	SITE NAME	COORDINATES FOR WIND SITE	LAND OWNER	ROUGHNESS LENGTH (m)	ELEVATION (m)	SLOPE (%)	WIND SPEED (m/s) @ 100m AGL	WIND SPEED (m/s) @ 150m AGL	WIND SPEED (m/s) @ 200m AGL	WIND AREA (m ²)	TURBINE MODEL	TURBINE RATING (MW)	HUB HEIGHT (m)	ROTOR DIAMETER (m)	WIND OF TURBINES (%)	NO. OF TURBINES	SPECIFIC TURBINE POWER (MW/m ²)	CAPACITY DENSITY (MW/m ²)	PEAK POWER (MW)	GROSS WIND (GWh per annum)	ASSUMED EFFICIENCY (%)	NET WIND (GWh per annum)	WIND REVENUE (\$/kWh @ 10¢)
1	Kelau Cogeneration Power Station	Kelau wind site	-15.67084° 103.20034°	Customary land	0.1	1205	7.8	8.57	8.57	8.57	469	17.5SWF-DD-142	4	126	142	38.07%	25	253	5.97	100	347	85%	295	8.85
2	Kariba North Bank Power Station	Kariba wind site	-16.46657° 28.76984°	Customary land	1	861	10.7	6.31	6.31	6.31	284	17.5SWF-DD-142	4	126	142	31.30%	25	253	5.97	100	274	85%	231	7.00
3	Kelau Cogeneration Lower Power Station	Kelau wind site	-15.52775° 103.24257°	Customary land	1	1327	3.3	6.71	6.71	6.71	469	17.5SWF-DD-142	4	126	142	40.20%	25	253	5.97	100	352	85%	300	8.99
4	Ilupatah Cogeneration Power Station	Ilupatah wind site	-15.52775° 103.24257°	Customary land	1	152	4	6.54	6.54	6.54	284	17.5SWF-DD-142	4	126	142	39.20%	25	253	5.97	100	344	85%	293	8.65
5	Ilupatah Cogeneration Upper Power Station	Ilupatah wind site	-15.52775° 103.24257°	Customary land	1	152	2	6.54	6.54	6.54	284	17.5SWF-DD-142	4	126	142	39.20%	25	253	5.97	100	344	85%	293	8.65
6	Lusua Power Station	Lusua wind site	-15.20265° 103.20265°	Customary land	0.1	1852	4.9	7.43	7.43	7.43	525	17.5SWF-DD-142	4	126	142	37.70%	25	253	5.97	100	321	85%	270	7.93
7	Masera Power Station	Masera wind site	-15.85887° 34.44310°	Customary land	0.1	1852	4.9	7.43	7.43	7.43	525	17.5SWF-DD-142	4	126	142	37.70%	25	253	5.97	100	321	85%	270	7.93
8	Chibimba Power Station	Chibimba wind site	-10.75501° 28.76721°	Customary land	1	1190	3.9	6.27	6.27	6.27	304	17.5SWF-DD-142	4	126	142	38.03%	25	253	5.97	100	338	85%	288	8.63
9	Shawangulu Power Station	Shawangulu wind site	-10.30511° 30.75244°	Customary land	1	1420	2.3	6.57	6.57	6.57	219	17.5SWF-DD-142	4	126	142	34.70%	25	253	5.97	100	304	85%	259	7.76
10	Lusua Area Hydro Power Station	Lusua wind site	-11.95141° 31.82247°	Customary land	1	1510	10.9	8.01	8.01	8.01	702	17.5SWF-DD-142	4	126	142	37.40%	25	253	5.97	100	326	85%	279	8.36
11	Mulungushi Hydro Power Station	Mulungushi wind site	-11.04087° 28.26581°	Customary land	0.1	1038	1.8	6.74	6.74	6.74	469	17.5SWF-DD-142	4	126	142	40.20%	25	253	5.97	100	353	85%	300	9.01
12	Victoria Falls Power Station	Victoria wind site	-11.05381° 28.72581°	Customary land	0.2	1121	1.2	6.25	6.25	6.25	194	17.5SWF-DD-142	4	126	142	37.30%	25	253	5.97	100	330	85%	281	8.40
13	Zigzag Power Station	Zigzag wind site	-17.95187° 25.24721°	Customary land	0.1	961	1.8	5.9	5.9	5.9	284	17.5SWF-DD-142	4	126	142	36.70%	25	253	5.97	100	322	85%	279	8.20
14	Zigzag Power Station	Zigzag wind site	-17.20265° 24.14621°	Customary land	0.1	1258	4.2	7.5	7.5	7.5	469	17.5SWF-DD-142	4	126	142	38.10%	25	253	5.97	100	325	85%	271	8.50

Note: Lusua wind site is about 2km from Masera.
 Note: Suboptimal values for the WorldBank and IFC project for these wind farm efficiency for 8 validation sites for Zambian (Dromo 85%, Welipanga 85%, Lusua 88%, Chibimba 88%, Kariba 88%, Masera 88%, Mulungushi 88%, Victoria 88%, Zigzag 88%, Lusua 88%, Masera 88%, Mulungushi 88%, Victoria 88%, Zigzag 88%).
 Note: The choice of a suitable wind turbine is an economical decision and depends on the project specifics. Generally, turbines with high specific power make more sense in regions with high average wind speeds. To reach the same capacity factor, turbines with high specific power need higher wind speeds than turbines with low specific power.
 Note: Turbine spacing using the 7D rule spacing (turbine distance perpendicular to prevailing wind direction) of 5D, where D is the rotor diameter.



Other Attributes

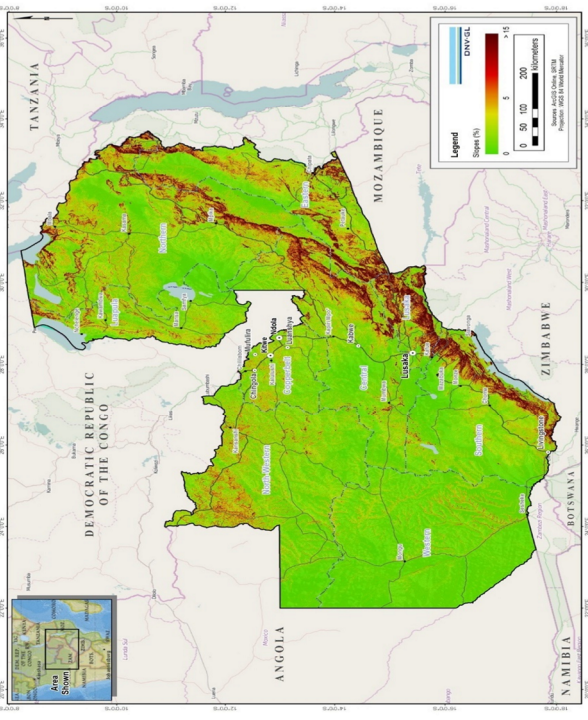
OTHER FPV SITE ATTRIBUTES

No.	WATER SITE	ACCESS ROAD NAME	DISTANCE (km)	PROTECTED ZONE
1	Kafue Gorge Upper	Power plant main access	2	No protected zone
2	Kariba North Bank	Power plant main access	2	No protected zone
3	Kafue Gorge Lower	Power plant main access	6	No protected zone
4	Itezhi-Tezhi	Power plant main access	2	No protected zone
5A	Lusiwasi Main Dam	Power plant main access	2	No protected zone
5B	Lusiwasi Lower Head Pond	Power plant main access	-	No protected zone
5C	Lusiwasi Diversion Weir	Power plant main access	-	No protected zone
6A	Musonda Main Dam	Power plant main access	10	No protected zone
6B	Musonda Head Pond	Power plant main access	-	No protected zone
6C	Musonda Diversion Weir	Power plant main access	-	No protected zone
7A	Chishimba Falls Dam	Power plant main access	2	No protected zone
7B	Chishimba Diversion Weir	Power plant main access	-	No protected zone
8	Shiwangandu Diversion Weir	Power plant main access	1	No protected zone
9	Lunsemfwa	Power plant main access	2	No protected zone
10A	Mulungushi Dam	Power plant main access	6	No protected zone
10B	Mulungushi Diversion Weir	Power plant main access	-	No protected zone
11	Victoria Falls Station C Head Pond	Power plant main access	2	No protected zone
12	Zengmina	Power plant main access	2	No protected zone

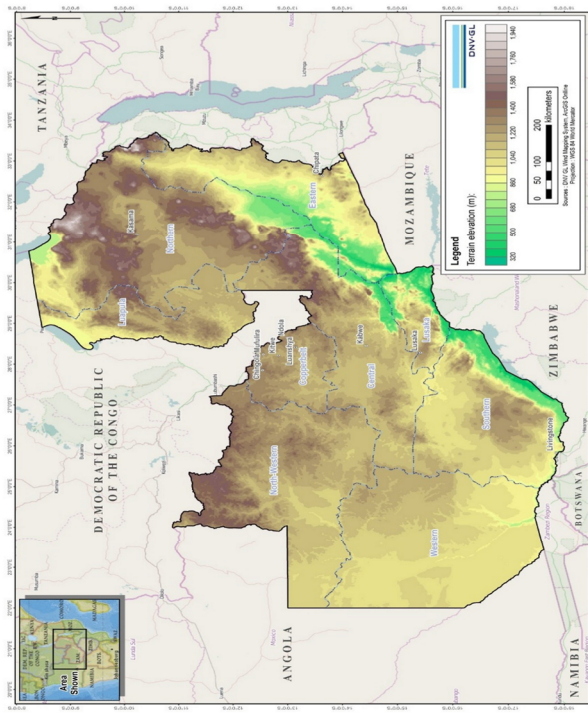
OTHER WIND SITE ATTRIBUTES

	SITE NAME	NAME OF ACCESS ROAD	DISTANCE (km)	PROTECTED ZONE
1	KGU wind site	Kafue road	14	No protected zone
2	Kariba wind site	M15	2.5	No protected zone
3	KGL wind site	Leopards hill	7.5	No protected zone
4	Itezhi-tezhi wind site	ITTZ road	1.35	No protected zone
5	Lusiwasi wind site	Road leading to Lusiwasi	3.5	No protected zone
6	Lunzua wind site	Mbala CBD	11	No protected zone
7	Musonda wind site	Mansa Nchelenge road	0.25	No protected zone
8	Chishimba wind site	Kasama Mporoko road	1	No protected zone
9	Shiwangandu wind site	Gravel road leading to D4	6	No protected zone
10	Lunsemfwa wind site	D200	3	No protected zone
11	Mulungushi wind site	D421	4.5	No protected zone
12	Victoria wind site	T1	3	No protected zone
13	Zengamina wind site	T5	5	No protected zone

Name of Site	Parallel to wind speed				Percentage Slope Values Relative to Wind Speed				Perpendicular to wind speed					
	Distance (km)		Path Average slope (%) @ km		Path Maximum slope (%)		Locality slope (%) @ km		Distance (km)		Path Average slope (%)		Path Maximum slope (%)	
KGU wind site	38.1	3% @ 17.8km	5.4	38.6	27.7	2.4% @ 15.5km	7.8	44						
Kariba wind site	18.5	7.3% @ 11.5km	10.7	41.4	31.9	9% @ 18.4km	7.4	52						
KGL wind site	19.4	0.2% @ 8.77km	1.9	23.8	20.7	1.3% @ 11.3km	3.3	23.6						
itezhi-tezhi wind site	110	1.2% @ 48.7km	1.4	11	85.5	1.1% @ 48km	1.4	15						
Lusiwasi wind site	15.9	1.9% @ 5.21km	2.1	11.5	14.6	1.4% @ 6km	1.3	5						
Lunzua wind site	68.6	0.8% @ 30.5km	4.9	37.1	75.5	1% @ 44.7km	2.6	7						
Musonda wind site	19.2	0.5% @ 8.94km	2.9	19.4	22.4	1.9% @ 13.2	3.9	24.1						
Chishimba wind site	50.9	0.1% @ 22.8	2.3	12.2	77.9	1.2% @ 52	1.9	21.2						
Shiwangangu wind site	16.7	7.1% @ 7.79km	10.9	37.1	21.7	1.3% @ 13km	4.4	32.9						
Lunsemfwa wind site	111	0.9% @ 44km	1.6	12.9	106	0.1% @ 63.2km	1.8	36.5						
Mulungushi wind site	10.7	1.8% @ 7.79km	2	9.2	12.1	1% @ 7.34km	1.8	5.7						
Victoria wind site	62.3	0.8% @ 28.5km	1.6	8.3	63.4	2.6% @ 38.1km	1.8	11.4						
Zengamina wind site	18.3	0.5% @ 9.15	4.2	39.4	20	4.5% @ 12.4km	3.4	27.3						



Map showing average terrain slope distribution in Zambia (source: World Bank & DNV-GI)



Map showing terrain elevation distribution (source: World Bank & DNV-GI)

Appendix B – Grid Assessment Models

Power System Modelling Data

Base MVA	100	
330kV Line Parameters		
R (p.u/km)	X (p.u/km)	B (p.u/km)
0.00004	0.000315	0.003708
220kV Line Parameters		
R (p.u/km)	X (p.u/km)	B (p.u/km)
0.000115	0.000682	0.001701
132kV Line Parameters		
R (p.u/km)	X (p.u/km)	B (p.u/km)
0.001224	0.002365	0.000486

Shunt Compensation

Station	Rating (MVAr)
Kitwe	20
Lumwana	20
Kansanshi	20

SVCs

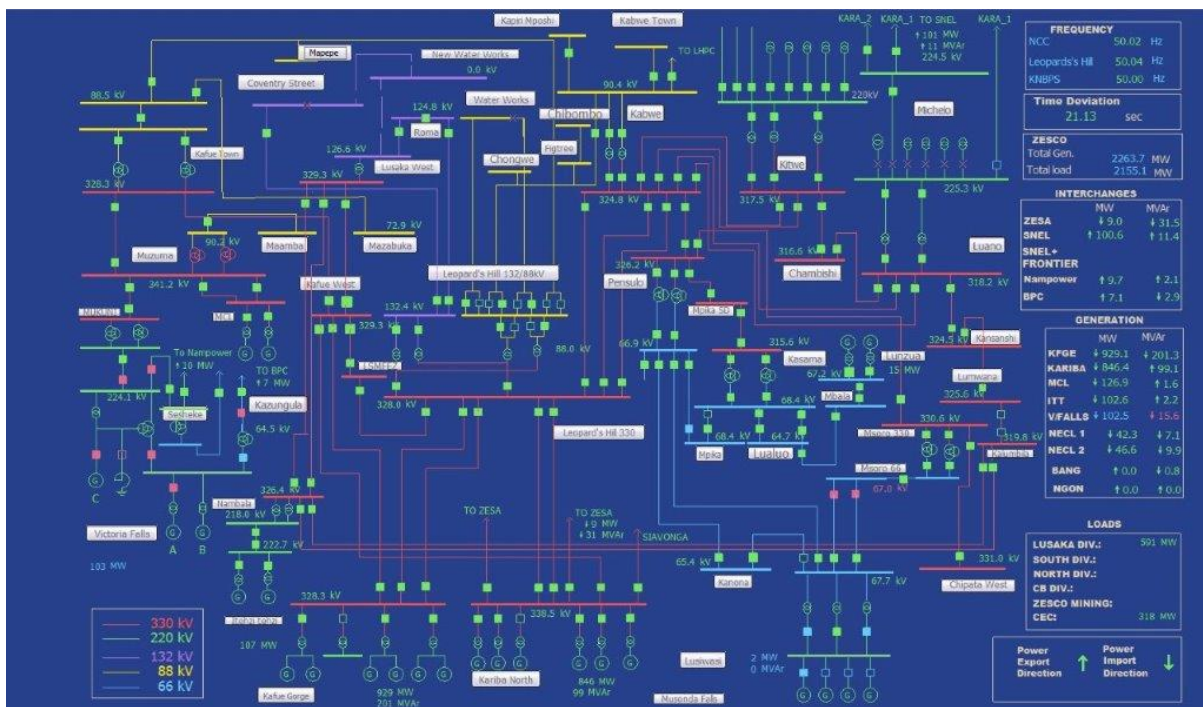
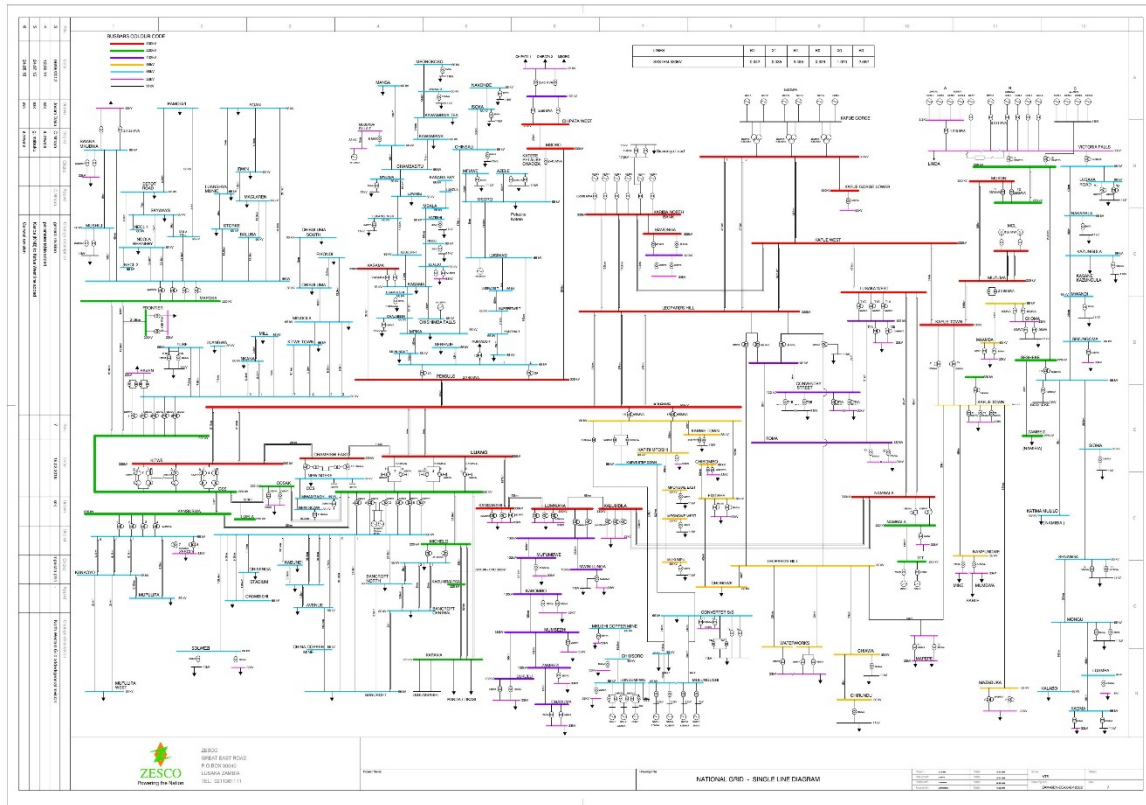
Station	Rating (MVA)
Kitwe	35
Luano	80

FROM	TO	km	R(p.u)	X(p.u)	B(p.u)	Voltage Level (kV)	Rating (MVA)
Kafue Gorge	Leopards Hill	47	0.00188	0.014805	0.174276	330	700
Kafue Gorge	Kafue West	43	0.00172	0.013545	0.159444	330	700
Kariba North	Leopards Hill	123	0.00492	0.038745	0.456084	330	700
Leopards Hill	Kabwe	97	0.00388	0.030555	0.359676	330	700
Kabwe	Kitwe	211	0.00844	0.066465	0.782388	330	700
Kabwe	Luano	247	0.00988	0.077805	0.915876	330	700
Kabwe	Pensulo	298	0.01192	0.09387	1.104984	330	700
Kitwe	Luano	40	0.0016	0.0126	0.14832	330	700
Kitwe	Chambishi	21.5	0.00086	0.0067725	0.079722	330	700
Chambishi	Luano	21.5	0.00086	0.0067725	0.079722	330	700
Luano	Kansanshi	196	0.00784	0.06174	0.726768	330	700
Kansanshi	Lumwana	72	0.00288	0.02268	0.266976	330	700
Kafue West	Lusaka West	51	0.00204	0.016065	0.189108	330	700
Kafue West	Kafue Town	3	0.00012	0.000945	0.011124	330	700
Kafue West	Leopards Hill	53	0.00212	0.016695	0.196524	330	700
VicFalls	Muzuma	159	0.018285	0.108438	0.270459	220	230
Muzuma	Kafue Town	189	0.021735	0.128898	0.321489	220	230
Luano	Michelo	44	0.00506	0.030008	0.074844	220	375
Michelo	Karavia	8	0.00092	0.005456	0.013608	220	375
Leopards Hill	Roma	28	0.034272	0.06622	0.013608	132	85
Leopards Hill	Coventry	28	0.034272	0.06622	0.013608	132	85
Roma	Lusaka West	21	0.025704	0.049665	0.010206	132	85
Lusaka West	Roma	21	0.025704	0.049665	0.010206	132	85

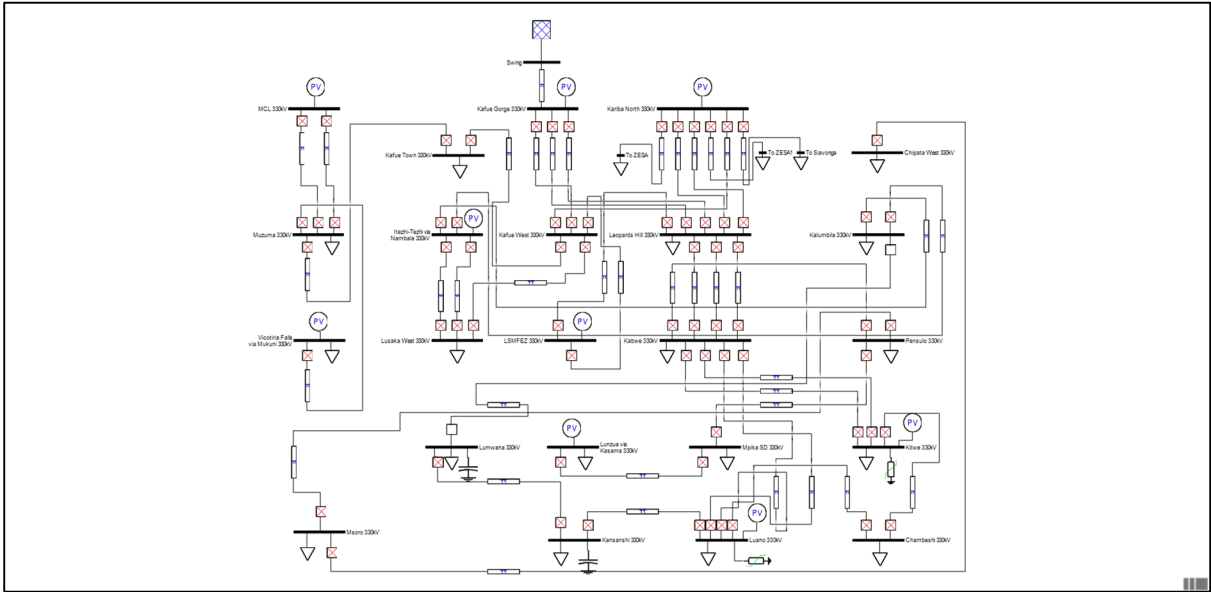
Transformers

Station	Qty	x(p.u)	Rating	Ratio
Kafue Town	1	0.185	60	220/88
Kafue Town	1	0.1707	60	330/88
Lusaka West	1	0.056	125	330/132
Leopard Hill	2	0.056	125	330/132
Kitwe	6	0.042	125	330/220
Luano	4	0.042	125	330/220

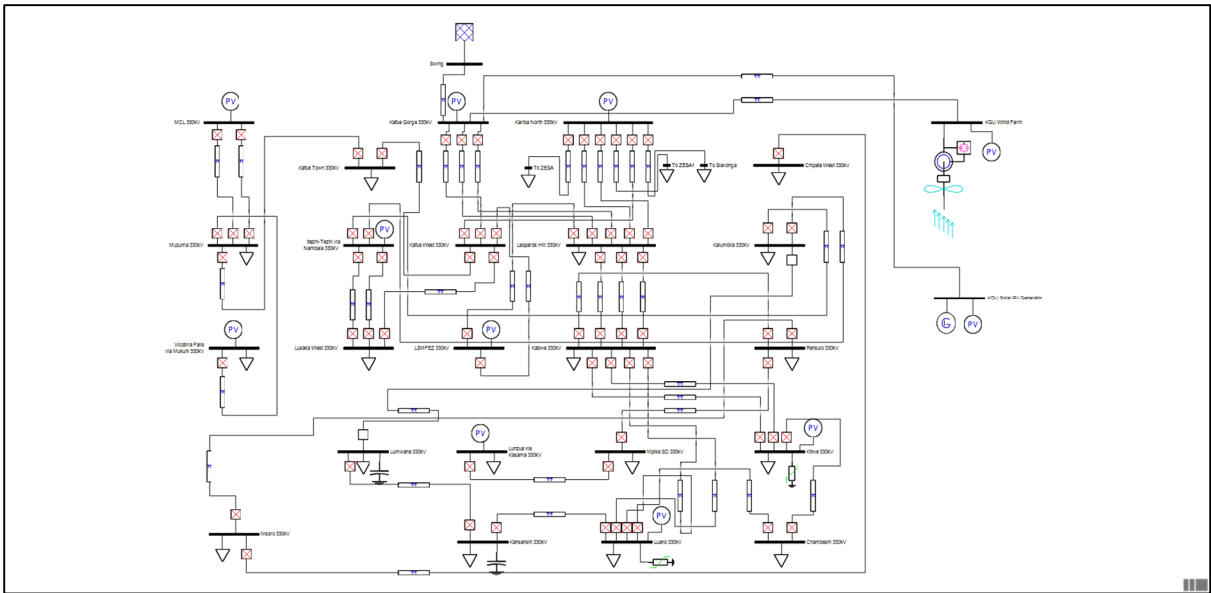
ZESCO Network Single Line Diagram



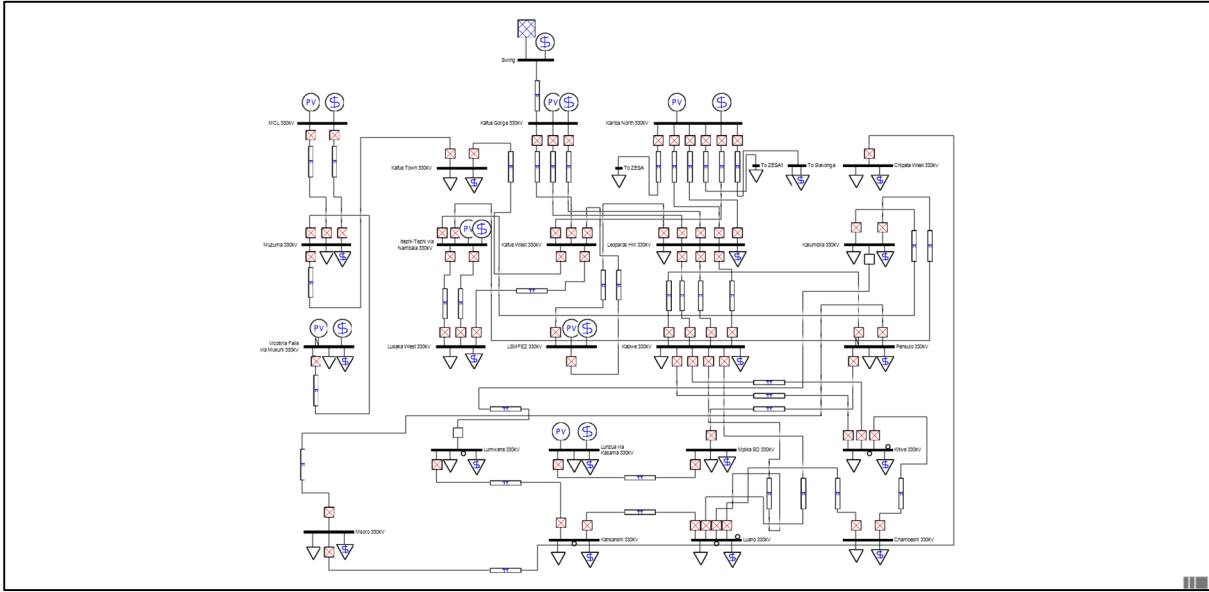
PSAT Single Line Diagram of Existing Network Model



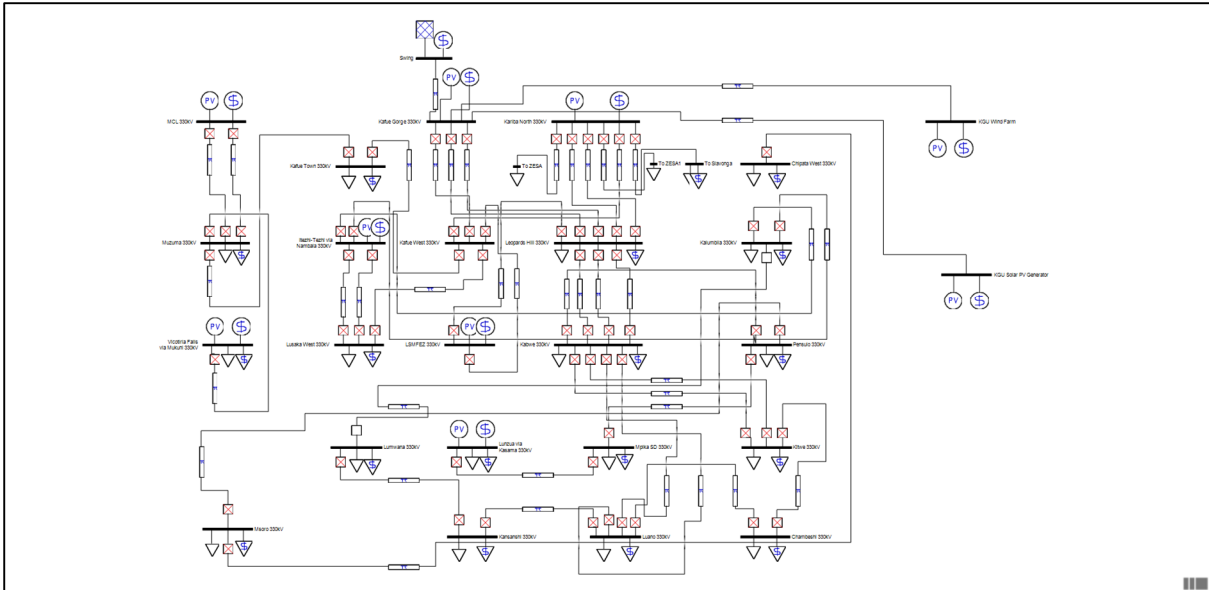
PSAT Single Line Diagram of VRES Integrated Model



PSAT SLD for the OPF Market Model of Existing Network



PSAT SLD for the OPF Market Model with VRES Integration



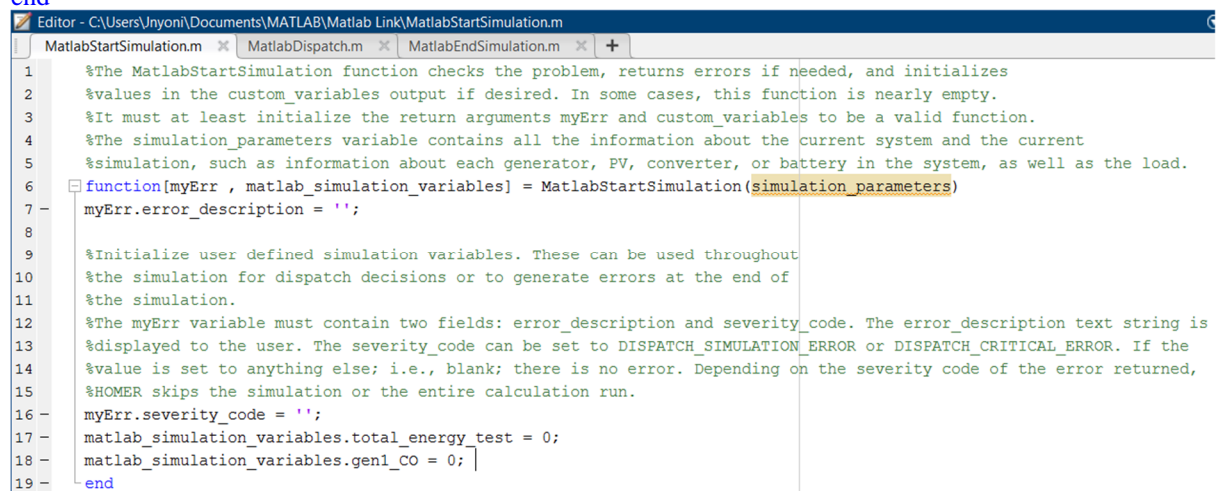
Appendix C – Matlab Link Dispatch Code

A MatlabStartSimulation Function

%The MatlabStartSimulation function checks the problem, returns errors if needed, and initializes
%values in the custom_variables output if desired. In some cases, this function is nearly empty.
%It must at least initialize the return arguments myErr and custom_variables to be a valid function.
%The simulation_parameters variable contains all the information about the current system and the current
%simulation, such as information about each generator, PV, converter, or battery in the system, as well as the
load.

```
function[myErr , matlab_simulation_variables] = MatlabStartSimulation(simulation_parameters)
myErr.error_description = '';
```

```
%Initialize user defined simulation variables. These can be used throughout
%the simulation for dispatch decisions or to generate errors at the end of
%the simulation.
%The myErr variable must contain two fields: error_description and severity_code. The error_description text
string is
%displayed to the user. The severity_code can be set to DISPATCH_SIMULATION_ERROR or
DISPATCH_CRITICAL_ERROR. If the
%value is set to anything else; i.e., blank; there is no error. Depending on the severity code of the error returned,
%HOMER skips the simulation or the entire calculation run.
myErr.severity_code = '';
matlab_simulation_variables.total_energy_test = 0;
matlab_simulation_variables.gen1_CO = 0;
end
```



```
Editor - C:\Users\jnyoni\Documents\MATLAB\Matlab Link\MatlabStartSimulation.m
MatlabStartSimulation.m x MatlabDispatch.m x MatlabEndSimulation.m x +
1 %The MatlabStartSimulation function checks the problem, returns errors if needed, and initializes
2 %values in the custom_variables output if desired. In some cases, this function is nearly empty.
3 %It must at least initialize the return arguments myErr and custom_variables to be a valid function.
4 %The simulation_parameters variable contains all the information about the current system and the current
5 %simulation, such as information about each generator, PV, converter, or battery in the system, as well as the load.
6 function[myErr , matlab_simulation_variables] = MatlabStartSimulation(simulation_parameters)
7 myErr.error_description = '';
8
9 %Initialize user defined simulation variables. These can be used throughout
10 %the simulation for dispatch decisions or to generate errors at the end of
11 %the simulation.
12 %The myErr variable must contain two fields: error_description and severity_code. The error_description text string is
13 %displayed to the user. The severity_code can be set to DISPATCH_SIMULATION_ERROR or DISPATCH_CRITICAL_ERROR. If the
14 %value is set to anything else; i.e., blank; there is no error. Depending on the severity code of the error returned,
15 %HOMER skips the simulation or the entire calculation run.
16 myErr.severity_code = '';
17 matlab_simulation_variables.total_energy_test = 0;
18 matlab_simulation_variables.gen1_CO = 0;
19 end
```

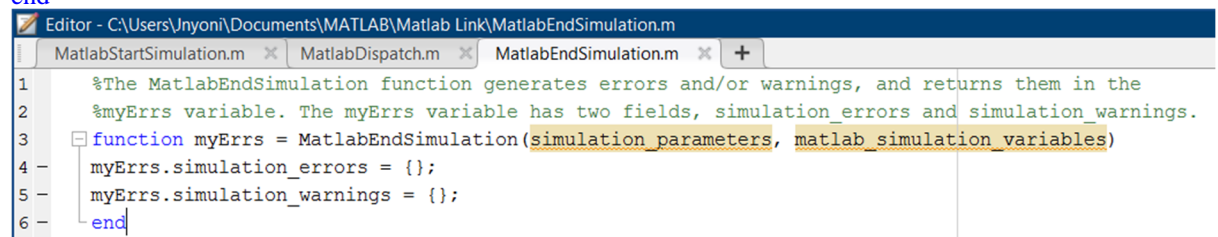
B MatlabEndSimulation Function

%The MatlabEndSimulation function generates errors and/or warnings, and returns them in the
%myErrs variable. The myErrs variable has two fields, simulation_errors and simulation_warnings.

```
function myErrs = MatlabEndSimulation(simulation_parameters, matlab_simulation_variables)
```

```
myErrs.simulation_errors = {};
myErrs.simulation_warnings = {};
```

```
end
```



```
Editor - C:\Users\jnyoni\Documents\MATLAB\Matlab Link\MatlabEndSimulation.m
MatlabStartSimulation.m x MatlabDispatch.m x MatlabEndSimulation.m x +
1 %The MatlabEndSimulation function generates errors and/or warnings, and returns them in the
2 %myErrs variable. The myErrs variable has two fields, simulation_errors and simulation_warnings.
3 function myErrs = MatlabEndSimulation(simulation_parameters, matlab_simulation_variables)
4 myErrs.simulation_errors = {};
5 myErrs.simulation_warnings = {};
6 end
```

C Matlab Dispatch Function

```

%The code utilizes and prioritizes variable renewable sources to save the load
%Homperpro/matlab does not support customized units for dispatch. The code works if the the customized
hydro is treated as a conventional generator
function[simulation_state, matlab_simulation_variables]= MatlabDispatch(simulation_parameters,
simulation_state, matlab_simulation_variables)

%Step1: Use all floating pv modules to serve the electrical load
if simulation_parameters.has_pv == true
    simulation_state.pvs(1).power_setpoint = simulation_state.pvs(1).power_available;
end

%Step2: Check unmet electrical load
unmet_load_after_pv = simulation_state.ac_bus.load_requested-simulation_state.pvs(1).power_available;

%Step3: Use all onshore wind if there is unmet load
if simulation_parameters.has_wind_turbine == true
    if unmet_load_after_pv >0
        power_available = simulation_state.wind_turbines(1).power_available;
        min_load = simulation_parameters.wind_turbines(1).minimum_load;
        simulation_state.wind_turbines(1).power_setpoint = max(min(power_available,unmet_load), min_load);
    else
        simulation_state.wind_turbines(1).power_setpoint = 0;
    end
end

%Step4: Check unmet electrical load
unmet_load_after_wind = simulation_state.ac_bus.load_requested-
max(min(power_available,unmet_load_after_pv), min_load);

%Step5: Use hydro generator to serve the unmet load. The generator will operate when the PV power alone
%is not enoguh to meet
if simulation_parameters.has_generator == true
    if unmet_load_after_wind >0
        power_available1 = simulation_state.generators(1).power_available;
        min_load1 = simulation_parameters.generators(1).minimum_load;
        simulation_state.generators(1).power_setpoint = max(min(power_available1, unmet_load_after_wind),
min_load1);
    else
        simulation_state.generators(1).power_setpoint = 0;
    end

%Step6: Serve the load
simulation_state.ac_bus.load_served = min(load_supplied_ac, simulation_state.ac_bus.load_requested);

%Step7: Set the excess electricity, unmet load, capacity served and capacity
%shortage
simulation_state.ac_bus.unmet_load = max(simulation_state.ac_bus.load_requested - load_supplied_ac, 0);
simulation_state.ac_bus.excess_electricity = max(load_supplied_ac - load_requested_ac, 0);
simulation_state.ac_bus.operating_capacity_served = operating_capacity_ac;
simulation_state.ac_bus.capacity_shortage = max(simulation_state.ac_bus.operating_capacity_requested -
operating_capacity_ac, 0);
end

```